JOURNAL OF APPLIED PHYSICS

JOURNAL OF APPLIED PHYSICS

Vol. 17, No. 12 DECEMBER, 1946

In This Issue

		Page
Report of the Electron Microscope Society of America's Committee on Resolution		989
Electron Microscope Examination of the Microphysical Properties of the Polymer Cuprene	JOHN H. L. WATSON AND K. KAUFMANN	996
Machine for the Application of Sand in Making Fourier Projections of Crystal Structures	DAN MCLACHLAN, JR. AND E. F. CHAMPAYGNE	1006
Radar Reflections from Long Conductors	F. BLOCH, M. HAMERMESH, AND M. PHILLIPS	1015
Viscometric Investigation of Dimethylsiloxane Polymers	ARTHUR J. BARRY	1020
Theory of Small Signal Bunching in a Parallel Electron Beam of Rectangular Cross Section	EUGENE FEENBERG AND DAVID FELDMAN	1025
On Vibrations of Shallow Spherical Shells	ERIC REISSNER	1038
Non-Uniform Transmission Lines and Reflection Coefficients	L. R. WALKER AND N. WAX	1043
Resonant Frequencies of the Nosed-In Cavity	ERNEST MAYER	1046
Study of a Certain Type of Resonant Cavity and Its Application to a Charged Particle Accelerator	E. S. AKELEY	1056
Millimeter-Wave Reflex Oscillator	J. M. LAFFERTY	1061
Resonant Circuit Modulator for Broad Band Acoustic Measurements	GORDON FERRIE HULL, JR.	1066
Transient Temperatures around Heating Pipes Maintained at Constant Temperature	ANDREW GEMANT	1076
Effect of Temperature on the Strength and Fatigue of Glass Rods	B. VONNEGUT AND J. L. GLATHART	1082
Plastic Flow, Creep, and Stress Relaxation. Part I. Plastic Flow	CHARLES MACK	1086
Plastic Flow, Creep, and Stress Relaxation. Part II. Creep	CHARLES MACK	1093
Plastic Flow, Creep, and Stress Relaxation. Part III. Creep and Elastic After-Effect	CHARLES MACK	1101
Asymptotic Solutions for the Normal Modes in the Theory of Microwave Propagation	C. L. PEKERIS	1108
Letters to the Editor:		
Concerning "Computer for Solving Linear Simultaneous Equations"	C. C. EAGLESFIELD; CLIFFORD E. BERRY	1125
Preparing Pigments for the Electron Microscope	A. M. CRAVATH	1125
Coordination Number in Solid Solutions—A Mathematical Paradox	DOUGLAS RENNIE HUDSON	1126
Note on a Paper of H. Bateman	F. W. J. OLVER	1127

Annual Indexes

Author Index to Volume 17	1132
Subject Index to Volume 17	1136
Volume Table of Contents	III

In Every Issue

Calendar of Meetings	1005
Here and There	1128
New Books	1139
New Booklets	1131
Index to Advertisers	xxxii

BOARD OF EDITORS

ELMER HUTCHISSON, *Editor*

Associate Editors

R. BOWLING BARNES
OTTO BEECK
W. F. BUSSE
S. H. CALDWELL
CLARK GOODMAN
SELIG HECHT
W. JAMES LYONS
PAUL E. SABINE
FREDERICK SEITZ
J. R. TOWNSEND

Publication of the American Institute of Physics

ADMINISTRATIVE STAFF

HENRY A. BARTON, *Director*

MARGARET S. GRIFFIN, *Publications Manager*

THEODORE VORBURGER, *Business Manager*

JOHN T. TATE, *Adviser on Publications*

GOVERNING BOARD

PAUL E. KLOPSTEG, *Chairman*

WALLACE WATERFALL, *Secretary*

GEORGE B. PEGRAM, *Treasurer*

R. B. DOW
L. A. DUBRIDGE
W. F. FAIR, JR.
FLOYD A. FIRESTONE
HARVEY FLETCHER
R. C. GIBBS
K. S. GIBSON
W. H. MARKWOOD, JR.
A. H. PFUND
JOHN T. TATE
L. W. TAYLOR
A. G. WORTHING

The JOURNAL OF APPLIED PHYSICS, published monthly at Prince and Lemon Sts., Lancaster, Pa., is devoted to physics in its role as the science basic to other natural sciences and to the arts and industries. Previous to 1937 this publication was known as PHYSICS. The JOURNAL OF APPLIED PHYSICS publishes editorials, news of physicists, and reviews, as well as technical papers of applied physics.

Manuscripts should be submitted to Elmer Hutchisson, Editor, Case School of Applied Science, Cleveland 6, Ohio.

Subscriptions and orders for back numbers should be addressed to Prince and Lemon Streets, Lancaster, Pa. or to the American Institute of Physics, 57 East 55 Street, New York 22, N. Y.

Subscription Price

	U.S. AND CANADA	ELSEWHERE
To members of scientific societies	$5.00	$5.70
To all others	7.00	7.70

Back Number Prices

Complete set: Vol. 1, July, 1931–Vol. 16, 1945—$101.50
Yearly back number rate: **$7.70**
Single copies: **$0.70** each.

Changes of address and proofs should be addressed to the Publications Manager.

Advertising rates supplied on request. Orders, advertising copy, and cuts should be sent to the American Institute of Physics.

Entered as second class matter January 22, 1937, at the Post Office at Lancaster, Pennsylvania, under the Act of March 3, 1879.
Accepted for mailing at the special rate of postage provided for in the Act of February 28, 1925, authorized May 2, 1932.

Copyright 1946, by the American Institute of Physics

Journal
of
Applied Physics

Volume 17, Number 12 December, 1946

Report of the Electron Microscope Society of America's Committee on Resolution

I. INTRODUCTION

THE opinions expressed in this report are those of the committee members and are based upon the personal experiences and experiments of those members, the published literature on the subject, and the answers received to a questionnaire sent out to all members of the Electron Microscope Society. There was not sufficient time available for the Committee, as such, to carry out experimental tests of the ideas and methods reported here. However, such experimental tests should be carried out, either by this or a subsequent committee or by interested members of the Society.

A suggestion was received from some members of the Society that the Committee examine various methods of measuring "resolving power" and recommend to the Society that one, the best of these methods in the opinion of the Committee, be adopted as *the* method of the Society. Consideration was given this suggestion but the Committee concluded that, for reasons to be explained later, such a suggestion could not be carried out practically. Consequently, the Committee does not, at this time, especially recommend any specific method of measurement.

It was decided that the interests of the Society could best be served by a critical review of the entire subject of resolving power and resolution, and of the various known or suggested methods for quantitative or qualitative evaluation of this factor. This report, therefore, contains the efforts of the Committee in such a direction.

II. DISCUSSION OF THE TERMINOLOGY USED

To obtain increased resolution is the fundamental reason for using an electron microscope. Such a statement should be obvious, yet careful consideration of it indicates the importance of any discussion of resolution. For much of the work with the microscope it is sufficient to know merely that the resolving power is about 2 orders of magnitude better than that of light microscopes. For example, if the thirty replies to the questionnaire sent to the members of the Society by this Committee give a representative cross section, only 30 percent of the micrographs taken with the instrument are examined at a total magnification of 50,000 times or greater. Now, unless this range of magnification is employed, the limiting factor in the detail to be seen is the resolving power of 0.2 mm for the human eye, and about 40A for the microscope.

Therefore, it should be realized that in about 70 percent of the work with present-day microscopes the question of resolution may be neglected as a limiting factor. However, the feeling was brought out in several replies that a greater percentage of high magnification work would be done if the resolving power of the microscope warranted it.

For the 30 percent of the micrographs which were examined at magnifications above 50,000×, however, the resolution does become important. In this connection, it was of interest to the Committee, as it will be to the Society, to obtain information on what members had determined

or believed to be their maximum resolution. The results of these replies are given in Fig. 1.

It is difficult to believe that the wide variation in this value is caused by actual variabilities in the instruments. Much of the differences must be caused by the lack of exact nomenclature associated with the subject. This may perhaps be traced to the fact that definitions commonly encountered are usually purely descriptive and invoke the concept of abstract mathematical points whose relation to physical particles is not always indicated. Furthermore, it is the opinion of the Committee that there are several aspects of resolutions or resolving power which are significantly different and should not be directly compared.

As examples of the descriptive types of definition, we may use those given by Webster's International Dictionary as follows:

"Optical resolving power—The power of an optical system using light of one color to form images of two point sources which are close together, so that the images may be recognized as distinct."

"Resolving power—The ability of an optical instrument to form distinct images of objects separated by small angular distances."

"Resolution—The act or property of rendering visible the separate parts of an object or of distinguishing between different sources of light."

Resolving power has also frequently been defined in the literature as the minimum distance between two points of the object whose images can still be resolved as separate.

It is the first recommendation of the Committee that the two terms, resolving power and resolution, be carefully distinguished in the following manner. As implied in the term "power" as well as in the Webster definition just given, *resolving power* should always be considered as an *ability* of the optical system while the term *resolution* should connote only the *realization* of that ability in a specific image. Resolving power should be the maximum resolution which *can be obtained* with the system. The actual resolution present in any specific image or picture may well be somewhat poorer. Thus, to speak of a series of published micrographs as having been obtained with an instrument whose resolving power is 20A is misleading. The actual resolution in the pictures shown or even possible

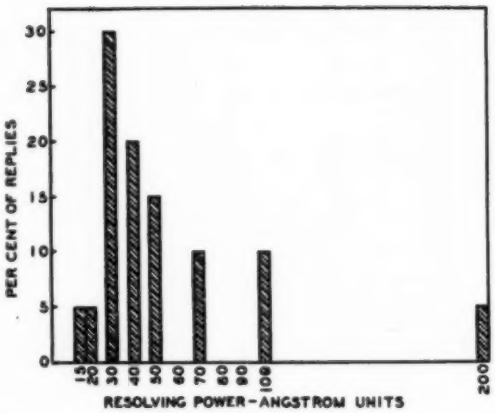

FIG. 1. A frequency diagram showing the resolving power which a number of individual electron microscopists considered to be the best they had obtained with their own instruments. The data were obtained from replies to a questionnaire sent to all members of the EMSA by the Committee on Resolution.

with the type of specimen studied may be considerably poorer, say 100A. In such cases, whereever possible, the resolution present in the original prints should be stated.

The Committee also suggests that the following distinctions be made in discussions on this subject in order to denote more definitely the type of resolving power or resolution which one is describing.

1. The *QUALITY* of a micrograph.
2. The *RESOLUTION* of a micrograph.
3. The *INSTRUMENTAL RESOLVING POWER* of a specific electron microscope.
4. The *CALCULATED LIMIT OF RESOLVING POWER* of an actual lens system.
5. The *THEORETICAL LIMIT OF RESOLVING POWER* of an electron beam.

These five divisions are described further as follows:

1. Quality. Basically the quality of a micrograph is determined by whether or not the picture gives the complete morphological information about the specimen. In a more practical sense, quality can be considered as a measure of the extent to which the micrograph provides the information which was sought in taking it. The Committee wishes only to point out here that quality and resolution are not synonymous but rather that resolution is but one factor contributing to quality. Many other factors, e.g., the population density and dispersion of the particles of the specimen, the absence of dirt,

etc., from the photographic plate, the lack of all artifacts, will likewise contribute to quality. Many of these will be quite independent of and have no effect on the resolution in the picture.

2. Resolution of a Micrograph. As already stated, the resolution in a micrograph is related to quality in that it sets a definite lower limit to the detail of structure which can be seen. However, there are other reasons for which one may be interested in resolution in a micrograph, particularly in its quantitative evaluation. Examples of such are:

a. To determine the minimum error in measurement of a size made on the micrograph particularly in determinations of particle size distributions where the sizes are near the resolution present.

b. In evaluating the effects upon resolution of various methods of specimen preparation and instrument adjustment.

c. In determining the extent to which physical properties of the specimen, density, thickness, etc., limit resolution.

d. In determining the extent to which the capabilities of the instrument have been utilized in a particular micrograph and as a means of detecting departure from the ideal performance of the instrument.

In general, the resolution in a micrograph is of interest either as a measure of the limiting detail available or as an integrated quantitative evaluation of the quality of the operation of the instrument.

In this connection, it should be pointed out that the resolution present will vary from point to point in a single micrograph, a fact which has been verified by measurements made by some of the Committee members and which is undoubtedly familiar to many electron microscopists. The phenomenon is probably due to the variation in the physical properties of the particles at those points, to different levels in the specimen, or to aberrations of the lens. It is brought out here merely to indicate the necessity for caution in attempting to measure the resolution in a single micrograph.

3. Instrumental Resolving Power. With this division we arrive at the categories concerning resolving power. Here we are considering capabilities, theoretical or actual, rather than the extent to which such capabilities have been realized in a particular application.

A prime but not sole factor determining the resolution in a micrograph is, of course, the resolving ability of the microscope used. This ability may be called the instrumental resolving power and it may be defined as the best resolution obtained with a given microscope when all conditions of specimen, photographic, and operational factors are ideal. It is, therefore, simply the best that instrument can do. It is significantly different from the previous category of resolution in that the choice of specimen is arbitrary in this determination.

A measurement of such instrumental resolving power would be of significance for several different purposes, for example:

a. To compare various designs, lens systems, etc.

b. To compare various microscopes of the same make or of different make.

c. To evaluate the effect of variations in different operating conditions such as apertures, angle of illumination, sources, etc.

d. To evaluate various photographic materials and processes.

From the results of answers to the questionnaire sent out to members of the Society a measurement of this type of resolving power is by far of greatest interest. Furthermore, it would probably be of advantage to have a standard method for measurement of this type of resolving power, particularly in comparisons between microscopes and microscopists. However, the Committee has not found a method which appears sufficiently accurate or sufficiently reproducible to recommend it for this purpose. It is possible, however, that experimental testing of some of the methods to be mentioned later will prove them suitable.

4 and 5. Calculated Limit of Resolving Power and Theoretical Limit of Resolving Power. The last two categories are described together because they have two points in common. First, both deal with limiting values obtained only mathematically and not in practice. Second, both are of considerably less interest to the Society as a whole although they are important to builders and manufacturers of microscopes.

The calculated limit of resolving power is that which one obtains for a specific instrument by the mathematical calculation of the effects of known limiting factors such as lens aberrations, electron velocity, etc. Whereas the instrumental resolving power is a measure of what an instru-

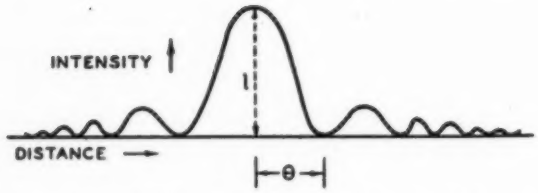

FIG. 2. The radial distribution of intensity in the image of a point source.

ment can do, the calculated limit of resolving power is a measure of what it should do according to theory. The ratio of these two is, therefore, a measurement of the efficiency of design of the instrument.

The theoretical limit of resolving power is merely the resolving ability of electron waves independent of any real instrument. It is commonly approximated by means of the Abbe formula, $d=\lambda/2N\cdot A$, or the Helmholtz or Rayleigh modifications of this. The validity of such approximations has been frequently questioned particularly in applying them to electron rather than light optics. However, a discussion of this point is believed beyond the scope of this report.

III. METHODS OF MEASUREMENT

From the experience of the Committee members, the published literature, and the answers to the questionnaire, it appears that there are seven possible types of measurements which may be made in connection with resolution or resolving power. These methods are briefly described at this time together with the Committee's evaluation of each.

1. Minimum Distance Between Particles. This method was indicated by nearly 50 percent of those giving positive replies to the question. "How do you measure resolution?" It is undoubtedly based upon the definition of resolution as a minimum distance between two points in the object whose images can be seen as separate. With this definition or with this method of measurement, the Committee has no disagreement. There are, however, several precautions to be exercised and several limitations of the method.

The first of these involves the translation in practice of the word *points* in the definition to the word *particles* in the method. It has been shown by physical optics[1] that the distribution of energy about the image of a *point* source produced by a lens of circular aperture follows a curve similar to that shown in Fig. 2. In this curve the distance, θ, is a function of the lens system, its aperture and aberrations, while the heighth l is a function of the intensity of the light source. Now, if we consider two points gradually approaching each other as in Fig. 3, it will be seen that their images begin to overlap significantly before the points themselves coincide and at some stage the two images will not be visually separable. At just what separation this occurs is determined by individual physiological factors, but for our purposes here we may adopt the frequently used conclusion[1] that, for the normal eye, the images will be undistinguishable when the first minimum of one image reaches the central maximum of the other, i.e., when $d=\theta$. At this stage the actual separation of the points in the object (d/magnification) is the resolving power of the system.

However, let us now consider the relations which exist in the images of actual particles. If, with the same optical system as before, we should determine the intensity distribution about an image of a self-luminous particle of diameter D and in a plane section along a diameter, we would find that the curve for such an image would be similar to that of the image of a point with one important exception. In the case of particles whose diameter, D, is of the same order of magnitude as the resolving power or longer, the θ_1 for the particle image will be determined by that particle size as well as by the resolving power for a point. When, therefore, one measures the minimum distance of approach of two such particles, the resolution obtained will also be determined by the size of such particles if the measurements are made from center to center in the images.

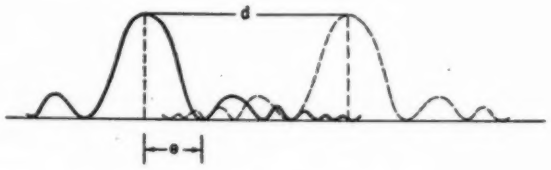

FIG. 3.

[1] John K. Robertson, *Introduction to Physical Optics* (D. Van Nostrand Company, New York, 1929), p. 233.

It, therefore, follows that the true resolving power of the system will be obtained only when the particles which are used as points are considerably smaller than the resolving power of the system. For electron microscopes this means that particles sufficiently small to behave as points must be only a few angstrom units in diameter or nearly of atomic dimensions. Some considerations regarding contrast of such particles toward electrons indicate that it may not be possible to see such particles, particularly those composed of low atomic number elements, even though the ability for linear resolution of the distance between them is available.

The significance of these considerations for this method of measuring resolving power lies in the fact that it shows that the measurement is always conservative for real particles of appreciable size, and, furthermore, that it requires particles of a size less than the resolving power being measured and of high contrast, *viz.*, of high atomic weight elements. For this reason it is suggested that the method be used to determine instrumental resolving power only when a suitable specimen is imaged, and that the specimen for that purpose be heavy metal particles of sufficiently fine size. The following specimens appear possible of application for such a purpose:

a. Evaporated metal films where the particles do not tend to coalesce or agglomerate. Evaporated films of 5–10A thick chromium appear excellent for this purpose.

b. Colloidal gold, silver, or platinum. Argyrol in 1:1000 dilution with water is fair although other materials are frequently present which obscure the picture.

As a test of the effect of different variables on the instrumental resolving power, the method suffers from the fact that one can never be certain that there is present somewhere in the field a pair of particles which are at the requisite minimum distance apart. For this reason, too, the method would appear to give conservative values of resolving power. Certainly micrographs of two different fields taken with two different microscopes cannot be quantitatively compared by such measurement except in a most approximate fashion. However, if it is possible to obtain a field in which the separation of uniformly small particles varies over wide values about the separation which can just be resolved, such a field could be used to ascertain the effects of variations in operating conditions.

Obviously a distinct advantage of this method is its convenience since it requires no auxiliary measuring device other than a ruled scale.

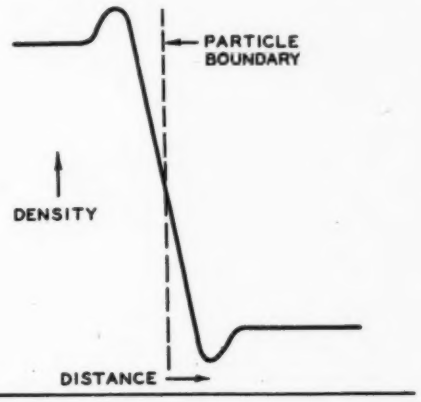

FIG. 4. A qualitative representation of the densitometric trace which is obtained across the photographic record of an electron microscope image.

2. Minimum Particle Diameter. It has been suggested that the diameter of the minimum sized particle present in the field be used as a measure of resolving power. As previously indicated it should be possible in theory to obtain images of particles of increasingly small diameter until the size of the image is no longer affected by the size of the particle. Such an image size should bear a distinct relation to the resolving power of the optical system. However, here again the important practical consideration of contrast must be taken into account. The Committee cannot state at the present time whether such a method would be of practical attainment—experimental tests should be carried out. It can be said, however, that this method suffers from the same disadvantages as that of minimum particle distance.

3. Contour Sharpness. If an in-focus image of a sharp and reasonably straight edge of a particle be recorded photographically in the electron microscope, a densitometer trace perpendicular to this edge appears as shown in Fig. 4. On such a curve one may measure a variety of constants which will bear some relation to the resolution present. Such measurements are as follows:

a. The lateral distance from maximum to minimum translated by magnification factors to a size in the object.

b. The slope of the straight line portion of the curve.

c. Following the suggestion of von-Ardenne,[2] the lateral distance, translated to the object, between points on the curve at 15 percent and 85 percent of the difference in intensity outside and inside the particle.

Such values are a direct measure of what one might call the sharpness of the image. This in turn is undoubtedly a direct function of the resolution present though just what function the Committee cannot say.

A significant advantage of this method lies in its reproducibility, particularly for different fields of the same specimen. It appears to be somewhat sensitive to changes in operating conditions also. It could, therefore, be used as a measure, though not a determination of the resolution in a micrograph or as a test procedure to study the effect of variations in operating conditions or of specimen preparation. Should it be possible to relate mathematically one of the values mentioned or a similar constant of the densitometric curve to the resolution present, it would be a convenient method of determining instrumental resolving power.

An interesting variation of this method is as follows: It is possible to predict from known values of lens aberrations and electron accelerating voltages the contour trace one should obtain in theory. Comparisons of this theoretical curve with that actually obtained gives a measure of the efficiency of the system. Such a test could be of interest in lens and instrument design.

4. Rounding of Particle Corners. A variation of the contour width measurement is found in the optical rounding of images of sharp corners

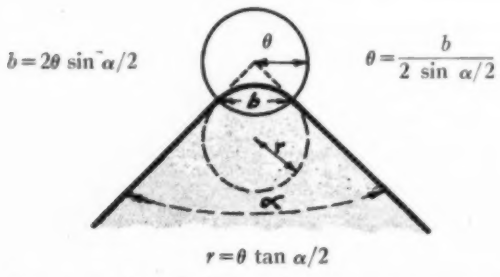

FIG. 5. A diagram illustrating the measurements used to determine the resolution in an electron micrograph from the apparent rounding of sharp corners.

of particles. This method is a development from the suggestion of Kausche and von Borries[3] as to the cause of such rounding. Essentially these authors assume that such a corner behaves as the ideal point and that, at the place where the circle of the first diffraction disk of that point intersects the straight edges of the particle, the deviation of the image from the true edge begins. This is shown in Fig. 5. The measurements which may be made thereon are indicated. Notice that these measurements are a function of the angle between the intersecting edges and such should be taken into account in any determination.

In actual practice the extent of rounding appears to be a more complex phenomena than the simple assumption of Kausche and von Borries. Determination of the distance, θ, are considerably larger than minimum particle distances. It seems quite likely that such rounding is more closely associated with the contour width and perhaps bears the same relation to resolution. More experimental work on this subject appears necessary. It is also known that contamination in the instrument due to the electron bombardment rounds the corners.

Such a method would prove of the same use as the contour width measurement. It has the advantage of not requiring a densitometer but the disadvantage of being less precise.

5. Rounding of Particle Intersections. A serious disadvantage of the method of measurements of rounded corners lies in the fact that one cannot be certain that the corners are not in physical reality rounded themselves, perhaps even by the bombardment of the electron beam. To avoid this a method has been suggested by Dr. Sergei Feitelberg[4] of the Mt. Sinai Hospital in which the rounding is measured not at a particle corner but at the intersection of the straight edges of two particles. There should at least in theory be no reason for more matter to be knocked off at such an intersection than along the remainder of the edge.

It would appear that otherwise the same statements apply to this method as given for the rounding of particle corners. The Committee

[2] Manfred von Ardenne, *Elektronen-Ubermikroskopie*. Reproduced under Authority of Alien Property Custodian (Edwards Brothers, Inc., Ann Arbor, Michigan, 1943), p. 279.

[3] B. von Borries and G. A. Kausche, Kolloid Zeits. **90**, 132–141 (1940).

[4] Sergei Feitelberg, private communication.

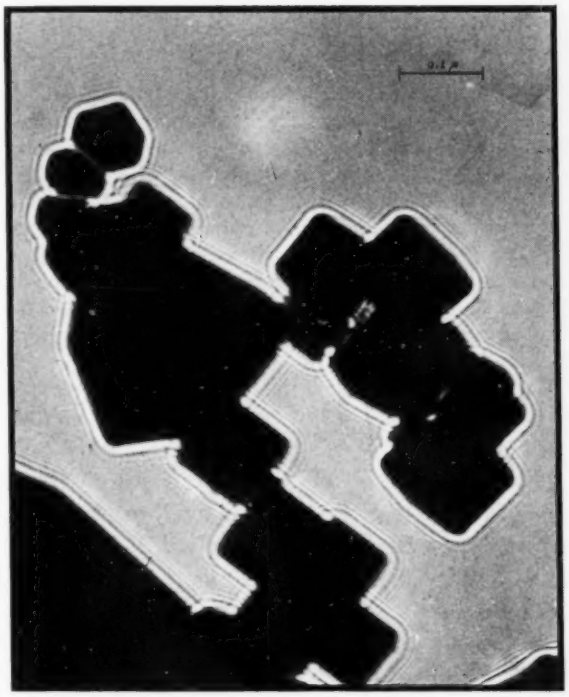

FIG. 6a. An out-of-focus electron micrograph of magnesium oxide smoke showing Fresnel fringes.

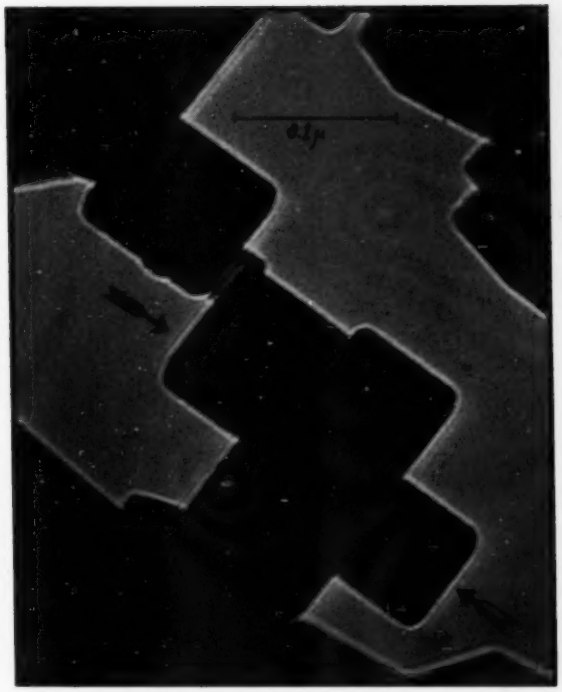

FIG. 6b. An electron micrograph of part of the same field of view as in (6a) which is only slightly out of focus and shows closely spaced Fresnel fringes.

would recommend the additional precautions that the two edges be as near as possible in the same focal plane and that there be no deposition of other materials at the intersection.

6. Quality Estimation. A method was recently described by Hillier[5] in which micrographs are visually graded for quality and this grade is expressed in terms of the maximum final magnification one estimates the picture quality will allow. Such a method has proven of value to him in evaluating over-all level of performance and progress in that direction. In such a method one examines the negative at about 10–20 times magnification. Quality may be judged by whatever factors are of particular interest—amount of contrast, accuracy of focus, symmetry of optical fringes or borders, exposure, distortion, and many others. Such a method could be useful for approximating "batting averages."

7. Measurements from Fresnel Fringes. A method of considerable promise for measuring instrumental resolving power is the measurement of Fresnel diffraction fringes in an out-of-focus micrograph of a straight edge of a particle. This method, suggested by Ruska,[6] and Hillier,[7] is an indirect result of work done by Boersch[8] though other authors have written on the subject. Images of such fringes are shown in Fig. 6. A densitometric trace perpendicular to such fringes is shown by Hillier.[7] The method consists briefly of measuring on such a trace the lateral distance between the maximum and minimum which can just be resolved. This distance, translated to the object plane by magnification factors, gives a value for instrumental resolving power.

To obtain such fringes in an electron microscope image requires the following conditions: First, the electron source must be as small as possible. This may be achieved either by using an extremely small condenser aperture—Boersch used a 5-micron aperture—or by obtaining a very small source free of secondary scattering.

The condenser current should be near maximum and the objective current should be somewhat lower than the in-focus value, i.e., the objective should be focused on a plane somewhat

[5] J. Hillier, J. App. Phys. **16**, 469 (1945).

[6] E. Ruska, Kolloid Zeits. **105**, 43–52 (1943).
[7] J. Hillier, J. App. Phys. **17**, 307 (1946).
[8] H. Boersch, Physik. Zeits. **44**, 202 (July 1943).

beyond the specimen in the direction of the condenser.

The phenomenon of Fresnel diffraction provides as the test for resolving power a series of secondary electron sources rather than physical particles. As one goes outward from the diffracting edge, the maxima and minima become increasingly closer both in angular direction and in intensity difference. It is not certain at the present time whether the limiting pair which are just visible are determined by their angular spacing and the resolving power of the microscope, or by the intensity difference and the contrast obtained therefrom on the photographic plate. Experimental tests might show this. Nevertheless, the method appears to be of considerable promise for testing the instrumental resolving power. While the out-of-focus condition of the objective changes the magnification somewhat from the in-focus value, an exact evaluation of the change can be made by a direct comparison of the in-focus and out-of-focus images.

IV. SUMMARY

In summary the Committee presents five quantities which are associated with resolving power and seven methods of measurement for such quantities. These are as follows:

1. The quality of a micrograph—probably best evaluated by visual inspection for the factor or factors of interest.
2. The resolution of a micrograph—there is no known method of obtaining this value for all micrographs. Probably the indirect measures of contour sharpness, or of corner or intersection rounding would serve this purpose best.
3. Instrumental resolving power—this value is probably best determined by measurements of Fresnel fringes. The minimum particle distance or the contour width may also be used.

4 and 5. Calculated and theoretical limits of resolving power—these values are mathematically evaluated and the computations involved are beyond the scope of this report.

As indicated several times, much experimental work seems desirable in this field. Until such methods have been thoroughly tested for preciseness and accuracy, the Committee cannot recommend that the Society standardize upon any one.

W. G. KINSINGER (*Chairman*)
J. HILLIER
R. G. PICARD
H. W. ZIELER

Electron Microscope Examination of the Microphysical Properties of the Polymer Cuprene

JOHN H. L. WATSON AND K. KAUFMANN
Plant Research Department, Shawinigan Chemicals Limited, Shawinigan Falls, Quebec
(Received July 10, 1946)

The microphysical structure of cuprene is described from electron micrographs and some suggestions are made concerning the mechanism of the formation of this substance. Cuprene samples prepared by polymerization of acetylene in the presence of finely divided cuprous oxide are shown to be composed of hollow fibers characterized by both longitudinal and transverse structure. The striking appearance in electron micrographs of this type of cuprene serves to identify it in clogging deposits taken from acetylene lines. This is illustrated by a deposit taken from a reactor used in the process of hydrogenation of acetylene to ethylene. Cuprene specimens formed by alpha-ray bombardment of acetylene gas are shown to be composed of round particles joined by short, straight, thick necks which are about 500 to 1000A in length. These are samples of cuprene which have been bombarded further by alpha-particles after their initial formation. An oxidized sample has round particles of mean diameter 4900A; an unoxidized sample has a mean diameter of 3800A for the round particles. There is evidence to suggest that alpha-ray cuprene is liquid in nature. The two types of cuprene are so different physically that a change in nomenclature is in order.

CUPRENE, PRODUCED CHEMICALLY IN A CATALYZED PROCESS

THE first references to cuprene are by Erdmann and Koethner.[1] It has been studied since by numerous investigators and comprehensive summaries are given by Calhoun[2]

[1] Erdmann and Koethner, Zeits. f. anorg. Chemie **18**, 48 (1898).
[2] Calhoun, Can. J. Research **15**, 208 (1937).

FIG. 1. Brown cuprene made chemically between 200 and 240°C with a cuprous oxide catalyst. Note longitudinal and transverse structure in the fibers. ×20,000.

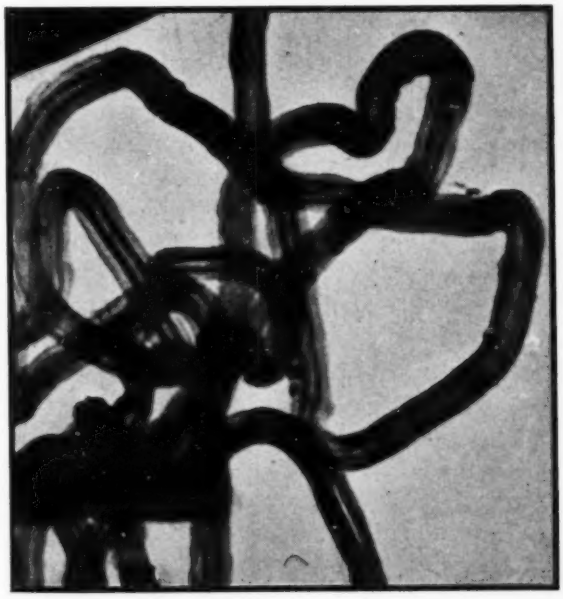

FIG. 2. An enlarged section of Fig. 1 to show longitudinal structure more clearly. ×36,000.

and others. It is a solid, amorphous material varying in color from a dark brown to a light yellow, and in physical appearance to the eye from a light, flocculent powder to a relatively dense, cork-like mass according to the conditions of preparation. Chemically, its nature is uncertain but it appears to be a polymer of acetylene with formula $(C_nH_m)_x$.

If it is prepared in the presence of copper or finely divided cuprous oxide as a catalyst, the polymerization starts at about 200°C, proceeds rapidly, and slows down gradually. Increase of temperature hastens the reaction but above 300°C carbon forms instead of cuprene. Solids resembling cuprene have been obtained also using tin, nickel, and cobalt as catalysts; and by the action of silent electric discharges, ultraviolet radiation, cathode rays, and alpha-particles upon acetylene gas.

The samples studied here were prepared by chemical means using finely divided cuprous

oxide as a catalyst between temperatures of 200°C and 240°C.

The cuprene presents a very striking appearance in electron micrographs and was photographed first by J. H. L. Watson and L. T. Newman with the electron microscope at the University of Toronto.[3] These pictures showed it to be composed of fibers which, from intensity characteristics in the micrographs, appeared to be tubular.

This cuprene is mounted for the electron microscope by rubbing the corky substance across a specimen holder with a Formvar film attached or across a filmless holder. Original magnifications of ×5000 are sufficient to show up detail existing within the fibers.

The fibrous, tubular nature of this cuprene formed chemically with a cuprous oxide catalyst is observed in both flat and stereoscopic electron micrographs. In addition, both a *transverse* (across the fiber) and a *longitudinal* (along the fiber) structure are observed (Figs. 1–3). Figure 2 is an enlarged section of Fig. 1.

FIG. 3. Brown cuprene made chemically with cuprous oxide catalyst. Note structure and loosened skin on fiber. ×20,000.

Considering first the *longitudinal* structure, two types are observed. From Fig. 2 and from certain stereoscopic views it is concluded that most of the larger fibers are composed of several finer ones lying parallel to each other and touching in a bundle. This is evident especially in those where the thickness is such that the electrons are able to penetrate with relatively small scattering. The finest longitudinal structures have diameters of the order of 80A. This is presumably the order of the diameter of the finest fibers and is equivalent to 50 to 60 carbon bond distances.[4]

There is great variety in both fiber shape and fiber diameter, but the tubular nature seems to be universal. For this reason a calculation of the approximate number of carbon atoms in the fiber circumference is in order. Again, if a fiber of circular cross section is considered with the minimum diameter 80A, it possesses 164 or 180 carbon bond distances in the length of its circumference, according as single or double bonding is assumed between the atoms.

Intensity variations over the micrographs signify either a true tube as the nature of the fibers, with carbon atoms clustered only at the skin of the tube; or merely that there is a *greater* concentration of carbon atoms at the skin than in the central regions. From stereoscopic views in general, as represented by Fig. 4 (location marked by the arrow), the tubes are seen to be hollow and are consequently true tubes with the atoms of the substance clustered at the edges. This stereoscopic pair is chosen as Fig. 4 because the tube marked is particularly interesting. It is not only hollow, and thin-skinned, but *hexagonal* in cross section. In addition it is noted that from the corners of the hexagon dark linear areas proceed down the fiber. These linear areas of apparently denser or thicker nature have been observed in other fibers of various shapes and contribute to a second type of longitudinal structure. They may account also for some of the longitudinal structure observed in Figs. 1 and 2.

[3] Burton and Kohl, *The Electron Microscope* (Reinhold Publishing Corporation, New York, 1946), second edition, p. 267.

[4] Values for single bond and double bond distances are 1.54A and 1.38A, respectively. Daniels: *Chemical Kinetics* (Cornell University Press, Ithaca, New York, 1938), p. 226.

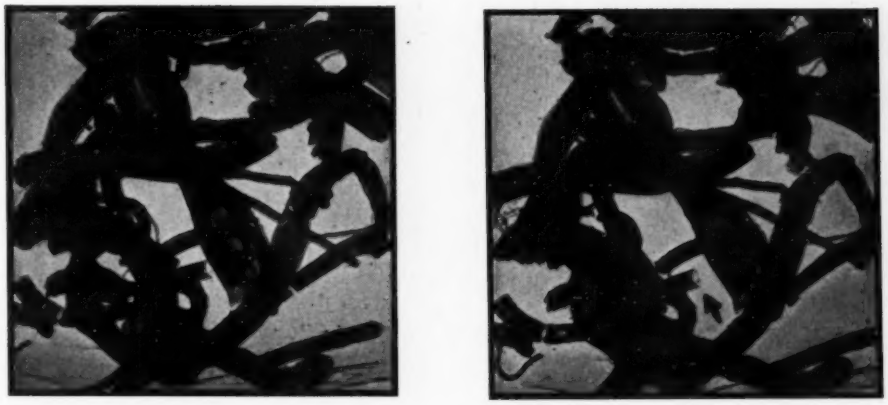

FIG. 4. A stereoscopic view of brown cuprene made with cuprous oxide catalyst. Note the hollow fiber of hexagonal cross section at ↖. ×8000.

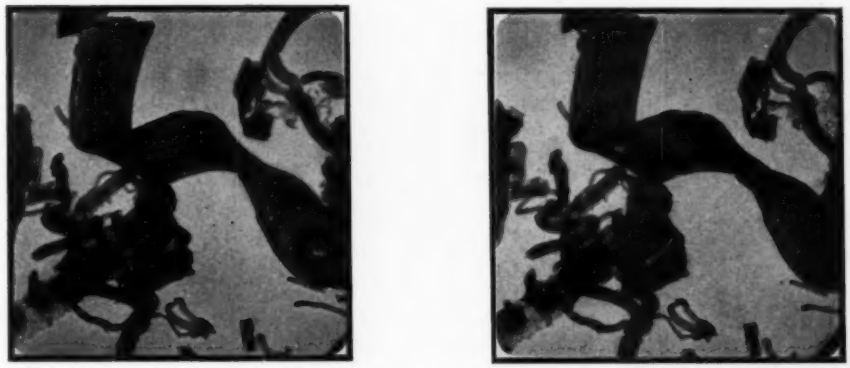

FIG. 5. A stereoscopic view of brown cuprene made with cuprous oxide catalyst. Note the ribbon-like, spiraled fiber. ×3800.

Cross-sectional areas of circular, oval, square, rectangular, ribbon-like, and hexagonal appearance have been recognized. Figure 5 is a stereoscopic pair of a ribbon-like fiber. It is suggested that the polymerizing fiber takes the cross-sectional shape of the particular small area or particle of catalyst upon which it begins to grow. There may be some information to be gained here concerning active centers on catalytic surfaces; a combination of active center properties and molecule sizes possibly may determine both size and shape of the fiber cross section.

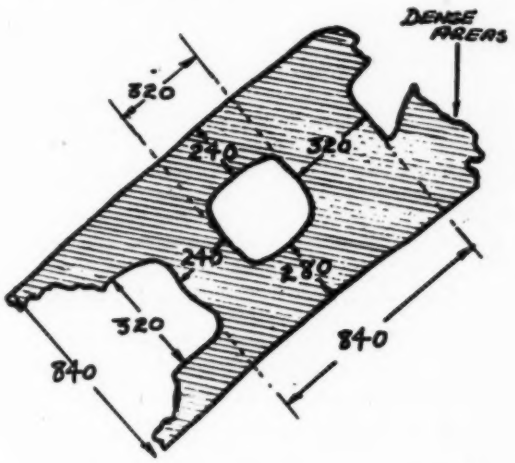

FIG. 6. Drawing to give the dimensions of the dense and light areas in a typical piece of cuprene possessing transverse structure. All dimensions are in angstrom units.

Perhaps more interesting than the longitudinal structure is the *transverse* structure evident throughout the micrographs. Typical occurrences are seen in Figs. 1 and 3 in fairly large fibers. These fibers appear to be divided by dense areas (recognized by dark regions in the micrographs) into cells, where presumably, again, the atoms of the substance are tending to cluster. Usually the length of one of these cells along a

FIG. 7. An enlarged section of Fig. 1 showing a fine fiber of diameter 170A which possesses transverse structure. ×65,000.

fiber is of the same order numerically as the value of the diameter of the particular fiber. At the mark of the arrow in Fig. 1 the transverse structure has dimensions approximating the values marked in the drawing in Fig. 6.

(A)

(B)

FIGS. 8A and B. Small filaments of newly formed cuprene grown upon an electron microscope specimen screen, showing small pieces of catalyst being carried along with the growing fiber of polymerizing cuprene. ×20,000.

FIG. 9. A sample of cuprene taken from a German reactor used in the hydrogenation of acetylene to ethylene with a palladium catalyst on silica gel. ×20,000.

From a few shadow cast specimens studied to date the observations of structure noted here have been substantiated but there is evidence to suggest that the structure is even more complicated in nature.

A skin is observed on the fibers in many micrographs as in Fig. 3 where it is apparently becoming loosened and is peeling off. This skin is observed chiefly with larger fibers. In the very tiny individual ones as reproduced in Fig. 7 there is no visible skin, nor longitudinal structure, but a definite suggestion of transverse structure still persists. Figure 7 is a much enlarged section of Fig. 1.

Intensity variations over electron micrographs are not easily interpreted but in general relatively darker areas in an image indicate either thicker, or else physically or atomically denser, parts of the specimen. The dark areas here indicate parts of the cuprene fiber where clustering of carbon atoms occurs. There is another possibility that copper or cuprous oxide is able to migrate along the fiber and does so along the dark image areas described. The percentage of

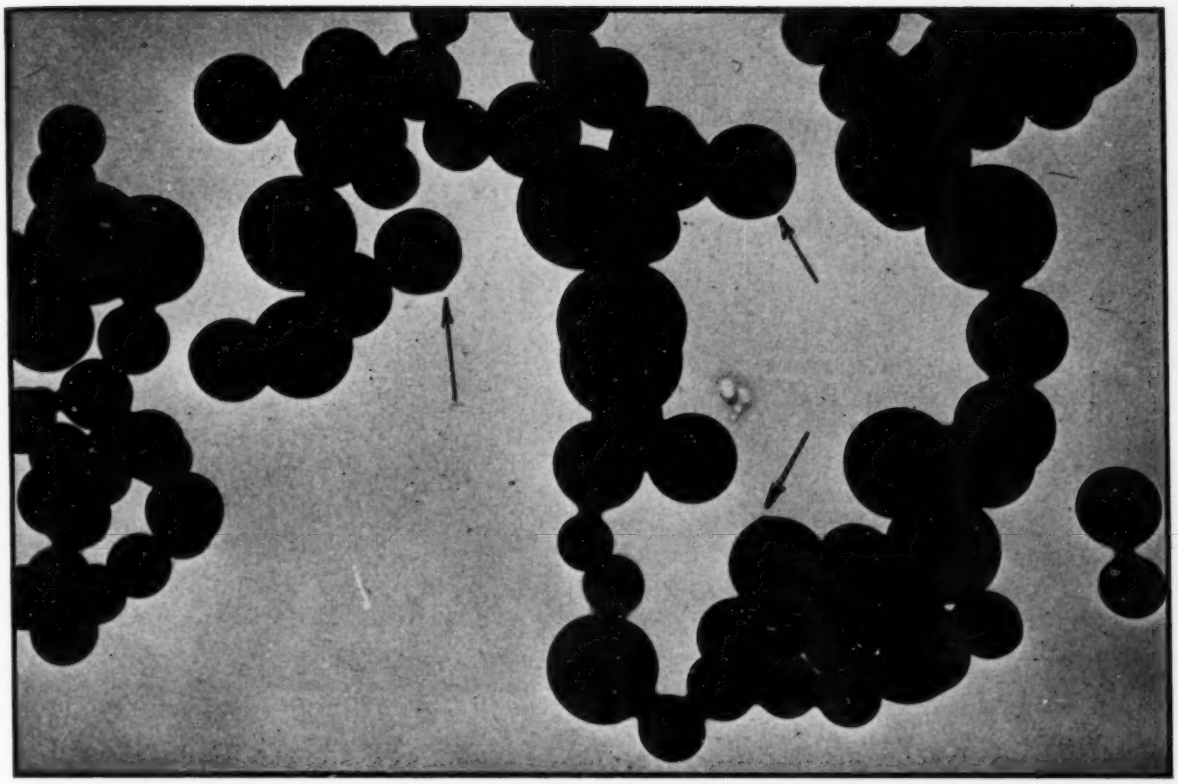

FIG. 10. Alpha-particle cuprene oxidized and bombarded with further alpha-particles after the original formation. ×20,000.

copper in cuprene is so small (3 percent) that it is most probable that clustering of carbon atoms in the preferred positions accounts for the structural pattern observed.

That metallic copper is actually associated with the fibers and is migrating along them, or is carried along with them, is supported by not very satisfactory transmission electron diffraction patterns of this cuprene where the only visible line was found corresponding to a grating space of 2.08A.[5] for the strongest line of metallic copper. Chemical tests also detect copper even in the very outermost parts of a cuprene growth far from the original catalyst. In the reducing atmosphere associated with cuprene formation it is likely that the cuprous oxide is reduced to metallic copper.

In order to study cuprene as it *first* begins to form it was grown upon copper specimen screens impregnated with cuprous oxide. It is found that the first forming cuprene begins its growth as a small spiraling fiber, as in Figs. 8A, and B. The spiral nature of the fibers persists in older samples. From observations of the newly formed, short fibers it is seen that they are carrying small pieces of some heavy material with them. We suggest that this is either cuprous oxide or metallic copper reduced from the oxide by hydrogen, and that it is carried along as the fiber grows, continuing in this way to catalyze the reaction. This mechanism would explain the presence of copper in the outer parts of the growth.

Some photographs were taken of cuprene, which had been raised in temperature slightly beyond 300°C. In addition to the usual fibers, small round particles of mean diameter 440A were detected. They were discrete and did not occur in chains although they are probably a type of acetylene black.

Cuprene is often a nuisance as it grows in acetylene lines. If cuprene is suspected to be the

[5] Hanawalt, Rinn, and Frevel, Ind. Eng. Chem. Anal. Ed. 10, 457 (1938).

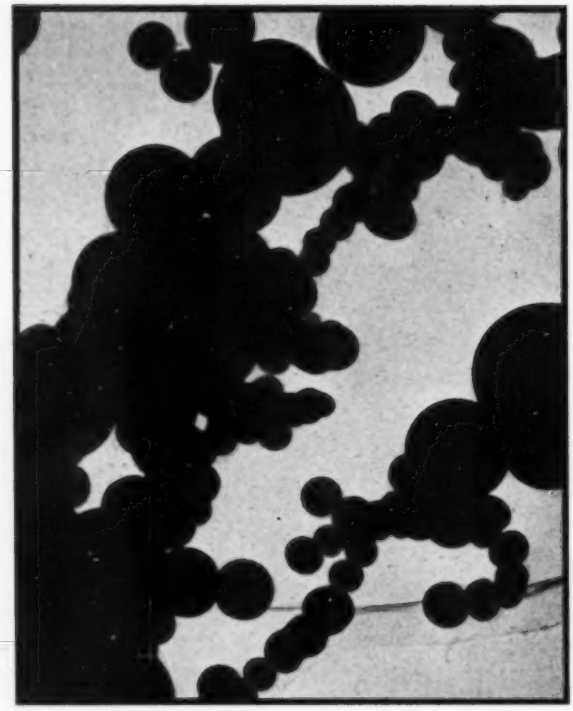

FIG. 11. Alpha-particle cuprene unoxidized, and bombarded with further alpha-particles after the original formation. ×20,000.

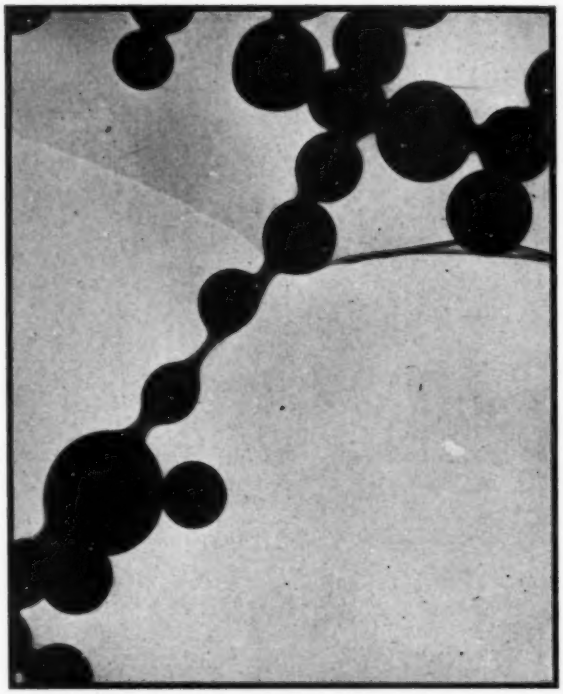

FIG. 12. Chains of alpha-particle cuprene stretched to show the existence of joining necks. ×20,000.

blocking agent in a line, it may be identified readily as such with the electron microscope because of its characteristic appearance when formed by a catalyzed chemical process. Figure 9 shows a deposit of a substance taken from a reactor which had been used in the process of hydrogenation of acetylene to ethylene at Anorgana, G.m.b.H., Gendorf, Bavaria, with a palladium catalyst on silica gel. This was a hard, rocky deposit, quite unlike Shawinigan cuprene to the eye, and had to be ground and mounted from a water suspension for the electron microscope. From electron micrographs the deposit was found to contain chiefly cuprene mixed with some other unidentified materials. No transverse structure was observed in the fibers but they do possess some longitudinal structure. There are many thin, film-like fragments which are probably wall structure from the ground fibers.

ALPHA-PARTICLE CUPRENE

Cuprene may be formed also when acetylene gas is bombarded by certain atomic particles,

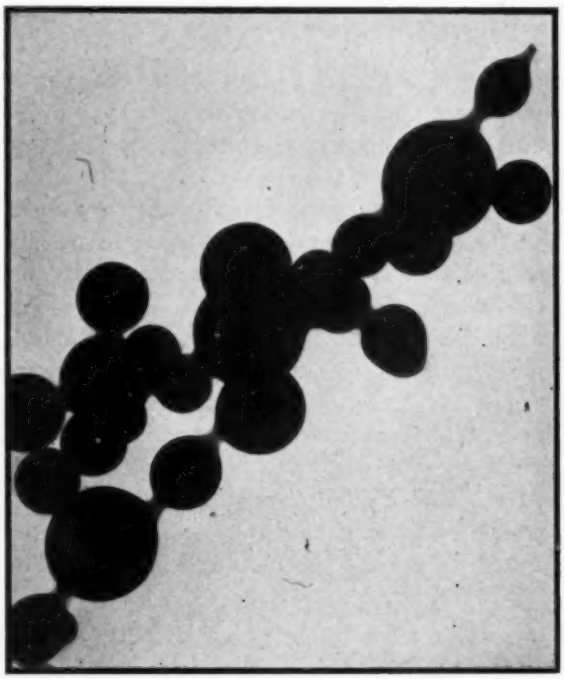

FIG. 13. Part of the same field as in Fig. 12 after the chain had broken, showing permanent deformation of the stretched particles and necks of cuprene. ×20,000.

such as alpha-particles from radon.[6] At ordinary temperatures and pressures a light yellow powder is deposited from the process.

Two samples of alpha-particle cuprene which were made some twenty years ago were secured from Dr. S. C. Lind.[7] That described as being "oxidized" was left open to the air for this time through a long, fine capillary and the probability is that it has oxidized slowly; alpha-ray cuprene adds about a quarter of its weight of oxygen in about three months time if it has free access to the air. The sample described as "unoxidized" was not open to the air. After their original formation both samples were subjected to further alpha-ray bombardment and probably lost some hydrogen in the process.

The physical appearance of this type of cuprene is distinctly different from that of cuprene formed by chemical means in the presence of a cuprous oxide catalyst. The alpha-ray cuprene is composed of comparatively large, round particles joined to each other by short, thick necks or rods of length approximating 500 to 1000A. These necks appear to join the particles at right angles. Figure 10 shows the oxidized sample wherein the particles and joining necks are seen. The unoxidized specimen has the same general characteristics and is shown in Fig. 11.

The existence of these necks is illustrated in Fig. 12 where a broken Formvar film has stretched a chain apart and lengthened the necks without breaking them. Figure 13 shows part of the same field after one link in the chain has broken. The distorted particle shape remains. In Fig. 14 several stretched cuprene necks can be seen over a breaking Formvar film, and in addition it is seen that the "droplets" of cuprene have been distorted about the holes in the Formvar. The observations mentioned in this paragraph indicate that this cuprene has the properties of a very viscous *liquid*, and can be compared to rubber latex in some of its particle characteristics. This would explain why the cuprene gives no x-ray diffraction pattern.

[6] Lind, *The Chemical Effect of Alpha Particles and Electrons* (The Chemical Catalog Company, New York, 1928).

[7] Lind, Bardnell, and Perry, J. Am. Chem. Soc. **48**, 1556 (1926).

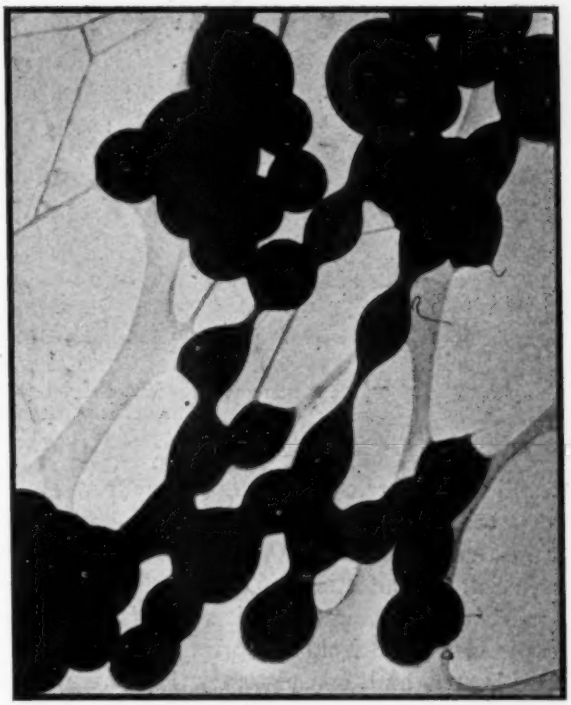

FIG. 14. Alpha-particle cuprene chains, showing stretching of the necks and deformation of the "droplets" about holes in the formvar film. ×20,000.

In a recent article by Stanton and Henson[8] a latex is described which possesses an appearance in electron micrographs very similar to that described here for the polymer cuprene. This property of large round particles joined by necks of the material would therefore appear to be common to some types of polymerized substances. On the other hand the fibrous structure of catalyzed cuprene is probably common to others, especially those grown upon a catalytic surface.

Little difference is immediately observable between the oxidized and unoxidized samples, but from particle size distribution studies of the "droplets," the mean diameter of the oxidized sample is found to be 4900A and of the unoxidized sample to be 3800A. This is a difference of 30 percent and is a significant difference for this type of counting procedure. The standard deviations for oxidized and unoxidized samples are 1300 and 2200A, respectively, indicating a greater spread of partizle sizes in the unoxidized

[8] Stanton and Henson, Ind. Eng. Chem. **18**, 468 (1946).

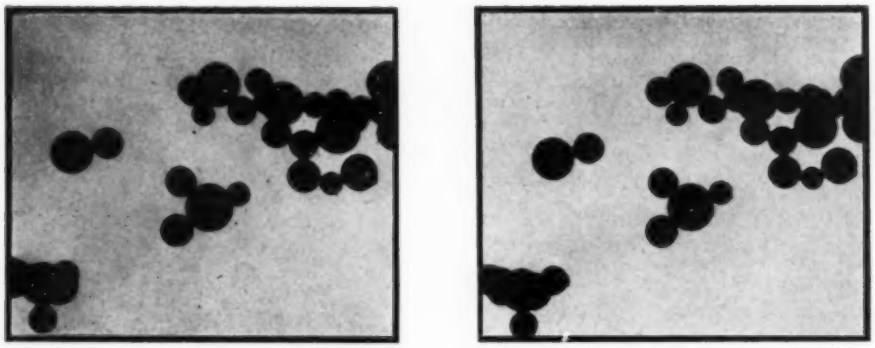

FIG. 15. A stereoscopic view of alpha-particle cuprene, oxidized, showing the "molecular model" appearance of the chains. ×8000.

sample. The particle diameters range from about 3000 to 10,000A, in the oxidized sample, and from about 1000 to 13,000A, in the unoxidized material. In addition to these differences in particle size measurements it seems from stereoscopic views and from flat prints that the necks are shorter and consequently less frequently observable in the unoxidized cuprene. Figure 15 is a stereoscopic view of the oxidized alpha-ray cuprene, showing the "molecular model" appearance of the chains.

A few of the smooth, round particles have slight protuberances on the side (see arrows in Fig. 10). This is probably caused by the method of mounting the specimens which involves rubbing the cuprene out over a Formvar film. This procedure tears some particles apart and leaves a roughened section behind.

According to the "cluster-ion" hypothesis of Lind and Glockler[9,10] some of the acetylene molecules are ionized by the bombardment process and these may either recombine to form smaller molecules or attract neutral molecules to form a cluster-ion. When the cluster-ion itself becomes finally neutralized a large molecule is formed. Lind[7] assumes that at least 19 neutral molecules of acetylene are formed around each $C_2H_2^+$. It is very questionable that the round particles observed here are identical with Lind's clusters; at any rate many more than 19 neutral molecules of acetylene would be involved in clusters of the size of these particles.

If Lind's theory is correct, then one of the clusters might be the initial point of condensation about which other clusters could gather to form the large particles shown here. Since the condensation will occur in an unrestricted gas space, the product might be expected to occur in spherical form. The limiting size of these particles would be of the order of 13,000A, i.e., the largest

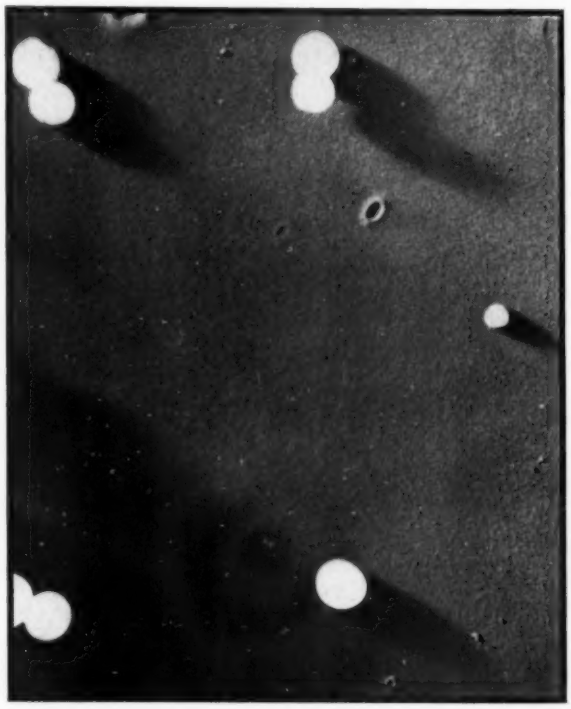

FIG. 16. A shadow cast specimen preparation of alpha-particle cuprene made with a filament height to specimen distance ratio of 1:4 with approximately 100A coating of chromium metal. ×10,000.

[9] Lind and Glockler, J. Am. Chem. Soc. **53**, 3355 (1931).
[10] Glockler and Lind, *The Electro-Chemistry of Gases and Other Dielectrics* (John Wiley & Sons, New York, 1939).

particle diameter measured in these investigations.

The appearance of alpha-ray cuprene at the moment of its first formation could be determined by placing prepared electron microscope specimen grids in the polymerization chamber so as to catch the original droplets for examination. Direct evidence might then be made available concerning the mechanism of this polymerization phenomenon.

Cuprene samples were shadow cast with a ratio of filament height to specimen distance of 1:4. Measurements made on the plates gave an average ratio of 1:3 for particle diameter to shadow length, signifying that, although the cuprene "droplets" appear to be spheres in the usual micrographs, in reality they are flattened somewhat as they lie on the Formvar film. This fact was not observable in stereoscopic pairs, and is further evidence that this material is a viscous liquid. Figure 16 is a shadow cast preparation of alpha-ray cuprene coated with approximately 100A of chromium metal at the angle described above.

No structure is visible within the alpha-ray cuprene and its appearance and other properties are so different from that formed chemically that it would probably be worth while to change the nomenclature and call it by a different name. Previously it had been supposed that all "cuprene" had the same physical structure. In this paper are three samples wherein differences are found. The Shawinigan cuprene is similar to the German sample in that each is fibrous, but the structure is different. Alpha-ray cuprene again is different to both.

From these results we may conclude that any "cuprene" made by a bombardment process (electrons, alpha-rays, photons, etc.) will possess a round-particle structure of some type; the polymerization process occurring in a discrete volume about the point of impact of the bombarding particle and a molecule. Whether the connecting necks will always occur is not known. On the other hand any catalyzed formation produced chemically on a surface will grow into a *fiber* of cuprene.

ACKNOWLEDGMENT

The authors wish to thank Dr. S. C. Lind, Dean of the Institute of Technology, University of Minnesota for the samples of alpha-ray cuprene, and Dr. Robley C. Williams of the Physics Staff of the University of Michigan for shadow casting several specimens.

Calendar of Meetings

December, 1946

17 Institute of Aeronautical Sciences, New York, New York
26–28 Geological Society of America, Chicago, Illinois
26–31 American Association for the Advancement of Science, Boston Massachusetts

January, 1947

3– 4 American Physical Society, Los Angeles, California
15–17 American Society of Civil Engineers, New York, New York
23–25 American Physical Society, New York, New York

February, 1947

20–22 Optical Society of America, New York, New York
24–28 American Society for Testing Materials, Philadelphia, Pennsylvania

May, 1947

1– 3 American Physical Society, Washington, D. C.

June, 1947

16–20 American Society for Testing Materials, Atlantic City, New Jersey

A Machine for the Application of Sand in Making Fourier Projections of Crystal Structures*

DAN MCLACHLAN, JR. AND E. F. CHAMPAYGNE
Stamford Research Laboratories, American Cyanamid Company, Stamford, Connecticut

(Received June 1, 1946)

This paper presents a method of using sand in building models of two-dimensional Fourier projections in crystal structure analysis. The machine for producing these models is described and the results are illustrated by projections of known structures. The mathematical principle of this method of summing Fourier series is identical to that which Bragg developed in England. The chief difference is in the use of sand instead of photographic film as the medium for producing contrasts in electronic density throughout the projection. The method herein described has a number of features which contribute to its usefulness: A two-dimensional Fourier projection comprising the addition of one hundred and fifty terms may be made in about four hours by a single worker. The time required is not determined by the size of the unit cell. The subdivisions of the projection face are sufficiently fine to assure an accuracy as great as the x-ray data from copper radiation will warrant when a scale of one angstrom to two centimeters is used. Upon embarking on a new structure problem, no changes in the equipment are necessary; as the initial set of templates suffices for all future work. The minimum interplanar spacing that the machine will accommodate is determined by the characteristics of copper radiation rather than the order (h, k, or l) by which the spacings are characterized. The resulting sand model of the projection is the same shape as the unit cell projection with regard to both the angle between the edges and the ratios of the edges of the cell. When the x-ray data warrant, a distinction can be made between heavy atoms and lighter atoms by the differences in the height of the sand. Photographs of the projections (see Figs. 7 and 9) portray atoms as distinct spots.

THE GENERAL CONCEPT OF WAVE ADDITION

WHEN a diffraction pattern of a single crystal is taken on any of the moving film types of camera, each diffraction spot presents three measurable parameters: two of position and one of intensity. When these measurements are used in making a projection of the crystal on one of its faces, the measured values are introduced into a Fourier series of the type

$$\rho_{xy}' = \sum_h \sum_k |F_{hko}| \cos [2\pi(hx+ky)-\alpha_{hko}], \quad (1)$$

in which there are as many terms as there are diffraction spots. Each term in the series

$$(S_{xy})_{hko} = |F_{hko}| \cos [2\pi(hx+ky)-\alpha_{hko}] \quad (2)$$

requires for its application the introduction of four measured parameters, h, k, F_{hko}, and α_{hko}. Of these four parameters, two, h and k, may be deduced from the two measurements of position of the diffraction spot on the film, and F_{hko} is directly related to the measured intensity, while the fourth term, α_{hko}, must be obtained by other means.

If Eq. (2) is plotted out as a two-dimensional graph, a surface is thereby produced whose shape resembles a piece of corrugated sheet iron as shown in Fig. 1. If a sinusoidal sheet of material, $ABCD$, passes through the imaginary plane, $EFGH$, the distance S (of any point at xy on the

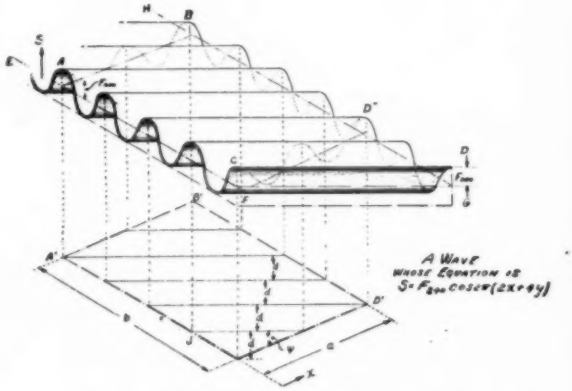

FIG. 1. The wave associated with the plane having Miller indices $hko=240$. The projection of the wave crests on the plane $A'B'D'$ shows the meaning of d and ψ. In this illustration $\alpha=0$.

* Presented in part before the Crystallographic Society in Northampton, Massachusetts, on March 23, 1946.

corrugated sheet) above or below the imaginary plane is expressed mathematically in terms of the coordinates x and y in the plane by Eq. (2). More specifically, Fig. 1 shows the corrugated sheet oriented in such a position with respect to the reference plane that the wave crests cut the x axis twice in the unit distance (a) and cut the y axis four times in the distance (b). This means, by definition, that h is 2 and k is 4. In the figure the amplitude F_{hko} is arbitrary and the phase α is zero. The expression

$$(S_{xy})_{240} = F_{240} \cos 2\pi(2x+4y) \qquad (3)$$

is the actual equation of the corrugated sheet shown in in Fig. 1 in terms of x and y and is applicable whether or not the x and y axes are perpendicular, as long as a and b are the unit distances. It is convenient that the perpendicular distance d_{hko} between the crests is equal to the interplanar distance found from the x-ray data

$$d_{hko} = n\lambda/2 \sin \theta, \qquad (4)$$

and the angle ψ that the wave crests make with the x axis is

$$\psi_{hko} = \text{arc sin } (hd_{hko}/a). \qquad (5)$$

This all means that for any crystal whose unit cell dimensions in the x and y directions are a and b, respectively, a wave of the type shown in Fig. 1 may be imagined as associated with every diffraction spot. The problem is to find a convenient method of adding together as many of these waves as there are diffraction spots in the x-ray pattern. Figure 2 shows a number of such waves in position for addition. The physical meaning of wave addition is illustrated in Fig. 3 where two simple waves corresponding to diffraction spots having Miller indices $hko = 020$ and 300, respectively, are added to form a warped sheet; and the contour map representing the warped sheet is projected on the base. The equation of the top wave is

$$S_{020} = 2 \cos 2\pi 2y \qquad (6)$$

and of the second wave is

$$S_{300} = 4 \cos 2\pi 3x, \qquad (7)$$

while the warped sheet obeys the equation

$$\rho_{xy}' = S_{020} + S_{300} = 2 \cos 2\pi 2y + 4 \cos 2\pi 3x. \qquad (8)$$

In the contour map dotted lines represent "valleys" while solid lines represent "hills" on

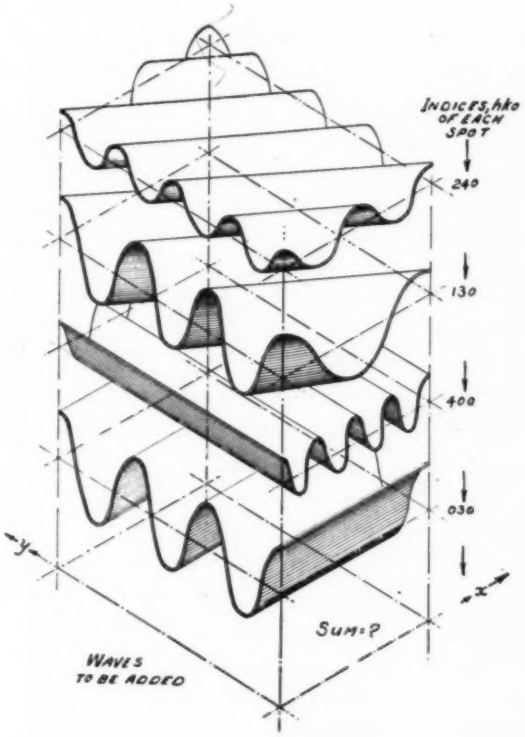

FIG. 2. A number of waves in position for adding on the basal xy plane.

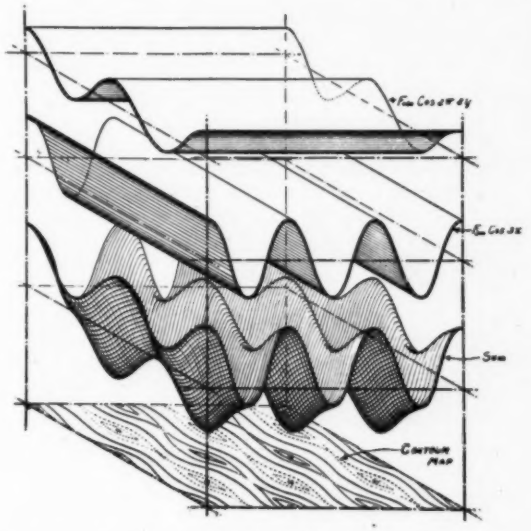

FIG. 3. The physical meaning of the addition of two waves and the relationship of their sum to a contour map.

the warped sheet. Such a contour map is the most common way of representing molecular structures projected on a plane, such maps being obtained from the analytical summation of the data from many dozens of x-ray diffraction spots.

THE BRAGG METHOD

W. L. Bragg[1] conceived a novel way of adding the waves associated with the terms in a Fourier series by using transparent photographic films. All of these films had one thing in common, that is, each film had on it a photographic impression consisting of parallel dark and light bands, so processed that the variation in the photographic density of the film in a direction perpendicular to the bands followed a modified sine law. Each film had, however, two characteristics which were unique: (a) the perpendicular distance between the parallel bands on any given film was proportional to d_{hko}, the interplanar spacing characteristic of a diffraction spot; and (b) the direction of the parallel bands corresponded to the direction that an *hko* family of planes cuts the *xy* face of the unit cell. It may be seen that any one of the Bragg strips has all the characteristics of a wave such as is shown in Fig. 1. The summation as performed by Bragg was accomplished by preparing films which had the spacing d_{hko} and direction ψ_{hko} governed by the position of the x-ray diffraction spots; then parallel light was shone through each film in succession upon a photographic plate. The sum of all these registered photographic impressions upon a single plate constituted a projection whose density depicted the molecular structure of the compound from which the x-ray data was obtained.

The amplitude, F_{hko}, in each of Bragg's films was incorporated in the time of exposure of the plate through each film.

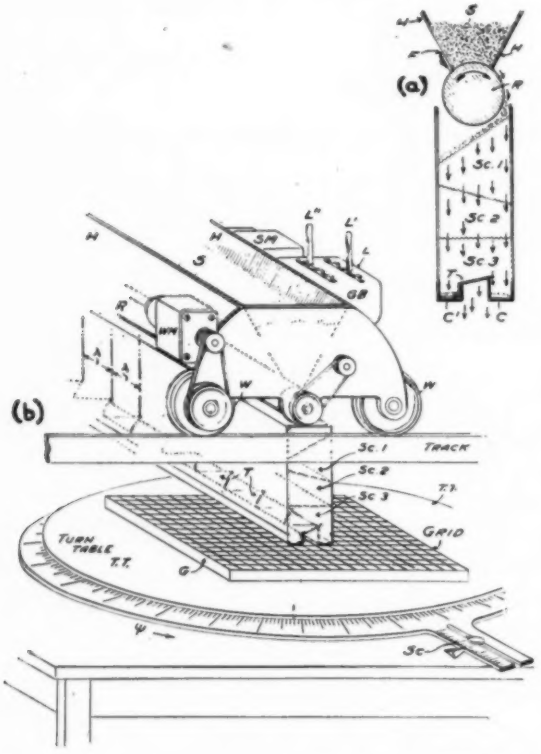

FIG. 4. A schematic drawing of the sand machine. (a) Diagram indicating action of the roller, screws, template and collector. (b) The sand machine. In this latter model, a variable speed motor is used instead of the gear box shown in Fig. 4.

[1] W. L. Bragg, Zeits. f. Krist. **A70**, 495 (1929).

THE SAND MACHINE

The machine herein described is based on the thought that any one of a great variety of substances might be forced to play the role that the photographic emulsion plays in the Bragg method. The choice of an alternate method is determined by (a) the ease by which a machine may be developed, (b) the convenience and speed in operation while projecting a particular structure, (c) the absence of extraneous labor in changing from one problem to another, (d) the accuracy of a chosen method, and (e) the need for a method which produces a projection to scale and which does not require distortion of the projection before interpretation. One of the most important decisions had to do with the choice of the substance to be distributed over the projection face to simulate electronic density. A substance which was found to be satisfactory was 100–140 mesh Ottawa sand. This material has a low angle of repose, is not affected by moisture, does not take on a noticeable electrostatic charge, is resilient on the bounce, and has other properties which add up to assuring reasonable duplication in flow measurements from rollers and screens.

Figure 4 shows schematically the principle of the sand machine. Sand, *S*, is loaded in a hopper, *H*, where it rests on a roller, *R*, which forms the

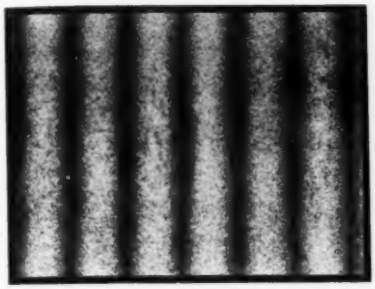

FIG. 5a. A single deposition of sand on felt.

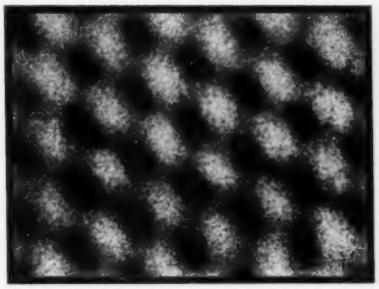

FIG. 5b. Two layers of sand; $\psi = 30°$

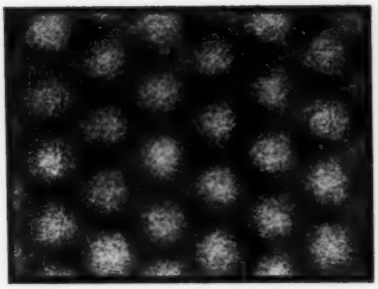

FIG. 5c. Three layers of sand (graphitic structure).

bottom of the truncated hopper. The rate that the sand pours from the hopper is determined by the speed of turning of the roller, this speed being governed by the settings of the levers L', L'', on the gearbox, GB, connected with the sand motor, SM. This method of obtaining an even and adjustable flow of sand was found to be the only successful one of several methods tried. Figure 4a shows a cross section of the sand hopper and the roller. The sand is prevented from escaping from one side of the hopper by a strip of felt, F, while the other side of the hopper is slightly opened to permit the sand to ride through on the turning roller. The sand after escaping from the hopper falls through three 30-mesh screens so adjusted that after passage through the third screen the originally thin sheet of sand has been distributed over a band about two centimeters wide. The band of sand strikes a sinusoidal paper template, T. Since the template is tilted at an angle of about 40°, the sand which strikes it bounces back into the collector, C'. Some of the sand falls into C but the sand which goes through the openings in the template escapes in a sinusoidal distribution into the receiving grid, G. When the entire hopper arrangement travels along the track on the wheels, W, turned by the motor, WM, the sand is distributed in parallel bands analogous to the bands on Bragg's lantern slides.[2]

Since the grid is mounted on a graduated turntable, $T.T.$, any desired angle, ψ, can be obtained. The template has a sinusoidal wavelength, λ, proportional in centimeters to the spacing d_{hko} in angstroms, and since the turntable can be shifted any desired fraction of d_{hko} perpendicular to the direction of motion of the hopper, any desired value of phase α may be selected.

Figures 5a, b, and c show three successive depositions of sand on black felt at ψ values 120°

TABLE I. Sample page of data for using the sand machine for projecting diopside.

Miller index *hol*	d_{hol} of template	Turntable angle ψ	Shift distance cm	F_{hol} expressed in sand speed Passes	Lever setting
002	13.8	0	6.9	4	2*H*
004	6.7	0	0	3	2*H*
$40\bar{2}$	8.5	321	4.25	2	2*H*
				1	1*H*
$60\bar{0}$	8.5	74	0	2	2*H*
				1	3*L*
$40\bar{4}$	5.4	342	0	2	2*H*
202	10.2	338	5.1	2	2*H*
602	8.5	71	4.25	1	2*H*
				1	1*H*
402	11.0	56	5.5	1	2*H*
				1	1*H*
404	6.7	31	0	2	1*H*
800	6.25	74	0	2	1*H*
$40\bar{6}$	3.95	343	1.97	2	1*H*
10, 02	4.4	304	2.2	1	2*H*
				1	6*L*
604	6.25	45	0	1	2*H*
				1	3*L*
10, 00	4.9	74	0	1	2*H*
				1	3*L*
$80\bar{2}$	5.2	307	2.6	1	1*H*
				1	4*L*
406	4.7	20	2.35	1	1*H*
				1	2*L*
202	13.8	32	0	1	2*H*
10, 02	5.2	82	2.6	1	2*H*
008	3.34	0	0	1	1*H*
206	4.7	10	2.85	1	1*H*
$80\bar{4}$	4.2	321	0	1	6*L*
				1	3*L*
802	6.7	79	3.85	1	5*L*
				1	4*L*
606	4.4	31	2.2	2	4*L*
$00\bar{6}$	4.4	0	2.2	2	4*L*
$20\bar{4}$	6.25	346	0	1	6*L*

[2] W. H. Bragg and W. L. Bragg, *The Crystalline State* (Bell and Sons, Ltd., London, 1933), Vol. I, p. 231.

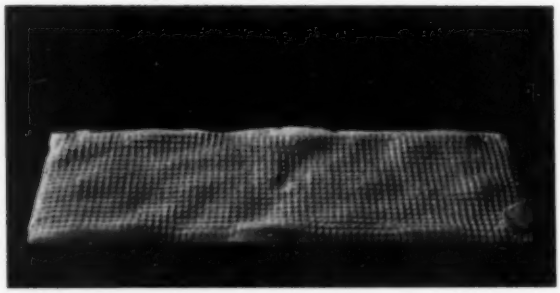

FIG. 6. Photograph showing the "hills" and "valleys" after the sand was dumped from the grid from a projection of diopside using Bragg's data (see reference 1).

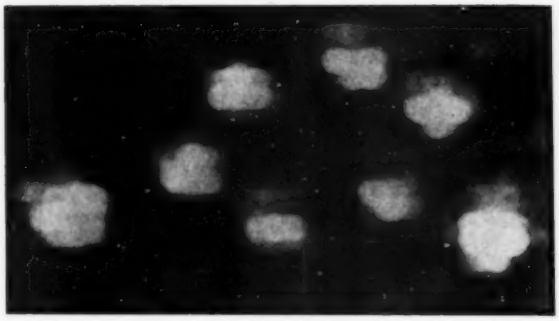

FIG. 7. Resorcinol as projected on the sand machine using the data of Robertson and Ubbelohde (see reference 4).

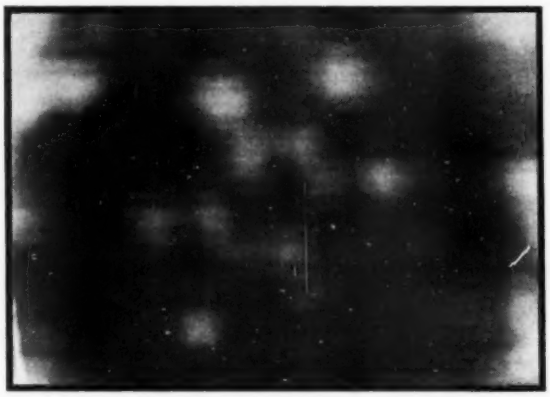

FIG. 8. Hexamethyl benzene projected into a grid having ¼-inch spacings.

apart to produce a structure very similar to that of graphite.

In using the machine it is convenient to have prepared a set of templates, each having a sinusoidal edge of the same amplitude of about one centimeter, but varying in wave-length by incremental steps between 0.8 centimeter to 20 centimeters. From the x-ray data the three quantities d_{hko}, ψ_{hko}, and F_{hko} and also the chosen value of α_{hko} are transformed to a table under the respective headings (a) template spacing, (b) turntable angle, (c) roller speed, and (d) shift distance. Table I shows a sample portion of such a tabulation of the data for the diopside structure. In this case the interplanar spacings d_{hol} were multiplied by a factor greater than the usual 1 centimeter per angstrom.

Illustrations of the Results from the Sand Machine

Figure 6 shows the sand after being poured out of the grid subsequent to making a projection of diopside.[1] It may be seen that there are "hills" corresponding to the positions of high electronic density where atoms are located and "valleys" between the hills. It is of academic interest to point out that, like the Bragg method, this method has no provisions for negative numbers since the sinusoidal distribution of sand for each traverse obeys Eq. (9) instead of Eq. (2).

$$S=|F_{hko}|+|F_{hko}|\cos[2\pi(hx+ky)-\alpha_{hko}], \quad (9)$$

and the final summation obeys Eq. (10) instead of Eq. (1).

$$\rho_{xy}'=\sum_h\sum_k|F_{hko}| + \sum\sum|F_{hko}|\cos[2\pi(hx+ky)-\alpha_{hko}]. \quad (10)$$

It was discovered that by illuminating the grid at an oblique angle from the sides while photographing it from directly above, a picture could be obtained which closely resembles the results obtained by Bragg[1] and Huggins.[3,4] Figure 7 shows the resorcinol molecule photographed in this manner after being projected according to the dictates of the data of Robertson and Ubbelohde.[5] Figures 8 and 9 show the hexamethyl benzene molecule using the data of Brockway and Robertson.[6] These two pictures, differing in resolution, are presented to demonstrate the advantages of using a fine mesh grid, because of theoretical reasons discussed later in the paper.

[3] M. L. Huggins, J. Am. Chem. Soc. **63**, 66 (1941).
[4] M. L. Huggins, J. Chem. Phys. **12**, 520 (1944).
[5] J. M. Robertson and A. R. Ubbelohde, Proc. Roy. Soc. London **A167**, 122 (1938).
[6] L. O. Brockway and J. M. Robertson, J. Chem. Soc. 1324 (1939).

THE ACCURACY OF THE METHOD

It is very difficult to derive a general law by which one may predict the accuracy to be expected from a Fourier summation in a crystal analysis on the basis of the known accuracies of the measured quantities used in the summation; nevertheless it should be understood that any machine which is developed for making the summations should be sufficiently accurate in its operation to make the fullest use of the accuracies of the x-ray data. Although it is known that in measuring the data from an x-ray film the accuracy of measuring the positions of the spots may be made extremely high (because these positions are so related to one another through the unit cell dimensions that statistics may be applied to their solution), the accuracies in measuring the intensities and ultimately the structure factor of the spots are not so easily handled. For example, if the crystal is not cylindrical in shape, the accuracy of the structure factors may be greatly dependent upon the accuracy of measuring the crystal dimensions. It is also observed that in ordinary microdensitometry the weakest diffraction spots are so badly distorted in value by the general background that no degree of accuracy can be claimed. Weak diffraction spots do not follow any general law in their location on the film but are very abundant in the regions of high Miller indices. Therefore, the best one can do in setting for himself a goal to be attained for a machine under construction is to make what may seem a reasonable guess. The goal chosen in this development is based on the assumption

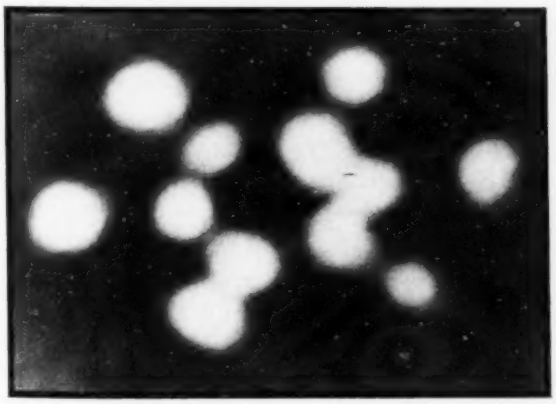

FIG. 9. Hexamethyl benzene projected into a grid having $\frac{1}{8}$-inch spacings.

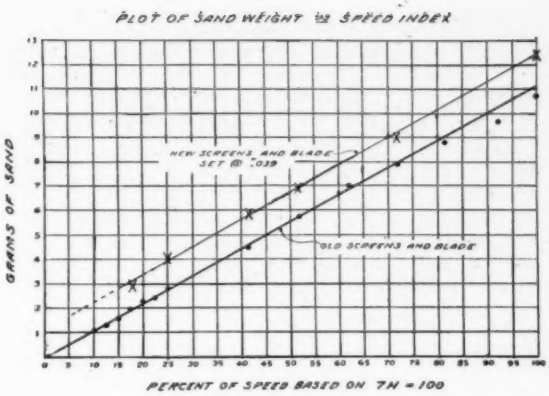
PLOT OF SAND WEIGHT VS SPEED INDEX
GRAMS OF SAND
NEW SCREENS AND BLADE SET @ .039
OLD SCREENS AND BLADE
PERCENT OF SPEED BASED ON 7H = 100

FIG. 10. Rate of sand flow plotted against the speed of rotation of the rod.

that the accuracy of the structure factors is 90 percent or greater for all spots corresponding to an interplanar spacing of one angstrom or more. To meet this goal, the amount of sand deposited by the machine in any single cavity in the grid should have an accuracy of 90 percent or more at the peak of a wave. The degree to which the various parts of the machine approach the goal are discussed separately.

The Rate of Sand Flow

The statement that the rate of sand flow is proportional to the rate of turning of the rod (*R*, Fig. 4) may be tested by experiment. In Fig. 10 the weight of sand discharged from the hopper in a set interval of time is plotted against the speed of rotation of the rod expressed as the percent of the fastest speed of rotation. The lower curve follows a straight line rather closely except at the faster speeds. This curve also passes through the origin corresponding (as one may expect) to zero flow at zero rate of turning. In the upper curve the knife blade above the rod was opened up to give a faster flow rate. This curve does not pass through the origin but indicates that there is a tendency for the sand to roll out independent of the peripheral motion of the rod. When the opening between the rod and the knife blade is too great, the slightest movement of the rod starts a small but continuous avalanche of sand. The second interesting characteristic of the upper curve is that its slope is very nearly the same as that of the lower curve. This suggests that the rotating rod has a

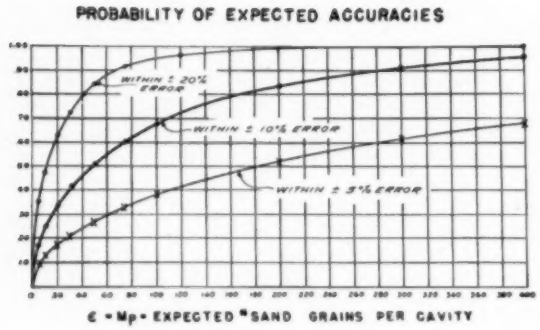

FIG. 11. A plot showing the probabilities of attaining inaccuracies within 5 percent, 10 percent, and 20 percent as a function of the number of grains of sand deposited in one grid cavity.

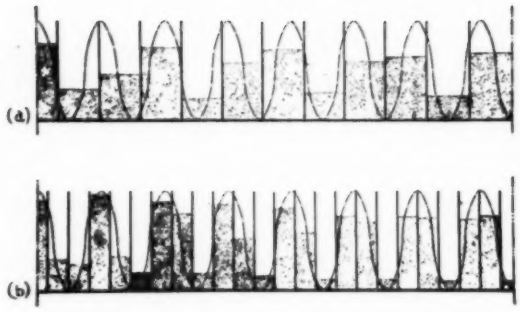

FIG. 12. (a) Distribution of sand in the cavities of the grid when $f=0.64$. (b) Distribution of sand in the cavities of the grid when $f=0.32$.

very definite depth of "bite" into the sand resting on it and when the opening is greater than this depth the rate of rotation is not a reliable measure of sand flow. In this work the opening of the knife blade has been kept below this upper limit. There is a lower limit for the size of the opening (at which point clogging occurs) which is easily avoided when sand grains of 100–140 mesh are used.

The Amount of Sand Required

If it were not for the ever present effects of statistical fluctuations in physical processes, it might be feasible to choose as the rate of flow of sand from the hopper for the lowest recorded structure factor that rate which would permit some small number (such as 10) grains of sand to fall into each cavity in the grid at the maxima of the waves and base all other rates on this standard. This is not possible. If the sand showers from the hopper through the screens and template into the grid in a perfectly statistical manner, there is a finite possibility that a cavity (into which 10 grains of sand were expected to have fallen) may be empty. According to probability theories, the percentage deviation from expectancy becomes smaller as the number of trials increases. It is required that we deposit into the grid enough sand to assure that any cavity in the grid at a wave crest will have a 9/10 probability of containing within 10 percent of the number of grains of sand that are expected. For this work we have used the normal law* and the tables in Fry's *Probability and Its Engineering Uses*. The central curve of Fig. 11 shows the probability of attaining an error of less than 10 percent plotted against the number of sand grains expected on the average to fall in each cavity in the grid. It may be seen that about 300 grains of sand are required to produce a 90 percent probability that the actual number of sand grains falling into any given cavity is within 10 percent of the number expected to fall in that cavity on the basis of a given rate of turning of the rod and a given rate of traverse of the hopper. The lower curve is added to show the tremendous number of sand grains required to attain an accuracy of 95 percent, and the upper curve shows the relatively few grains necessary to attain 80 percent.

The Size of the Cavities in the Grid

If the sand which drops through the template could be forced to "stick fast" to the exact position that it strikes the base of the grid, then partitions in the grid would be unnecessary. The fact that partitions in the grid force the sand to stay approximately in its initial position assures us that the use of grid sections only approximately enforces the desired effect. Since the accuracy is greater for smaller grid cavities, it is important to decide how small they should be.

When sand falls into a grid cavity, the vibration of the mechanism causes the sand to become leveled out although the sand may have de-

* As pointed out at the Northampton meeting of the Crystallographic Society by D. Harker, the Poisson equation is more appropriate than the normal law for this particular work. The computations were not repeated, however, because the two laws give almost identical values in the working regions of the curves.

posited initially in a manner far from level. For this reason, the grid behaves as a sampling and averaging mechanism over an interval of area. For example, suppose that a curtain of sand were deposited across a grid according to the cosine equation

$$S = F_0 + F_0 \cos (2\pi/d_{hol})P, \qquad (11)$$

where P is the distance from the origin. Figure 12a shows a curve of this type. If a grid is used to sample and average such a curve, the height of sand in any cavity is

$$h_m = F_0 + \frac{F_0}{2\pi f} \sin 2\pi f(m+\tfrac{1}{2}) - \sin 2\pi f(m-\tfrac{1}{2}), \qquad (12)$$

where f is the relative width, w, of the grid spacing expressed as a fraction of the wave-length d_{hko}

$$f = w/d_{hko}, \qquad (13)$$

and m is the serial number of each cavity when the cavities are numbered from left to right as shown in Fig. 12a. In Fig. 12a the heights of sand are shown as the dotted areas with grid separations so spaced that $f=0.64$. It can be seen that the height of the sand in the grid does not bear a very close relationship to the amount of sand actually deposited at specific points. Figure 12b shows the improvement obtained by using $f=0.32$. The reason that these specific values of f are used in the illustrations is that $f=0.64$ is the value resulting from the use of the quarter-inch grid for the 1 angstrom spacing and $f=0.32$ resulted from the one-eighth inch grid. A comparison of the hexamethyl benzene projections, Figs. 8 and 9, demonstrates the practical results obtained from small grid cavities. It may be stated that when f is less than 0.5 the largest error in representing a wave crest by a grid is

$$\text{percent } E = 100\left(0.5 - \frac{\sin 2\pi f}{4\pi f}\right). \qquad (14)$$

Using this equation, Fig. 12b should show only a 73 percent accuracy which may be verified by reading the accuracy directly off Fig. 12b at its worst peak at $m=18$. By actually solving for that value of f which permits an accuracy of 90 percent one finds that f must be about 0.18. This means that the eighth-inch grid spacing is about twice as great as it should be for a scale of one angstrom per centimeter. Such fine grids, however, are more difficult to assemble, and the accuracy of 90 percent is obtained with an eighth-inch grid by enlarging the scale to one angstrom per two centimeters.

The Depth of the Grid

One may readily calculate the depth that the grid must be to assure that it will not run over before a summation is complete. Choosing a grid size of one-eighth inch square and knowing that 300 grains are the minimum number for the peak of the weakest wave, one may assume that a summation might require 200 wave additions with structure factor values whose ratios range from 1 to about 12 with a mean value of about six times the smallest measured value. If the sand has an average radius of about 0.01 cm and when loosely packed incorporates about 40 percent void space, then the total depth of sand in a cavity in which all 200 waves should contribute their maximum is about $1\frac{1}{2}$ inches.

The Required Number of Templates

The accuracy required in cutting the templates is also determined by accuracy of the x-ray data. If one wishes to have on hand a series of templates covering the range of wave-lengths from 0.8 cm to 20 cm so that he is prepared to project any structure whose interplanar spacings fall in this range, and if the accuracy of measurement of the F values is 90 percent, then there is no need to cut the templates more accurately than 93 percent. The choice of 93 percent or (100−7) percent is based on the fact that the peak value

TABLE II. A proposed set of template wave-lengths.

Template No.	λ cm	Template No.	λ cm	Template No.	λ cm	Template No.	λ cm	Template No.	λ cm
1	0.80	11	1.56	21	4.52	31	8.84	41	17.34
2	0.86	12	1.72	22	4.83	32	9.46	42	18.56
3	0.90	13	1.84	23	5.16	33	10.12	43	19.86
4	0.96	14	1.97	24	5.52	34	10.80		
5	1.03	15	2.10	25	5.90	35	11.56		
6	1.12	16	3.24	26	6.31	36	12.37		
7	1.20	17	3.46	27	6.75	37	13.23		
8	1.28	18	3.70	28	7.22	38	14.15		
9	1.37	19	3.96	29	7.72	39	15.14		
10	1.46	20	4.23	30	8.26	40	16.20		

TABLE III. Description of parts of the sand machine.

Sand	Ottawa, 100–200 mesh (obtained from American Grade Sand Company, Chicago, Illinois).
H	Sheet metal hopper, 7″ wide at top, 4½″ deep, 31¼″ long, sides tilt approximately 30° and converge at roller, *R*.
R	Steel tubing, 1/16″ wall, approximately .540″ O.D., 31″ long.
SM	Bodine Universal Motor, Thyratron controlled continuously between 15 and 200 r.p.m. (Gerald Heller Product, Baltimore, Maryland).
K	Knife, ½″ sq. C.R. steel bar, supported in bearings just above roller, *R*; one edge rotated to or from the roller to adjust opening to about .025″.
Sc	Screens, No. 30 mesh, 2¾″ wide, stainless steel, fastened to 5/16″ brass supporting bars which rest in bearings allowing tilt of screen for optimum sand distribution; 2 top screens tilt about 20° in same direction, bottom screen horizontal. All screens 3″ apart, screen chamber about 7″×3″. Both sides of screen chamber are closed in with sheets of cellulose acetate to prevent sand escaping to outside. *Note:* Ends of hopper, *H*, and screen chamber are of ⅜″ brass stock.
C	Sand collector, 1⅝″ deep, 4¼″ wide, 31¼″ long; contains template holder consisting of two ⅛″ brass bars both mounted on edge to restrict a 9/16″ opening along the center of collector, one bar 1.0″ wide and the other 1½″ wide. The difference in the two bars creates an angle, approximately 40°, across the two edges on which to rest the paper template.
T	Templates, 4½ cm over-all width, 30½″ length, peak amplitude 3 cm, leaving 1½ cm for holding (cut from heavy weight graph paper).
WM	Carriage motor drive, Bodine, 10 r.p.m., 30 in. oz., reversible, drive sprocket—16 teeth, driven sprocket—14 teeth.
Carriage assembly	Face plates, 12″ wide, wheels 1¼″ diameter, ½″ thick, flange ¼″×⅛″, C.R. steel, 2 wheels on one shaft for drive, 2 wheels mounted on independent shafts, all wheels mounted on ⅜″ roller bearings.
Track	1¼″×1¼″×3/16″ iron T-bar stock, 56″ long mounted 6½″ from table on 1½″ round brass posts with flanges attached for mounting to table.
Table	32″ high, 61½″ long, 43″ wide, constructed of 4″×4″ legs, ⅞″ framing, and ¾″ plywood top surfaced with 3/16″ Masonite.
T.T.	Turntable, ⅛″ aluminum, 30″ diameter, indexed at the edge throughout 360°, pivots on ⅛″ pin, the latter supported by a ⅛″×4″×40″ slide strip which slides between fixed runners, also indexed on one edge in intervals of 1 mm over 15-cm distance.
G	Grid, 20″ square, ¾″ deep, constructed of .002″ corrugated brass shim stock laid side by side with alternate partitions to form ⅛″ cells supported by a ¾″ angle iron frame, mounted on 4 posts projecting from the turntable and high enough to provide clearance for a ¾″ plywood false bottom which can be dropped a uniform distance from the bottom of the grid as the grid fills before completion of run; thus making the effective depth of the grid increase from ¾″ to about 1¼″.

of a cosine curve is in error 10 percent at about 25° or about 7 percent of a cycle. Table II furnishes a proposed set of template wave-lengths, each wave-length being about 7 percent greater than the preceding one. One then selects, from the prepared set, that template which is the nearest in value to the wave-length desired.

In Table III the parts of the sand machine are given for convenience in duplicating this apparatus. The captions in this table correspond to those used in Fig. 4.

ACKNOWLEDGMENTS

The authors wish to thank the American Cyanamid Company for furnishing the facilities for carrying on this work and Dr. R. Bowling Barnes, director of the Physics Division of the Stamford Research Laboratories, for his enthusiasm and encouragement. We are also indebted to the Mining Division and to a number of machinists, draftsmen, and photographers of these Laboratories for their assistance and fruitful suggestions.

Radar Reflections from Long Conductors*

F. Bloch

Stanford University, Palo Alto, California,

M. Hamermesh

New York University, University Heights, New York, New York,

and

M. Phillips

Brooklyn College, Brooklyn, New York

(Received August 12, 1946)

The distribution of the backscattered radiation of a long straight conductor shows a sharp return lobe perpendicular to its orientation. In horizontal observation such a "rope" would therefore give an appreciable echo only if it were almost exactly vertical. In practice no such effect will be observed since, because of wind and other disturbances, the rope will never be straight but actually over its whole length will pass through regions of space where the phase of the incident wave will change many times through its full range 2π. The effect of these irregularities will be to make the sharp dependence of the cross section upon the orientation of the rope disappear, and to give a cross section proportional to the total length L of the rope. In Section I, the wave-length λ is assumed to be large compared to the transverse dimensions of the rope. In Section II, the results are extended to include the case where the wave-length λ of the incident radiation is not necessarily large but is comparable with or even small compared to the width d of a ribbon-shaped rope. It is found that the cross section of such a rope can be written generally in the form $\sigma = KAf(\pi d/\lambda)$, where K is a numerical constant depending upon the deviations of the rope from the vertical and where $A = Ld$ is the area of the ribbon. The length L is assumed to be much greater than λ. The function f is evaluated by the use of a method developed by Morse and Rubenstein.

DURING the past few years the design of radar reflectors has been studied extensively. These reflectors are used to produce strong echoes at the radar—as identifying or locating signals, or to confuse the enemy radar operator by presenting large numbers of false targets in addition to the true target. When such reflectors are to be used by aircraft, considerations of compactness, weight, and ease of handling are paramount in importance. This has, except for special applications, prevented the use of flat-sheet or spherical reflectors. Instead resonant dipoles have been used. If such dipoles are cut properly so as to resonate to the radar frequency, they will produce large intensities of reflection per unit weight. At longer wave-lengths, however, the resonance length becomes inconvenient and the dipoles tend to break. In this long wave-length region, long rolls of metallized strip have been used. These long strips have been referred to as "ropes." The material is wound on spools in lengths of several hundred feet; after the spool is dropped from the aircraft, simple attachments (e.g., a cardboard attached to the free end of the rope) can be used to cause the roll to stream off the spool. In practice, ropes have usually been devised so that they are suspended approximately vertically during their fall.

In designing such reflectors one must know the value of the "radar cross section," σ, of the rope, i.e., the cross section for backscattering to the radar. Though in most cases the transverse dimensions of the rope (e.g., the width of the strip) are small compared to the wave-length, the dependence of the cross section on the transverse dimensions is of interest.

I

We consider first a circular cylindrical rope, of radius a small compared to the wave-length λ,

* This work reported in this paper was done at the Radio Research Laboratory of Harvard University under contract with the Office of Scientific Research and Development, National Defense Research Committee, Division 15.

and of length l large compared to λ. We assume the rope to be straight and vertical and to be irradiated by a vertically polarized plane wave incident in the horizontal direction. The electric field, E, of this plane wave will be parallel to the axis of the rope and uniform along its length. The current induced in the rope will, except for end-effects which are unimportant since $l \gg \lambda$, also be uniform along the rope. If the material of the rope is perfectly conducting, the tangential component of the *total* electric field must vanish on the surface of the material. If I is the total current, then this condition is expressed by the equation

$$\frac{Ik}{2\pi ic}\int_0^{2\pi} d\varphi \int_{-\infty}^{+\infty} \frac{\exp\left[ik(z^2+\rho^2)^{\frac{1}{2}}\right]}{(z^2+\rho^2)^{\frac{1}{2}}}dz = -E, \quad (1)$$

where z is the coordinate along the rope and $k = 2\pi/\lambda$.

For $\rho \ll \lambda$ $(k\rho \ll 1)$,

$$\int_{-\infty}^{+\infty} \frac{\exp\left[ik(z^2+\rho^2)^{\frac{1}{2}}\right]}{(z^2+\rho^2)^{\frac{1}{2}}}dz \simeq 2\ln(2/\gamma k\rho) + i\pi,$$

where $\gamma = 1.781$. From Fig. 1, $\rho = 2a \sin(\varphi/2)$, so that

$$E = -\frac{2Ik}{ic}\left[\ln(2/\gamma ka) + i\pi/2\right]. \quad (2)$$

The current I, uniform along the rope of length l, produces at a distance R, perpendicular to the rope and large compared to l, a field E' given by

$$E' = \frac{k}{ic}\frac{e^{ikR}}{R}Il. \quad (3)$$

The cross section is defined as

$$\sigma = 4\pi R^2 |E'|^2/|E|^2,$$

so that

$$\sigma = \frac{\pi l^2}{\left[\ln(\lambda/\pi\gamma a)\right]^2 + (\pi/2)^2}. \quad (4)$$

For arbitrary values of θ (the angle between the direction of incidence and the axis of the rope), and φ (the angle between the field E and the plane of incidence), a similar derivation gives

$$\sigma = \frac{\pi l^2 \sin^2\theta}{\left[\ln(\lambda/\pi\gamma a \sin\theta)\right]^2 + (\pi/2)^2} \cdot \left[\frac{\sin(2\pi l/\lambda\cos\theta)}{2\pi l/\lambda\cos\theta}\right]^2 \cdot \cos^4\varphi. \quad (5)$$

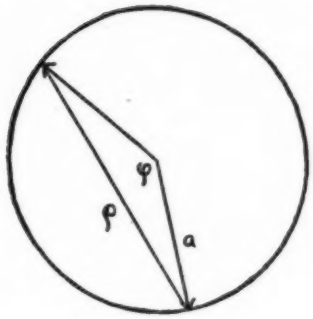

FIG. 1.

These formulas have been obtained previously by L. J. Chu (unpublished).

If the rope is a thin metallic strip of width d, the results are changed only slightly, the quantity a is replaced by $d/4$ in Eqs. (4) and (5).

According to Eq. (5) the reflection pattern of a long straight rope has a sharp lobe covering an angular range $\lambda/2\pi l$ around $\theta = 90°$. Thus for horizontal observation the rope will produce only a weak echo unless it is almost exactly vertical. In practice the rope will never be perfectly straight but will deviate from a vertical line by distances of several wave-lengths. These deviations will eliminate the strong angular dependence indicated by Eq. (5) and lead to a cross section more or less independent of the instantaneous shape and orientation of the rope, and proportional to its length l.

To derive such an "effective" cross section we shall assume that the rope consists of independently scattering sections, each of which is a full helical turn about the vertical axis. The angle α between the rope and the vertical is assumed to be small; the radius, r, of the helix is assumed to be large compared to λ. Let the vertical be the z direction and $x = x(z)$, $y = y(z)$ be the equation of the helix. For a wave incident along the x direction, the field at the rope will now be $Ee^{ikx(z)}$. The induced current will show this same phase variation along the rope provided

the phase varies only slightly within one wavelength along the rope. This condition is fulfilled if α is small. Then

$$I(z)=-\frac{icEe^{ikz(z)}}{2k[\ln(2/\gamma ka)+i\pi/2]}. \quad (6)$$

The field at a large distance R is

$$E'=\frac{k}{ic}\frac{e^{ikR}}{R}\int_0^h I(z)e^{ikz(z)}dz, \quad (7)$$

where h is the vertical projection of the helical turn. Thus

$$E'=-\frac{e^{ikR}}{R}\frac{E}{\ln(2/\gamma ka)+i\pi/2}\int_0^h e^{2ikz(z)}dz. \quad (8)$$

For a helix with angle α and radius r,

$$x=r\cos(z/r\cot\alpha), \quad h=2\pi r\cot\alpha.$$

Thus, if $\varphi=z/r\cot\alpha$,

$$E'=-\frac{e^{ikR}}{R}\frac{Er\cot\alpha}{\ln(2/\gamma ka)+i\pi/2}\int_0^{2\pi} e^{2ikr\cos\varphi}d\varphi. \quad (9)$$

For $kr\gg 1$, this becomes

$$E'\simeq-\frac{e^{ikR}}{2R}\frac{2\pi E\cot\alpha}{\ln(2/\gamma ka)+i\pi/2}\left(\frac{r}{\pi k}\right)^{\frac{1}{2}}\times\cos(2kr-\pi/4). \quad (10)$$

Thus the cross section will be

$$\sigma=4\pi R^2|E'|^2/|E|^2$$

$$=\frac{4\pi^3\cot^2\alpha}{[\ln(2/\gamma ka)]^2+(\pi/2)^2}\frac{r}{\pi k}\cos^2(2kr-\pi/4). \quad (11)$$

Since $kr\gg 1$ and we are interested only in average values, we may replace $\cos^2(2kr-\pi/4)$ by $\frac{1}{2}$. Also using $r=h/2\pi\cot\alpha$, $k=2\pi/\lambda$, and $h=l\cos\alpha$, we obtain

$$\sigma=\frac{l\lambda}{2}\frac{1}{[\ln(\lambda/\gamma\pi a)]^2+(\pi/2)^2}\cdot\frac{\cos^2\alpha}{\sin\alpha}. \quad (12)$$

If now we consider a rope consisting of helical turns with varying l and α, we may assume that the scattering of the separate turns adds incoherently to produce the total cross section of the rope. Thus we obtain the final formula

$$\sigma=K\frac{L\lambda/2}{[\ln(\lambda/\gamma\pi a)]^2+(\pi/2)^2}, \quad (13)$$

where K is the average value of $\cos^2\alpha/\sin\alpha$ (weighted in proportion to the length of the rope section), and L is the total length of the rope.

A quantitatively similar formula is obtained if, instead of the above procedure, one assumes the rope to consist of straight sections of varying length which contribute incoherently to the cross section. If one assumes that the inclinations to the vertical, α, are distributed uniformly between zero and a maximum value $\alpha_{\max}$, one obtains the same final expression (13), except that K is now $\pi/2\sin\alpha_{\max}$. Obviously one cannot assign an exact numerical value to K without knowledge of the exact shape of the rope; qualitatively, at least, both procedures lead to the same result.

II

We can extend the calculation to the case where λ is comparable with or even small compared to the transverse dimensions of the rope. We shall consider the rope to be a flat strip of width d, and introduce the quantity $c=\pi d/\lambda$. ($c\ll 1$ is equivalent to $\lambda\gg d$.) Then Eq. (13) can be written as

$$\sigma=KA\frac{\pi}{2c}\frac{1}{[\ln(4/\gamma c)]^2+(\pi/2)^2}, \quad (14)$$

where $A=Ld$ is the actual area of the ribbon. Equation (14) can be generalized for arbitrary λ by writing

$$\sigma=KAf(c). \quad (15)$$

Comparing with (14) we see that

$$f(c)=\frac{\pi}{2c}\frac{1}{[\ln(4/\gamma c)]^2+(\pi/2)^2} \quad \text{for } c\ll 1. \quad (16)$$

A method for computing $f(c)$ for arguments c not necessarily small compared to one has been developed by Morse and Rubenstein.[1] Actually one finds in their paper an expression for the ratio of scattered intensity I' to incident inten-

[1] P. M. Morse and P. J. Rubenstein, Phys. Rev. **54**, 895 (1938).

sity I_0 at distances R, large compared to λ and d, but small compared to the length L of the rope. In this case the scattered intensity I' is of course proportional to $1/R$ whereas for distances large even compared to L it is proportional to $1/R^2$. Since the definition of a cross section can be meaningful only where the intensity follows a $1/R^2$ law, one must first convert their results.

Let I'/I_0 be the ratio of scattered to incident intensity for $R \ll L$, and I/I_0 the ratio for $R \gg L$. In either case the scattered intensity is proportional to the absolute square of the integral

$$H = \int_{-L/2}^{+L/2} \frac{\exp\left[ik(R^2+z^2)^{\frac{1}{2}}\right]}{(R^2+z^2)^{\frac{1}{2}}} dz. \qquad (17)$$

For $kR \gg 1$, i.e., for distances large compared to the wave-length, this integral becomes

$$H = \left(\frac{2\pi i}{kR}\right)^{\frac{1}{2}} e^{ikR}, \quad \text{for } R \ll L. \qquad (18)$$

If, on the other hand, R is so large that both $kR \gg 1$ and $kL^2/R \ll 1$, it becomes

$$H = (L/R)e^{ikR}. \qquad (19)$$

The ratio of the absolute square of the two expressions (18) and (19) is

$$(2\pi/kR)(R^2/L^2) = 2\pi R/kL^2 = R\lambda/L^2.$$

Thus

$$I/I_0 = (L^2/R\lambda)I'/I_0. \qquad (20)$$

Since I'/I_0 is proportional to $1/R$, we thus obtain the proper $1/R^2$ proportionality for I/I_0. The factor L^2 which appears in (20) originates from the fact that this expression is derived for incidence and observation normal to a perfectly straight rope. Just as in Section I, even small deviations from straightness result in a scattered intensity and therefore a cross section σ which is proportional to the *first* power of L, or, as indicated in (15), to the area A covered by the rope. The result is that instead of L^2 in (20) there appears the factor $KL\lambda/2\pi$. Making this substitution and writing further $(I/I_0) = (\sigma/4\pi R^2)$, we obtain from (20)

$$\sigma = 2KRL(I'/I_0), \qquad (21)$$

which, with the expression of Morse and Rubenstein for I'/I_0, leads to an expression of the form (15) for the cross section.

There is another feature of the problem that has to be taken into account before the results of Morse and Rubenstein can be applied. The scattered intensity will in general depend not only on the wave-length but also on the relative orientation of the plane of the ribbon with respect to the directions of incidence and observation. We are here interested only in return signals, where the direction of the scattered radiation is equal and opposite to that of incidence and is perpendicular to the longitudinal axis of the ribbon. In this case there remains only the dependence of the backscattered radiation on the azimuthal angle ψ by which the ribbon can rotate around its axis. As long as λ is large compared to d, i.e., $c \ll 1$, this dependence is negligible; even if the ribbon is viewed edgewise the strong diffraction of the waves around it makes it scatter almost as much as in front view. For $c \gg 1$, i.e., for λ small compared to the width of the ribbon, this dependence becomes, of course, very marked, since here one obtains a return signal only if the plane of the ribbon is practically perpendicular to the direction of incident and scattered radiation. In practice, the ribbon will always be twisted many times around its perpendicular axis. It is, therefore, the average value of I'/I_0 or of σ over the azimuthal angle ψ which is of practical interest. The function $f(c)$ which appears in (15) is thus always to be understood as this average value over ψ. $f(c)$ has been computed for various values of c, by use of the tables of Morse and Rubenstein.[2] (See Table I.)

The evaluation of $f(c)$ becomes rather troublesome for large values of the argument, since more and more terms in a certain double sum have to be evaluated. We therefore found it

TABLE I.

c	.1	.2	.4	.6	.8	1.0	1.2	1.4
$f(c)$	1.085	.767	.576	.479	.426	.391	.369	.364

[2] Cf. reference 1. The backscattering for electromagnetic waves with the electric vector parallel to the ribbon axis is derived from the first of Eqs. (12), p. 898, with the angle of incidence u equal to $\pi - \psi$ and the whole averaged over ψ. Similarly, the results for waves polarized so that the electric vector is perpendicular to the ribbon axis follow from Eq. (10), p. 897. The quantity which we call I'/I_0 is d/R times the expressions given in (10) and (12) of Morse and Rubenstein, averaged over ψ.

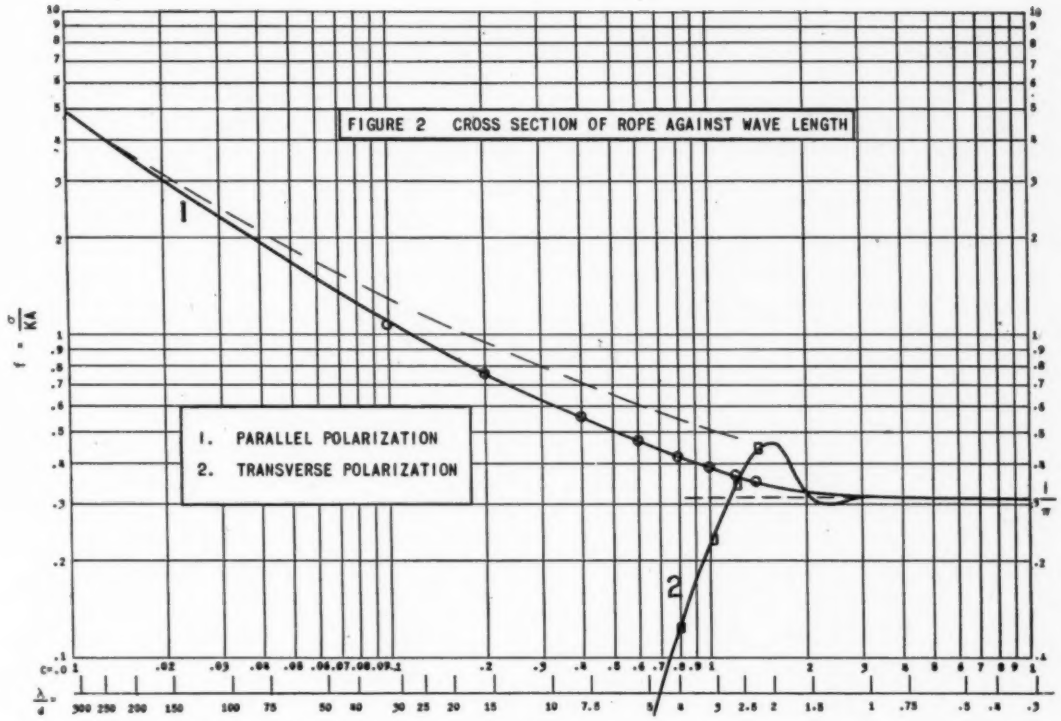

FIG. 2.

useful to derive the limiting expression of $f(c)$ for $c \gg 1$.

The method of obtaining this limiting value is essentially that used for the approximate treatment of diffraction phenomena. It consists of determining the current set-up by the external field in the ribbon at each point, neglecting the edge effects, i.e., treating it as though the ribbon were infinitely extended. From the expression for the current thus derived, one then determines the reradiated field by the usual radiation formulas. For a distance $R \ll L$, one thus obtains

$$\frac{I'}{I_0} = \frac{\sin^2\psi}{2\pi kR} \frac{\sin^2(kd\cos\psi)}{\cos^2\psi}, \tag{22}$$

where ψ is the azimuthal angle of twist of the ribbon mentioned above, and where $\psi = \pi/2$ refers to an orientation of the plane of the ribbon perpendicular to the common direction of incidence and scattering. For $kd = 2\pi d/\lambda = 2c \gg 1$, one obtains an appreciable backscattering only in the neighborhood of the "specular" orientation $\psi = \pi/2$. The average value of (22) over ψ for $kd \gg 1$ gives

$$\langle (I'/I_0) \rangle_{Av} = d/2\pi R. \tag{23}$$

Inserting this value for I'/I_0 in (21) we obtain

$$\sigma = \frac{K}{\pi} Ld = KA/\pi, \tag{24}$$

and, therefore, by comparison with (15) it is evident that

$$f(c) = 1/\pi \quad \text{for} \quad c \gg 1. \tag{25}$$

While Eqs. (16) and (25) give the values of $f(c)$ in the two limiting cases $c \ll 1$ and $c \gg 1$, the intermediate region is covered by Table I, values computed from the tables of Morse and Rubenstein.

It is interesting to note that for $c = 0.1$ one obtains, from (16), $f(c) = 1.288$ instead of 1.085 and that the limiting value of $f(c)$ from (25) is 0.318, while for $c = 1.4$ it is actually 0.364. This means that Table I extends through a sufficient region so that both for smaller and larger values of c the much simpler limiting formulas (16) and (25) are good approximations. In curve 1 of Fig. 2 we have plotted $f(c)$ against c or λ/d, using the computed points of Table I and joining on to the dotted lines which represent the limiting expressions for small and large arguments.

TABLE II.

c	.4	.6	.8	1.0	1.2	1.4
$f(c)$	.011	.075	.125	.237	.36	.46

So far we have assumed that the incident radiation is polarized parallel to the axis of the rope. As long as $\lambda \gg d$, any transverse component produces a negligible scattered intensity, of order $(d/\lambda)^4$ as compared to the parallel component. If, however, d becomes comparable to λ, the transverse component will also be scattered appreciably. In fact for $\lambda \ll d$, $f(c)$ will equal $1/\pi$ for either polarization. Table II gives the values of $f(c)$ for transverse polarization. These were obtained from the equations of Morse and Rubenstein in a manner similar to that for parallel polarization. These values are plotted in curve 2. For large arguments c this curve reaches the same constant $1/\pi$ as curve 1. While the value of $f(c)$ is negligible compared to that for parallel polarization below $c=\pi d/\lambda=\frac{1}{2}$, it becomes equal for $c=1.25$ and even exceeds it for $c=1.4$. The numerical calculations have not been carried beyond that point and from there on the curve 2 is drawn somewhat schematically, keeping in mind only that it must approach the same value $1/\pi$ as curve 1. It seems plausible, however, that it should have a maximum in the neighborhood of $c=\pi d/\lambda=1.5$, since this corresponds to a width approximately equal to $\lambda/2$. Since for transverse polarization the ribbon can be thought of as being composed of infinitely many infinitesimally narrow half-wave dipoles, the occurrence of such a maximum can be expected. Because of the strong coupling between these dipoles this maximum is quite broad and not very pronounced. For the same reason one can even expect additional maxima for larger arguments. Since they will be even less pronounced than the first maximum and have not been actually computed, they have been omitted in the drawing of curve 2. Even in the least reliable region between $c=1.4$ and $c=3$, we estimate the error to be no more than 20 percent.

Viscometric Investigation of Dimethylsiloxane Polymers*

ARTHUR J. BARRY
The Dow Chemical Company, Midland, Michigan

(Received July 29, 1946)

The intrinsic viscosities of an extended series of linear methyl polysiloxane fluids, having dimethylsiloxane (Me_2SiO) as the repeating unit, have been determined in toluene solution. These values have been correlated with their molecular weights, determined chemically and by osmotic pressure and light scattering measurements. The Staudinger equation was found applicable only for fluids of relatively low molecular weights, i.e., up to about 2500; for the higher polymers, the best correlation of intrinsic viscosity with number average molecular weight was found to be:

$$[\eta]=2\times10^{-4}M_n^{0.66}.$$

This held reasonably well for molecular weights from 2500 to about 200,000. The bulk viscosities of the polysiloxane fluids were found to conform to the Flory relationship for melt viscosities; the expression:

$$\log \text{visc. (cs. at } 25°\text{C)} = 1.00+0.0123M_n^{\frac{1}{2}}$$

appears to be reasonably valid for molecular weights above 2500.

THE silicone fluids have recently become of considerable commercial and technical importance. They consist of a series of methylpolysiloxanes; details relating to their methods of preparation and description of properties are now appearing in the literature. McGregor and Warrick[1] described a number of low and high polymer oils of cyclic and linear structures which were derived from the hydrolysis chiefly of dimethyldiethoxysilane. Intensive studies of the cyclic dimethylsiloxanes have been reported re-

* This paper, a contribution of the Dow Corning Corporation, was presented before the American Physical Society at the New York Meeting, January 26, 1946.

[1] R. R. McGregor and E. L. Warrick, U.S.P. 2,384,384 (1945).

cently by Hurd,[2] Patnode and Wilcock,[3] Hunter, Hyde, Warrick, and Fletcher,[4] and Wilcock.[5] The linear low polymers containing trimethylsiloxy groups as endblocking units are described in three of these papers[2,3,5] while the high polymer members of this homologous series are described along with the low polymer species in a paper[6] which has been submitted for publication.

The viscometric investigation of this important class of fluids, correlated with their molecular weight data, is of considerable practical as well as academic interest. The present paper is concerned principally with the linear members of the dimethylsiloxane polymers endblocked by ethoxyl or trimethylsiloxyl groups.

TABLE I. Methylpolysiloxane properties.

	Viscosity* (cs./25°C)	Intrinsic viscosity	Molecular weight	*MW* method	Calc'd *MW***
Trimethylsiloxy endblocked species					
Hexamer	2.63	.0066	458	*a, b*	
Heptamer	3.24	.0077	532	*a, b*	
Octamer	3.88	.0088	606	*a, b*	
Nonamer	4.58	.0098	680	*a, b*	
Ethoxy endblocked species					
Heptamer	3.28	.0093	592	*a, b, c*	
Octamer	3.86	.0104	666	*a, b, c*	
Nonamer	4.50	.0119	740	*a, b, c*	
Decamer	5.17	.0124	814	*a, b, c*	
Ethoxy endblocked polymers					
	6.30	.0139	837	*c*	
	7.71	.0168	1,005	*c*	
	9.90	.0189	1,150	*c*	
	13.5	.0235	1,468	*c*	
	21.7	.0302	2,170	*c*	
	24.1	.0328	2,535	*c*	2,200
	37.4	.040	2,840	*c*	2,950
	48.0	.047	3,800	*c*	3,800
	76.8	.058	5,170	*c*	5,170
	82.0	.062	5,030	*c*	5,700
	102.0	.070	7,140	*c*	7,000
	156.0	.082	8,250	*c*	8,700
	290.0	.104	14,100	*c*	12,500
High polymer fluids					
	930.0	.159	25,300	*s*	23,500
	1,722.0	—	40,700	*s*	—
	1,698.0	.185	36,800	*s*	30,000
	1,960.0	.185	—		30,000
	3,060.0	.210	50,800	*s*	36,000
	10,600	—	70,800	*p*	—
	14,600	.310	—		65,000
	23,360	.340	69,900	*s*	75,000
	32,900	.374	—		87,000
	40,000	—	85,400	*p*	—
	65,000	.390	—		93,000
	125,000	.459	—		118,500
	310,000	.479	—		126,000
	746,000	.556	148,000	*p*	158,000

(*a*) Ultimate analysis.
(*b*) Boiling point elevation.
(*c*) Ethoxyl end-group analysis (reference 7).
(*p*) Osmotic pressure in methyl amyl ketone (reference 8).
(*s*) Light scattering in toluene (reference 9).
* Bulk viscosity of the silicone oil in centistokes at 25°C.
** Calculated from $[\eta] = 2.00 \times 10^{-4} M^{0.66}$.

[2] C. B. Hurd, J. Am. Chem. Soc. **68**, 364 (1946).
[3] W. Patnode and D. F. Wilcock, J. Am. Chem. Soc. **68**, 358 (1946).
[4] M. J. Hunter, J. F. Hyde, E. L. Warrick, and H. J. Fletcher, J. Am. Chem. Soc. **68**, 667 (1946).
[5] D. F. Wilcock, J. Am. Chem. Soc. **68**, 691 (1946).
[6] M. J. Hunter, E. L. Warrick, J. F. Hyde, and C. C. Currie, paper submitted for publication.

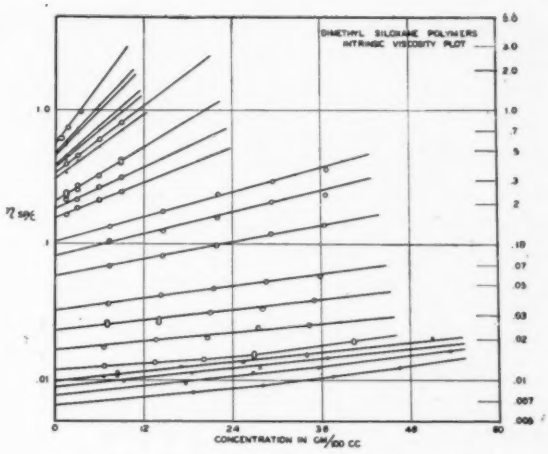

FIG. 1. Determination of intrinsic viscosities of methylpolysiloxane fluids.

MATERIALS

Fluids of a wide range of viscosities and chain lengths were investigated as grouped in Table I. The first group is comprised of distilled species of trimethylsiloxy endblocked polymers of low molecular weight determined by ultimate analysis as well as by boiling point elevation. The first member listed has the structure:

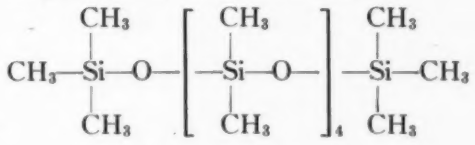

Tetradecamethylhexasiloxane

The second group is comprised of distilled species of ethoxy endblocked polymers whose molecular sizes were established as above and confirmed by endgroup analysis. The first member listed has the structure:

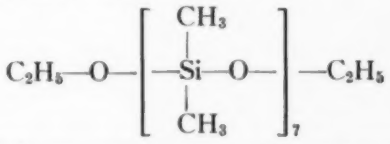

Diethoxytetradecamethylheptasiloxane

Each fluid in the third group consists of a mixture of intermediate polymers of the preceding type. They were prepared by partial hydrolysis of diethoxydimethylsilane followed by aspiration at elevated temperatures to remove the distillable low polymer.[7] The number average molecular weights were estimated from their

[7] Unpublished work by M. J. Hunter and H. J. Fletcher.

ethoxyl analyses determined by a modified Zeisel method.[8]

The high polymer fluids were mixtures and were of molecular weights too great for sensitive determination by chemical methods of analysis. A number of them were characterized by average molecular weights estimated by osmotic pressure[9] and light scattering[10] methods using solutions in heptanone-2 and toluene, respectively.

EXPERIMENTAL

For this study, toluene solutions of the above samples were employed in concentrations up to 60 g/100 cc for the low polymer species, 37 g/100 cc for the intermediate polymers, and 9 g/100 cc for the high polymer fluids. The relative viscosities were determined at 20°±.05°C using Ostwald tubes of 1.8–2.3 cc effluent volume and 10-cm capillary length. The discharge times for solvent were generally in the range of 0.8 to 1.4 minutes though tubes of 3.8 and 12.5 minute solvent efflux times were frequently used for checks. A kinetic energy error of about 2 percent was calculated for the intrinsic viscosities so determined; the correction was not applied.

The specific viscosity was determined conventionally:

$$\eta_{sp} = \eta_r - 1 = \left(\frac{t \cdot d}{t_s \cdot d_s} - 1\right)$$

where η_{sp} and η_r = specific and relative viscosities respectively, t = solution time, t_s = solvent time, d = density of solution, and d_s = density of solvent. Expressing the concentration, c, in g/100 cc, the values of $\eta_{sp/c}$ were calculated and plotted on logarithmic scale against the concentrations as shown in Fig. 1. The intrinsic viscosity, $[\eta]$ the limiting value of $\eta_{sp/c}$ as the concentration approaches zero, was read off the graph as the intercept upon extrapolation of each curve. The intrinsic viscosities are entered in Table I.

DISCUSSION

With the exception of the very low polymers, the curves for which show some curvature in the semi-logarithmic plot, the points representing $\eta_{sp/c}$ as a function of concentration fall in straight lines, permitting very good extrapolations and conforming to the Martin[11] relationship:

$$\log (\eta_{sp/c}) = \log [\eta] + k'[\eta]c.$$

While Martin reports the value of k' to be unique for a polymer-homologous series in a given solvent, this does not prove true in the present work. Here the value of k' varies as an inverse function of the size of the molecule. To illustrate, a few of the k' values are: 0.315, 0.222, 0.148, 0.135, 0.124 for the 7.7, 24, 290, 930, and 23,300 cs. fluids, respectively. They seem to approach 0.11 as a limit. The Huggins equation[12] does not yield a value of k' for any one polymer which is independent of solution concentration. If a limiting value of k' be determined for each polymer by extrapolating to zero concentration the plot of k' *vs.* concentration using the Huggins equation, it is found that the limiting k_0'-values diminish through the polymer series in the same manner as the Martin k'-value. Thus for the 24, 290, 930, and 23,300 cs. fluids, the k_0'-values were found to be 0.46, 0.33, 0.31, 0.29, respectively, approaching about 0.25 as an apparent limit for the series.

It is difficult to ascribe k' values to the lower polymer species of the first two groups, because of some curvature of their plots in Fig. 1. Nevertheless, some preliminary observations on the comparison of the plots of these open chain low polymers with those of a few corresponding cyclic polymers are of significance in the attempt to correlate k' values with structure. It was noted that the cyclic pentamer, hexamer, and octamer, $(Me_2SiO)_n$, showed lower intrinsic viscosities than their linear counterparts while their ($\eta_{sp/c}$ *vs.* concentration) slopes, and consequently their k' values, were greater. These data suggest that the compact rather fixed structure of the cyclic siloxanes contribute relatively little to flow resistance of dilute solutions yet have a pronounced effect in higher concentrations due to greater molecular interaction than is manifest in the open chain polymers. A greater molecular interaction is further reflected in the higher bulk viscosities of the cyclic polymers and in the

[8] E. P. Samsel and J. A. McHard, Ind. Eng. Chem. Anal. Ed. **14**, 750 (1942).
[9] R. M. Fuoss and D. J. Mead, J. Phys. Chem. **47**, 59 (1943).
[10] P. Debye, J. App. Phys. **15**, 338 (1944).
[11] A. F. Martin, paper presented at the Memphis Meeting of the American Chemical Society, April 1942, "Cellulose and cellulose derivatives," edited by Emil Ott (Interscience Publishers, Inc., New York, 1943), p. 966.
[12] M. L. Huggins, J. Am. Chem. Soc. **64**, 2716 (1942).

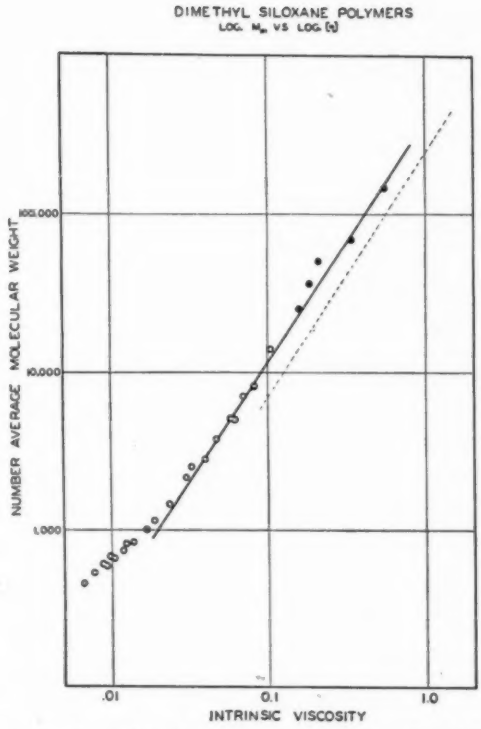

FIG. 2. Logarithmic plot of intrinsic viscosities of methylpolysiloxanes *vs.* molecular weights determined by: ○ chemical analysis; ⊕ light scattering; ◒ osmotic pressure. The dotted line represents Flory's data on polyisobutylene polymers (reference 14).

greater change of their viscosities with temperature change.

The first twelve polymers listed in Table I show exceedingly low intrinsic viscosities, which interestingly fall below the 0.025 limit of the Einstein equation when the concentrations are corrected to its fraction volume basis:

$\eta_r = 1 + 2.5\ v/V$ or $\eta_{sp} = 2.5\ v/V = 0.025\ v/100$ cc,

where v = volume of solute and V = volume of solvent. Similar failure of the Einstein equation has been indicated previously by Meyer and Van der Wijk[13] who reported on the viscosities of a series of paraffin hydrocarbons from $C_{17}H_{36}$ to $C_{34}H_{70}$ in CCl_4 solution.

The intrinsic viscosity data for the ethoxy endblocked species and the intermediate polymers up to a molecular weight of 1500 fit the simple form of the Staudinger equation $[\eta] = K \cdot M$ where $K = 1.62 \times 10^{-5}$. The intrinsic viscosities of the trimethylsiloxy endblocked species are somewhat lower and $K = 1.43 \times 10^{-5}$. To compensate for the fact that the chain of a polymer of the ethoxy endblocked type is longer, by two C_2H_5O-groups, than the corresponding member of the other series, it is interesting to correlate the intrinsic viscosity with the chain length, L, in atom units. If this is done, totaling all the C, O, and Si atoms in the chain, the relation becomes $[\eta] = K_l \cdot L$ where $K_l = 5 \times 10^{-4}$. This holds reasonably well for either type of polymer up to 80 atoms in length ($M = 2840$).

For the polymer mixtures of higher molecular weights, it was necessary to supplant the simple Staudinger equation by an exponential form. For such an evaluation, the intrinsic viscosities were plotted against the molecular weights using double logarithmic coordinates as shown in Fig. 2. The data fall on a reasonably straight line from which may be drawn the relationship:

$$[\eta] = K \cdot M^a,$$

where $[\eta]$ is the intrinsic viscosity, M is the number average molecular weight, K is a constant $= 2.00 \times 10^{-4}$, and a is an exponent $= 0.66$.

It is recognized that the molecular weights determined by light scattering are weight average values whereas all the other points are number average. Since the high viscosity fluids were commercial samples from which the lower polymers were removed by distillation at reduced pressure, the molecular weight distribution of the several species contributing to the average is upset from a normal probability function. Hence the conventional factor of $\frac{1}{2}$ for deriving number average molecular weights from weight average data is not applicable to the values determined by light scattering. However, there should be some negative correction in applying these molecular weight data to the graph which is otherwise drawn to number average molecular weights. With this qualification, the above relationship is quite reliable and fair practical agreement is shown between the reported molecular weights and the values estimated from the equation, as entered in the last column of Table I. A program involving fractionation of a high polymer mixture to provide specimens of narrow molecular weight ranges for similar study is projected.

It is interesting to view the analogy in structure between the polydimethylsiloxanes and the polyisobutylenes:

[13] K. H. Meyer and A. Van der Wijk, Helv. Chim. Acta. **18**, 1067 (1935); Kolloid Zeits. **76**, 278 (1936).

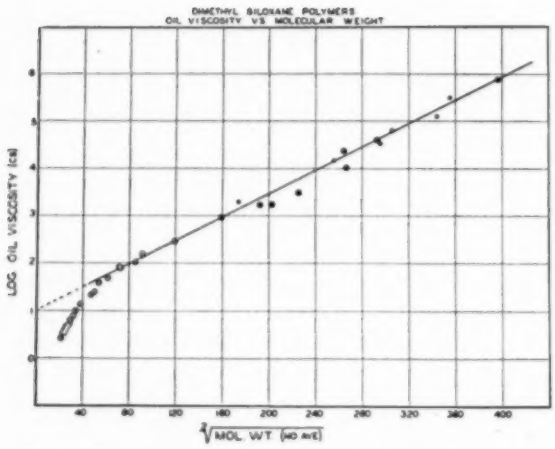

FIG. 3. Flory relationship plot for methylpolysiloxane fluids. Molecular weights determined by: ○ chemical analysis; ⊕ light scattering; ◒ osmotic pressure; ○ calculation from intrinsic viscosity equation.

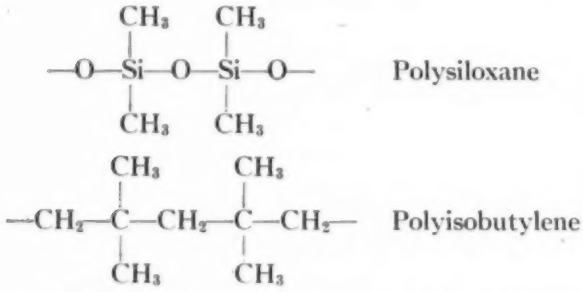

Flory[14] investigated a series of polyisobutylene fractions. Determining the viscosities in diisobutylene, he found the following equation to be valid for molecular weights above 5000:

$$[\eta] = K \cdot M^a,$$

where $K = 3.60 \times 10^{-4}$ and $a = 0.64$. This expression is represented in Fig. 2 by the broken line displaced toward higher intrinsic viscosities. The comparable slopes (a^{-1}) suggest a similar degree of chain kinking or spiral configuration for these structural analogs. This kinked structure may be reflected as one factor in the relative insensitivity to temperature of the viscosities, i.e., low viscosity/temperature slopes, observed for the polysiloxane fluids. Increase in temperature may tend to open out the kinked structure, invoking greater molecular interaction, and so compensate to some extent the normal decrease of viscosity with temperature rise.

When the logarithms of the oil viscosities (in centistokes at 25°C) were plotted against the square roots of the molecular weights, as illustrated in Fig. 3, it was found that the Flory relationship[15] for melt viscosities was applicable. Over most of the range, a straight line was obtained, the equation for which was found to be:

$$\log \eta_{(\text{cs./25°C})} = a + cM_n^{\frac{1}{2}}$$

where

$$a = 1.00, \quad c = 0.0123.$$

The expression appears to be reasonably valid for molecular weights above 2500. It should be noted that number average molecular weights were considered in the above formula. That a straight line plot was so obtained indicates that the several fluids are characterized by relatively narrow ranges of molecular weight or by comparable types of molecular weight distribution.

ACKNOWLEDGMENT

The author is indebted to Dr. M. J. Hunter, Mr. C. C. Currie, and Mr. H. J. Fletcher for providing the fluids studied. The author also wishes to thank Mr. R. F. Lind for osmotic pressure determinations and Mr. R. S. Spencer for light scattering measurements of molecular weight on several of the samples.

SUMMARY

The intrinsic viscosities of an extended series of linear methyl polysiloxane fluids, having dimethylsiloxane (Me_2SiO) as the repeating unit, have been determined in toluene solution. These values have been correlated with their molecular weights, determined chemically and by osmotic pressure and light scattering measurements. The Staudinger equation was found applicable only for fluids of relatively low molecular weights, i.e., up to about 2500; for the higher polymers, the best correlation of intrinsic viscosity with number average molecular weight was found to be:

$$[\eta] = 2 \times 10^{-4} M_n^{0.66}.$$

This held reasonably well for molecular weights from 2500 to about 200,000. The bulk viscosities of the polysiloxane fluids were found to conform to the Flory relationship for melt viscosities; the expression:

$$\log \text{visc. (cs. at 25°C)} = 1.00 + 0.0123 M_n^{\frac{1}{2}}$$

appears to be reasonably valid for molecular weights above 2500.

[14] P. J. Flory, J. Am. Chem. Soc. **65**, 372 (1943).

[15] P. J. Flory, J. Am. Chem. Soc. **62**, 1057 (1940).

Theory of Small Signal Bunching in a Parallel Electron Beam of Rectangular Cross Section

EUGENE FEENBERG* AND DAVID FELDMAN**
Washington Square College, New York University, New York, New York
(Received August 8, 1946)

The phenomenon of bunching which takes place in a velocity modulated electron beam can be described in purely kinematical terms if space charge effects are negligible. However, the non-uniform distribution of charge in the bunched beam gives rise to a field which opposes the bunching process so that the kinematic solution may be validly applied only for a limited length of drift space. An accurate solution of the bunching process requires the integration of the dynamical and field equations. These reduce to a linear homogeneous system under the assumption of "small signal" conditions. The device of a high frequency "surface charge" is employed in formulating the boundary conditions at the surface of the beam. In the non-relativistic approximation the dynamical and field equations yield solutions which are classified as non-solenoidal or solenoidal accordingly as the motion produces or does not produce a high frequency charge density within the beam. There exists a non-solenoidal type of motion which generates no field outside the beam. The actual physical problem is solved by taking a suitable linear combination of both solutions. Under conditions met with in practice, a large part of the actual solution may be of the solenoidal type. The high frequency component of beam current appears as a sum of a volume current and a "surface current," the latter term arising from the longitudinal motion of the high frequency "surface charge." Again, under conditions met with in practice, a large part of the high frequency component of beam current may occur in the form of "surface current." The theory contains three debunching wave numbers: one identical with that which occurs in Webster's debunching theory for a beam of unlimited cross section, and two which depend upon the transverse dimensions of the beam and drift tube, the current density, frequency, and beam velocity.

1. INTRODUCTION

AN adequate treatment of the bunching process in a velocity modulation tube must take account of the debunching action arising from the non-uniform distribution of charge in the bunched beam. Space charge effects become especially important in small signal amplifiers where the transit time in the drift space is made large in order to secure the maximum possible voltage gain. A satisfactory discussion of the bunching phenomenon therefore cannot be based on a purely kinematic treatment, but requires the integration of the dynamical and field equations which relate the motion of the electrons to the debunching field subject to suitable boundary conditions.[1] The method which is used here follows very closely that employed by one of the authors for the treatment of small signal bunching in a parallel beam of circular cross section.[2]

In this paper we are concerned with a parallel electron beam of rectangular cross section centered in a rectangular drift tube. In order to simplify the analysis, we take the width of the beam to be infinite; this has the advantage of making the problem two-dimensional. The results that are derived on the basis of this assumption will hence be applicable in practice to a ribbon electron beam whose width is much greater than its depth. We make the following additional approximations:

$$\text{(1) Beam velocity/velocity of light} \ll 1. \quad (1)$$

This has the consequence that the equations of motion may be written in non-relativistic form; it also permits a simple description of the electromagnetic field generated by the bunching process.

* Now at Washington University, St. Louis, Missouri.
** Now at Harvard University, Cambridge, Massachusetts.

[1] A method of solution in terms of an infinite set of characteristic solutions which must be combined in the correct proportions to obtain a solution of the actual physical problem has been given by W. C. Hahn, Gen. Elec. Rev. **42**, 258 (1939); W. C. Hahn and G. F. Metcalf, Proc. I.R.E. **27**, 106 (1939); S. Ramo, Proc. I.R.E. **27**, 757 (1939). This procedure is especially well adapted to the case of an infinitely strong longitudinal magnetic field which completely suppresses all transverse motion. The opposite extreme of no magnetic field is the only condition considered in this paper.

[2] We make repeated reference to a volume on the theory and practice of klystron design and operation now in process of publication under the editorship of E. Ginzton. The authors of the volume are present and former members of the Tube Laboratory of the Sperry Gyroscope Company, Garden City, New York.

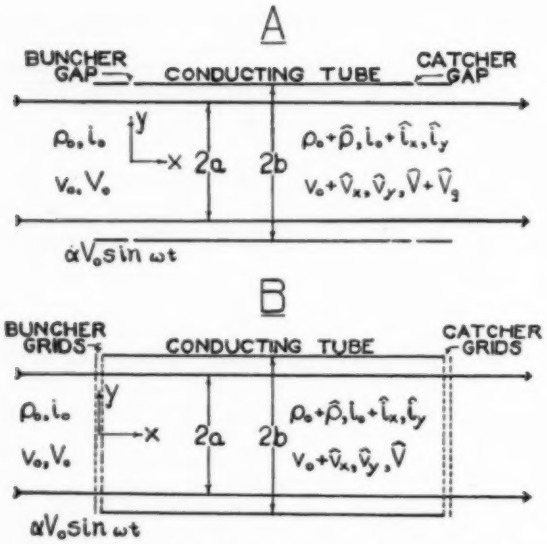

FIG. 1. A. Parallel ribbon electron beam centered between plane parallel conducting sheets. Gaps in the drift tube provide coupling to the input and output resonators.
B. Parallel ribbon electron beam centered between plane parallel conducting sheets. Beam traverses grid sections which form part of the input and output resonators.

(2) Buncher voltage/beam voltage$\ll 1$ (2a)

and

High frequency component of beam current/total beam current$\ll 1$. (2b)

We are thus effectively restricting the discussion to the case of "small signals." Under these circumstances, the equations of motion and the field equations reduce to a linear system.

(3) We assume finally that there is an accumulation of positive ions in sufficient numbers to neutralize the time average field due to the bunched beam. In other words, in the absence of hf (high frequency) fields, there is no field at all acting on the unbunched beam in the drift space; in the presence of hf fields, the debunching action arises from the non-uniform distribution of charge in the bunched beam.

The type of coupling between the beam and the modulating hf field will influence the choice of boundary conditions and hence the results obtained to a large degree. We shall consider two types of coupling. In the first case (illustrated in Fig. 1A), coupling is achieved through gaps in the drift tube; each gap forms part of a resonant circuit or cavity resonator such that an electromagnetic field in the resonant circuit or cavity produces a field within the drift tube in the neighborhood of the gap. In the second case (illustrated in Fig. 1B), the drift tube is closed at either end by a pair of closely spaced plane grids (each such pair forming the capacity section of a re-entrant cavity resonator) which serve to couple the beam to the buncher and catcher fields, respectively.

2. LIST OF SYMBOLS

All electrical quantities are stated in m.k.s. units. The subscript o and boldface type designate steady-state and the hf components, respectively; the additional subscripts x and y distinguish between longitudinal and transverse components. The following symbols are of importance in the calculations:

$\mathbf{V}_g$	The potential in the charge free drift space resulting from an hf voltage across the buncher gap. (Note that $\mathbf{V}_g=0$ for a tube with grids.)
$\mathbf{V}$	The additional potential resulting from the hf fluctuations in charge density. ($\mathbf{V}$ is the total hf potential in the drift space for a tube with grids.)
v	Velocity.
ρ	Charge density.
$\mathbf{i}_x=(\rho_0+\boldsymbol{\rho})(v_0+\mathbf{v}_x)-\rho_0 v_0$ $\cong\boldsymbol{\rho} v_0+\rho_0\mathbf{v}_x$	Longitudinal hf current density.
$\mathbf{i}_y\cong\rho_0\mathbf{v}_y$	Transverse hf current density.
D	Transit angle in radians across the buncher grid space or gap opening.
$\mu=2/D\cdot\sin D/2$	Beam coupling coefficient.
$\mu_x=\mu\cosh(\eta y/a)/\cosh(\eta b/a)$ $\mu_y=\mu\sinh(\eta y/a)/\cosh(\eta b/a)$	Beam coupling coefficients in a gap system.
λ'	"Beam wave-length" or the average distance traveled by an electron in one cycle.
$k'=2\pi/\lambda'$	"Beam wave number."
$\eta=k'a,\ \eta'=k'b$	
$G_0=2ai_0/V_0$	Beam admittance per unit width of the beam.
$\beta_0=v_0/c$	Ratio of beam velocity to the velocity of light.
$h=(\rho_0/2\epsilon_0 V_0)^{\frac{1}{2}}$	Debunching wave number. To compute h we use the equivalent expression where G_0 is in mhos per meter.
$ha=(30\pi aG_0/\beta_0)^{\frac{1}{2}}$	
α	Ratio of hf voltage to beam voltage.
τ	Phase at which an electron enters the drift space ($x=0$).
$\langle f\rangle$	Average value of the function f over the cross section of the beam.

Throughout most of the analysis, it will prove to be useful to express the potential, velocity, current density, and charge density in terms of a basic set of units in order to effect a consider-

able simplification in the appearance of many of the equations. The set used consists of $2V_0$, v_0, i_0, and ρ_0 for the potential, velocity, current density, and charge density, respectively. To transform an expression involving reduced units into ordinary units, we must then make the following substitutions:

$$V \rightarrow V/2V_0,$$
$$v \rightarrow v/v_0,$$
$$i \rightarrow i/i_0,$$
$$\rho \rightarrow \rho/\rho_0.$$

Unless otherwise stated, reduced units are employed.

3. FIELD EQUATIONS AND EQUATIONS OF MOTION

In view of the assumption contained in Eq. (1), the magnetic field of the beam may be neglected in computing the force acting on an electron in the beam; furthermore, the electric field may be derived from a quasistatic potential function $\mathbf{V}(x, y, t)$. The net error in the expression for the force due to these two simplifications consists in the neglect of a term of order β_0^2 relative to the leading term which is retained.[3] The resulting field equations are quite analogous to those which hold for an electrostatic field, *viz.*,

$$\mathbf{E} = -\nabla \mathbf{V} \quad \text{and} \quad \nabla \cdot (\epsilon_0 \mathbf{E}) = \varrho,$$

so that

$$\Delta \mathbf{V} = -\varrho/\epsilon_0$$

in ordinary units, and in reduced units

$$\Delta \mathbf{V} = -h^2 \varrho. \tag{3}$$

Conservation of charge may be expressed by the equation

$$\nabla \cdot \mathbf{i} + \partial \varrho/\partial t = 0$$

in ordinary units, which in terms of our reduced units becomes

$$v_0 \nabla \cdot \mathbf{i} + \partial \varrho/\partial t = 0. \tag{4}$$

We have finally the equations of motion

$$m\dot{\mathbf{v}}_x = -e\partial \mathbf{V}/\partial x, \quad m\dot{\mathbf{v}}_y = -e\partial \mathbf{V}/\partial y$$

in ordinary units, which become, on substituting reduced units,

$$\dot{\mathbf{v}}_x = -v_0 \partial \mathbf{V}/\partial x, \quad \dot{\mathbf{v}}_y = -v_0 \partial \mathbf{V}/\partial y. \tag{5}$$

Equations (3)–(5) constitute the theoretical system for our problem.

Throughout the remainder of this report, we make use of the fact that in practice $h \ll k'$; we assume this inequality in the form $ha \ll \eta$. In seeking solutions of Eqs. (3)–(5), it therefore proves convenient to employ a perturbation procedure with the quantity ha/η as expansion parameter. A first-order perturbation calculation is all that is desired so that we shall consistently neglect terms of order $(ha/\eta)^2$ with respect to the leading term in all of our equations. On the other hand, it should be noted that it is not necessarily true that hx is a small quantity, whence all powers of hx must be kept in the expressions for hf quantities.

An analogous situation occurs in Webster's kinematic bunching theory[4] which employs the quantity α as expansion parameter in a first order perturbation calculation. Here, terms of order α^2 with respect to the leading term may be neglected in all expressions. However, the quantity $\alpha \cdot k'x$ which is simply the product of α by the transit angle in radians in the drift space is not necessarily small, so that all powers of $\alpha \cdot k'x$ must be retained.

4. BOUNDARY CONDITIONS

We next impose boundary conditions on the various quantities appearing in (3)–(5), *viz.*, on the potential function, the entering hf components of the longitudinal and transverse velocities, and the entering hf component of beam current density (or charge density). The specific nature of the boundary conditions will be determined by the type of coupling between the beam and the hf modulating field.

The gap system has been treated in detail.[2] It has been shown that the velocity modulation produced by an hf gap may be expressed in terms of the beam coupling coefficients μ_x and μ_y as though produced instantaneously at the plane $x=0$. Actually the gap field is confined to a region about the plane $x=0$, attenuating exponentially in either direction. An explicit consideration of $\mathbf{V}_g$ is unnecessary however since the

[3] See, for example, the discussion of the forces acting on and due to electrons in uniform motion given in Jeans, *The Mathematical Theory of Electricity and Magnetism* (Cambridge University Press, Cambridge, 1945), fifth edition, p. 560.

[4] D. L. Webster, J. App. Phys. **10**, 501 (1939).

beam coupling coefficients μ_x and μ_y essentially express the over-all effect of $\mathbf{V}_g$.

For a gap system, we therefore have the following boundary conditions:

$$\left.\begin{aligned}&\mathbf{V}(x, b, t)=\mathbf{V}(0, y, t)=0\\&\left.\begin{aligned}\mathbf{v}_x&=\tfrac{1}{2}\alpha\mu_x \sin\tau\\ \mathbf{v}_y&=\tfrac{1}{2}\alpha\mu_y \cos\tau\\ \varrho&=0.\end{aligned}\right\}\text{ at } x=0\end{aligned}\right\}GAP.$$

For a system with grids, we have correspondingly:

$$\left.\begin{aligned}&\mathbf{V}(x, b, t)=\mathbf{V}(0, y, t)=0\\&\left.\begin{aligned}\mathbf{v}_x&=\tfrac{1}{2}\alpha\mu \sin\tau\\ \mathbf{v}_y&=0\\ \mathbf{i}_x&=0.\end{aligned}\right\}\text{ at } x=0\end{aligned}\right\}GRID.$$

The formulas for $\mathbf{v}_x$ and $\mathbf{v}_y$ for the gap system are obtained by integrating the equations of motion of an electron (moving in a charge free drift space) across the region in which the gap field is appreciable, and retaining only linear terms in α. The beam coupling coefficients μ_x and μ_y which appear in these formulas are essentially the Fourier transforms of the longitudinal and transverse quasistatic electric fields generated in the charge free drift space by the voltage across the gap. To derive the explicit expressions for μ_x and μ_y which are listed in Section 2, the components of electric field are first expressed as Fourier integrals in which the integrands contain a product of an exponential function of the longitudinal coordinate and a hyperbolic function of the transverse coordinate; the specific nature of these functions is determined by the fact that, subject to the inequality $\beta_0\eta' \ll 1$, the hf electric field in the drift space due to an hf gap is a quasistatic field and a solution of Laplace's equation. With the aid of suitable boundary conditions on the electric field components and the Fourier integral theorem, the remainder of the derivation may be carried through without difficulty. The procedure which is outlined here is taken from unpublished notes of W. W. Hansen. See also reference 2.

Inasmuch as the expressions for μ_x and μ_y which are listed in Section 2 have been derived for a charge free drift space, they may not be applied validly beyond a first-order perturbation calculation with ha/η as expansion parameter.

The boundary condition on the hf charge density for the gap system is based on the fact that it may be shown that the hf charge density ϱ vanishes everywhere (to within quadratic terms in α) when space charge effects[2] are neglected. The range of application of this boundary condition is again limited to a first-order perturbation calculation in terms of ha/η.

Finally, the expression for $\mathbf{v}_x$ for a system with grids may be derived by integrating the equation of motion of an electron moving across the buncher grid space and retaining only linear terms in α.

It is at this point desirable to consider in some detail what takes place at points near the surfaces $y=\pm a$ (the surfaces of the unbunched beam). It is evident from a qualitative consideration of the effect of the space charge perturbation arising from the non-uniform distribution of charge that the beam alternately expands and contracts, such that points near the surfaces $y=\pm a$ are alternately inside and outside the beam with consequent violent fluctuations of charge density at these points. A literal representation of this state of affairs would not lend itself to a perturbation procedure whose validity requires that all hf quantities vary continuously with the perturbation parameter ha/η. For our purpose it is sufficient to replace the fluctuating boundary by an hf surface charge density (with consequent longitudinal surface current density) on the surfaces $y=\pm a$.

Let $\mathbf{y}(x, y_0, t)$ denote the transverse coordinate of an electron which enters the drift space at $y=y_0$. The surface charge density then equals

$$\varrho_s(x, a, t)=\mathbf{y}(x, a, t)-a. \tag{6}$$

Similarly, for the surface current density we obtain

$$\mathbf{i}_s(x, a, t)=\mathbf{y}(x, a, t)-a. \tag{7}$$

There are analogous expressions for the surface charge density and surface current density for the boundary at $y=-a$. However, in view of the perfect symmetry which exists with respect to the surface $y=0$, we shall in all future discussions confine our attention to the surface at $y=a$.

Having introduced a surface charge density, we require two additional boundary conditions. First, the potential is continuous at the boundary

of the beam, i.e.,

$$\mathbf{V}_+(x, a, t)=\mathbf{V}_-(x, a, t), \tag{8}$$

where the subscripts + and − designate the approach to $y=a$ from without and within the beam, respectively. Second, there is a discontinuity in the transverse component of the electric displacement with the amount of discontinuity determined by the surface charge density. In ordinary units, this relation is

$$(\partial\mathbf{V}/\partial y)_- - (\partial\mathbf{V}/\partial y)_+ = \varrho_s/\epsilon_0.$$

In our reduced units, we get

$$(\partial\mathbf{V}/\partial y)_- - (\partial\mathbf{V}/\partial y)_+ = h^2\varrho_s. \tag{9}$$

5. CLASSIFICATION OF SOLUTIONS

Before actually applying the boundary conditions just outlined, we examine the consequences of the dynamical and field Eqs. (3)–(5). It is first convenient to remove the factor $\exp j(\omega t-k'x)$ from all hf quantities. If we then put for each hf quantity in (3)–(5) an expression of the form

$$\mathbf{f}(x, y, t)=f(x, y)\exp j(\omega t-k'x),$$

the field equations and equations of motion may be restated to give

$$\{(\partial/\partial x-jk')^2+\partial^2/\partial y^2\}\,V=-h^2\rho, \tag{3'}$$

$$(\partial/\partial x-jk')v_x+\partial v_y/\partial y+\partial\rho/\partial x=0, \tag{4'}$$

$$\left.\begin{aligned}\partial v_x/\partial x&=-(\partial/\partial x-jk')\,V,\\ \partial v_y/\partial x&=-\partial V/\partial y.\end{aligned}\right\} \tag{5'}$$

In the derivation of (5′) we have used the approximation

$$\begin{aligned}d/dt&=\partial/\partial t+v_x\partial/\partial x+v_y\partial/\partial y\\ &\cong\partial/\partial t+v_0\partial/\partial x.\end{aligned}$$

Now, differentiating (4′) with respect to x and using (5′), we get

$$\{(\partial/\partial x-jk')^2+\partial^2/\partial y^2\}\,V=\partial^2\rho/\partial x^2, \tag{10}$$

whence, comparing (3′) and (10), we have

$$(\partial^2/\partial x^2+h^2)\rho=0. \tag{11}$$

A consideration of (11) shows that there are two possible kinds of motion which may take place. In the first, there exists an hf charge density (i.e., the flow is non-solenoidal) with the consequent implication that all hf quantities $(V, \rho, v_x, v_y, i_x, i_y)$ have the general form

$$\begin{aligned}f_{12}(x, y)=&\exp(-jhx)f_1(y)\\ &+\exp(jhx)f_2(y).\end{aligned} \tag{12}$$

The non-solenoidal solution thus contributes two traveling waves, with the quantity h entering here as a debunching number.

In the second, the hf volume charge density vanishes identically (i.e., the flow is solenoidal). Then, both (3′) and (10) degenerate into the same equation, *viz.*, Laplace's equation. In fact, any potential function V which is a solution of Laplace's equation will give rise to a solenoidal type of motion. In what follows, we shall use the subscript 3 to denote solenoidal solutions.

It is important to note that, in Eq. (12) and the statement immediately preceding it, we have employed the term "non-solenoidal solution" in a special sense; evidently the motion which results from the addition of any arbitrary solenoidal solution to a non-solenoidal solution which is specified by (12) is non-solenoidal in the general sense of the word but is no longer characterized by (12) (except for the hf charge density ρ). However, for the purpose of classifying solutions, any general non-solenoidal motion may be considered as made up of a solenoidal flow plus a non-solenoidal flow which takes the form of Eq. (12). It is with this restricted meaning that we speak of a non-solenoidal solution throughout this paper.

In the following two sections, we discuss the general nature of the solenoidal and non-solenoidal solutions which may be used to describe an electron beam with elongated rectangular cross section, subject only to boundary conditions (8) and (9), with the additional requirement that $V(x, b)=0$. Finally, in the last two sections we seek linear combinations of both types of solutions so as to satisfy the remaining boundary conditions whose nature is determined by the type of coupling between the beam and the modulating field.

6. THE SOLENOIDAL SOLUTION

For the solenoidal type of motion, the potential function V_3 must satisfy the following (Laplace's) equation:

$$\{(\partial/\partial x-jk')^2+\partial^2/\partial y^2\}\,V_3=0. \tag{13}$$

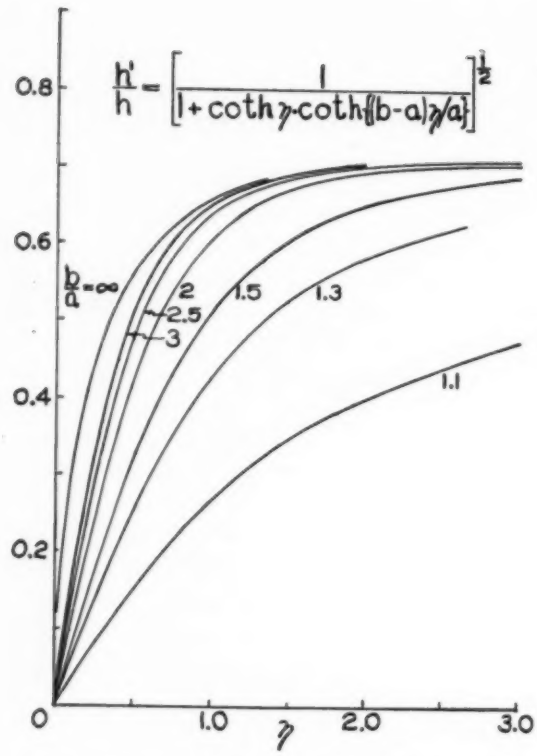

FIG. 2. The quantity h'/h as a function of η and b/a; h' is the leading term in the expansions for both h_+ and h_- (the debunching numbers arising from the solenoidal solution).

Separating variables in (13), we may write for the potential function in the beam $(-a \leqslant y \leqslant a)$

$$V_3(x, y) = \sum_\sigma V_3^{(\sigma)} \cdot \cosh\,(u_\sigma y/a)/\cosh\,u_\sigma \cdot \exp\, j(\eta - u_\sigma)x/a. \quad (14)$$

The dependence on the transverse coordinate y is chosen so as to make V_3 an even function of y. Equations (5′) suggest that we try similar type expressions for the hf velocities, *viz.*,

$$v_{x3}(x, y) = \sum_\sigma v_{x3}^{(\sigma)} \cdot \cosh\,(u_\sigma y/a)/\cosh\,u_0 \cdot \exp\, j(\eta - u_\sigma)x/a, \quad (15)$$

$$v_{y3}(x, y) = \sum_\sigma v_{y3}^{(\sigma)} \cdot \sinh\,(u_\sigma y/a)/\cosh\,u_\sigma \cdot \exp\, j(\eta - u_\sigma)x/a, \quad (16)$$

with the algebraic relations

$$v_{x3}^{(\sigma)} = v_{y3}^{(\sigma)}/j = u_\sigma/(\eta - u_\sigma) \cdot V_3^{(\sigma)}. \quad (17)$$

Outside the beam, for $a \leqslant y \leqslant b$, Eq. (8) plus the requirement that the potential function shall vanish at the drift tube suggest that we write

$$V_3^*(x, y) = \sum_\sigma V_3^{(\sigma)} \cdot \sinh\,\{(b-y)\mu_\sigma/a\}/\sinh\,\{(b-a)u_\sigma/a\} \cdot \exp\, j(\eta - u_\sigma)x/a. \quad (18)$$

It is clear that (18) is a solution of (13) and satisfies the boundary conditions

$$V_3^*(x, b) = 0; \quad V_3^*(x, a) = V_3(x, a). \quad (19)$$

For the determination of the u_σ's we use boundary condition (9). Now the transverse displacement $\mathbf{y}_3(x, a, t) - a$ may be expressed as the time integral of $\mathbf{v}_{y3}(x, a, t)$ (in ordinary units) along the orbit of the electron; in reduced units this may be written

$$\mathbf{y}_3(x, a, t) - a = v_0 \int_{\tau/\omega}^{t} \mathbf{v}_{y3}\{x(t'), a, t'\}dt'. \quad (20)$$

If we carry out the integration along the undisturbed orbit of the electron in place of its actual orbit, we may then consider the factor $\exp\, j(\omega t - k'x)$ as a constant of the motion so that Eq. (20) may be restated to give

$$y_3(x, a) = \int_0^x v_{y3}(x', a)dx', \quad (21)$$

where we have set $dt' = dx'/v_0$. Note that the amplitude factor $y_3(x, a)$ refers not to the transverse coordinate but to the transverse displacement from the surface $y = a$, i.e.,

$$\mathbf{y}_3(x, a, t) - a = y_3(x, a)\, \exp\, j(\omega t - k'x).$$

Hence, using (16) and (21), we get for the transverse displacement

$$y_3(x, a)/a = \sum_\sigma v_{y3}^{(\sigma)} \tanh\, u_\sigma \cdot [\{\exp\, j(\eta - u_\sigma)x/a\} - 1]/j(\eta - u_\sigma). \quad (22)$$

There is an additive term in (22) which is independent of x; the significance of this term will

TABLE I. Several limiting cases for the function $W(\eta) = [1 + \coth\,\eta \cdot \coth\,\{(b-a)\eta/a\}]^{-1}$.

Condition	$W(\eta)$
$\eta \to 0$, b/a finite	$(b-a)/a \cdot \eta^2$
$\eta \to \infty$, $(b-a)/a \geqslant 1$	$\frac{1}{2} \cdot \{1 - \exp\,(-2\eta)\}$
$\eta \to \infty$, $1 \geqslant (b-a)/a \geqslant 0$	$\frac{1}{2} \cdot [1 - \exp\,\{-2\eta(b-a)/a\}]$
η finite, $b \to a$	$(b-a)/a \cdot \eta \tanh\,\eta$
η finite, $b/a \to \infty$	$(1 + \coth\,\eta)^{-1}$

be discussed following the analysis of the nonsolenoidal solution.

Boundary conditions (8) and (9) must hold separately for each component of potential, where a component of potential is specified by a particular functional dependence on x. Substituting (14), (18), and (22) into (9) and equating the coefficients of $\exp j(\eta-u_\sigma)x/a$ to zero, we have

$$\coth\{(b-a)u_\sigma/a\} = -\tanh u_\sigma\cdot\{1+(ha)^2/(j\eta-ju_\sigma)^2\}. \quad (23)$$

We seek solutions of (23) where we neglect terms of order $(ha/\eta)^2$. First take ju_σ to be a real quantity; then (23) reduces to

$$\cosh(u_\sigma b/a)\cong 0,$$

or

$$ju_\sigma b/a\cong(\sigma+\tfrac{1}{2})\pi, \quad \sigma=0, 1, \cdots \quad (24)$$

and at the same time

$$\sinh\{(b-y)u_\sigma/a\}/\sinh\{(b-a)u_\sigma/a\} \cong\cosh(u_\sigma y/a)/\cosh u_\sigma. \quad (25)$$

It is evident from a consideration of the potential terms which (24) and (25) contribute when substituted into (14) and (18) that these terms are damped waves which, subject to the inequality $(ha/\eta)^2\ll 1$, are identical with the waves which may be set up in a charge free drift tube.

We can also get solutions for u_σ out of (23) for u_σ real. Thus, we restate (23) in the form

$$u_\pm=\eta\pm h_\pm a, \quad (26)$$

with

$$h_\pm=h[1+\coth u_\pm\cdot\coth\{(b-a)u_\pm/a\}]^{-\frac{1}{2}}, \quad (27)$$

where the $\pm$ replaces the σ subscript.

The potential terms contributed to (14) and (18) by (26) are obviously traveling waves, with the quantities h_+ and h_- serving as debunching numbers. There are hence a total of three such numbers, h, h_+, and h_-, of which only the first appears in the theory of an unlimited plane beam.

We observe that under the usual restriction, $(ha/\eta)^2\ll 1$,

$$h_+\cong h_-\cong h' \equiv h[1+\coth\eta\cdot\coth\{(b-a)\eta/a\}]^{-\frac{1}{2}} \quad (28)$$

and

$$|u_\pm-\eta|\ll\eta. \quad (29)$$

We digress briefly to consider the behavior of the function $W(\eta)$ where we define the latter as follows:

$$h'=h\{W(\eta)\}^{\frac{1}{2}} \quad (30)$$

or

$$W(\eta)=[1+\coth\eta\cdot\coth\{(b-a)\eta/a\}]^{-1}. \quad (31)$$

Table I lists several limiting expressions for this function. Figure 2 contains a plot of the quantity h'/h as a function of η and b/a.

We list the expressions for V_3, v_{x3}, v_{y3}, and y_3 obtained from Eqs. (14)–(16) and (22), respectively, upon substituting the values of u_σ given in (24) and (26); we use the notation $P_\sigma=(\sigma+\frac{1}{2})\pi$.

$$V_3(x,y)=V_{3+}\cdot\cosh(u_+y/a)/\cosh u_+\cdot\exp(-jh_+x)+V_{3-}\cdot\cosh(u_-y/a)/\cosh u_-\cdot\exp(jh_-x) +\exp(jk'x)\sum_{\sigma=0}^{\infty}V_{3\sigma}\cdot\cos(P_\sigma y/b)/\cos(P_\sigma a/b)\cdot\exp(-P_\sigma x/b), \quad (32)$$

$$v_{x3}(x,y)=-u_+/h_+a\cdot V_{3+}\cdot\cosh(u_+y/a)/\cosh u_+\cdot\exp(-jh_+x) +u_-/h_-a\cdot V_{3-}\cdot\cosh(u_-y/a)/\cosh u_-\cdot\exp(jh_-x) +\exp(jk'x)\sum_{\sigma=0}^{\infty}-jP_\sigma/(\eta'+jP_\sigma)\cdot V_{3\sigma}\cdot\cos(P_\sigma y/b)/\cos(P_\sigma a/b)\cdot\exp(-P_\sigma x/b), \quad (33)$$

$$v_{y3}(x,y)=-ju_+/h_+a\cdot V_{3+}\cdot\sinh(u_+y/a)/\cosh u_+\cdot\exp(-jh_+x) +ju_-/h_-a\cdot V_{3-}\cdot\sinh(u_-y/a)/\cosh u_-\cdot\exp(jh_-x) +\exp(jk'x)\sum_{\sigma=0}^{\infty}-jP_\sigma/(\eta'+jP_\sigma)\cdot V_{3\sigma}\cdot\sin(P_\sigma y/b)/\cos(P_\sigma a/b)\cdot\exp(-P_\sigma x/b), \quad (34)$$

$$y_3(x,a)/a=u_+/(h_+a)^2\cdot V_{3+}\tanh u_+\cdot\{\exp(-jh_+x)-1\}+u_-/(h_-a)^2\cdot V_{3-}\tanh u_-\cdot\{\exp(jh_-x)-1\} +\sum_{\sigma=0}^{\infty}(-P_\sigma b/a)/(\eta'+jP_\sigma)^2\cdot V_{3\sigma}\tan(P_\sigma a/b)\cdot\{\exp(jk'-P_\sigma/b)x-1\}. \quad (35)$$

The formula for $V_3^*(x, y)$ may be obtained directly from Eq. (32) by writing

$$\sinh\{(b-y)u_\sigma/a\}/\sinh\{(b-a)u_\sigma/a\}$$

for $\cosh(u_\sigma y/a)/\cosh u_\sigma$.

Summarizing this section, the application of boundary condition (9) has yielded two traveling solenoidal waves plus an infinite number of damped waves. The function of the former is to contribute to the propagation of the velocity modulation; the latter help satisfy the boundary conditions at $x=0$, particularly the condition $\mathbf{V}(0, y, t)=0$.

7. THE NON-SOLENOIDAL SOLUTION

Our point of departure in the consideration of the non-solenoidal solution is once again boundary conditions (8) and (9). Making use of the functional dependence of all non-solenoidal hf quantities (as given in (12)) in conjunction with Eq. (5′), we get

$$\left.\begin{aligned} v_{x1} &= -(1+k'/h)V_1, \\ v_{x2} &= -(1-k'/h)V_2, \\ v_{y1} &= 1/jh\cdot\partial V_1/\partial y, \\ v_{y2} &= -1/jh\cdot\partial V_2/\partial y. \end{aligned}\right\} \quad (36)$$

These relations together with an equation corresponding to (21) lead to the following expression for the transverse displacement function for the non-solenoidal case:

$$y_{12}(x, a) = 1/h^2\cdot[(\partial V_1/\partial y)_a\{\exp(-jhx)-1\} + (\partial V_2/\partial y)_a\{\exp(jhx)-1\}]. \quad (37)$$

We defer the discussion of the additive term (independent of x) appearing in (37), which is the analog of the corresponding additive term in (22), until the close of this section.

Now in the space between the beam and the drift tube ($a\leqslant y\leqslant b$), the potential function $V_{12}^*(x, y)$ must have the form of Eq. (12) and simultaneously be a solution of Laplace's equation (13). We then get the following expression:

$$V_{12}^*(x, y) = V_1(a)\cdot\sinh\{(k'+h)(b-y)\}/\sinh\{(k'+h)(b-a)\}\cdot\exp(-jhx) + V_2(a)\cdot\sinh\{(k'-h)(b-y)\}/\sinh\{(k'-h)(b-a)\}\cdot\exp(jhx). \quad (38)$$

The form of the functional dependence of $V_{12}^*(x, y)$ on the transverse coordinate y is suggested by Eq. (18).

Applying boundary condition (9), we obtain, in view of Eq. (37),

$$(\partial V_1^*/\partial y)_a=(\partial V_2^*/\partial y)_a=0, \quad (39)$$

where we have ignored, for the moment, the constant term in (37). The immediate consequence of (38) and (39) is that

$$\left.\begin{aligned} &V_1(a)=V_2(a)=0, \\ \text{whence}\quad &V_1^*(y)=V_2^*(y)\equiv 0, \end{aligned}\right\} \quad (40)$$

or $V_{12}^*(x, y)$ vanishes identically.

In other words, the field outside the beam for the non-solenoidal type of motion is zero. The hf surface charge is such as to neutralize exactly the field due to the hf volume charge at all external points, i.e., the surface charge distribution is equal but opposite in sign to the Green's equivalent stratum corresponding to the volume charge distribution.[5] Equation (40) is quite reasonable since the use of (12) and (13) requires that $V_{12}^*(x, y)$ be both non-solenoidal and solenoidal at the same time; this is clearly a contradiction which is resolved by the identical vanishing of $V_{12}^*(x, y)$.

We now rewrite Eq. (3′) to read

$$\{\partial^2/\partial y^2-(k'+h)^2\}V_1=-h^2\rho_1 \quad (41)$$

plus a similar relation obtained from (41) by putting the subscript 2 in place of 1, and $-h$ for h.

It remains to guess at a suitable form for V_1 and V_2, whence from (41) we will have expressions for ρ_1 and ρ_2. Toward this end we are guided first, by the nature of the expressions obtained for the potential due to the traveling solenoidal waves (the first two terms on the right-hand side of Eq. (32)) and second, by our use of the inequality $(ha/\eta)^2\ll 1$ as the basis for a perturbation procedure. We, therefore, try

$$V_1=\{h/(k'+h)\}^2\rho_1^0+\sum_{\sigma=0}^{\infty}V_{1,\sigma+1}\cdot 1/\sigma!\cdot\partial^\sigma/\partial\eta^\sigma\cosh(\eta y/a)/\cosh\eta, \quad (42)$$

whereupon

$$\rho_1=\rho_1^0-1/(ha)^2\cdot\sum_{\sigma=0}^{\infty}[V_{1,\sigma+3}+2\eta V_{1,\sigma+2}-\{2\eta ha+(ha)_2\}V_{1,\sigma+1}]\cdot 1/\sigma!\cdot\partial^\sigma/\partial\eta^\sigma\cosh(\eta y/a)/\cosh\eta. \quad (43)$$

[5] Jeans, reference 3, p. 182.

Corresponding relations for V_2 and ρ_2 are got from (42) and (43) by substituting the subscript 2 for the subscript 1, and $-h$ for h.

Using (40), Eq. (42) implies that

$$\left.\begin{aligned}\rho_1^0 &= -(1+\eta/ha)^2 V_{1,1},\\ \rho_2^0 &= -(1-\eta/ha)^2 V_{2,1}.\end{aligned}\right\} \tag{44}$$

We pause briefly to discuss the significance of the constant term appearing in the expression for y_{12} (given by (37)) as well as that of the analogous term in the corresponding equation for y_3 (given by (22)). As already pointed out in the discussion immediately preceding Eq. (23), boundary conditions (8) and (9) must hold separately for each component of potential, where a component of potential is specified by a particular functional dependence on x. It is then a direct consequence of Eqs. (8) and (9) that the constant term which appears in the total transverse displacement function y_3+y_{12} must vanish. This requirement (to which we shall refer as the consistency condition) follows since the constant term would otherwise contribute a traveling wave moving with beam velocity to the transverse displacement function, but there are no such terms in any of the other hf quantities (cf. Eqs. (12), (32) through (35)), and in particular in the expressions for the potentials or their transverse derivatives.

The problem which remains is to combine the solenoidal and non-solenoidal solutions so as to satisfy the consistency condition plus the boundary conditions (at $x=0$) for the gap and grid coupled systems, respectively. A complete solution for either case, therefore, requires the determination of explicit formulas for the potential coefficients V_{3+}, V_{3-}, $V_{3\sigma}$, $V_{1,\sigma+1}$, $V_{2,\sigma+1}$ ($\sigma=0,\ 1,\ \cdots$) to within a sufficient degree of accuracy so as to enable the calculation of the leading term and the term of order ha/η relative to the leading term for each of the hf quantities (v_x, v_y, ρ, $y(x, a)$) which are in turn needed to evaluate the leading and first-order terms for the longitudinal volume and surface current densities.

We now assume for both the gap and grid systems that the coefficients $V_{3\sigma}$, arising from the infinite set of damped solenoidal waves, are all of the order $(ha/\eta)^2$ or higher. With this hypothesis, it is found possible to satisfy the consistency condition as well as the boundary conditions on the entering hf components of the longitudinal and transverse velocities and the entering hf component of beam current density (or charge density), and so evaluate V_{3+}, V_{3-}, $V_{1,\sigma+1}$, $V_{2,\sigma+1}$ explicitly. The remaining requirement, *viz.*, that the potential vanish at $x=0$, leads to two conditions on the potential coefficients, the one holding outside the beam, and the other within the beam. These conditions not only verify the assumption on the $V_{3\sigma}$'s but also provide a means for their determination correct to terms in $(ha/\eta)^2$, although we have no actual need of them.

8. GAP COUPLING

The absence of an hf charge density at $x=0$ makes it possible to satisfy all the boundary conditions at the entering plane as well as the consistency condition without using the non-solenoidal waves. In discarding the latter, we are implicitly assuming that the contributions to the hf components of the longitudinal and transverse velocities by the non-solenoidal waves are of the order $(ha/\eta)^2$ relative to the leading terms in the hf velocities. We verify these statements by showing that it is indeed possible to construct a solution which will satisfy the boundary conditions and the consistency condition by simply using the two traveling solenoidal waves. In view of the remarks at the end of Section 7, we also neglect the infinite sum of damped waves.

Equations (9) and (35) then yield for the consistency condition

$$u_+/(h_+a)^2\cdot V_{3+}\tanh u_+ + u_-/(h_-a)^2\cdot V_{3-}\tanh u_-\cong 0. \tag{45}$$

The boundary conditions on the entering hf velocity components assume the form (making use of (33) and (34))

$$\alpha\mu/2j\cdot\cosh(\eta y/a)/\cosh\eta'\cong -u_+/h_+a\cdot V_{3+}\cdot\cosh(u_+y/a)/\cosh u_+ + u_-/h_-a\cdot V_{3-}\cdot\cosh(u_-y/a)/\cosh u_-, \tag{46}$$

$$\alpha\mu/2j\cdot\sinh(\eta y/a)/\cosh\eta'\cong -u_+/h_+a\cdot V_{3+}\cdot\sinh(u_+y/a)/\cosh u_+ + u_-/h_-a\cdot V_{3-}\cdot\sinh(u_-y/a)/\cosh u_-. \tag{47}$$

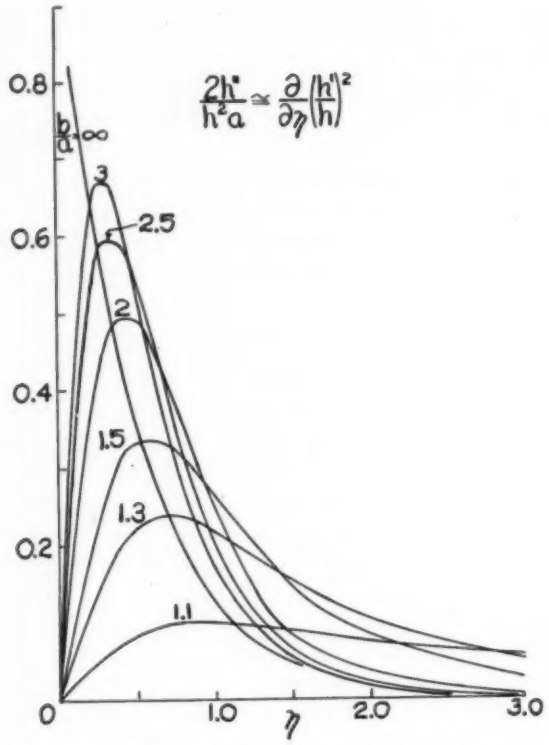

FIG. 3. The quantity $2h''/h^2a$ as a function of η and b/a; h'' and $-h''$ are the first correction terms in the expansions for h_+ and h_-, respectively (where h_+ and h_- are the debunching numbers arising from the solenoidal solution).

In (45)–(47) we have neglected terms of order $(ha/\eta)^2$ relative to the leading terms.

If we expand the quantities cosh $(u_\pm y/a)$ and sinh $(u_\pm y/a)$ into Taylor series about the point η, and make use of the substitutions

$$f(u_+)+f(u_-)=2f(\eta)\{1+0((ha/\eta)^2)\}$$

and

$$f(u_+)-f(u_-)=2h'a\cdot\partial/\partial\eta f(\eta)\cdot\{1+0(ha/\eta)\},$$

then (46) and (47) are not independent relations but reduce to the same equation, *viz.*,

$$\alpha\mu/2j\cdot 1/\cosh\eta'\cong -u_+/h_+a\cdot V_{3+}\cdot 1/\cosh u_+ + u_-/h_-a\cdot V_{3-}\cdot 1/\cosh u_-, \quad (48)$$

where we neglect terms of order $(ha/\eta)^2$.

Equations (45) and (48) possess the solution

$$-u_\pm/h_\pm a\cdot V_{3\pm}=\pm\alpha\mu/4j\cdot h_\pm/h'\cdot\sinh\eta/\cosh\eta'\cdot\coth u_\pm\cdot\{1+0_\pm((ha/\eta)^2)\}, \quad (49)$$

where 0_+ and 0_- are remainder functions with leading terms of the second order in ha/η.

It follows from (36) that the hf components of potential contributed by the two non-solenoidal waves are of the third order in ha/η, whence the total potential function at $x=0$ will equal a known function (quadratic in ha/η) arising from the traveling solenoidal waves plus an infinite sum of local damped waves with coefficients $V_{3\sigma}$. Inasmuch as $V(0, y)=V^*(0, y)=0$, all of the coefficients $V_{3\sigma}$ are quadratic in ha/η. We have, therefore, verified our initial assumption about the order of magnitude of the $V_{3\sigma}$'s.

It is now a straightforward procedure to compute the total hf longitudinal and transverse velocities, the transverse displacement function, and finally the effective beam volume and surface currents. For the remainder of this section, we state all quantities in ordinary units.

It will prove convenient to use the notation

$$2h''=h_+-h_-\cong h^2a\cdot\partial/\partial\eta(h'/h)^2. \quad (50)$$

The quantity $2h''/h^2a$ is plotted in Fig. 3 as a function of η and b/a.

Inserting (49) into (33), (34) and (35), we get

$$v_x/v_0\cong\alpha\mu/2j\cdot\sinh\eta/\cosh\eta'\cdot\exp(-jh''x)\cdot[\cos(h'x)\cdot\cosh(\eta y/a)/\sinh\eta - j\sin(h'x)\cdot\partial/\partial\eta\{h'a\cdot\cosh(\eta y/a)/\sinh\eta\}], \quad (51)$$

$$v_y/v_0\cong\alpha\mu/2\cdot\sinh\eta/\cosh\eta'\cdot\exp(-jh''x)\cdot[\cos(h'x)\cdot\sinh(\eta y/a)/\sinh\eta - j\sin(h'x)\cdot\partial/\partial\eta\{h'a\cdot\sinh(\eta y/a)/\sinh\eta\}], \quad (52)$$

$$y(x, a)\cong\alpha\mu/2\cdot\sinh\eta/\cosh\eta'\cdot\exp(-jh''x)\cdot\sin(h'x)/h'. \quad (53)$$

In (51)–(53) terms of order $(ha/\eta)^2$ with respect to the leading terms are neglected. There is no zero-order term in (53) because of the consistency condition.

To calculate the volume and surface current densities, we need simply put $i_x=\rho_0 v_x$ and $i_s=i_0 y(x, a)$. For a gridless catcher, the hf current becomes a physically significant quantity only if it is the "effective current," i.e., each element of longitudinal current must be multiplied by the longitudinal beam coupling coefficient. For the effective volume current we then

have

$$\mathbf{I}_v/I_0=\langle v_x/v_0\cdot\mu\cosh(\eta y/a)/\cosh\eta'\rangle \times\exp j(\omega t-k'x)$$

$$\cong\alpha\mu^2/2j\cdot[\tfrac{1}{2}\{1+\sinh(2\eta)/2\eta\}\cdot 1/\cosh^2\eta'] \cdot\cos(h'x)\cdot\exp j\{\omega t-(k'+h'')x\}. \quad (54)$$

In similar fashion, we write for the effective surface current

$$\mathbf{I}_s/I_0=\mu\cosh\eta/\cosh\eta'\cdot y(x,a)/a\cdot\exp j(\omega t-k'x)$$

$$\cong\alpha\mu^2/2\cdot\{\sinh(2\eta)/2\eta\cdot 1/\cosh^2\eta'\} \cdot k'/h'\cdot\sin(h'x)\cdot\exp j\{\omega t-(k'+h'')x\}. \quad (55)$$

The quantity in the curly brackets in Eq. (55) is plotted in Fig. 4 as a function of η and b/a.

In deriving Eqs. (54) and (55), we have retained leading terms only. Hence the first neglected term in $\mathbf{I}_v$ is of the order ha/η; the first neglected term in $\mathbf{I}_s$ is also of the order ha/η since the transverse displacement function (53) has no zero-order term.

Comparing the relative orders of magnitude of $\mathbf{I}_s$ and $\mathbf{I}_v$, we note that the hyperbolic function enclosed in the brackets in (55) is always larger than the corresponding function in (54) for $\eta>0$ and equal to it for $\eta=0$; this statement follows readily from the inequality $\sinh(2\eta)/2\eta\geq 1$ for $\eta\geq 0$. Furthermore, $\mathbf{I}_v$ is of the order h'/k' (a quantity smaller than ha/η) with respect to $\mathbf{I}_s$, and our entire procedure has been based on the assumption that $(ha/\eta)^2\ll 1$.

The total hf current is the sum of the surface and volume currents. Noting that the leading terms in $\mathbf{I}_s$ and $\mathbf{I}_v$ are 90° out of phase, it follows from the preceding two paragraphs that the amplitude factor for the total current, which equals $(|\mathbf{I}_s|^2+|\mathbf{I}_v|^2)^{\frac{1}{2}}$, contains a leading term of order $(k'/h')^2$ contributed by the surface current, with the following term of zero order, contributed by both the volume and surface currents. The volume current is therefore insignificant except in the immediate vicinity of zeros of $\sin(h'x)$.

Retaining only the surface current, maximum hf current occurs for a drift tube length determined by the first maximum of $\sin(h'x)$; this length corresponds to maximum gain for a single stage amplifier at low input levels. Hence

$$x_{\max}=\pi/2h'. \quad (56)$$

The perturbation procedure is no longer valid when the transverse displacement (53) exceeds $b-a$. When this happens, current flows directly to the drift tube in hf pulses while at the same time the hf beam current drops considerably. This effect should become sharp for $(b-a)/a\ll 1$, i.e., there will exist a critical input level such that below this level the system will behave as an amplifier with a given "small signal" voltage or power gain, but above this level the output will remain fairly constant.

The critical input level is determined by the relation

$$|y(x,a)|=b-a. \quad (57)$$

For a tube designed to give a maximum gain at low input levels, (53) and (57) yield

$$\alpha=2ha/\mu\cdot(\eta\coth\eta)^{\frac{1}{2}}\cdot\{(b-a)/a\}^{\frac{1}{2}}, \quad (58)$$

where we have assumed $(b-a)/a\ll 1$ together with the expression for h' given in Table I for this condition.

9. GRID COUPLING

We return once more to the use of reduced units. Our input conditions on the longitudinal current density and velocity are $\mathbf{i}_x=\rho+\mathbf{v}_x=0$ and $\mathbf{v}_x=\alpha\mu/2j\cdot\exp(j\omega t)$; so that, in view of (12),

$$\rho_1+\rho_2=-\alpha\mu/2j. \quad (59)$$

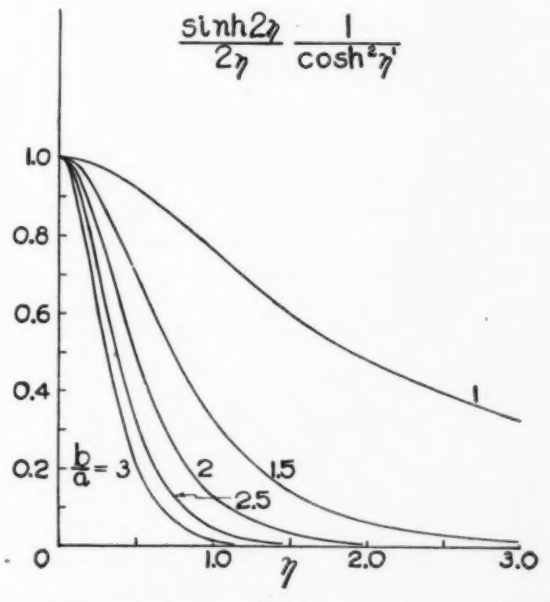

FIG. 4. A coefficient required to evaluate the effective surface current with gap coupling (refer to Eq. (55)).

In terms of (43) and (44), Eq. (59) yields the following two relations:

$$\{1+(\eta/ha)^2\}\cdot(V_{1,1}+V_{2,1})+2\eta/ha\cdot(V_{1,1}-V_{2,1}) = \alpha\mu/2j, \quad (60)$$

$$2\eta/ha\cdot(V_{1,\sigma+1}-V_{2,\sigma+1}) = -(V_{1,\sigma+1}+V_{2,\sigma+1}) + 2\eta/(ha)^2\cdot(V_{1,\sigma+2}+V_{2,\sigma+2}) + 1/(ha)^2\cdot(V_{1,\sigma+3}+V_{2,\sigma+3}), \quad \sigma=0,1,\cdots. \quad (61)$$

We again make the hypothesis that the potential coefficients $V_{3\sigma}$, which specify the damped local solenoidal waves, are all of the order $(ha/\eta)^2$. This means that in the statement of the boundary conditions on the entering longitudinal and transverse velocities and of the consistency condition, terms due to these local waves may be omitted. This hypothesis will be verified along the lines given in the discussion toward the end of Section 7.

With the help of Eqs. (12), (33), (36), (42), and (44), the boundary condition on the longitudinal velocity at $x=0$ yields the following relation:

$$\{(V_{1,1}+V_{2,1})+\eta/ha\cdot(V_{1,1}-V_{2,1})\} - \sum_{\sigma=0}^{\infty}\{(V_{1,\sigma+1}+V_{2,\sigma+1})+\eta/ha\cdot(V_{1,\sigma+1}-V_{2,\sigma+1})\} \cdot 1/\sigma!\cdot\partial^\sigma/\partial\eta^\sigma\cosh(\eta y/a)/\cosh\eta - u_+/h_+a\cdot V_{3+}\cdot\cosh(u_+y/a)/\cosh u_+ + u_-/h_-a\cdot V_{3-}\cdot\cosh(u_-y/a)/\cosh u_- \cong \alpha\mu/2j. \quad (62)$$

Setting up the corresponding boundary condition on the transverse velocity at $x=0$, where we now employ Eq. (34) in place of (33) in the above listing, we get, following a single differentiation with respect to y plus a rearrangement of terms,

$$\sum_{\sigma=0}^{\infty}\{\eta/ha\cdot(V_{1,\sigma+1}-V_{2,\sigma+1})+2/ha\cdot(V_{1,\sigma+2}-V_{2,\sigma+2}) + 1/\eta ha\cdot(V_{1,\sigma+3}-V_{2,\sigma+3})\}\cdot 1/\sigma! \cdot\partial^\sigma/\partial\eta^\sigma\cosh(\eta y/a)/\cosh\eta + u_+/\eta\cdot u_+/h_+a \cdot V_{3+}\cdot\cosh(u_+y/a)/\cosh u_+ - u_-/\eta\cdot u_-/h_-a \cdot V_{3-}\cdot\cosh(u_-y/a)\cosh u_- \cong 0. \quad (63)$$

Finally, using (35) and (37) and applying the consistency condition, we obtain the relation

$$1/(ha)^2\cdot\sum_{\sigma=0}^{\infty}\{\eta(V_{1,\sigma+1}+V_{2,\sigma+1}) + (V_{1,\sigma+2}+V_{2,\sigma+2})\}\cdot 1/\sigma!\cdot\partial^\sigma/\partial\eta^\sigma\tanh\eta + u_+/(h_+a)^2\cdot V_{3+}\cdot\tanh u_+ + u_-/(h_-a)^2\cdot V_{3-}\cdot\tanh u_- \cong 0. \quad (64)$$

Note that in Eqs. (62)–(64) additive terms of order $(ha/\eta)^2$ have been discarded.

The foregoing set of Eqs. ((60) through (64)) is adequate to evaluate explicitly the potential coefficients V_{3+}, V_{3-}, $V_{1,\sigma+1}$, $V_{2,\sigma+1}$ within an accuracy determined by our hypothesis on the order of magnitude of the coefficients $V_{3\sigma}$. The calculations required for this evaluation are given in reference 2. We list the results:

$$V_{1,1}+V_{2,1} = -\alpha\mu/2j\cdot(ha/\eta)^2/(1-(ha/\eta)^2),$$
$$V_{1,1}-V_{2,1} = \alpha\mu/2j\cdot(ha/\eta)/(1-(ha/\eta)^2),$$
$$V_{1,2}+V_{2,2} = \alpha\mu/2j\cdot(ha/\eta)^2\eta\{1+0((ha/\eta)^2)\},$$
$$V_{1,\sigma+3}+V_{2,\sigma+3} = \alpha\mu/2j\cdot 0((ha/\eta)^4), \quad \sigma=0,1,\cdots, \quad (65)$$
$$V_{1,\sigma+2}-V_{2,\sigma+2} = \alpha\mu/2j\cdot 0((ha/\eta)^3), \quad \sigma=0,1,\cdots,$$
$$u_\pm/h_\pm a\cdot V_{3\pm} = \mp\alpha\mu/4j\cdot\{1\pm ha/\eta\cdot K + 0_\pm((ha/\eta)^2)\},$$
$$ha/\eta\cdot K = h''/h'\cdot(1+0(ha/\eta)).$$

There is one final requirement which the potential coefficients must satisfy arising from the boundary condition on the potential at $x=0$, *viz.*, $V(0,y)=V'(0,y)=0$. Setting up the potential function within and without the beam with help of (12), (32), (42), and (44) together with the statement immediately following (35), and using the potential coefficients for the traveling solenoidal and non-solenoidal waves given in (65), we obtain a known function (quadratic in ha/η) plus an infinite sum of damped waves with coefficients $V_{3\sigma}$. Since the potential vanishes at $x=0$, all the coefficients $V_{3\sigma}$ are quadratic in ha/η, thus justifying our initial assumption.

Equation (65) constitutes a complete solution of the problem. We proceed to list some im-

portant hf quantities, returning once more to the use of ordinary units.

$$\rho/\rho_0 \cong \alpha\mu/2\cdot\{k' \sin(hx)/h + j\cos(hx)\}, \tag{66}$$

$$v_x/v_0 \cong \alpha\mu/2j\cdot[\{\cosh(\eta y/a)/\cosh\eta\}\{\exp(-jh''x)\cdot\cos(h'x)-\cos(hx)\}+\cos(hx)], \tag{67}$$

$$y(x,a)/a \cong \alpha\mu/2\cdot[(\tanh\eta/\eta)\{k'\exp(-jh''x)\cdot\sin(h'x)/h'-k'\sin(hx)/h\}$$
$$+j(\partial/\partial\eta\tanh\eta)\{\exp(-jh''x)\cdot\cos(h'x)-\cos(hx)\}]. \tag{68}$$

The terms which are neglected in (66)–(68) are of the order ha/η.

To calculate the volume and surface current densities, we use the relations

$$i_x/i_0 = \rho/\rho_0 + v_x/v_0 \quad \text{and} \quad i_s/i_0 = y(x,a).$$

The total volume current then equals

$$I_v/I_0 = \langle i_x/i_0\rangle$$
$$\cong \alpha\mu/2\cdot[k'\sin(hx)/h - j(\tanh\eta/\eta)$$
$$\cdot\{\exp(-jh''x)\cdot\cos(h'x)-\cos(hx)\}]. \tag{69}$$

For the total surface current, we obtain

$$I_s/I_0 = y(x,a)/a, \tag{68'}$$

and it is hence given directly by Eq. (68).

We compute finally the total current:

$$I_t/I_0 = I_v/I_0 + I_s/I_0$$
$$\cong \alpha\mu/2\cdot[(\tanh\eta/\eta)\cdot k'\exp(-jh''x)\cdot\sin(h'x)/h' + (1-\tanh\eta/\eta)\cdot k'\sin(hx)/h$$
$$+j(\eta\partial/\partial\eta\tanh\eta/\eta)\{\exp(-jh''x)\cdot\cos(h'x)-\cos(hx)\}]. \tag{70}$$

The hyperbolic function coefficients appearing in (68)–(70) are plotted in Fig. 5.

The importance of the surface current in the usual design of klystron amplifier with grid coupling is established by Figs. 2 and 5. It is easily possible for the first term in Eq. (70) to exceed the second by a factor of three or four. Indeed, for $\eta < 1$, the first term in (70) is the only one of importance, and the motion becomes solenoidal.[6] The length of drift tube for maximum hf current is then given by the relation which we obtained previously for the gap system, *viz.*,

$$x_{max} = \pi/2h'. \tag{56}$$

The corresponding maximum of current has the value

$$(I_t/I_0)_{max} \cong \alpha\mu k'/2h' = \alpha\mu/2\cdot\eta/ha\cdot h/h'. \tag{71}$$

We note finally that, as $\eta\to\infty$, Eq. (70) reduces to the correct limiting expression for an unbounded beam,

$$(I_t/I_0)_{\eta\to\infty} \cong \alpha\mu/2\cdot k'\sin(hx)/h. \tag{72}$$

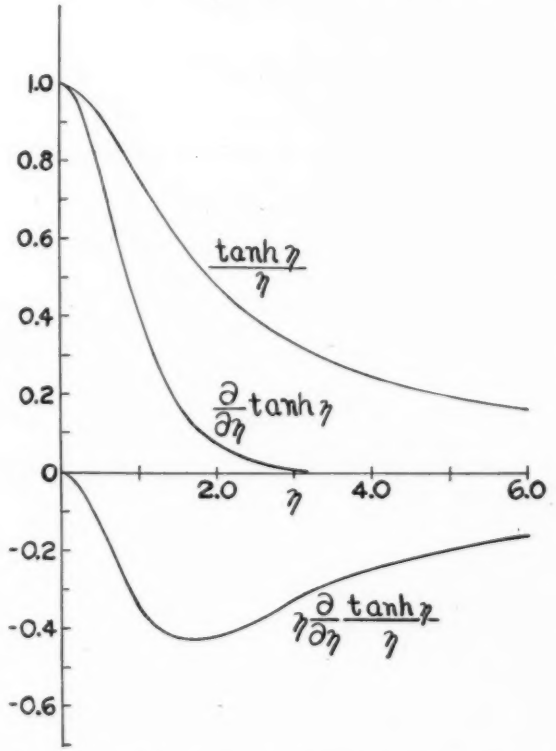

FIG. 5. Coefficients required to evaluate the volume, surface and total currents with grid coupling (refer to Eqs. (69)–(70)).

[6] R. H. Varian has shown, by a physical argument, that the flow must become solenoidal for a beam of circular cross section in the limiting case of extremely small radius (for a fixed total current). For a given amount of velocity modulation, it follows from Gauss's theorem in electrostatics that the longitudinal field due to space charge approaches a finite limiting value as the cross section is made smaller. At the same time, the radial field at the edge of the beam increases without limit (roughly inversely as the radius of the beam). Hence the bunching process is such as to tend toward expansion and contraction at constant density as the cross section is reduced. It is of interest to note that, in the case treated in this paper, we also approach a solenoidal flow as the transverse dimension of the beam is reduced for a fixed current density, although Varian's argument is no longer applicable.

On Vibrations of Shallow Spherical Shells

ERIC REISSNER
Massachusetts Institute of Technology, Cambridge, Massachusetts
(Received July 30, 1946)

The problem of the axi-symmetrical vibrations of a shallow spherical shell is reduced to two simultaneous differential equations for the tangential and normal components of displacement. The solution of these equations is obtained in terms of Bessel functions. With this solution the third-order determinant for the frequencies of a shell segment with clamped edge is given but not evaluated. Instead, an approximate value for the lowest frequency is calculated by means of the Rayleigh-Ritz procedure [Eq. (40)]. It is found that very little curvature is needed to modify appreciably the corresponding flat-plate frequency. The approximations which are made are those customary for shallow shells: (1) omission of the transverse shear term in the tangential force equilibrium equation, and (2) relations between couples and changes of curvatures as in the theory of flat plates.

1. INTRODUCTION

IN this note we consider the problem of the rotationally symmetric vibrations of a thin, shallow, elastic, spherical shell. Our aim is to arrive at a formula which contains the modifying effect of the curvature of the shell on the corresponding formulas for the flat plate. We take the basic equations as in an earlier paper on the statics of shallow spherical shells.[1] These equations are reduced to two simultaneous equations for normal and tangential components of displacement. It is found that these two equations have a symmetrical structure of such a kind that their complete solution in terms of Bessel functions is possible. Determination of the frequencies of a shell segment with one boundary requires the evaluation of a third-order determinant having as its elements products of Bessel functions and rational functions. For a shell segment with two boundaries a corresponding sixth-order determinant occurs.

An upper bound for the lowest frequency of a shell segment with clamped edge is obtained by means of the Rayleigh-Ritz procedure. This formula shows the expected pronounced effect of even small curvature on the values of the frequency.

After the work of this paper had been completed it was found that similar results had been obtained earlier by K. Federhofer.[2] As our method of derivation is quite different from Federhofer's, and as moreover Federhofer's work is published in a relatively inaccessible place, it is thought that publication of the present developments still may be of some interest.

2. FORMULATION OF THE PROBLEM

We take the equation of the middle surface of the shell in the form

$$z=(R^2-r^2)^{\frac{1}{2}}-(R-h), \tag{1}$$

where R is the radius of the shell, h the distance between base plane and apex of the shell, and r the radius vector in the base plane (Fig. 1). Let $r=a$ be the intersection of the shell surface with the plane $z=0$, so that according to (1),

$$a^2=2hR-h^2. \tag{2}$$

For a shallow shell we have the order of mag-

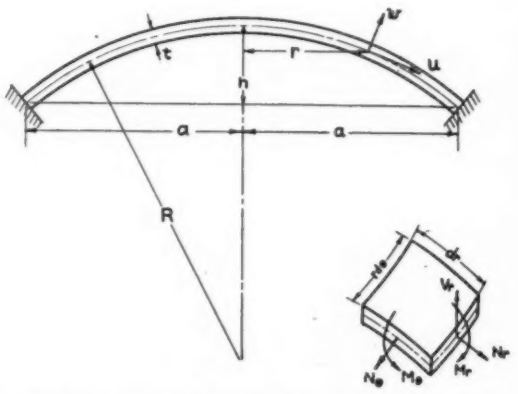

FIG. 1. Section of shallow spherical shell segment and element of shell, with indication of symbols used in text.

[1] E. Reissner, J. Math. and Phys. **25**, 80–85 (1946).
[2] K. Federhofer, Sitz. Akad. d. Wiss. Wien **146**, 57–69 (1937).

nitude relation

$$\frac{dz}{dr}=-\frac{r}{(R^2-r^2)^{\frac{1}{2}}}\sim-\frac{r}{R}=o(1), \tag{3}$$

which must hold for all $r\leqslant a$. As a consequence of (3) we have that $h\ll R$, and Eq. (2) may be replaced by

$$a=(2hR)^{\frac{1}{2}}. \tag{4}$$

We restrict attention to rotationally symmetric vibrations with circular frequency ω and omit the time factor in the equations of the problem. We then have as equations of equilibrium

$$(rN_r)'-N_\theta+t\rho\omega^2ru=0, \tag{5a}$$

$$(rV_r)'-(r/R)(N_r+N_\theta)+t\rho\omega^2rw=0, \tag{5b}$$

and

$$(rM_r)'-M_\theta-rV_r=0. \tag{5c}$$

In (5) primes denote differentiation with respect to r; u and w are the meridional and normal component of displacement; N_r and N_θ are direct stress resultants; V_r is the transverse shear stress resultant; and M_r and M_θ are the bending stress couples. Equation (5a) has been simplified by the omission of the transverse shear term.[1]

We take as stress strain relations[1]

$$N_r=C\left[u'+\frac{w}{R}+\nu\left(\frac{u}{r}+\frac{w}{R}\right)\right], \tag{6a}$$

$$N_\theta=C\left[\frac{u}{r}+\frac{w}{R}+\nu\left(u'+\frac{w}{R}\right)\right], \tag{6b}$$

$$M_r=-D\left(w''+\frac{\nu}{r}w'\right), \tag{6c}$$

and

$$M_\theta=-D\left(\frac{w'}{r}+\nu w''\right), \tag{6d}$$

where

$$C=\frac{Et}{1-\nu^2}\quad\text{and}\quad D=\frac{Et^3}{12(1-\nu^2)}. \tag{7a, b}$$

From (6c, d) and (5c) we obtain for a shell of constant thickness t

$$V_r=-D(w''+w'/r)', \tag{8}$$

thereby expressing all resultants and couples in terms of the components of displacement.

3. THE DIFFERENTIAL EQUATIONS FOR THE COMPONENTS OF DISPLACEMENT

We introduce (6a) and (6b) into (5a) and obtain

$$ru''+u'-u/r+(1+\nu)rw'/R+(t\rho\omega^2/C)ru=0. \tag{9}$$

We next introduce (6a), (6b), and (8) into (5b) and obtain

$$[rw'''+w''-w'/r]'+((1+\nu)C/RD)[ru'+u+2rw/R]-(t\rho\omega^2/D)rw=0. \tag{10}$$

The system (9) and (10) which corresponds to one differential equation of the sixth order can be transformed in such a way that its complete solution is expressed in terms of Bessel functions.

To see this we use the identity

$$rf''+f'-f/r\equiv r[r^{-1}(rf)']' \tag{11}$$

and introduce an operator L defined by

$$L(g)\equiv r[r^{-1}g']'. \tag{12}$$

With (11) and (12) we write (9) and (10) in the form

$$L(ru)+(1+\nu)rw'/R+(t\rho\omega^2/C)ru=0 \tag{13}$$

and

$$[L(rw')]'+((1+\nu)C/RD)[(ru)'+2rw/R]-(t\rho\omega^2/D)rw=0. \tag{14}$$

In (13) and (14) the quantities u and w occur principally in the form ru and rw'. This suggests that we introduce two new dependent variables y and z defined as

$$y=ru\quad\text{and}\quad z=rw'. \tag{15a, b}$$

Furthermore, we divide (14) by r, differentiate the result, and then multiply by r. If this is done equations (13) and (14) become

$$L(y)+(t\rho\omega^2/C)y+(1+\nu)z/R=0 \tag{16}$$

and

$$LL(z)-(t\rho\omega^2/D)z+((1+\nu)C/RD)[L(y)+2z/R]=0. \tag{17}$$

When $R=\infty$, Eqs. (16) and (17) are equivalent to known equations for the uncoupled extensional and flexural vibrations, with no radial nodes, of circular plates.

We put as abbreviations in (16) and (17)

$$t\rho\omega^2/C=(1-\nu^2)\rho\omega^2/E=\alpha^2, \tag{18a}$$

$$t\rho\omega^2/D=12(1-\nu^2)\rho\omega^2/Et^2=k^4, \tag{18b}$$

$$(1+\nu)R=2(1+\nu)h/a^2=m_1^2, \tag{18c}$$

$$(1+\nu)C/RD=24(1+\nu)h/a^2t^2=m_2^2, \tag{18d}$$

$$2(1+\nu)C/R^2D=96(1+\nu)h^2/a^4t^2=k^4-\beta^4 \tag{18e}$$

and have

$$L(y)+\alpha^2y+m_1^2z=0 \tag{19}$$

and

$$LL(z)-\beta^4z+m_2^2L(y)=0. \tag{20}$$

4. SOLUTION OF THE DIFFERENTIAL EQS. (19) AND (20)

We note that the equation

$$L(f)+\mu^2f=0 \tag{21}$$

has the Bessel-function solution

$$f=rZ_1(\mu r). \tag{22}$$

We set in (19) and (20)

$$y=ArZ_1(\mu r), \quad \text{and} \quad z=BrZ_1(\mu r) \tag{23a, b}$$

and obtain

$$\left.\begin{aligned}(\alpha^2-\mu^2)A+m_1^2B=0\\ -m_2^2\mu^2A+(\mu^4-\beta^4)B=0\end{aligned}\right\}. \tag{24a, b}$$

The condition of vanishing determinant of (24) is

$$(\alpha^2-\mu^2)(\mu^4-\beta^4)+m_1^2m_2^2\mu^2=0. \tag{25a}$$

If we multiply (25a) by a^6, where a may be the radius of the base of the shell segment, we obtain, with (18),

$$\left[(1-\nu^2)\frac{\rho\omega^2a^2}{E}-(\mu a)^2\right]\left[(\mu a)^4-12(1-\nu^2)\frac{\rho\omega^2a^4}{Et^2}+96(1+\nu)\frac{h^2}{t^2}\right]+48(1+\nu)\frac{h^2}{t^2}(\mu a)^2=0. \tag{25b}$$

It follows from (25b) that the three roots μ_1, μ_2, and μ_3 of (25) are of the form

$$\mu a=f\left[\frac{a^2}{t}\omega\left(\frac{(1-\nu^2)}{E}\rho\right)^{\frac{1}{2}},\frac{h}{t},\frac{h}{a},\nu\right]. \tag{26}$$

From (24a) follows for the amplitude ratios

$$A/B=m_1^2/(\alpha^2-\mu^2). \tag{27}$$

Combining the solutions corresponding to different values of μ and taking J_1 as well as Y_1 as part

of Z_1, we may write

$$z=rw'=r\{B_1J_1(\mu_1r)+C_1Y_1(\mu_1r)+B_2J_1(\mu_2r)+C_2Y_1(\mu_2r)+B_3J_1(\mu_3r)+C_3Y_1(\mu_3r)\}, \tag{28}$$

and

$$y=ru=rm_1^2\left\{\frac{B_1J_1(\mu_1r)}{\alpha^2-\mu_1^2}+\frac{C_1Y_1(\mu_1r)}{\alpha^2-\mu_1^2}+\frac{B_2J_1(\mu_2r)}{\alpha^2-\mu_2^2}+\frac{C_2Y_1(\mu_2r)}{\alpha^2-\mu_2^2}+\frac{B_3J_1(\mu_3r)}{\alpha^2-\mu_3^2}+\frac{C_3Y_1(\mu_3r)}{\alpha^2-\mu_3^2}\right\}. \tag{29}$$

For an annular shell all six constants of integration are needed in order to satisfy three boundary conditions on each edge. For a complete shell segment with no singularity at the apex we must have $C_1=C_2=C_3=0$.

Integrating (27) we obtain for the deflection w,

$$w=-B_1J_0(\mu_1r)/\mu_1-C_1Y_0(\mu_1r)/\mu_1-B_2J_0(\mu_2r)/\mu_2-C_2Y_0(\mu_2r)/\mu_2-B_3J_0(\mu_3r)/\mu_3-C_3Y_0(\mu_3r)/\mu_3. \tag{30}$$

5. FREQUENCY EQUATION FOR SHELL SEGMENT WITH CLAMPED EDGE

As an example of the form which the equation determining the frequency assumes, we consider the motion of a shell determined by the conditions that there is no singularity for $r=0$ and that along the edge $r=a$ there is complete restraint,

$$w(a)=w'(a)=u(a)=0. \tag{31a, b, c}$$

We substitute (28) to (30) in (31) and obtain three simultaneous homogeneous equations for B_1, B_2, and B_3. The possible frequencies follow from the determinantal equation

$$\begin{vmatrix} J_0(\mu_1a)/\mu_1 & J_0(\mu_2a)/\mu_2 & J_0(\mu_3a)/\mu_3 \\ J_1(\mu_1a) & J_1(\mu_2a) & J_1(\mu_3a) \\ \dfrac{J_1(\mu_1a)}{(\alpha a)^2-(\mu_1a)^2} & \dfrac{J_1(\mu_2a)}{(\alpha a)^2-(\mu_2a)^2} & \dfrac{J_1(\mu_3a)}{(\alpha a)^2-(\mu_3a)^2} \end{vmatrix}=0. \tag{32}$$

In Eq. (32) we must introduce the values of μ_1, μ_2, and μ_3 which follow from the cubic (25). Comparison of (32) and (26) shows that the frequencies of free vibrations are determined by a formula of the form

$$\omega=\frac{t}{a^2}\left[\frac{E}{(1-\nu^2)\rho}\right]^{\frac{1}{2}}F\left(\frac{h}{t},\frac{h}{a},\nu\right). \tag{33}$$

For a flat plate ($h=0$) Eq. (33) becomes, for flexural vibrations, $\omega=(t/a^2)[E/(1-\nu^2)\rho]^{\frac{1}{2}}\times$const., and for extensional vibrations, $\omega=(1/a)[E/(1-\nu^2)\rho]^{\frac{1}{2}}\times$const.

The simultaneous solution of (32) and (25), by numerical methods, is presumably not an easy matter and is not given in this note. Instead, a simple approximate formula is derived in what follows by means of the Rayleigh-Ritz procedure.

6. APPROXIMATE DETERMINATION OF LOWEST FREQUENCY BY VARIATIONAL METHOD

The variational form of the equations of motion is according to (13) and (14)

$$\int_0^a C[L(ru)+m_1^2rw'+\alpha^2ru]\delta u+D[\{L(rw')\}'+m_2^2(ru)'-\beta^4rw]\delta w\}dr=0. \tag{34}$$

To obtain an approximate value of the lowest frequency we set in (34)

$$\delta u=(\delta A)\frac{r}{a}\left(1-\frac{r}{a}\right), \tag{35a}$$

and

$$\delta w=(\delta B)(1-r^2/a^2)^2, \tag{35b}$$

which leads to the following two simultaneous equations for A and B:

$$\left[\frac{1}{60}(\alpha a)^2-\frac{1}{4}\right]A-\frac{11}{105}m_1^2aB=0 \tag{36a}$$

and

$$\frac{11}{105}m_2^2a^3A-\left[\frac{1}{10}(\beta a)^4-\frac{32}{5}\right]B=0. \tag{36b}$$

The condition of vanishing determinant of (36) may be written in the form

$$\lambda^2-\left[\frac{80}{9}+8(1+\nu)\frac{h^2}{t^2}+15\frac{a^2}{t^2}\right]\lambda+\frac{a^2}{t^2}\left[\frac{400}{3}+120(1+\nu)\frac{h^2}{t^2}-96\left(\frac{11}{21}\right)^2(1+\nu)^2\frac{h^2}{t^2}\right]=0, \tag{37}$$

where

$$\lambda=(1-\nu^2)\omega^2\rho a^4/Et^2. \tag{38}$$

As $(t/a)\ll 1$ and $(h/a)\ll 1$, the smaller of the two roots of (37) simplifies to

$$\lambda=\frac{80}{9}\left[1+\left(\frac{9}{10}-\frac{242}{1225}(1+\nu)\right)(1+\nu)\frac{h^2}{t^2}\right], \tag{39}$$

and the lowest characteristic frequency is then approximated by the simple formula

$$\omega=2.98\frac{t}{a^2}\left(\frac{E}{\rho(1-\nu^2)}\right)^{\frac{1}{2}}\left(1+(1+\nu)[.90-.20(1+\nu)]\frac{h^2}{t^2}\right)^{\frac{1}{2}}. \tag{40}$$

In the limiting case of a flat plate Eq. (40) gives a value which lies within about one percent of the exact value.

It may be noted that had one used, instead of (35), the still rougher approximation $u=0$ and $w=B(1-r^2/a^2)^2$, then instead of (40), an approximate value for ω would have been obtained where the term $.90-.20(1+\nu)$ is replaced by $.90$.[3] This indicates that the upper limit for ω, which is given by (40), should be improved, especially for appreciable values of h/t, either by solving the determinantal equation (32) or by using additional terms in the Rayleigh-Ritz procedure.

[3] By using $u=(r/a)(1-r^2/a^2)$ instead of (35a), Federhofer obtains a result which may be transformed into an expression of the form (40), with the difference that the factor .20 is replaced by a factor .19.

Non-Uniform Transmission Lines and Reflection Coefficients

L. R. WALKER AND N. WAX
Bell Telephone Laboratories, Inc., New York, New York
(Received July 30, 1946)

A first-order differential equation for the voltage reflection coefficient of a non-uniform line is obtained and it is shown how this equation may be used to calculate the resonant wave-lengths of tapered lines.

THE usual method of treating non-uniform (or tapered) transmission line problems consists in solving a second-order differential equation in either the voltage or current along the line. Pierce[1] has shown, recently, how one may obtain a first-order differential equation for the input impedance of a non-uniform line. It is the purpose of this note to derive a first-order differential equation for the voltage reflection coefficient of a non-uniform line and to show how this equation may be used to calculate the resonant wave-lengths of tapered lines.

The equations satisfied by the voltage, V, and current, I, at a point x along any transmission line are

$$dV/dx = -Z(x)I, \tag{1}$$

$$dI/dx = -Y(x)V, \tag{2}$$

where $Z(x)$ and $Y(x)$ are the series impedance and shunt admittance per unit length of line, respectively. The nominal characteristic impedance, $K(x)$, and nominal propagation factor $\Gamma(x)$, are defined by the relations

$$K(x) = \left[\frac{Z(x)}{Y(x)}\right]^{\frac{1}{2}}, \tag{3}$$

$$\Gamma(x) = [Z(x)\,Y(x)]^{\frac{1}{2}}. \tag{4}$$

The voltage reflection coefficient, q_v, is defined by

$$q_v = \frac{\frac{V}{I} - K(x)}{\frac{V}{I} + K(x)}. \tag{5}$$

Making use of the above equations one finds that q_v satisfies the first-order non-linear differential equation

$$\frac{dq_v}{dx} - 2\Gamma(x)q_v + \frac{1}{2}\frac{d\log K(x)}{dx}(1-q_v^2) = 0. \tag{6}$$

Introducing the complex phase angle, θ, by means of the relation $q_v = e^{i\theta}$, Eq. (6) becomes

$$\frac{d\theta}{dx} = -2i\Gamma(x) + \frac{d\log K(x)}{dx}\sin\theta \tag{7}$$

or, in integral form,

$$\theta = -2i\int^x \Gamma(x)dx + \int^x \sin\theta \frac{d}{dx}[\log K(x)]dx. \tag{8}$$

The first term on the right-hand side of Eq. (8) represents a generalization of the usual expression for the phase shift along a uniform line that takes into account the variations in propagation factor. The second term is in the nature of a correction term which depends not only on the changes in nominal characteristic impedance but also on the phase at the point.

Thus far no assumptions have been made concerning the properties of the transmission line. If one now assumes, as will be done in the rest of this paper, that the line is loss-less, then the nominal characteristic impedance will be real and the propagation factor will be purely imaginary, $\Gamma(x) = i\beta(x)$. A new variable, y, may be defined by

$$y = \int_0^x \beta(x)dx.$$

Equations (7) and (8) then become

$$\frac{d\theta}{dy} = 2 + \frac{d\log K(x)}{dy}\sin\theta, \tag{9}$$

$$\theta = \theta(0) + 2y + \int_0^x \sin\theta \frac{d}{dx}[\log K(x)]dx, \tag{10}$$

where $\theta = \theta(0)$ at $x = 0$.

[1] J. R. Pierce "Note on the transmission line equations in terms of impedance," Bell Sys. Tech. J. **22**, 263–265 (1943).

It may be instructive to consider Eq. (7) from the viewpoint of transducer theory. The relation between the reflection coefficients q_{v1} and q_{v2} (looking in the same direction) on the two sides of a loss-less, linear, passive, four-terminal network is

$$q_{v1}=\exp(-i\alpha_1)\frac{\gamma+\exp(i\alpha_2)q_{v2}}{1+\gamma\exp(i\alpha_2)q_{v2}}, \quad (11)$$

where α_1, α_2, γ are all real, and $|\gamma|\leqq 1$. Equation (11) may be obtained in a variety of ways, for example from the definition of the voltage reflection coefficient and the known relationships between the voltages and currents on the two sides of the network. Let $q_{v1}=\exp(i\theta_1)$ and $q_{v2}=\exp(i\theta_2)$. Then Eq. (11) becomes

$$\tan\left(\frac{\theta_2+\alpha_2}{2}\right)=\Delta\tan\left(\frac{\theta_1+\alpha_1}{2}\right), \quad (12)$$

where $\Delta=(1+\gamma)/(1-\gamma)$. If one now considers a small element of the transmission line as an elementary four-terminal network, then $\theta_2=\theta_1+\delta\theta$, $\alpha_1=\delta\alpha_1$, $\alpha_2=\delta\alpha_2$, and $\Delta=1+\delta\Delta$. One finds that

$$\delta\theta=(\delta\alpha_1-\delta\alpha_2)+\delta\Delta\sin\theta_1, \quad (13)$$

and comparing this with Eq. (7)

$$\delta\alpha_1-\delta\alpha_2=\beta(x)\delta x, \quad (14)$$

$$1+\delta\Delta=1+\delta\log K(x)=\frac{K(x)+\delta K(x)}{K(x)}. \quad (15)$$

An equivalent representation for each small section of a non-uniform line is, therefore, two small lengths of uniform line with the characteristic impedance of one line that of the nominal characteristic impedance at the beginning of the section, and that of the other the characteristic impedance at the end of the section.

Equation (10) may be solved by the method of iteration; the approximations converge rapidly when the change in $\log K(x)$ over the interval considered is sufficiently small. The nth-order approximation will be

$$\theta_n=\theta(0)+2y+\int_0^x\sin\theta_{n-1}\frac{d}{dx}[\log K(x)]dx. \quad (16)$$

The zero-order approximation is given by

$$\theta_0=\theta(0)+2y \quad (17)$$

and the first-order approximation by

$$\theta_1=\theta(0)+2y+\int_0^x\sin\theta_0\frac{d}{dx}[\log K(x)]dx. \quad (18)$$

Equations (16)–(18) enable one to solve Eq. (10) when the propagation factor is known. The calculation of the resonant wave-lengths of non-uniform lines presents a somewhat different problem in that the propagation factor is the quantity to be determined.

It is convenient to make two more assumptions now. One is that the line is terminated in a pure reactance at $x=0$; this makes θ a real quantity. The other is that the propagation factor is a constant as a function of x; an important special class of non-uniform lines satisfies this condition. Equation (10) becomes, then,

$$\theta=\theta(0)+\frac{4\pi}{\lambda}x+\int_0^x\sin\theta\frac{d}{dx}[\log K(x)]dx, \quad (19)$$

where $\beta(x)=\beta$; $\beta=2\pi/\lambda$.

Resonance will occur when $\theta=m\pi$, where m is an even positive integer, anti-resonance when m is an odd positive integer.

Let $x=a$ when $\theta=m\pi$; in solving Eq. (19) by the method of iteration one sets all approximations equal to $m\pi$ at $x=a$.

The nth-order approximation to λ is given by

$$\lambda_n=\frac{4a}{m-\frac{\theta(0)}{\pi}-\frac{1}{\pi}\int_0^a\sin\theta_{n-1}\frac{d}{dx}[\log K(x)]dx} \quad (20)$$

with the zero-order approximation

$$\lambda_0=\frac{4a}{m-\frac{\theta(0)}{\pi}} \quad (21)$$

and the first-order approximation

$$\lambda_1=\frac{4a}{m-\frac{\theta(0)}{\pi}-\frac{1}{\pi}\int_0^a\sin\theta_0\frac{d}{dx}[\log K(x)]dx}. \quad (22)$$

Resonant wave-lengths of a few non-uniform lines have been obtained by the standard meth-

ods and by means of Eq. (22); the results were in agreement when the taper was small. The appendix gives the results of such a calculation for a particular class of non-uniform lines, together with the errors arising from the use of the first approximation.

APPENDIX

If one assumes that the propagation factor is constant, and that $K(x)$ varies as a power of x, then Eq. (9) will be of the form

$$\frac{d\theta}{dx}=2\beta-\frac{1\pm 2v}{x}\sin\theta \qquad \text{(A1)}$$

with β and v real constants.

A new variable w may be introduced by means of the transformation

$$\frac{1}{w}\frac{dw}{dx}=\pm\frac{v}{x}-\beta\tan\theta/2. \qquad \text{(A2)}$$

Using (A1) and (A2) one obtains Bessel's equation

$$\frac{d^2w}{dx^2}+\frac{1}{x}\frac{dw}{dx}+\left(\beta^2-\frac{v^2}{x^2}\right)w=0, \qquad \text{(A3)}$$

with solutions, therefore, of the form

$$w=AJ_v(\beta x)+BY_v(\beta x) \qquad \text{(A4)}$$

A and B are constants.

If $w=0$ at $x=a$ and at $x=b$ then (A4) yields

$$J_v(\beta b)\,Y_v(\beta a)=J_v(\beta a)\,Y_v(\beta b). \qquad \text{(A5)}$$

From (A2), the zeros of w are the poles of $\tan\theta/2$, for $x\neq 0$; the corresponding boundary conditions on (A1) are then $\theta=(2m+1)\pi$ at $x=a$, $\theta=(2n+1)\pi$ at $x=b$, where m and n are integers. The eigenvalues of (A1), subject to these boundary conditions, are thus the roots of (A5). One may readily obtain a first approximation to the eigenvalues of (A1), and therefore to the roots of (A5) by using the method of iteration. This yields

$$\beta_1=\frac{1}{b-a}\left\{s\pi-\frac{1\pm 2v}{2}\right.$$
$$\times\left[\left(Si\left(\frac{2s\pi\alpha}{\alpha-1}\right)-Si\left(\frac{2s\pi}{\alpha-1}\right)\right)\cos\frac{2s\pi}{\alpha-1}\right.$$
$$\left.\left.+\left(Ci\left(\frac{2s\pi\alpha}{\alpha-1}\right)-Ci\left(\frac{2s\pi}{\alpha-1}\right)\right)\sin\frac{2s\pi}{\alpha-1}\right]\right\}, \qquad \text{(A6)}$$

$s=m-n$, $\alpha=b/a>1$, Si and Ci are the sine- and cosine-integrals, respectively.

Roots of (A5) may be obtained quite quickly by means of (A6) and are of fair accuracy when v and α are small. The percentage error for $v=0$ and $\alpha\leqq 4$ is less than 2.5 percent for the first five roots; for $v=\frac{1}{3}$ and $\alpha\leqq 4$ it is less than 6.2 percent for the first three roots; for $v=1$ and $\alpha\leqq 2.5$ it is less than 5.5 percent for the first four roots. When $v=2$ and $\alpha=2$, the first root is in error by 13.2 percent. In all cases computed the percentage error decreased rapidly as s increased.

The above approximation has been compared with the McMahan[2] series solution for (A5). It was found that for $\alpha<4$, $v<2$, a single root could be obtained with about equal speed by the two methods, for comparable accuracy. However, the above approximation has two advantages over the McMahan series: (1) that approximate roots may be obtained very quickly for many values of α, and (2) that even a single root may be obtained with greater speed for $\alpha>4$, since the McMahan series converges slowly for these values.

ACKNOWLEDGMENTS

The authors wish to thank their colleagues at the Bell Telephone Laboratories and in particular Dr. S. A. Schelkunoff for his help during the preparation of this paper, and Miss M. E. Moore for computing aid.

[2] A. Gray, G. B. Mathews, and T. M. MacRobert, *A Treatise on Bessel Functions* (The Macmillan Company, New York, 1922), Appendix III (VI), p. 261.

Resonant Frequencies of the Nosed-In Cavity

ERNEST MAYER*
Westinghouse Research Laboratories, East Pittsburgh, Pennsylvania
(Received June 13, 1946)

In this paper the resonant frequency of the nosed-in cavity is studied as a function of the cavity dimensions. Maxwell's differential equations and boundary conditions are converted into an integral equation which is solved approximately by the Ritz variational method. The size and shape of the cavity are fixed by specification of the dimensions (cf. Fig. 1) r_1 and r_2, the inner and outer radii; ϵ^{I}, the post length and ϵ^{II}, the gap space. If the cavity is to resonate to the wave-length λ, only three of its dimensions can be given independently; the fourth will be a function of the given three and the wave number $k=2\pi/\lambda$. For fixed r_1/r_2 the dependence of $k\epsilon^{\mathrm{I}}$ on $k\epsilon^{\mathrm{II}}$ is calculated with a precision of 1 percent.

I. INTRODUCTION

THE present article is based almost entirely on a Westinghouse Research report.[1] A number of mathematical details and proofs not given here and additional references will be found in the above-mentioned report.

Much interest has developed recently in the nosed-in type of cavity of large gap spacing shown in Fig. 1. In this article we obtain curves which relate the resonant frequency of the cavity to its dimensions. These dimensions are: ϵ^{I}, the post length; ϵ^{II}, the gap space; r_1, the post radius; and r_2, the outer radius of the cavity. As the cavity is a figure of revolution we use cylindrical polar coordinates (r, φ, z) with the z axis along the axis of symmetry and the $z=0$ plane along the tip of the post. We are interested in the fundamental mode of resonance. In this mode the angular component of the electric field, E_φ is zero and the angular component of the magnetic field, H_φ, is independent of φ. Since the mode has angular symmetry, H_φ satisfies the partial differential equation

$$\frac{\partial^2 H_\varphi}{\partial r^2}+\frac{1}{r}\frac{\partial H_\varphi}{\partial r}+\frac{\partial^2 H_\varphi}{\partial z^2}+\left(k^2-\frac{1}{r^2}\right)H_\varphi=0, \quad (1)$$

together with the boundary condition that, on all conducting surfaces,

$$\frac{\partial}{\partial n}(rH_\varphi)=0, \quad (2)$$

where $\partial/\partial n$ denotes differentiation in the direction normal to the conducting surface, and $k=2\pi/\lambda$ is the wave number. H_φ can serve as a potential function for the other two non-vanishing components of the field:[2]

$$ikE_z=-\frac{1}{r}\frac{\partial}{\partial r}rH_\varphi, \quad (3)$$

$$ikE_r=-\frac{\partial H_\varphi}{\partial z}. \quad (4)$$

For the cavity in Fig. 1 no explicit solution of (1) has been given. Only approximate methods are available for calculating the frequency of such a resonator. A practical procedure is to divide the interior of the cavity by a suitably chosen surface S into regions I and II, in each of which the variables of (1) can be separated. In these regions the solutions H_φ^{I} and H_φ^{II}, respectively, can be set up so as to satisfy (2) at the conducting surfaces. However, owing to the fact that neither region is completely surrounded by conducting walls, each solution will contain an infinite number of arbitrary constants; furthermore, the wave

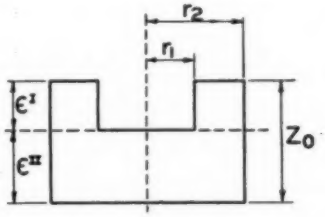

FIG. 1.

* Now at The M. W. Kellogg Company, Jersey City, New Jersey.

[1] T. Holstein and E. Mayer, Research Report SR-281, "Resonent frequencies of the nosed-in cavity."

[2] E. U. Condon, Rev. Mod. Phys. **14**, 341 (1942).

number k is undetermined. In order for H_φ^{I} and H_φ^{II} to represent the solution of (1) in the whole cavity, they must obey the following continuity conditions on the surface S:

$$H_\varphi^{\mathrm{I}} = H_\varphi^{\mathrm{II}}, \tag{5}$$

$$\partial H_\varphi^{\mathrm{I}}/\partial n = \partial H_\varphi^{\mathrm{II}}/\partial n, \tag{6}$$

where $\partial/\partial n$ denotes differentiation in the direction normal to S. The imposition of these continuity conditions determines not only the arbitrary constants but also the wave number k.

This procedure has been applied by Hansen[3] to the nosed-in resonator of small gap space. In his paper the surface S is chosen at $r=r_1$. The interior is thereby divided into two regions in each of which H_φ can be expanded as a Fourier-Bessel summation, the amplitudes of the terms being determined by the condition that both summations yield the same value of the tangential electric field E_z on the dividing surface S. This condition, which is equivalent to (6), together with (5) can be used to determine the unknown amplitudes and the wave number k.

Hansen now assumes an analytic form $E_z(z)$ to approximate the component of the actual field on S. The assumed $E_z(z)$ is expanded into two Fourier series over the intervals ϵ^{II} and $\epsilon^{\mathrm{I}}+\epsilon^{\mathrm{II}}=z_0$, corresponding to the regions into which Hansen's S divides the interior of the cavity. Substitution of the Fourier expansions into (3) permits evaluation of the amplitudes and therefore satisfies (6) by construction. The determination of the only remaining unknown, k, is now effected by a matching of H_φ^{I} and H_φ^{II} at z_1, a particular value of z on the surface S employed by Hansen. With the value k thus found, say k_1, the matching indicated in (5) is in general not satisfied at $z \neq z_1$, because the analytic form of $E_z(z)$ is only an approximation. Had E_z been the correct function, the k obtained from matching at a particular z would have guaranteed satisfaction of (5) everywhere on S. Hansen shows that k_1 is close to the correct k as it is not very sensitive to the error in E_z or to the choice of z_1. In practical calculations it turns out that his method begins to be inaccurate for resonators whose total height z_0 exceeds $\pi/2k$.

A more general approach to the problem has been made by J. Schwinger. According to his method E_z (or, more generally, the tangential electric field on S) is left undetermined. The amplitudes of the Fourier terms are expressed by means of (3) and (6) as integrals of the unknown E_z. Substitution in (5) leads to an integral equation in E_z of which solutions exist only for a denumerably discrete set of k's. In applying such integral equations to wave guide problems Schwinger has shown how approximate solutions can be obtained by variational methods.

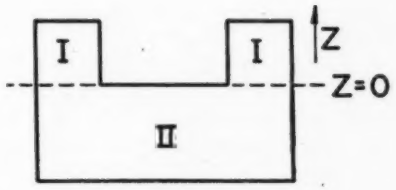

FIG. 2.

The frequency calculations presented in this paper extend beyond the range treated by Hansen, i.e., the method presented here is practical for $z_0 > \pi/2k$. These calculations are based on an integral equation of the form

$$\int \psi(r) G(r, r') dr' = 0, \tag{7}$$

in which the kernel $G(r, r')$ is a function of the cavity dimensions and the wave number k. The steps leading to (7) are stated below. The solution of the integral equation will be achieved by methods analogous to those employed by Schwinger.

II. THE INTEGRAL EQUATION

The derivation of the integral equation proceeds as follows. We divide the cavity interior into regions I and II by choosing* S along $z=0$ as shown in Fig. 2. The solutions of (1) in both regions are of the form

$$H_\varphi = Z_1(k_r r) e^{ik_z z},$$

where

$$k_r^2 + k_z^2 = k^2$$

and $Z_1(k_r r)$, the first-order cylindrical function, is a linear superposition of Bessel and Neumann

[3] W. W. Hansen, J. App. Phys. **10**, 1 (1939).

* This choice of S is merely a matter of mathematical convenience. The variational method applied here can be applied also when S is chosen at $r=r_1$ as in Hansen's paper (see reference 3).

functions

$$Z_1(k_r r) = aJ_1(k_r r) + bN_1(k_r r),$$

a and b being constants of integrations. Using H_φ as a potential from which E_z and E_r can be derived according to (3) and (4), we can now impose the boundary condition that the tangential electric field shall vanish on all conducting surfaces, and thereby arrive at relations between a and b and between k_z and k from which simplified expressions for H_φ^{I} and H_φ^{II} can be written in closed form.

We start with region II, in which $b=0$ since the Neumann function is excluded because of its singularity at $r=0$. Further, the boundary condition $E_z=0$ at $r=r_2$ leads to $J_0(k_r^{\mathrm{II}} r_2)=0$. Hence, k_r^{II} can have any of the values j_n/r_2, where j_n is the n'th root of the zero-order Bessel function. In cavities of practical interest $kr_2 < j_1 = 2.405$, and, therefore, all the k_z^{II}'s are imaginary with

$$-(k_z^{\mathrm{II}})^2 = (j_n/r_2)^2 - k^2 = (k_n^{\mathrm{II}})^2, \quad k_n^{\mathrm{II}} \text{ real.} \quad (8)$$

We can thus express H_φ^{II} as

$$H_\varphi^{\mathrm{II}} = \sum A_n^{\mathrm{II}} \cosh k_n^{\mathrm{II}}(z+\epsilon^{\mathrm{II}}) J_1(j_n r/r_2). \quad (9)$$

Here the phase of the cosh term has been adjusted to make E_r zero on the wall at $z=-\epsilon^{\mathrm{II}}$.

In region I we find that in order for E_z to vanish at $r=r_1$ and $r=r_2$ we must have

$$Z_0(k_r^{\mathrm{I}} r_1) = 0 \quad \text{and} \quad Z_0(k_r^{\mathrm{I}} r_2) = 0.$$

From the latter two conditions we can, in the first place, solve for a/b so that we can write Z_1 as

$$Z_1(k_r^{\mathrm{I}} r) = -N_0(k_r^{\mathrm{I}} r_1) J_1(k_r^{\mathrm{I}} r) + J_0(k_r^{\mathrm{I}} r_1) N_1(k_r^{\mathrm{I}} r) \quad (10)$$

and secondly we find that k_r^{I} must satisfy

$$J_0(k_r^{\mathrm{I}} r_1) N_0(k_r^{\mathrm{I}} r_2) - N_0(k_r^{\mathrm{I}} r_1) J_0(k_r^{\mathrm{I}} r_2) = 0. \quad (11)$$

Introducing the notation $\zeta = k_r^{\mathrm{I}} r_2$ we rewrite (11):

$$J_0(\zeta r_1/r_2) N_0(\zeta) - N_0(\zeta r_1/r_2) J_0(\zeta) = 0. \quad (11')$$

The solutions $\zeta = \zeta_n$ of this equation are listed in Jahnke-Emde's[4] *Tables of Functions*. As ζ_n is always larger than the corresponding j_n, we again have imaginary k_z's or

$$-(k_z^{\mathrm{I}})^2 = (\zeta_n/r_2)^2 - k^2 = (k_n^{\mathrm{I}})^2, \quad k_n^{\mathrm{I}} \text{ real.} \quad (12)$$

In addition to the Z_1's listed in (10) the function $1/r$ is a solution for the case $k_r=0$ since it satisfies (1) and its boundary conditions. Thus the complete solution of (1) in region I is

$$H_\varphi^{\mathrm{I}} = A_0^{\mathrm{I}} \cos k(z-\epsilon^{\mathrm{I}})/r + \sum A_n^{\mathrm{I}} \cosh k_n^{\mathrm{I}}(z-\epsilon^{\mathrm{I}}) Z_1(\zeta_n r/r_2), \quad (13)$$

where the dependence on z has been so adjusted that E_r vanishes on the wall at $z=\epsilon^{\mathrm{I}}$.

We now define $\psi(r)$ by the relation

$$\psi(r)/r = \partial H_\varphi/\partial z = -ikE_r \quad \text{at} \quad z=0. \quad (14)$$

This is the ψ which appears in (7) as the unknown function. In solving (7) for the wave number k we shall obtain, as a by-product of the calculations, the dependence of ψ on r and hence the functional form of E_r.

Following the procedure outlined above we solve for the amplitude A_n as integrals of the tangential field (in this case E_r) on S. Substitution of (9) and (13) in (14) gives

$$\frac{\psi(r)}{r} = \sum A_n^{\mathrm{II}} k_n^{\mathrm{II}} \epsilon^{\mathrm{II}} J_1(j_n r/r_2), \quad (15)$$

$$\frac{\psi(r)}{r} = A_0^{\mathrm{I}} k \sin k\epsilon^{\mathrm{I}}/r - \sum A_n^{\mathrm{I}} k_n^{\mathrm{I}} \sinh k_n^{\mathrm{I}} \epsilon^{\mathrm{I}} Z_1(\zeta_n r/r_2). \quad (16)$$

To solve for A_m^{II} we multiply in (15) by $J_1(j_m r/r_2) r dr$ and integrate over S obtaining

$$A_m^{\mathrm{II}} = \frac{2k_m^{\mathrm{II}} \int_{r_1}^{r_2} J_1(j_m r'/r_2)\psi(r')dr'}{(k_m^{\mathrm{II}} r_2)^2 \sinh k_m^{\mathrm{II}} \epsilon^{\mathrm{II}} J_1^2(j_m)}. \quad (17)$$

[4] E. Jahnke and F. Emde, *Tables of Functions* (Dover Publications, New York, 1943), p. 205. The tables from which ζ_n can be obtained contain a number of errors. New and more accurate values were taken from tables by A. N. Lowan and A. Hillman, J. Math. Phys. **22** (Dec., 1943). These tables contain suitable information in the range $r_2/r_1 \leq 4$. For $r_2/r_1 > 4$ we calculated ζ_n's from asymptotic expansions quoted by Lowan and Hillman.

An analogous integration of (16) with $Z_1(\zeta_m r/r_2)rdr$ leads to

$$A_m^{\mathrm{I}}=\frac{-2k_m^{\mathrm{I}}\int_{r_1}^{r_2} Z_1(\zeta_m r'/r_2)\psi(r')dr'}{(k_m^{\mathrm{I}}r_2)^2\sinh k_m^{\mathrm{I}}\epsilon^{\mathrm{I}}[Z_1^2(\zeta_m)-(r_1/r_2)^2Z_1^2(\zeta_m r/r_2)]}. \tag{18}$$

The Z_1's in the denominator of (18) can be expressed in terms of J_0's[5] so that A_m^{I} becomes

$$A_m^{\mathrm{I}}=-\frac{\frac{\pi^2}{2}k_m^{\mathrm{I}}\zeta_m^2\int_{r_1}^{r_2} Z_1(\zeta_m r'/r_2)\psi(r')dr'}{(k_m^{\mathrm{I}}r_2)^2\sinh k_m^{\mathrm{I}}\epsilon^{\mathrm{I}}[(J_0(\zeta_m r_1/r_2)/J_0(\zeta_m))^2-1]}. \tag{18'}$$

Finally to obtain A_0^{I} we integrate (16) with $1/r\cdot rdr$ and get

$$A_0^{\mathrm{I}}=\int_{r_1}^{r_2}\frac{\psi(r')}{r'}dr'\Big/k\sin k\epsilon^{\mathrm{I}}\log\frac{r_2}{r_1}. \tag{19}$$

Having obtained the expressions for A_n we can formulate the boundary condition (5) as

$$H_\varphi^{\mathrm{I}}-H_\varphi^{\mathrm{II}}=0=\int_{r_1}^{r_2}\psi(r')G(r,r')dr', \tag{7'}$$

where

$$G(r,r')\equiv\frac{\cot k\epsilon^{\mathrm{I}}}{k\log r_2/r_1}\frac{1}{r}\frac{1}{r'}-\frac{\pi^2}{2}\sum\frac{k_n^{\mathrm{I}}\coth k_n^{\mathrm{I}}\epsilon^{\mathrm{I}}\zeta_n^2 Z_1(\zeta_n r/r_2)Z_1(\zeta_n r'/r_2)}{(k_n^{\mathrm{I}}r_2)^2[(J_0(\zeta_n r_1/r_2)/J_0(\zeta_n))^2-1]}$$
$$-2\sum\frac{k_n^{\mathrm{II}}\coth k_n^{\mathrm{II}}\epsilon^{\mathrm{II}}}{(k_n^{\mathrm{II}}r_2)^2J_1^2(j_n)}J_1(j_n r/r_2)J_1(j_n r'/r_2). \tag{20}$$

III. THE EQUIVALENT VARIATIONAL PROBLEM

The solution of the integral Eq. (7') is achieved by the solution of the equivalent variational problem, which we shall now proceed to formulate. We define

$$U=\int\int\frac{\psi(r)G'(r,r')\psi(r')drdr'}{\frac{\cot k\epsilon^{\mathrm{I}}}{k\log r_2/r_1}\int\int\frac{\psi(r)}{r}\frac{\psi(r')}{r'}drdr'}, \tag{21}$$

where

$$G'(r,r')=\frac{\cot k\epsilon^{\mathrm{I}}}{k\log r_2/r_1}\frac{1}{r}\frac{1}{r'}-G(r,r')$$

and all the integrations extend, as in the subsequent expressions where the limits are omitted, from r_1 to r_2. The two equations

$$U=1 \tag{22}$$

and

$$\delta U=0, \tag{23}$$

where δU is the variation in U arising from an arbitrary variation $\delta\psi$ of ψ, then constitute a variational problem equivalent to (7').

[5] G. N. Watson, *Theory of Bessel Functions* (Cambridge, 1922), p. 76.

To prove this equivalence we perform the variation

$$\delta U=\frac{2\int\delta\psi(r)dr}{\int\int\frac{\cot k\epsilon^{\mathrm{I}}}{k\log r_2/r_1}\frac{\psi(r)}{r}\frac{\psi(r')}{r'}drdr'}\left[\int G'(r,r')\psi(r')dr'\right.$$

$$\left.-\frac{\int\int\psi(r)G'(r,r')\psi(r')drdr'\int\frac{\cot k\epsilon^{\mathrm{I}}}{k\log r_2/r_1}\frac{\psi(r')dr'}{rr'}}{\int\int\frac{\cot k\epsilon^{\mathrm{I}}}{k\log r_2/r_1}\frac{\psi(r)}{r}\frac{\psi(r')}{r'}drdr'}\right]=0.$$

Since $\delta\psi$ is arbitrary, the bracketed quantity must vanish; or, in view of (21)

$$\int G'(r,r')\psi(r')dr'-U\int\frac{\cot k\epsilon^{\mathrm{I}}}{k\log r_2/r_1}\frac{\psi(r')}{rr'}dr'=0 \tag{23'}$$

which, for $U=1$, is identical with (7').

IV. PROPERTIES OF THE SOLUTION

The theory of integral equations asserts that the solution of (23) (or its equivalent (23')) is in general an infinite set of eigenfunctions ψ_n which belong to corresponding terms of a set of eigenvalues U_n of U. Owing to the particular form of $G'(r,r')$ a number of special features of the solution, outlined below in (a), (b), and (c), can be proved.[1] These features serve to guide us in the application of approximate methods for solving (23).

For specified values of ϵ^{I}, ϵ^{II}, r_1, r_2, and k in the range

$$kr_2<j_1=2.405,\quad k\epsilon^{\mathrm{I}}<\pi/2, \tag{24}$$

the following theorems hold:

(a) There exist only one eigenvalue (denoted by U_0) and one corresponding eigenfunction (denoted by ψ_0) which satisfy (23).

(b) Equation (22) with $U=U_0$, that is $U_0=1$, constitutes an equation among the five parameters from which ϵ^{I} can be evaluated uniquely when the other four are specified. (The value of ϵ^{I} so obtained will be denoted by $\epsilon_0{}^{\mathrm{I}}$.)

(c) The value of ϵ^{I} obtained from (22) with an arbitrary ψ cannot exceed $\epsilon_0{}^{\mathrm{I}}$; i.e., $\epsilon^{\mathrm{I}}\leq\epsilon_0{}^{\mathrm{I}}$.

In view of (c) we may expect that[6] if we find a sequence of ψ's such that the corresponding ϵ^{I}'s form a monotonically increasing series, the limit of this series is $\epsilon_0{}^{\mathrm{I}}$.

[6] R. Courant and D. Hilbert, *Methoden der Mathematischen Physik* (Interscience Publishers, Inc., New York, 1943), Vol. 1, p. 146.

V. THE RITZ VARIATIONAL METHOD

In this section we describe the Ritz procedure by which an approximate solution of (22) and (23) can be obtained. We select n functions $\psi_j(r)$ each of which can be made to satisfy the boundary conditions on $\psi(r)$ and set up

$$\psi(r)=\sum_{j=1}^{n}\alpha_j\psi_j(r). \tag{25}$$

Variations in ψ are now effected by variations in α_j. With (25) substituted in (22) and (23) we can determine α_j and solve for ϵ^{I} as a function of ϵ^{II}, r_1, r_2 and k.

In using (25) we find the following notation convenient:

$$G_{ij}=\int\int\psi_i(r)G'(r,r')\psi_j(r')drdr'=G_{ji},$$

$$I_{ij}=\frac{\cot k\epsilon^{\mathrm{I}}}{k\log(r_2/r_1)}\int\int\frac{\psi_i(r)}{r}\frac{\psi_j(r')}{r'}drdr'=I_{ji}.$$

With these formulas we convert (22) and (23) into

$$\frac{\sum_i\sum_j\alpha_i\alpha_jG_{ij}}{\sum_i\sum_j\alpha_i\alpha_jI_{ij}}=1$$

and

$$\delta\frac{\sum_i\sum_j\alpha_i\alpha_jG_{ij}}{\sum_i\sum_j\alpha_i\alpha_jI_{ij}}=0,\quad i,j=1,2\cdots n,$$

respectively. The variation is performed on α; giving

$$\frac{2\sum_j\delta\alpha_j}{\sum_i\sum_j\alpha_i\alpha_jI_{ij}}\Big[\sum_i\alpha_iG_{ij}-\sum_i\alpha_iI_{ij}\frac{\sum_i\sum_j\alpha_i\alpha_jG_{ij}}{\sum_i\sum_j\alpha_i\alpha_jI_{ij}}\Big]=0.$$

As the $\delta\alpha_j$'s are arbitrary, the bracketed term must vanish; or, after simplification,

$$\sum_{i=1}^{n}\alpha_i(G_{ij}-I_{ij})=0;\quad j=1,2\cdots n.$$

This system of n linear equations for the $n\alpha_i$'s has a non-trivial solution if, and only if, the determinant formed from the coefficients of the α_i's vanishes;

$$\begin{vmatrix}G_{11}-I_{11} & G_{12}-I_{12} & \cdots\\ G_{21}-I_{21} & G_{22}-I_{22} & \cdots\\ \cdots & \cdots & \end{vmatrix}\equiv 0. \tag{26}$$

This expression constitutes a transcendental equation from which it is possible to solve for ϵ^{I} when the other four parameters are specified.

VI. THE CHOICE OF Ψ'S

In choosing suitable ψ_j's, we take into account the behavior of the correct solution ψ_0 and its derivatives on S. Thus as $r=r_2$, we must have $E_z\to 0$ and hence from (14) and

$$\operatorname{div}E=\frac{\partial}{\partial r}rE_r+r\frac{\partial E_z}{\partial z}=0,$$

it follows that

$$\partial\psi_0/\partial r=0\quad\text{at}\quad r=r_2. \tag{27a}$$

When $r\to r_1$, $E_r\to\infty$ as $(r-r_1)^{-\frac{1}{3}}$ so that we have

$$\psi_0(r)\propto(r-r_1)^{-1/3},$$
$$\partial\psi_0/\partial r\propto(r-r_1)^{-4/3},\quad\text{as } r\to r_1. \tag{27b}$$

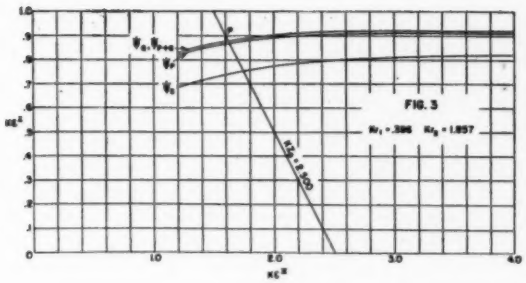

FIG. 3.

Finally, from the analogous two-dimensional case it is to be expected that

$$\partial^2\psi_0/\partial r^2>0\text{ on }S. \tag{27c}$$

Now, we seek a set of ψ_j's which can be combined according to (25) to make ψ behave approximately as ψ_0. A vital property of our ψ_j's must be, however, that they permit the evaluation of the integrals for G_{ij} and I_{ij}. The question of this integrability is important enough to warrant the relaxation of some of the conditions in (27) in order that a practical set of ψ_j's be found.

After a number of trials it was found that a family of ψ_j's which can be made to agree satisfactorily with conditions (27) and also permit evaluation of $G_{ij}-I_{ij}$ without undue difficulty consists of power series in r. The basic ψ_n's considered in this family are

$\psi_c=1$, a constant,

$\psi_p=\alpha_1+\alpha_2[(r-r_2)^2-a_p]$, a parabolic ψ_n,

$\psi_q=\alpha_1'+\alpha_3'[(r-r_2)^4-a_q]$, a quartic ψ_n,

and

$$\psi_{p+q}=\alpha_1''+\alpha_2''[(r-r_2)^2-a_p]+\alpha_3''[(r-r_2)^4-a_q],$$

a superposition of parabolic and quartic ψ_n's. The constants a_p and a_q are determined from

$$\int\frac{(r-r_2)^2-a_p}{r}dr=\int\frac{(r-r_2)^4-a_q}{r}dr\equiv 0,$$

which will insure that all the I_{ij}'s vanish except

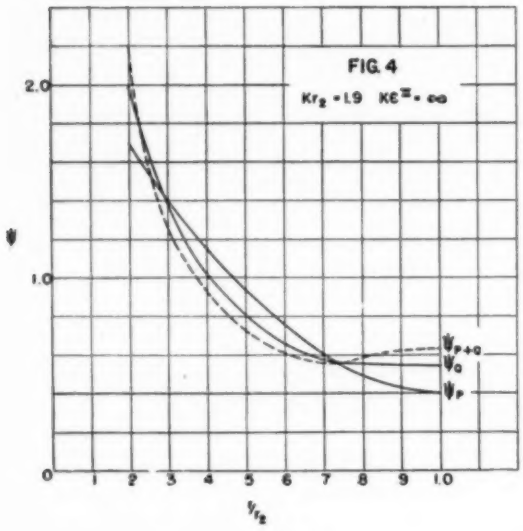

FIG. 4.

I_{11}. For ψ_c the determinantal equation reduces to

$$G_{11}-I_{11}=0 \qquad (26')$$

from which values of $k\epsilon^{I}$ as function of $k\epsilon^{II}$ with fixed kr_1 and kr_2 have been calculated (Fig. 3). In view of more accurate* final curves, the value of $k\epsilon^{I}$ thus obtained is about 10 percent below $k\epsilon_0{}^{I}$.

Considerable improvement over the ψ_c curve is obtained by use of the parabolic ψ_p, which leads to the determinantal equation

$$\begin{vmatrix} G_{11}-I_{11} & G_{12} \\ G_{21} & G_{22} \end{vmatrix} = 0. \qquad (26'')$$

Further increase in the calculated value of $k\epsilon^{I}$ is obtained by use of ψ_q. When the more general ψ_{p+q} is employed, there is no appreciable increase in $k\epsilon^{I}$ over the result with ψ_q, as shown in Fig. 3. The convergence of the Ritz process illustrated in Fig. 3 indicates that ψ_q is sufficiently good for the calculation of characteristics of the nosed-in resonator, and therefore this function was employed in preference to more general functions, with which the numerical work becomes exceedingly laborious without compensating gain in accuracy. The calculations with ψ_q are given in greater detail in the next section.

The experimental check on these curves was obtained at the Westinghouse Research Laboratories. The resonator of total height $kz_0=k(\epsilon^{I}+\epsilon^{II})=2.5$ having $k\epsilon^{I}$ and $k\epsilon^{II}$ corresponding to point P on Fig. 3 shows an agreement within 2.5 percent of the calculated value. Further measurements at the Bloomfield Division of Westinghouse Electric Corporation led to similar agreement, the experimental values of $k\epsilon^{I}$ lying about 2.5 percent above the calculated curves. The disagreement is ascribed to the deviation of the actual cavity from that treated by the theory. Instead of the smooth top shown in Figs. 1 and 2 the actual cavity is provided with a corrugated diaphragm (to permit tuning).

The radial variation of ψ_p, ψ_q, and ψ_{p+q} is illustrated in Fig. 4. It is to be noted that (27b) is not satisfied by these ψ's, but this does not result in serious trouble because the infinity of ψ_0 at $r=r_1$ is integrable.

VII. SUMMARY OF PROCEDURE AND RESULTS

A practical set of ψ_n's consists of the two functions

$$\psi_1=\psi_c=1 \quad \text{and} \quad \psi_3=\psi_q=(r-r_2)^4-a_q,$$

where the constant a_q, defined by

$$\int_{r_1}^{r_2} \psi_q dr/r=0,$$

is

$$a_q=r_2{}^4\frac{12\log r_2/r_1-25+48(r_1/r_2)-36(r_1/r_2)^2+16(r_1/r_2)^3-3(r_1/r_2)^4}{12\log r_2/r_1}.$$

From the definitions of I_{11} and G_{ij} we are led to the following formulas for these terms:

$$I_{11}=r_2\frac{\log r_2/r_1}{kr_2}\cot k\epsilon^{I},$$

* Since from (c) in Section IV $\epsilon_0{}^{I}$ is the upper limit of the ϵ^{I} that can be calculated from an arbitrary ψ, the highest curve on Fig. 3 is the most accurate.

$$G_{11}=2r_2\sum\frac{\coth k_n^{II}\epsilon^{II}}{(k_n^{II}r_2)}\frac{1}{j_n^2}\frac{J_0^2(j_nr_1/r_2)}{J_1^2(j_n)},$$

$$G_{13}=8r_2^5\sum\frac{\coth k_n^{II}\epsilon^{II}J_0(j_nr_1/r_2)}{(k_n^{II}r_2)j_n^2J_1^2(j_n)}E_{3n}^{II}(r_1/r_2)=G_{31},$$

$$G_{33}=32r_2^9\left\{\sum\frac{\coth k_n^{I}\epsilon^{I}[E_{3n}^{I}(r_1/r_2)]^2}{(k_n^{I}r_2)\zeta_n^2\left[\left(\frac{J_0(\zeta_nr_1/r_2)}{J_0(\zeta_n)}\right)^2-1\right]}+\sum\frac{\coth k_n^{II}\epsilon^{II}[E_{3n}^{II}(r_1/r_2)]^2}{(k_n^{II}r_2)j_n^2J_1^2(j_n)}\right\}.$$

In these formulas the E's, which are functions only of the ratio r_1/r_2 are defined by

$$E_{3n}^{I}=\frac{J_0(\zeta_nr_1/r_2)}{J_0(\zeta_n)}[1/\zeta_n-4/\zeta_n^3-\frac{\pi}{2}H_0(\zeta_n)(1-3/\zeta_n^2)]$$
$$-[(3-3r_1/r_2+(r_1/r_2)^2)/\zeta_n-4/\zeta_n^3-\frac{\pi}{2}H_0(\zeta_nr_1/r_2)(1-3/\zeta_n^2)],$$

$$E_{3n}^{II}=J_1(j_n)[1/j_n-4/j_n^3-\frac{\pi}{2}H_0(j_n)(1-3/j_n^2)]$$
$$-r_1/r_2J_1(j_nr_1/r_2)\left[(3-3r_1/r_2+(r_1/r_2)^2)\Big/j_n-4/j_n^3-\frac{\pi}{2}H_0(j_nr_1/r_2)(1-3/j_n^2)\right]$$
$$+r_1/r_2J_0(j_nr_1/r_2)\left[\left(-\frac{2}{j_n^2}+\frac{3}{2}\right)(r_1/r_2)-(r_1/r_2)^2+\tfrac{1}{4}(r_1/r_2)^3\right.$$
$$\left.+\frac{(1-a_q/r_2^4)}{4r_1/r_2}-\frac{\pi}{2}H_1(j_nr_1/r_2)(1-3/j_n^2)\right],$$

where the H_0 and H_1 are the zero and first-order Struve functions, respectively. Next we set up the determinantal equation

$$\begin{vmatrix}G_{11}-I_{11} & G_{13}\\ G_{31} & G_{33}\end{vmatrix}=0, \qquad (26''')$$

which connects the wave number k and the geometric parameters ϵ^I, ϵ^{II}, r_1, and r_2. If, now, k is assigned, this equation can be solved for ϵ^I when the other three parameters are specified provided that $kr_2<j_1=2.405$.

It is convenient to fix the value of r_1/r_2 and let $k\epsilon^{II}$ assume an arbitrary set of values corresponding to which $k\epsilon^I$ is determined by (26'''). Expanding the latter into

$$I_{11}=G_{11}-G_{13}^2/G_{33}, \qquad (28)$$

we note that $k\epsilon^I$ appears on the left in I_{11} and $k_n^I\epsilon^I$ on the right in G_{13}, which, however, is not very sensitive to variations in ϵ^I. We can thus first obtain $k\epsilon^I$ approximately from $I_{11}=G_{11}$, calculate from (12)

$$\coth k_n^I\epsilon^I=\coth k\epsilon^I[\zeta_n^2/(kr_2)^2-1]^{\frac{1}{2}}$$

and substitute this in G_{13}. It turns out that only $\coth k_1^I\epsilon^I$ need be calculated in this manner because for $n>1$ $\coth k_n^I\epsilon^I\approx1$. Similarly, we have from (8) $\coth k_1^{II}\epsilon^{II}=\coth k\epsilon^{II}[j_1^2/(kr_2)^2-1]^{\frac{1}{2}}$ and for $n>1$ $\coth k_n^{II}\epsilon^{II}\approx1$.* With these expressions for the coth's the summations in the right member of (28) are readily performed up to a

* In order for this approximation to hold $k\epsilon^{II}$ must not be taken much smaller than unity.

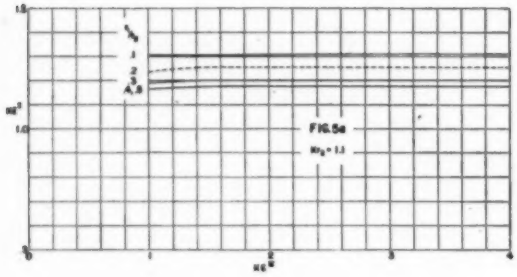

FIG. 5a.

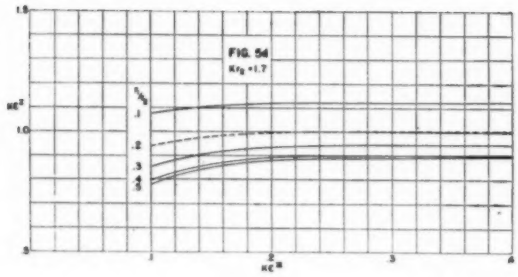

FIG. 5d.

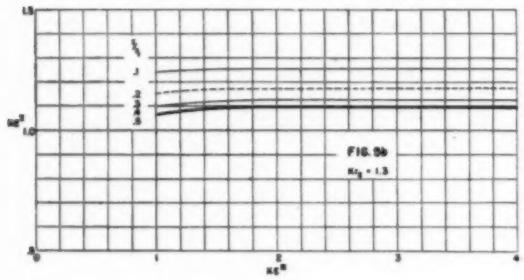

FIG. 5b.

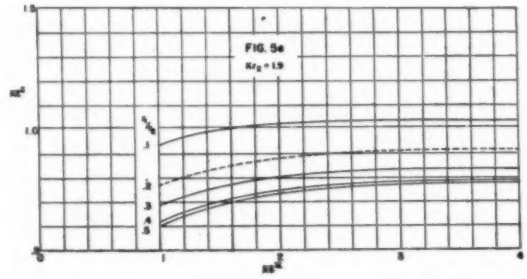

FIG. 5e.

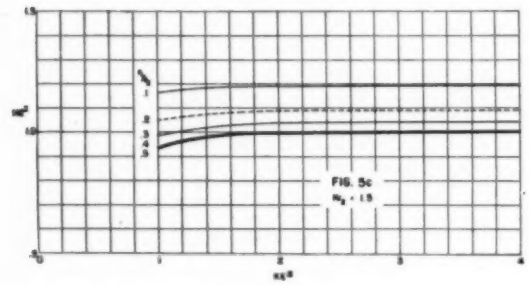

FIG. 5c.

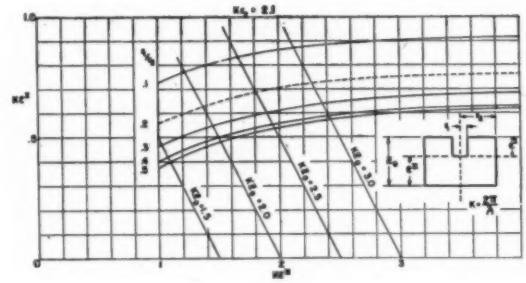

FIG. 5f.

number of terms N which depends on the accuracy desired. The number N increases as the ratio r_1/r_2 is taken smaller.

With $k\epsilon^{II} \geq 1$ as the independent variable the full-lined curves in Figs. 5a–f were calculated giving $k\epsilon^{I}$ for the following fixed values of the other parameters: $r_1/r_2 = .1, .3, .4, .5$; $kr_2 = 1.1, 1.3, 1.5, 1.7, 1.9, 2.1$. A precision of 1 percent was obtained with five terms in the summations deriving from region I and seven terms in the summations from region II.

By drawing on Fig. 5 the straight lines $kz_0 = \text{constant}$ (shown only on Fig. 5f) and taking the intersections of the latter with the $k\epsilon^{I}$ curves corresponding to the values of r_1/r_2 we obtain the points from which we plot Fig. 6a–f giving $k\epsilon^{I}$ *vs.* r_1/r_2 for fixed total heights kz_0. On these curves the ordinate and the slope at $r_1/r_2 = 0$ are obtained directly from (28) as limiting values for $kr_1 \to 0$ are taken. We can write

$$\lim_{kr_1 \to 0} \cot k\epsilon^{I} = \frac{f(r_1/r_2)}{\log r_2/r_1},$$

where $f(r_1/r_2)$ is a function which remains finite, and hence

$$k\epsilon^{I} \to \pi/2 - \frac{f(r_1/r_2)}{\log r_2/r_1},$$

with the slopes becoming infinite as $r_2/r_1 \log r_2/r_1$.

From Figs. 6a–f we can now read the ordinates

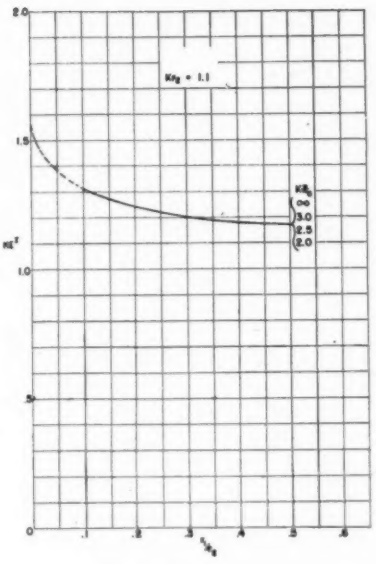

FIG. 6a.

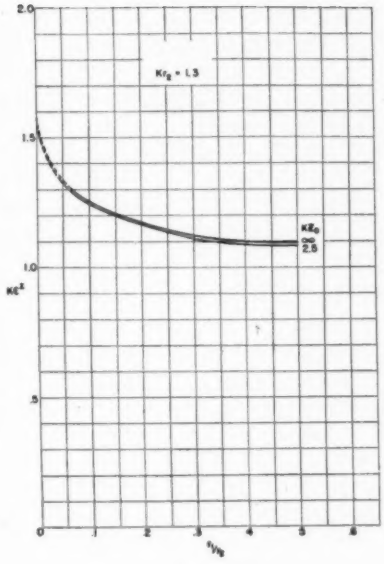

FIG. 6b.

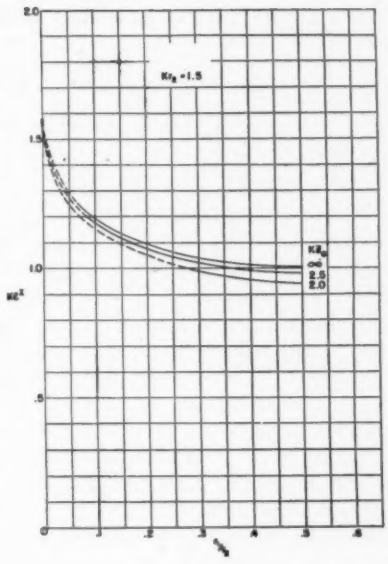

FIG. 6c.

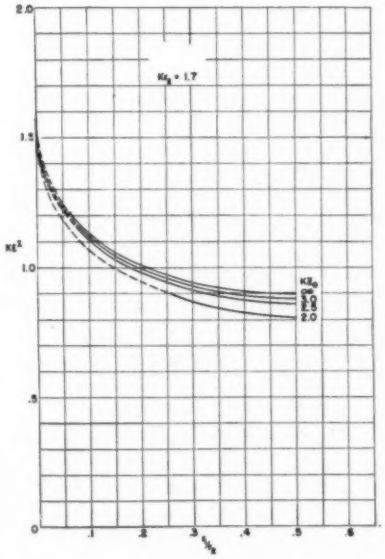

FIG. 6d.

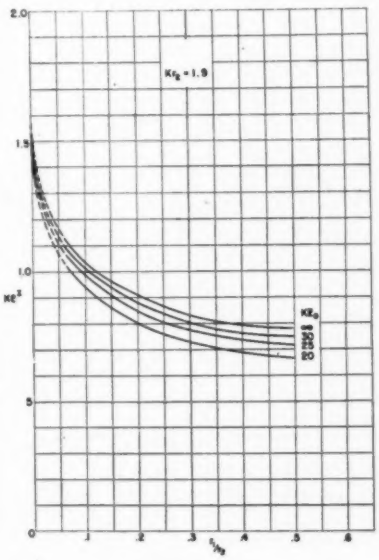

FIG. 6e.

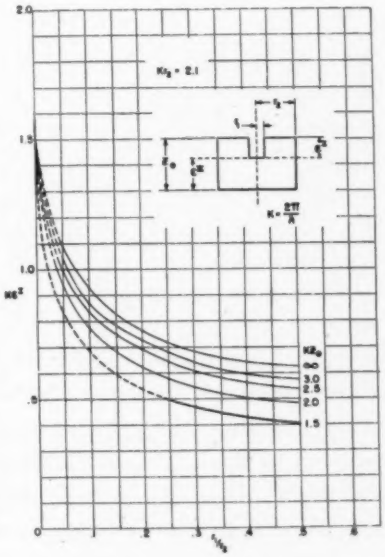

FIG. 6f.

for other values of r_1/r_2 and obtain by interpolation curves for $k\epsilon^{I}$ *vs.* $k\epsilon^{II}$. On 5a–f the curves for $r_1/r_2=.2$, indicated by the dotted lines were plotted in this manner. A check was obtained on the interpolation by a direct calculation for $kr_2=1.9$.

The Study of a Certain Type of Resonant Cavity and Its Application to a Charged Particle Accelerator

E. S. Akeley
Department of Physics, Purdue University, Lafayette, Indiana
(Received November 20, 1945)

A linear accelerator for charged particles, consisting of a number of cavity resonators placed end to end with the inside end plates removed, and thus forming a wave guide with two closed ends, is discussed. The shape of each section must be so chosen that the velocity of the particle will correspond to the phase velocity of the radiation of the cavity. In order to determine possible shapes for the cavity, the stationary TM_{01} modes between two parallel conducting planes are determined. In Part 1, excitation of a single mode is discussed, including the shape of the conducting surface that can be used to connect the planes and thus form a cavity. Three cases are considered—when the phase velocity in the cavity is greater than, equal to, and less than that of light. If only one mode is excited, and the phase velocity is not greater than that of light, then the radius of the cavity becomes infinite at the two plates. In Part 2, the simultaneous excitation of two modes is considered. The phase velocity of one mode is that of light; the other has a phase velocity $1/n$ that of light, where n is an odd integer. The cavity can be made finite by a suitable choice of the relative amplitude of the two modes, and the radius of one end of the cavity. This requires a rather elaborate discussion. This case is of particular interest for the acceleration of electrons. It is shown, furthermore, that only the first mode contributes to the acceleration of the electron. In Section 4, the application of the methods used in Part 3 to the case of an accelerator for heavy particles is touched upon.

INTRODUCTION

IN the electron accelerator patented by W. W. Hansen in 1937, energy is imparted to an electron by letting it pass a number of times through a cavity resonator. J. R. Woodyard[1] thought of modifying this arrangement by placing a number of such resonators end to end and removing their inside end plates. He showed that it should be possible in this way to produce electrons of many hundred million volts electron energy. The shape of the cavity in such an accelerator must be such that the phase velocity of the radiation along the axis corresponds to the velocity of the electrons. Furthermore, the shape should be chosen to give as small as possible a rate of dissipation of energy caused by the finite conductivity of the walls of the cavity. This paper is concerned with the first of these two problems.

PART 1

If one stipulates rotational symmetry relative to an axis, and a finite field on this axis, the stationary TM_{01} modes for the region between two infinite parallel planes of infinite conductivity are of the form

$$E_z=\cos h_n z J_0[(k^2-h_n^2)^{\frac{1}{2}}r],$$
$$H_\phi=\cos h_n z \frac{J_1[(k^2-h_n^2)^{\frac{1}{2}}r]}{(k^2-h^2)^{\frac{1}{2}}}, \qquad (1\text{-}1)$$
$$E_r=h_n \sin h_n z \frac{J_1[(k^2-h_n^2)^{\frac{1}{2}}r]}{(k^2-h_n^2)^{\frac{1}{2}}},$$

with $h=n\pi/L$, where n is a positive integer and L the distance between the plates. (z, r, ϕ) are cylindrical coordinates, z being the distance along the axis, r the perpendicular distance from the axis, and ϕ the azimuth. $Ee^{+i\omega t}$ and $He^{+i\omega t}$ are the electric and magnetic field strengths, respectively. h_n is 2π divided by the wave-length in the guide, and k is 2π divided by the wave-length of radiation of the same frequency in space. Each n defines a mode, and these modes can exist independently. However, if the planes are connected by a surface of revolution of infinite conductivity, the relative intensity of the modes excited will be determined by the requirement that the tangential component of E and the normal component of H are zero on the surface, whose differential equation is

$$E_z dz+E_r dr=0. \qquad (1\text{-}2)$$

This equation states that E is normal to the surface. The requirement that H be tangential to the surface is automatically satisfied as H_ϕ is

[1] Private communication, to be published soon.

the only component of H different from zero. First, let us determine the shape of the bounding surface required for the excitation of a single mode. It is convenient to introduce the notation $hz=x$ and $hr=y$ which normalizes the unit of distance relatively to the wave-length. Also let $y_c=y(\pi/2)$ and $y_0=y(0)$. There are three cases to consider:

Case 1. $k^2>h^2$.

$$E_z=\cos x J_0\left[\left(\frac{k^2}{h^2}-1\right)^{\frac{1}{2}}y\right],$$
$$E_r=\frac{h\sin x}{(k^2-h^2)^{\frac{1}{2}}}J_1\left[\left(\frac{k^2}{h^2}-1\right)^{\frac{1}{2}}y\right], \tag{1-3}$$

and

$$J_0\left[\left(\frac{k^2}{h^2}-1\right)^{\frac{1}{2}}y\right]=J_0\left[\left(\frac{k^2}{h^2}-1\right)^{\frac{1}{2}}y_c\right][\sin x]^{h^2/k^2-h^2} \tag{1-4}$$

as the equation of the bounding surface. From (1-4) it follows that

$$J_0\left[\left(\frac{k^2}{h^2}-1\right)^{\frac{1}{2}}y_0\right]=0.$$

There are two cases to be considered:

(a) $J_0\left[\left(\frac{k^2}{h^2}-1\right)^{\frac{1}{2}}y_c\right]=0$, so that $y=y_c(x)$. This is the ordinary cylindrical cavity resonator oscillating in the TM_{01} mode.

(b) $J_0\left[\left(\frac{k^2}{h^2}-1\right)^{\frac{1}{2}}y_c\right]\neq 0$, where y is no longer constant but variable as determined by Eq. (1-4).

Cases (a) and (b) represent the same mode of oscillation, only the bounding surface is different.

Case 2. $k^2<h^2$.

$$E_z=\cos x I_0\left[\left(1-\frac{k^2}{h^2}\right)^{\frac{1}{2}}y\right],$$
$$E_r=\frac{h\sin x}{(h^2-k^2)^{\frac{1}{2}}}I_1\left[\left(1-\frac{k^2}{h^2}\right)^{\frac{1}{2}}y\right] \tag{1-5}$$

with the equation

$$I_0\left[\left(1-\frac{k^2}{h^2}\right)^{\frac{1}{2}}y\right]=I_0\left[\left(1-\frac{k^2}{h^2}\right)^{\frac{1}{2}}y_c\right][\sin x]^{-h^2/h^2-k^2} \tag{1-6}$$

for the bounding surface.

Case 3.

$$k^2=h^2,\quad E_z=\cos x,\quad E_r=\frac{y}{2}\sin x, \tag{1-7}$$

with the equation

$$y^2=y_c^2-4\log\sin x \tag{1-8}$$

for the bounding surface.

Case 1 cannot be used for a particle accelerator as the phase velocity is greater than that of light. Case 2 is of interest for particle accelerators in general, as the phase velocity is less than that of light. Case 3 is of particular interest for an electron accelerator after the electron has an energy of more than 10^6 electron volts, when it is moving very nearly with the velocity of light. It is to be noted that only in the first case is the surface finite in size. In all cases of interest for a particle accelerator, the radius of the surface becomes infinite at the two conducting planes. In Part 2, it will be shown for Case 3 above that the addition of another mode, if properly chosen, will give a surface of finite radius.

PART 2

Cavities Suitable of High Velocity Electrons

We shall now consider the simultaneous excitation of two modes, $h_1=k$ and $h_n=nk$, when n is an odd integer. (If n were even, an unsymmetry would be introduced into the shape of the cavity, and it would not be possible to remove the infinity at both ends.) y_0 finite requires that $E_z=0$ at the point of contact of the surface and plane. This condition determines the relative intensity of the two modes, and one finds

$$E_z=\cos x-\frac{I_0[(n^2-1)^{\frac{1}{2}}y]}{I_0[(n^2-1)^{\frac{1}{2}}y_0]}\cos nx,$$
$$E_r=\frac{y}{2}\sin x-\frac{n}{(n^2-1)^{\frac{1}{2}}}\frac{I_1[(n^2-1)^{\frac{1}{2}}y]}{I_0[(n^2-1)^{\frac{1}{2}}y_0]}\sin nx, \tag{2-1}$$
$$dy/dx=-E_z/E_r. \tag{2-2}$$

An integral of this differential equation for the bounding surface has not yet been obtained. Computations by numerical integration are in progress. However, certain characteristics of the solution can be deduced. For this purpose, the following results are of importance:

(a) $$\left.\frac{1}{x}\frac{dy}{dx}\right|_{x=0} = \frac{1-n^2}{y_0 - \dfrac{(3n^2-1)I_1[(n^2-1)^{\frac{1}{2}}y_0]}{(n^2-1)^{\frac{1}{2}}I_0[(n^2-1)^{\frac{1}{2}}y_0]}}. \quad (2\text{-}3)$$

Therefore, the surface meets the planes at right angles, and the curve $y(x)$ makes parabolic contact with the line $y=y_0$.

(b) $$\left.\frac{1}{\left(\frac{\pi}{2}-x\right)}\frac{dy}{dx}\right|_{x=\pi/2} = -\frac{n+1}{\dfrac{y_c}{2}+\dfrac{n}{(n^2-1)^{\frac{1}{2}}}\dfrac{I_1[(n^2-1)^{\frac{1}{2}}y_c]}{I_0[(n^2-1)^{\frac{1}{2}}y_0]}}. \quad (2\text{-}4)$$

Therefore the curve $y(x)$ makes parabolic contact with the line $y=y_c$ and is convex toward the x axis at $x=\pi/2$.

(c) Let Y_1 be the value of y for which

$$(E_r/x)_{x=0}=0. \quad (2\text{-}5)$$

Then Y_1 satisfies the transcendental equation

$$Y_1=\frac{2n^2}{(n^2-1)^{\frac{1}{2}}}\frac{I_1[(n^2-1)^{\frac{1}{2}}Y_1]}{I_0[(n^2-1)^{\frac{1}{2}}Y_1]}. \quad (2\text{-}6)$$

Also let Y_2 be the value of y for which

$$\left.\frac{1}{x}\frac{dy}{dx}\right|_{x=0}=0. \quad (2\text{-}7)$$

Y_2 satisfies the transcendental equation

$$Y_2=\frac{3n^2-1}{(n^2-1)^{\frac{1}{2}}}\frac{I_1[(n^2-1)^{\frac{1}{2}}Y_2]}{[I_0(n^2-1)^{\frac{1}{2}}Y_2]}. \quad (2\text{-}8)$$

It is quite easy to compute Y_1 and Y_2 for any n by successive approximation, and to show that $Y_2>Y_1$ and that both Y_1 and Y_2 increase monotonically with n.

(d) The values of (x, y) for which $E_z=0$ are given by the equation

$$1=\frac{I_0[(n^2-1)^{\frac{1}{2}}y]}{[I_0(n^2-1)^{\frac{1}{2}}y_0]}\frac{\cos nx}{\cos x}. \quad (2\text{-}9)$$

Now since $\cos nx/\cos x$ decreases monotonically from 1 to 0 as x increases from 0 to $\pi/2n$, it follows that y increases monotonically from y_0 to ∞ in this interval, while the interval $\pi/2n < x < \pi/n$, Eq. (2-9) is not satisfied by any real value of y.

Another relation that is easily verified is that $y_0=Y_1$ is the point where curvature of $y(x)$ is equal to the curvature of (2-9). Furthermore, for $y_0<Y_1$, $y(x)$ lies below (2-9) in the neighborhood of $x=0$, while for $y_0>Y$, $y(x)$ lies above (2-9) in the same neighborhood.

(e) The values of (x, y) for which $E_r=0$ are given as solutions of

$$y_1=\frac{2n}{(n^2-1)^{\frac{1}{2}}}\frac{I_1[(n^2-1)^{\frac{1}{2}}y]}{I_0[(n^2-1)^{\frac{1}{2}}y_0]}\frac{\sin nx}{\sin x}. \quad (2\text{-}10)$$

One can deduce:

(1) If $x=0$ and $y_0=Y_1$, then $y_1=Y_1$.

(2) $\left.\dfrac{dy}{dx}\right|_{\substack{E_r=0\\ x=0}} > 1$. Therefore if $y_0<Y_1$ then $y_1(0)<y_0<Y_1$, and if $y_0>Y_1$, then $y_1(0)>y_0>Y_1$.

(3) As $(\sin nx)/(\sin x)$ decreases monotonically from n to 0 in the interval from 0 to π/n, it follows that y_1 increases monotonically from a given value $y_1(0)$ to ∞ in the same interval.

Making use of the relationships contained in paragraphs (a), (b), (c), (d), and (e), it is now possible to discuss the character of the curves for various values of y_0. In particular, it is possible to show, for certain values of y_0, that $y(x)$ either becomes infinite or multiple valued at some point. The curves, for which this occurs, are of no interest for a particle accelerator. Therefore, as soon as it is found that a curve has such a characteristic, that curve is not discussed any further. We now discuss separately three cases:

Case $y_0<Y_1$. Figure 1 shows graphically the relationships of y_0, Y_1, and the curves $E_r=0$ and $E_z=0$ for this case where (1) $y_1(0)<y_0<Y_1$, (2) $y(x)$ lies below $E_z=0$ in the neighborhood of

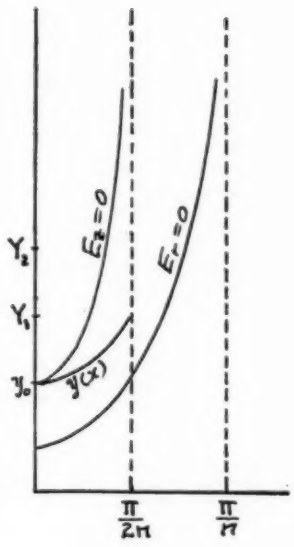

FIG. 1.

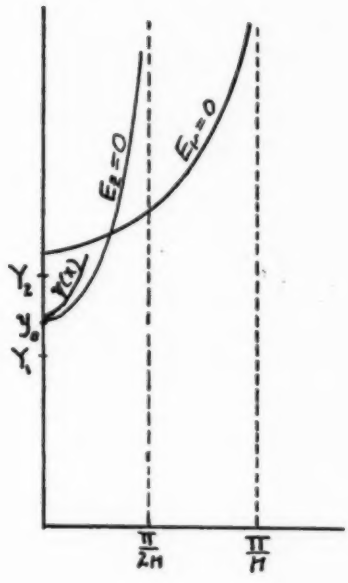

FIG. 2.

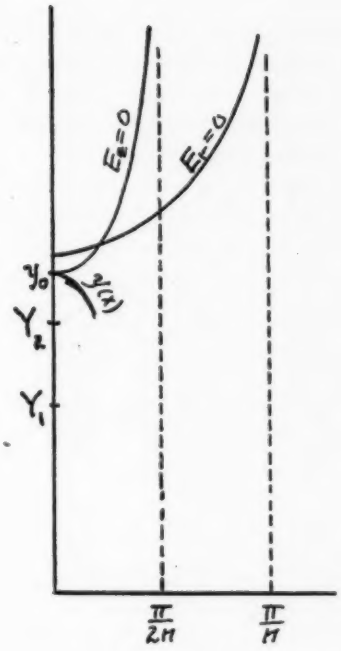

FIG. 3.

$x=0$, and (3) dy/dx is positive in the neighborhood of $x=0$. Now as x increases, dy/dx cannot change sign unless it touches one of the curves $E_z=0$ or $E_r=0$. Now, if it should meet $E_z=0$, it must be horizontal at the point of contact, and that is only possible if $y(x)$ bends backward into a region of negative slope, forming a curve that would not be useful. If it does not meet $E_z=0$, then it must meet $E_r=0$, and if so it must meet the latter tangentially and with infinite slope. This can only occur at $x=\pi/n$. Therefore, $y(\pi/n)=\infty$. Therefore, this case is excluded, not having further interest for us.

Case $Y_1<y_0<Y_2$. Figure 2 shows graphically the relationships of the quantities involved. Here $y_1>y_0>Y_1$, $y(x)$ lies above $E_z=0$ in the neighborhood of $x=0$, and dy/dx is positive in the same neighborhood. If $y(x)$ should meet $E_r=0$, $dy/dx=\infty$ at contact, and the slope would become negative on crossing this curve. The curve would then bend back toward the y axis. If $y(x)$ does not do this, it must meet $E_r=0$. Then $dy/dx=0$ on crossing, and it will then pass into region of negative slope. There is a possibility that this case would be interesting from the accelerator. If so, it would probably occur for y_0 very slightly greater than Y_1. A numerical integration will be performed to determine this point.

Case $y_0>Y_2$. Figure 3 shows the qualitative relationships for this case. The chief difference from the previous case is that dy/dx is negative near $x=0$. It will continue to have a negative slope as x increases until it reaches the line $x=\pi/2$, where it will have zero slope, unless it touches one of the lines $E_z=0$ or $E_r=0$. If it does not meet one of these lines, it would be a suitable shape for a cavity, in the latter case probably not. It would seem to be very difficult to determine necessary and sufficient conditions for obtaining a suitable curve in this case. However, such curves must exist. If y_0 is chosen only slightly greater than Y_2, $y(x)$ will have a large negative slope. After y has diminished about four units in value, the shape of the curve for greater values of x, would be very close to the type (1-8), and will therefore behave properly. On the other hand, if y_0 is much greater than Y_2, then the curve will start out flatter, and it may meet parts of the graphs of $E_r=0$ or $E_r=0$, in regions where $x>\pi/n$.

Therefore, for suitable shapes for a cavity resonator for an accelerator, to choose y_0 slightly

greater than Y_2 is most promising, but there may also be possibilities for y_0 slightly greater than Y_1 and for y_0 considerably greater than Y_2, but these are the only possibilities with only two modes excited.

Let us in conclusion to this section consider the influence of one of these modes on an electron moving along the axis with the velocity of light. The equation of its motion is $z=c(t-t_0)$. The energy imparted to the electron per unit charge in its passage between the two planes is

$$\int_0^L dzE_z=\int_0^L dze^{-i\omega t}\cos\frac{n\pi z}{L}$$

$$=e^{-i\omega t_0}\int_0^L dze^{-ikz}\cos nkz$$

$$=0 \quad (n\neq 1)$$

$$=e^{-i\omega t}/2 \quad (n=1).$$

It therefore follows that only the mode $h=k$ imparts energy to the electron. The other modes, however, will dissipate energy in the form of heat, caused by the finite conductivity of the walls. One of the considerations in choosing a suitable shape will be to keep this loss as low as possible.

PART 3

Cavities Suitable for Low Velocity Particles

The excitation of the modes h and k with $h>k$, which is of interest when the velocity of the particle is appreciably less than that of light can be treated in the same way as for high speed particles in Part 1. Equations corresponding to (2-1)–(2-4) are easily obtained, and it should not be difficult to determine suitable types of cavity. The shape of each cavity would be determined by the velocity of the entering particle and the amplitude of excitation of that cavity. However, the velocity of the particle and the shape and size of the cavity would change progressively as one passes along the wave guide. Furthermore the velocity of the particle entering any cavity would depend upon the amplitude of excitation of the other cavities, and at the same time the relative excitation of the cavities would depend upon their relative sizes. Thus the accelerator for low velocity particles would appear to have more difficulties both theoretical and experimental connected with it, than are involved in the accelerator for high speed particles.

It might furthermore be interesting to excite more than two modes. Each mode introduces an additional arbitrary constant.

A Millimeter-Wave Reflex Oscillator

J. M. LAFFERTY
General Electric Research Laboratory, Schenectady, New York
(Received July 10, 1946)

The factors which affect the frequency limitation of reflex oscillators are discussed. General design considerations are given for the construction of oscillators of the shortest possible wave-length. The performance of several tubes is given. The highest frequency obtained was 72,000 megacycles.

INTRODUCTION

IN the early part of 1942 Dr. H. V. Neher of the M.I.T. Radiation Laboratory made the first reflex oscillator[1] which operated at centimeter wave-lengths. After that several laboratories placed considerable effort on the design of microwave reflex oscillators in this wave-length region. During the construction of these tubes it was realized that an upper frequency limit had not yet been reached. The material which follows describes the results of experiments performed in an effort to obtain oscillations of the shortest possible wave-length.

In the design of reflex oscillators at extremely high frequencies, the electron gun is of prime importance. The purpose of the gun is to focus electrons from all points of an extended source into a beam of small diameter. The maximum frequency at which the reflex oscillator may be expected to operate is limited by the current density of the electron beam at the position where it passes through the cavity resonator. It can be shown that if the resonator has negligible external loading, the starting current density is proportional to the five-halves power of the frequency. Therefore, the main objective is to design a gun which will transmit as much current as possible through a given diameter aperture for a given beam voltage. Definite upper limits for the value of this current are set by several factors,[2] the three most important of which are thermal emission velocity of the electrons, aberrations of the gun lens system, and mutual repulsion (space charge) of the electrons.

From thermal velocity considerations it can be shown that the radius of curvature of the cathode should be made small and the beam angle large to obtain large beam current densities. Just how far one can go in this direction depends primarily on the spherical aberration of the lens system. The use of high beam voltages and cathodes with high emission densities at low temperatures also tend to increase the beam current density. The use of accurately focused wide angle beams would seem to show greatest promise for improvement.

The electric field is greatest in the reflector space. In the absence of appreciable space charge it has a value given by

$$E=20{,}240(V_0^{\frac{1}{2}}/\lambda\theta), \qquad (1)$$

where E is in volts per centimeter if V_0 is the beam voltage, λ the wave-length in millimeters, and θ the transit time of the electrons in the retarding space expressed in cycles.

Having increased the beam voltage near the point where breakdown occurs, the current density in a given beam is limited primarily by the current density at the cathode surface. Anything which can be done to increase the emission current density of cathodes will extend the upper frequency limit of the reflex oscillator.

To obtain the shortest waves possible from the reflex oscillator, the proportions of the resonator gap must also be given careful consideration. The minimum beam current required to start oscillations is obtained when the beam voltage and gap spacing are adjusted so that the gap transit angle is approximately one-half cycle. For this case, the condition for self-

[1] W. C. Hahn and G. F. Metcalf, Proc. I.R.E. **27**, 106 (1939). H. E. Hollman and A. Thoma, Hoch: Tech. u. Elek: akus. **56**, 181 (1940). A. E. Harrison, J. App. Phys. **15**, 709 (1944). J. R. Pierce, Proc. I.R.E. **33**, 112 (1945). C. C. Wang, Phys. Rev. **68**, 284 (1945). E. L. Ginzton and A. E. Harrison, Proc. I.R.E. **34**, 97 (1946). S. Gvosdover and V. Lopukhin, J. Phys. U.S.S.R. **10**, 275 (1946).

[2] For a detailed discussion of these factors see J. R. Pierce, "Physical limitations in electron ballistics," Bell Sys. Tech. J. **24**, 305 (1945).

starting oscillations becomes[3]

$$I > 8.04 \times 10^5 \left[\frac{(d/\lambda)^2}{R}\right] \frac{1}{p+\frac{1}{4}}, \qquad (2)$$

where I, the beam current, is expressed in amperes if d is the gap spacing and λ the wave-length, both expressed in the same units, R is the equivalent shunt resistance of the resonator and load expressed in ohms, p is an integer, and $p+\frac{1}{4}$ is the number of cycles spent by the electrons in the retarding field space. If it is assumed that the electron gun supplies a sufficiently large beam so that the effective current which passes through the resonator may be taken as proportional to the area of the aperture, then I may be replaced by $\pi r^2 J$, where r is the radius of the aperture in the resonator and J is the current density at the aperture. Making this substitution, relation (2) becomes

$$J > 2.56 \times 10^5 \left[\frac{(d/\lambda)^2}{r^2 R}\right] \frac{1}{p+\frac{1}{4}}. \qquad (3)$$

For a resonator of given material and negligible external loading, the expression in the brackets depends only on the dimensions of the gap and associated resonator. For a given wave-length the value of d will be determined by the beam voltage used and there remains the problem of selecting a value of r which will make the product Rr^2 a maximum.

In cases where grids are not used across the apertures in the resonator, the optimum value of r obtained by making Rr^2 a maximum may be too large for best operational performance. As the apertures are increased in diameter the d.c. equipotential surfaces between the cavity and reflector are pushed into the cavity by the negative reflector. This has the bad effect of reducing the effective beam voltage in the modulator gap region. In addition the r-f electric field in the gap is reduced because it fringes out through the openings. As a result of these effects, the effective gap coefficient is reduced. The gap coefficient at the edge of the apertures will be the same as that obtained with grids present. However, calculations show that the gap coefficient at the center of the beam will drop to nearly 0.5 the edge value for an aperture diameter of one-half cycle.

When grids are used, there are several factors to be considered. The grids should intercept a minimum amount of beam current and at the same time give the most effective electrostatic shielding possible. This is accomplished by using grid wire of extremely small diameter. The wire should also be a good r-f conductor and have a low vapor pressure at high temperatures. The smallest wire which is commercially available and suitable for grids is 0.0003-inch diameter tungsten.[4] The spacing between the wires used in the grid nearest the reflector must be sufficiently small to insure a uniform transit time for all the electrons passing into the retarding space at the same instant of time. The wires used in the grid nearest the gun should be sufficiently close to prevent the r-f field from fringing badly.

Some consideration must also be given to the maximum power which the grids will dissipate. For a grid wire which operates at a high temperature and is very long compared to its diameter, nearly all the power loss at the center is by radiation. The power loss is thus proportional to the surface and hence to the diameter of the wire. The power received by the wire due to current interception is proportional to its projected area and hence to its diameter. Thus, to a first approximation the operating temperature of the grid is independent of wire size.

It appears from expression (3) that the beam current density required for starting oscillations is reduced if the tube is operated under conditions in which p is large. This corresponds to long transit angles for the electrons in the retarding space. If p is made too large, the bunching action in the retarding space is inhibited by space charge effects. Experimental evidence would indicate that there is little advantage in trying to operate with values of p greater than eight or nine. The maximum power output also drops off as p is increased according to the relation[5]

$$P = \frac{0.40}{p+\frac{1}{4}} V_0 I_0, \qquad (4)$$

[3] J. M. Lafferty, "Velocity-modulated reflex oscillator," to appear soon in Proc. I.R.E.

[4] Available from the Cleveland Wire Works, 1131 Chardon Road, Euclid, Ohio.

[5] Lafferty, reference 3, Eq. (48).

where P is in watts if V_0 and I_0, the beam voltage and current, are expressed in volts and amperes, respectively. The reason for low power output for large values of p is easily understood. For long transit angles the electrons are bunched to the optimum degree by a low r-f modulating voltage. With such a low voltage, little power can be developed in the load.

GENERAL DESIGN CONSIDERATIONS

Perhaps one of the first factors which must be decided upon before proceeding with the design of a reflex oscillator is the beam voltage. Previous experience has indicated that 2000 volts is about the maximum practical beam voltage, taking into account insulation problems, spark over in the tube, and life limitation of an oxide-coated cathode due to positive ion bombardment. The transit angle expressed in cycles for an electron crossing an r-f gap is

$$\theta = 12.85(d/\lambda)\,V_0^{\frac{1}{2}}, \qquad (5)$$

where d = gap spacing in mils (.001″), λ = wavelength in mm, and V_0 = beam potential in volts. Since the gap spacing varies as the square root of the beam voltage, there is little to be gained by going to high voltages. For example, if $\lambda = 5$ mm, a beam voltage of 1600 volts gives a gap spacing of 7.8 mils for a half-cycle gap. Increasing the beam voltage to 2500 volts makes the insulation problems considerably more difficult, but increases the gap spacing only about two mils. In view of these considerations it was decided to use 1600 volts for the beam voltage.

Another question which has to be decided upon is whether or not grids are to be used at the r-f gap. For a 1600-volt beam at five millimeters the gap coefficient at the center of a gridless gap will drop to less than one-half the edge value if the gap diameter exceeds 8 mils. To focus the beam current through such a small aperture would, indeed, place very stringent conditions on the gun design. It is doubtful if a gun could be designed to deliver sufficient starting current (estimated at 30 ma) within a crossover diameter of 8 mils. It was thus decided to use grids and make the aperture larger.

The grids were made from 0.0003-inch diameter tungsten wires spaced 3 mils apart. The maximum variation in the transit time of the electrons in the retarding space was found to be less 0.5 percent over the non-uniform part of the field. The effective r-f field strength in the gap is reduced about 25 percent for paths which lie midway between grid wires. The beam power transmission densities required for oscillation would melt the grids if the tube were operated continuously. Pulsed operation therefore was required.

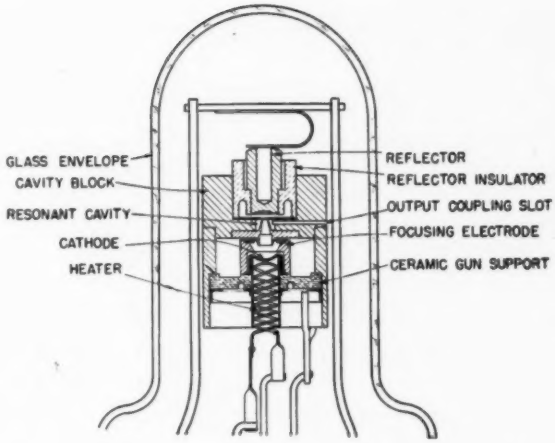

FIG. 1. A millimeter-wave reflex oscillator with a glass envelope. The r-f power radiates from the coupling slot out through the glass envelope.

Several types of guns were tried. The ones which performed best are shown in Figs. 1 and 2. The gun shown in Fig. 1 has a special shaped focusing electrode which operates at cathode potential. This gun was designed according to the method described by Samuel.[6] The gun shown in Fig. 2 has a cylindrical focusing electrode which operates at a negative potential. This potential can be adjusted to give optimum focusing for each tube. Higher beam current densities could be obtained with this gun and it was used in the oscillators which operated below six millimeters. The cathode is $\frac{1}{8}$ inch in diameter and has a radius of curvature of 0.077 inch. It was found that the grids were not damaged or the oscillator performance impaired if the duty cycle did not exceed 0.01. It was found convenient to pulse the beam voltage at a 60-cycle repetition rate with pulses ranging in length from 50 to 160 microseconds. Beam

[6] A. L. Samuel, Proc. I.R.E. **33**, 233 (1945).

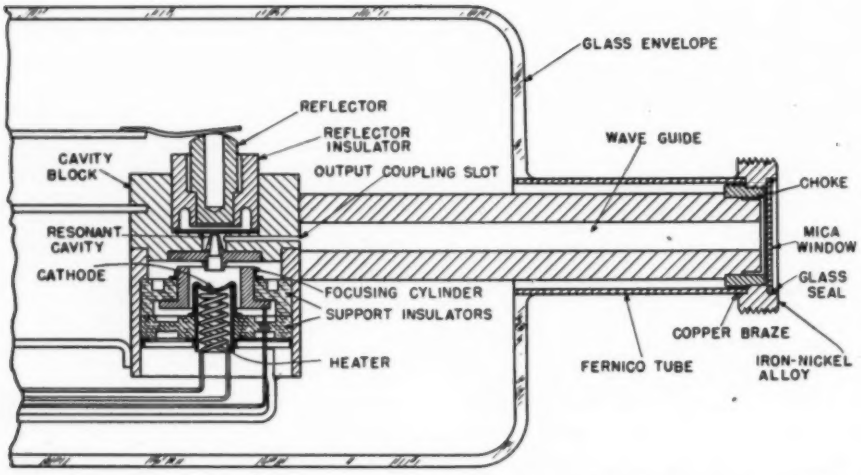

FIG. 2. A millimeter-wave reflex oscillator with a wave guide output. The r-f power is transmitted through the non-resonant mica window with negligible loss.

currents with peak values of 50 milliamperes were focused through a 0.028-inch diameter aperture under these conditions with a 1600-volt beam. This represented about 75 percent of the total cathode current.

The reflector consisted of a plane electrode spaced 30 mils from the gap. The aperture near the reflector was made 20 percent larger than the aperture in the cone near the electron gun to accommodate the returning beam. Under an extreme condition such as this where the beam travels less than one diameter into the retarding space, very little is necessary in the way of focusing to insure a large percentage of the beam returning across the gap.

For a 5.5-millimeter oscillator the cavity resonator was 82 mils in diameter and 43 mils high. The coupling slot was 37 mils wide and 20 mils high. The reentrant cone has an included angle of 35° and a 28-mil diameter opening for the electron beam. The gap spacing was 7 mils. For shorter wave-lengths the external dimensions of the cavity, coupling slot, and gap were correspondingly smaller. The dimensions of the cone were kept the same.

TUBE PERFORMANCE

Two types of tubes were constructed as shown in Figs. 1 and 2. In the first type no attempt was made to incorporate a wave guide output or window in the structure. The radiation from these tubes was picked up in a short section of wave guide placed next to the glass envelope opposite the output coupling slot as shown on the right in Fig. 3. This section of guide contained a wave meter branch, a crystal, and a shorting plunger in the end opposite the tube. An absorption type wave meter was used. Resonance was detected by observing the dip in the crystal current. Wave-length, electronic tuning, starting current, and relative-power output measurements of the various modes could be made. Omitting the wave guide and window on the tube simplified the structure considerably and permitted a large number of experiments to be made on the gun, grids, and cavity with a minimum of effort.

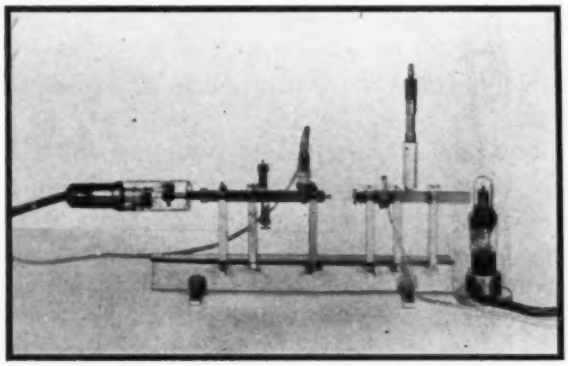

FIG. 3. Set-up for making power and wave-length measurements. A wave guide output tube connected to a bolometer is shown on the left. On the right is shown a tube without a wave guide output in position for making wave-length measurements.

TABLE I. Starting current data.

Tube number	λ	V_0	V_c	I_s	I_0	Relative power
26	9.60	1500	−455	23.9	32.2	100
			−245	20.6		67
			−100	19.8		26
			− 35	19.6		7
58	6.05	1500	−810	22.6	56.0	100
			−510	20.7		56
			−310	19.3		26
			−190	18.7		11
			− 95	17.4		4
			− 20	14.7		2
64	5.45	1500	−370	16.5	20.7	100
			−190	15.2		73
			− 60	13.8		50

In order to measure the total power output, a wave guide and window were added to some of the tubes. This structure is shown in Fig. 2 with the gun using the cylindrical focusing electrode.

All tubes were operated by pulsing the beam voltage 60 times a second with 50 to 160 microsecond pulses. The pulsating crystal current thus obtained was fed into a type 208 DuMont oscilloscope. With the crystal used (Sylvania 1N26), a one-inch deflection on the scope corresponded to an r-f power of approximately 0.1 milliwatt.

Table I shows some data taken on the starting current and relative power output for the various modes of oscillation. The more negative reflector voltages correspond to shorter transit times in the retarding space. It will be observed that the starting current and power output both increase with the shorter transit time modes as would be expected from theoretical considerations. The starting current at different wavelengths cannot be readily compared because of structural variations in the various tubes.

The minimum starting current I_s was determined by operating the cathode at a temperature reduced to the point where oscillations could just be detected. This beam current was then collected and measured as reflector current by operating the reflector a few volts positive with respect to the cavity. The operating current I_0 is the reflector current thus obtained with the cathode operating at normal temperature.

TABLE II. Power output measurements.

Tube number	λ	V_0	V_c	I_s	I_0	P
70	5.80	1750	− 40	32	70	12.7
77	5.60	1600	− 50	31	48	5.5
78	4.51	1700	− 45	38	49	2.6
87	4.15	1700	−350	16	25	0.2

V_0 = beam voltage
V_c = reflector voltage
I_s = peak starting current in ma
I_0 = peak operating current in ma
λ = wave-length in mm
P = peak power output in milliwatts.

The power output obtained from several tubes constructed with wave guide outputs is summarized in Table II. The r-f power was measured with a thermister type bolometer connected across a wave guide section which was coupled to the tube. The wave guide contained a double stub tuner and shorting plunger for impedance matching as shown on the left of Fig. 3. A Type D-162046 unmounted thermister bead was used with an M.I.T. Radiation Laboratory TBN-3EV (Type W) thermister bridge.

The electronic tuning obtained by varying the reflector voltage was found to be about 80 megacycles for most of the tubes below six millimeters.

It was found in all cases that an increase in beam current (by increasing the cathode temperature) resulted in a larger power output. This means that the equivalent shunt impedance of the cavity and load is too low for the available beam current and explains the rather low power output and efficiency obtained at these short wave-lengths. At shorter wave-lengths this condition becomes even more acute and a point is soon reached where oscillations cannot be obtained because of insufficient beam current.

The frequency and power output obtained with these tubes are considerably greater than those obtained by Cleeton and Williams[7] and Richter[8] with magnetrons. The reflex oscillator has an additional advantage over the magnetron in that no magnetic field is required. It is doubtful if oscillations of wave-lengths appreciably shorter than four millimeters can be obtained by the velocity modulation reflex principle until new cathodes are developed with considerably higher emission current densities, or some

[7] E. E. Cleeton and N. H. Williams, Phys. Rev. **50**, 1091 (1936).
[8] H. Richter, Hoch: Tech. u. Elek: akus. **51**, 10 (1938).

radically new gun design is invented for producing electron beams of extremely high current densities.

The power output obtained from the tubes described in Table II should be ample for making dielectric measurements and absorption studies of gases. By making one side of the resonant cavity flexible, it should be possible to construct tubes which may be continuously tuned over a 10 to 15 percent wave-length range.

Resonant Circuit Modulator for Broad Band Acoustic Measurements

GORDON FERRIE HULL, JR.*
Wilder Laboratory, Dartmouth College, Hanover, New Hampshire
(Received July 23, 1946)

A modulation method is described whereby a broad band frequency response is obtained for recording of sound. In particular low frequency sound approaching 0 c.p.s. can be recorded. The theory of the resonant circuit modulating principle is first discussed followed by a description of the apparatus which was constructed for this purpose.

INTRODUCTION

THE resonant circuit modulator was developed for the purpose of recording sound over a broad frequency band, and particularly to record low frequency sounds. The principle upon which the modulator is based is the following. Consider a series resonant circuit having an inductance L, resistance R, and capacity C connected to a sinusoidal source of constant e.m.f. and of constant frequency. As the capacity C is varied, the current through the resonant circuit will vary and hence the voltage across the capacity will vary. If for the capacity C, we substitute a condenser transmitter and tune the resonant circuit off resonance, then as the capacity of the transmitter is varied by the sound field the voltage across the transmitter will vary according to the shape of the resonance curve. It will be shown that this action produces amplitude (and also phase) modulation of the carrier frequency.

This principle has been suggested by Hans Riegger[1] for converting sound into electrical energy. It is also the general basic principle of the ultra micrometer, a device for the measurement of small displacements, which was developed by R. Whiddington[2] and in the Bell Telephone Laboratories by J. R. Haynes.[3]

The discussion of the resonant circuit modulator and broad band recording system is divided into two parts, the theory of its operation and the experimental apparatus.

THEORY

Series Resonant Circuit, Constant Voltage Source

We begin the analysis of the resonant circuit modulator by considering a series resonant circuit. A constant voltage generator $E=E_0e^{j\omega t}$ of constant frequency ω and of zero internal impedance is impressed upon the series resonant circuit composed of inductance L, resistance R, and capacity C. We will define C_0 by $1/LC_0=\omega^2$ as the capacity when the circuit is tuned to resonance, and $Q=\omega L/R=1/\omega C_0R$, the circuit Q at resonance. We wish to find the voltage V_c across the condenser as a function of the circuit Q and the capacity of the condenser C. The current flowing in the circuit is

$$i=\frac{E_0}{Z_s}e^{j(\omega t-\varphi)}, \quad \text{where} \quad \tan\varphi=\frac{\omega L-(1/\omega C)}{R}$$

and

$$Z_s=\left[R^2+\left(\omega L-\frac{1}{\omega C}\right)^2\right]^{\frac{1}{2}}$$

---

* This research was carried out while the author was a member of the Technical Staff of the Bell Telephone Laboratories, Incorporated, Murray Hill, New Jersey.

[1] Hans Riegger, Wiss. Veröff. a.d. Siemens-Konzern **3**, No. 2, 67 (April 16, 1924).

[2] R. Whiddington, Phil. Mag. **40**, 634 (1920).

[3] J. R. Haynes, Bell Lab. Record **13**, 337 (1935).

is the impedance of the series resonant circuit. Hence the voltage across the condenser is

$$V_c=\frac{i}{j\omega C}=\frac{E_0}{\omega CZ_s}e^{j(\omega t-\varphi-(\pi/2))}.$$

It is convenient to define $\alpha=C/C_0$ as the ratio of the capacity of the condenser off resonance to the capacity at resonance. Rewriting the equations for Z_s and V_c in terms of α and Q we obtain

$$\frac{Z_s}{R}=\frac{1}{\alpha}[\alpha^2+Q^2(\alpha-1)^2]^{\frac{1}{2}},$$

$$\frac{V_c}{E_0}=\frac{Q}{\alpha Z_s/R}e^{j(\omega t-\varphi-(\pi/2))}.$$

Neglecting the time factor

$$\frac{V_c}{E_0}=\frac{Q}{\alpha Z_s/R}. \tag{1}$$

Equation (1), which can be written:

$$\frac{V_c}{QE_0}=[1+Q^2(\alpha-1)^2]^{-\frac{1}{2}} \text{ when } Q\gg\alpha$$

is plotted independent of Q in Fig. 1 as curve (1). It will be observed that curve (1) has the shape of a resonance curve.

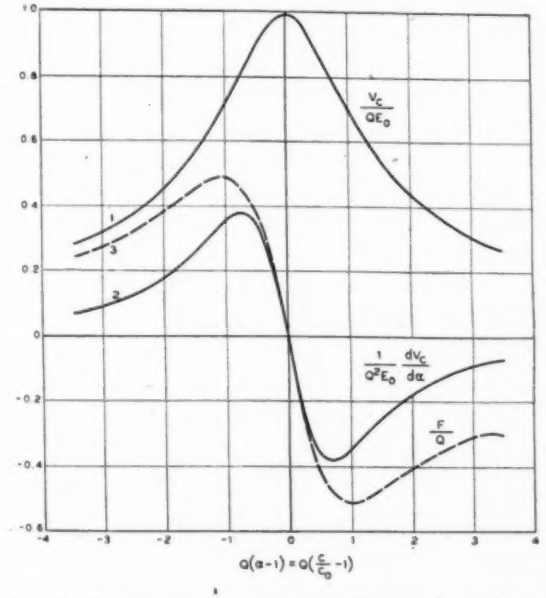

FIG. 1. Generalized voltage-capacity characteristics of resonant circuit.

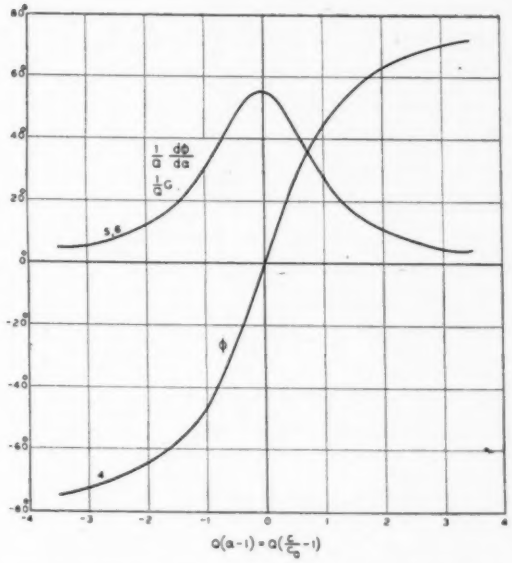

FIG. 2. Generalized phase-capacity characteristics of resonant circuit.

To use the resonant circuit as a modulator, the circuit is detuned from resonance to a point on the resonance curve such that the voltage change produced by a variation of capacity will be a maximum. To find this point it is necessary to find the point at which the slope of curve (1) is a maximum. Consequently we obtain the slope $dV_c/d\alpha$ or what is more convenient to use $(1/QE_0)(dV_c/d\alpha)$. This is

$$\frac{1}{QE_0}\frac{dV_c}{d\alpha}=-\frac{1}{\alpha^2(Z_s/R)^3}\left[Q^2\left(\frac{\alpha-1}{\alpha}\right)+1\right]. \tag{2}$$

The degree of modulation as a function of α is dV_c/V_c and we obtain for it

$$\frac{dV_c}{V_c}=F\frac{d\alpha}{\alpha}=F\frac{dC}{C}, \tag{3}$$

where

$$F=-\frac{1}{(Z_s/R)^2}\left[Q^2\left(\frac{\alpha-1}{\alpha}\right)+1\right].$$

Equations (2) and (3) when $Q\gg\alpha$ are plotted as curves (2) and (3) in Fig. 1. It is observed from curve (2) that the slope of curve (1) is a maximum at a point on the curve 0.8 of the maximum of curve (1). This can also be shown analytically, by setting $d^2V_c/d\alpha^2=0$, and solving for α in terms of Q. When this value of α is substituted in Eq. (1), $V_c=0.8QE_0$ is obtained. Hence the

greatest change in voltage for a given change in capacity will occur when the resonant circuit is detuned to 0.8 of the maximum voltage across the condenser. Also in the neighborhood of this point, the slope is changing the least, and, consequently, the greatest linearity of voltage change *versus* change in capacity is to be expected. Although the maximum degree of modulation does not occur at this point, but at a point 0.7 of the maximum of curve (1), the degree of modulation at the 0.8 point is of sufficiently high magnitude.

What has been discussed so far is the amplitude modulation. Phase modulation also occurs since

$$\varphi = \arctan Q\left(\frac{\alpha-1}{\alpha}\right). \tag{4}$$

It is also desirable to know the slope of (4) and also the value of phase modulation. These are

$$\frac{1}{Q}\frac{d\varphi}{d\alpha} = \frac{1}{\alpha^2\{Z_s/R\}^2} \tag{5}$$

and

$$d\varphi = G\frac{d\alpha}{\alpha} = G\frac{dC}{C},$$

where

$$\frac{1}{Q}G = \frac{1}{\alpha\{Z_s/R\}^2}. \tag{6}$$

Generalized forms of Eqs. (4)–(6) independent of Q when $Q \gg \alpha$ are plotted in Fig. 2. It is not convenient to plot Eqs. (5) and (6) as two separate curves because they differ very little from each other, more specifically by the factor $1/\alpha$.

Before continuing the discussions of the series resonant circuit with constant voltage source, let us consider other ways in which a resonant circuit can be used as a modulator.

Series Resonant Circuit, Constant Current Source

If we substitute a constant current generator $i = i_0 e^{j\omega t}$ for the constant voltage generator in the series resonant circuit, the analysis of its behavior as a modulator is as follows. The voltage across the condenser is

$$V_c = \frac{i}{j\omega C} = \frac{i_0}{\omega C} e^{j(\omega t - (\pi/2))}.$$

Neglecting the time factor,

$$V_c = \frac{i_0}{\omega C}$$

and

$$dV_c = -\frac{i_0}{\omega C}\frac{dC}{C} \quad \text{or} \quad \frac{dV_c}{V_c} = -\frac{dC}{C}.$$

It is evident that amplitude modulation results and no phase modulation. Furthermore the degree of modulation is independent of the resonance curve. In some applications this may be of advantage. However, the degree of modulation is greater in the constant voltage case than in the constant current case by the factor F, and therefore is more desirable to use in spite of the phase modulation which also occurs.

Parallel Resonant Circuit

If a constant current generator $i = i_0 e^{j\omega t}$ of constant frequency ω and of infinite internal impedance is impressed upon a parallel resonant circuit, then the voltage V_c across the condenser is

$$V_c = Z_p i_0 \exp\left[j(\omega t - \varphi_1 - \varphi_2)\right],$$

where

$$Z_p = \frac{\left[\left(\frac{L}{C}\right)^2 + \left(\frac{R}{\omega C}\right)^2\right]^{\frac{1}{2}}}{\left[R^2 + \left(\omega L - \frac{1}{\omega C}\right)^2\right]^{\frac{1}{2}}}$$

is the impedance of the parallel resonant circuit and

$$\tan\varphi_1 = \frac{R}{\omega L} = \frac{1}{Q}, \quad \tan\varphi_2 = \frac{\omega L - \frac{1}{\omega C}}{R} = Q\left(\frac{\alpha-1}{\alpha}\right).$$

If $L/C \gg R/\omega C$ and we neglect $R/\omega C$ which is usually permissible, then in terms of Q and α we obtain

$$V_c = \frac{Q^2 R}{\alpha\frac{Z_s}{R}} i_0 e^{j(\omega t - \varphi)},$$

where

$$\varphi = \varphi_2 = \arctan Q\left(\frac{\alpha-1}{\alpha}\right).$$

Hence we see that a series resonant circuit with

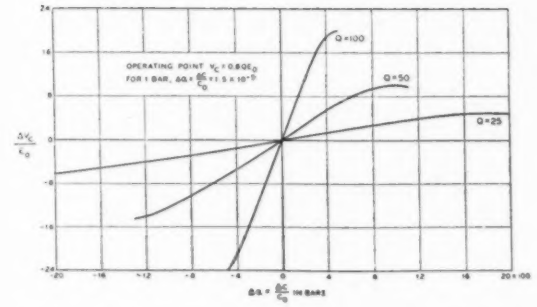

FIG. 3. Voltage-capacity operating characteristics of resonant circuit modulator using type 640 Western Electric condenser transmitter. Change in capacity $\Delta C/C_0$ expressed in equivalent bars pressure.

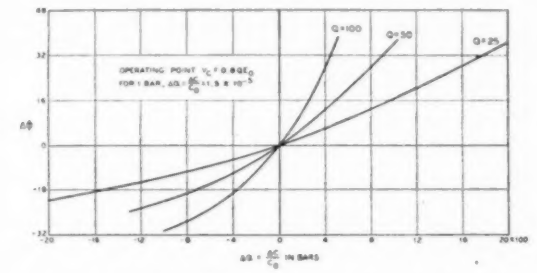

FIG. 4. Phase-capacity operating characteristics of resonant circuit modulator using type 640 Western Electric condenser transmitter. Change in capacity $\Delta C/C_0$ expressed in equivalent bars pressure.

a constant voltage source is equivalent to a parallel resonant circuit with a constant current source, provided we substitute $E_0 = QRi_0 e^{i\pi/2}$. Hence all the previous analysis for the series resonant circuit applies to the parallel resonant case.

If, however, a constant voltage source is impressed upon the parallel resonant circuit, then it is evident that the voltage across the condenser will always be a constant irrespective of the manner in which the capacity may change. Hence this circuit will produce no modulation.

Frequency Modulation

If a resonant circuit is used as the frequency determining element of an oscillator, and the capacity of the circuit is varied, frequency modulation (and also amplitude modulation) will result, since for this case $\alpha = 1$, $\omega^2 = 1/LC = 1/LC_0$. Whence

$$2\frac{d\omega}{\omega} = -\frac{dC}{C} = -\frac{d\alpha}{\alpha};$$

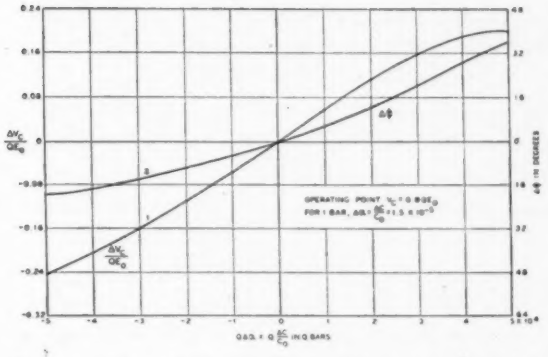

FIG. 5. Generalized voltage-capacity (1) and phase-capacity (2) operating characteristics of resonant circuit modulator using type 640 Western Electric condenser transmitter. Change in capacity $\Delta C/C_0$ expressed in equivalent Q bars pressure.

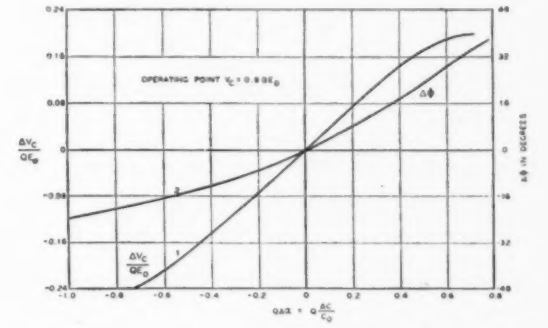

FIG. 6. Generalized voltage-capacity (1) and phase-capacity (2) operating characteristics of resonant circuit modulator for any condenser transmitter.

or twice the fractional frequency variation equals the corresponding capacity variation. Amplitude modulation is also present because V_c is a function of the circuit Q and Q is proportional to ω. The amplitude modulation is not important in this discussion because a limiter circuit would be used to eliminate amplitude modulation.

If the frequency modulated carrier is now impressed on a resonant circuit which is tuned off resonance, then the frequency modulation is converted into amplitude modulation. To show this, define $\omega_0^2 = 1/LC$. Retain the definitions $\omega^2 = 1/LC_0$, $Q = \omega L/R = 1/\omega C_0 R$. Set $\omega/\omega_0 = \beta$ and $d\omega/\omega_0 = d\beta$. Then $(\omega/\omega_0)^2 = C/C_0 = \beta^2 = \alpha$ and $2d\omega/\omega = dC/C = 2d\beta/\beta = d\alpha/\alpha$. Hence frequency modulation is equivalent to amplitude modulation provided we substitute β^2 for α in our previous analysis, Eqs. (1)–(6), and, consequently, the curves in Figs. 1 and 2 can be used for the frequency modulation case.

TABLE I. Operating point $V_c=0.8QE_0$, $\varphi=\pm 37°$.

Q	Percentage modulation $\Delta V_c/V_c$ for 1 bar	Phase modulation $\Delta\varphi$ for 1 bar
25	.0188%	.014°
50	.0375%	.028°
100	.075%	.056°

Phase Modulation

Evidently the resonant circuit can also be used as a phase modulator. From the curves in Fig. 2 it is seen that the maximum phase shift with capacity change and greatest linearity occur when the resonant circuit is tuned to resonance. The value of phase shift for a given circuit Q and capacity change can be readily calculated from Eq. (6) and the curves in Fig. 2. This phase modulation will also be accompanied by some amplitude modulation as can be seen by referring to curve (1) in Fig. 1.

Application to the Western Electric Type 640 Condenser Transmitter

Modulation

The type 640 condenser transmitter, which is used in the resonant circuit modulator, has a capacity of 50 $\mu\mu$f and is normally operated with a polarizing potential of 200 volts. When so used it has a sensitivity of 52 db below 1 volt per bar (dyne per cm^2). A simple calculation shows that the change in capacity, produced by a 1 bar sound field is $\Delta C=7.5\times10^{-4}$ $\mu\mu$f and so the fractional capacity change is $\Delta C/C_0=1.5\times10^{-5}$ per bar. When the transmitter is used in the modulator, and the circuit detuned from resonance such that $V_c=0.8QE_0$, the curves in Figs. 1 and 2 can be replotted with origin of coordinates at the operating point $V_c=0.8QE_0$. This has been done in Fig. 3 and Fig. 4 in which $\Delta V_c/E_0$ and $\Delta\varphi$ are plotted against $\Delta C/C_0$ expressed in equivalent bars pressure. The curves are generalized in Fig. 5 for any circuit Q and in Fig. 6 for any circuit Q and for any condenser transmitter.

It is of some interest to know the degree of modulation which will be produced by the resonant circuit modulator using a type 640 condenser transmitter. This can be obtained from Eq. (3) and the curves in Figs. 1 and 3 or by the approximation $F\cong\frac{1}{2}Q$ in $dV_c/V_c=FdC/C$. The phase modulation can be obtained from Eq. (6) and the curves in Figs. 2 and 4 which give $G=37Q$ in $d\varphi=GdC/C$. It is of interest to note that the degree of modulation and the phase modulation increase linearly with Q. In Table I are listed the percentage modulation per bar for the type 640 condenser transmitter as well as the phase modulation per bar.

From Table I it is seen that a large percentage modulation is obtained only with large sound fields (of the order of 1000 bars) for circuit Q's of 25 to 100. For sound fields of the order of 10 bars, Q's of 100 times as great are required, or else carrier suppression must be used. This will be discussed in a later section.

Distortion

Amplitude distortion produced in the modulator is readily obtainable from the curves in Fig. 3 as well as from curve (1) in Figs. 5 and 6 and is measured by the departure of these curves from a straight line. This gives the total harmonic distortion. Evidently the amount of distortion depends upon the sound field and the circuit Q. The phase distortion is another matter, however, because we are concerned ultimately with the phase distortion in the audio signal. This is given by the ratio of the audiofrequency to the carrier frequency multipled by the total phase excursion of the carrier, as discussed in a later section.

Response

The audiofrequency response of the resonant circuit modulator is the same as that of the condenser transmitter without d.c. bias. This is so because the amplitude modulation is proportional to the change in capacity of the transmitter, which in turn is a function of the sound field pressure acting on the diaphragm of the transmitter.

Noise

The question of noise produced by the modulator is an important one and can be calculated from the expression[4]

$$\bar{V}^2=4kT\int_{f_1}^{f_2}Z_r df,$$

[4] J. B. Johnson, Phys. Rev. **32**, 97 (1928); H. Nyquist, Phys. Rev. **32**, 110 (1928).

where k is Boltzmann's constant, T the absolute temperature, $Z_r=R/\omega^2C^2Z_s^2$ the real part of the complex impedance Z_p, and f_2-f_1 the band width. To evaluate the noise, some assumptions and approximations will be made. First let us restrict ourselves to a carrier frequency of 4 mc and we will take $C=50$ $\mu\mu$f, the capacity of the type 640 condenser transmitter. Since ω and C are now constants, the inductance L must be a constant and hence R is the only variable in Z_r. If we choose an operating point $V_c=0.8QE_0$, then $R=0.8(C/C_0)Z_s$. We can now put Z_r in terms of Q, since $Q=1/\omega C_0R$, and we have $Z_r=0.64Q/\omega C$. If Z_r is assumed to be a constant over the frequency band f_2-f_1, which is approximately correct, then $\bar{V}^2=2.56kT(Q/\omega C)(f_2-f_1)$. The frequency band of interest is that in the region of the carrier frequency which ultimately will appear in the rectified audio output, for it is only those noise frequencies in the neighborhood of the carrier frequency which are large in amplitude, because Z_r is large in this frequency band, and which will be transmitted through tuned radiofrequency amplifiers between the modulator and rectifier. Let us assume that the audio band is 10 kc wide, then since the rectifier is a non-linear circuit element, the carrier will beat with those noise frequencies lying in a band ±10 kc wide on either side of the carrier frequency, thus producing noise in the 10-kc audio band of the rectifier output. Consequently we take $f_2-f_1=20$ kc. The noise voltage $\bar{V}$ can now be calculated. It is desirable, however, to obtain the noise level of the modulator in db referred to a 1 bar sound field. This is $-20\log_{10}(dV_c/\bar{V})$. Since $dV_c\cong\frac{1}{2}QV_cdC/C$, the noise level becomes $-20\log_{10}(22.7Q^{\frac{1}{2}}V_c)$ for a carrier frequency of 4 mc a capacity of 50 $\mu\mu$f and an audio band width of 10 kc.

In Table II are listed noise levels for three values of Q and one volt across the condenser transmitter ($V_c=1$ volt). Evidently for sound fields of the order of 1 bar, noise should not be a troublesome factor.

Other sources of noise are also present, but in general they will be small compared to the one we have discussed. Such sources of noise are the load resistance in the rectifier circuit, the input resistance of the d.c. amplifier, and tube noise. These will contribute little to the noise developed in the modulator, for the latter has been amplified along with the modulated carrier in passing through the radiofrequency amplifier in the receiver. The noise level which has been calculated represents then a minimum noise level for the recording system which, as we shall discuss later, consists of the modulator, a receiver, a d.c. amplifier, and a string oscillograph.

Wave Form of Modulated Carrier

When the resonant circuit modulator is used to produce amplitude modulation, the wave form of the modulated carrier is important, because of the associated phase modulation and, as we will discuss later, because of the desirability of using carrier suppression for low sound fields. Let us assume a sound wave of the form $\cos pt$ striking the diaphragm of the condenser transmitter. The capacity of the condenser transmitter will vary according to

$$dC=[dC]_{\max}\cos pt,$$

where $[dC]_{\max}$ is the amplitude of the capacity change. The voltage across the condenser transmitter is given by

$$V_c=\frac{E_0}{\omega CZ_s}e^{j(\omega t-\varphi-(\pi/2))}=|V_c|\cos(\omega t-\varphi),$$

where

$$|V_c|=E_0/\omega CZ_s.$$

Then

$$dV_c=\cos(\omega t-\varphi)d|V_c|+|V_c|\sin(\omega t-\varphi)d\varphi.$$

Now

$$d|V_c|=|V_c|F\frac{dC}{C}\quad\text{and}\quad d\varphi=G\frac{dC}{C}$$

from Eqs. (3) and (6). Let

$$\delta=F\frac{[dC]_{\max}}{C}\quad\text{and}\quad\epsilon=G\frac{[dC]_{\max}}{C}.$$

Hence

$$dV_c=|V_c|[\delta\cos(\omega t-\varphi)+\epsilon\sin(\omega t-\varphi)]\cos pt.$$

TABLE II. Operating point $V_c=0.8QE_0=1$ volt, $\varphi=\pm37°$.

Q	Noise level in db below 1 bar
25	41
50	44
100	47

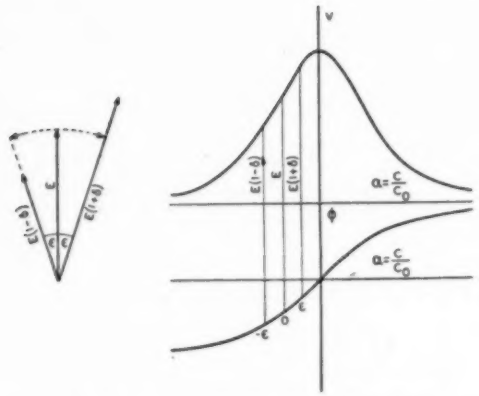

FIG. 7. Vector representation of amplitude and phase modulation of carrier as produced by resonant circuit modulator.

Therefore the wave form of the voltage across the condenser transmitter when a sound wave strikes it is

$$(V_c+dV_c)=|V_c|\{\cos(\omega t-\varphi)+[\delta\cos(\omega t-\varphi)+\epsilon\sin(\omega t-\varphi)]\cos\rho t\}.$$

This can be written in the form

$$V=E\cos(\omega t-\varphi)+\delta E\cos\rho t\cos(\omega t-\varphi)+\epsilon E\cos\rho t\sin(\omega t-\varphi)$$

or

$$V=E\cos(\omega t-\varphi)+\tfrac{1}{2}\delta E\{\cos[(\omega+\rho)t-\varphi]+\cos[(\omega-\rho)t-\varphi]\}+\tfrac{1}{2}\epsilon E\{\sin[(\omega+\rho)t-\varphi]+\sin[(\omega-\rho)t-\varphi]\},$$

where we have set $(V_c+dV_c)=V$ and $|V_c|=E$. The first term represents the unmodulated carrier, the second term the amplitude modulation which is in phase with the carrier, and the third term the phase modulation which is 90° out of phase with the carrier. Both modulation terms contain the sum and difference frequencies $(\omega+\rho)$ and $(\omega-\rho)$. This equation holds only for small amplitudes of modulation. For large amplitudes the correct equation is:

$$V=E(1+\delta\cos\rho t)\cos[\omega t-(\varphi+\epsilon\cos\rho t)]$$

which reduces to the first equation for small amplitudes. The meaning of this equation can be readily understood by means of the vector representation as shown in Fig. 7.

The effect of the phase modulation on the rectified signal of frequency ρ is negligible provided the carrier frequency ω is much higher than ρ and provided the receiver does not cut off any of the significant side bands of the phase modulation, for the phase modulation of the rectified signal equals the phase modulation of the carrier multiplied by ρ/ω. If the ratio is 0.01, which is reasonable in practice, then a phase modulation of the carrier of ±30° will yield only a phase modulation of ±0.3° of the rectified signal. In general the phase modulation or phase distortion of the rectified signal can be made as small as desired by increasing the carrier frequency ω.

Carrier Suppression

In general to obtain a reasonable degree of amplitude modulation for low sound fields, it is necessary to suppress some of the carrier after the carrier has been modulated, or to increase the resonant circuit Q to a very high value, which may prove impractical. In view of the phase modulation present amplitude distortion may arise because of suppression of the carrier. In Fig. 8 the vector E representing the carrier is shown modulated in phase through the angle $\pm\epsilon$ and modulated in amplitude from $E(1-\delta)$ to $E(1+\delta)$. From these vectors is subtracted a fraction γ of E. The resulting vectors A and B represent the new magnitudes through which the suppressed carrier is amplitude modulated. In order that no amplitude distortion occur, the difference $B-A$ must vary linearly with the sound field pressure for a given value of γ, the degree of carrier suppression. From geometry it is evident that

$$A^2/E^2=[(1-\delta)^2+\gamma^2-2\gamma(1-\delta)\cos\epsilon],$$
$$B^2/E^2=[(1+\delta)^2+\gamma^2-2\gamma(1+\delta)\cos\epsilon].$$

We are interested in the value of $(B-A)/E$ as a

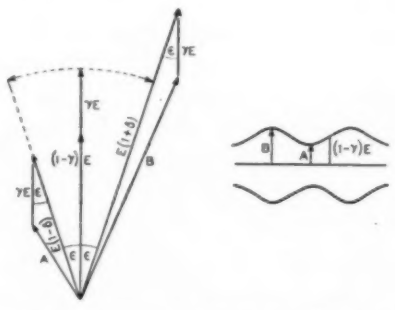

FIG. 8. Vector representation of amplitude and phase modulation of carrier as produced by resonant circuit modulator when carrier suppression is imposed.

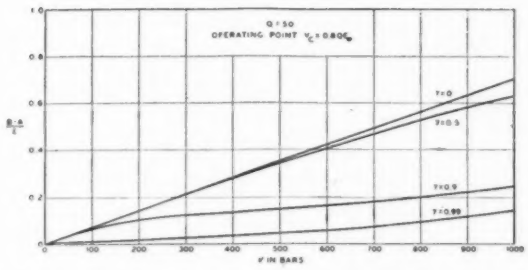

FIG. 9. Magnitude $(B-A)/E$ of amplitude modulation *vs.* sound field pressure ν in bars with various degrees of carrier suppression γ for resonant circuit modulator using type 640 Western Electric condenser transmitter.

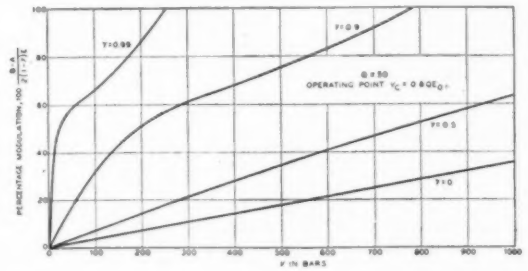

FIG. 10. Percentage modulation *vs.* sound field pressure ν in bars with various degrees of carrier suppression γ for resonant circuit modulator using type 640 Western Electric condenser transmitter.

function of γ and the sound field pressure, and also in the percentage modulation $100\ (B-A)/[2(1-\gamma)E]$. These have been worked out for the case of the type 640 condenser transmitter in the resonant circuit modulator with $Q=50$ and the operating point $V_c=0.8QE_0$. For this case $F=23.64, G=31.51, [dC]_{\max}/C=1.5\times10^{-5}\nu$, where ν is in bars pressure, and so $\delta=F[dC]_{\max}/C=35.47\times10^{-5}\nu$ and $\epsilon=G[dC]_{\max}/C=47.26\times10^{-5}\nu$. The results are plotted in Figs. 9 and 10. It is seen that for $\gamma=0$ (no carrier suppression) $(B-A)/E$ increases linearly with ν and at $\nu=1000$ bars, the percentage modulation is about 37.5 percent as obtained by the approximate method. For $\gamma=0.9$ (90 percent of the carrier suppressed), the maximum sound field which is permissible without distortion is $\nu=100$ bars and the percentage modulation for this sound field is about 37.5 percent. And last for $\gamma=.99$ (99 percent of the carrier suppressed), it is seen from the curves that the maximum permissible sound field without appreciable distortion is $\nu=10$ bars with about the same percentage modulation as before.

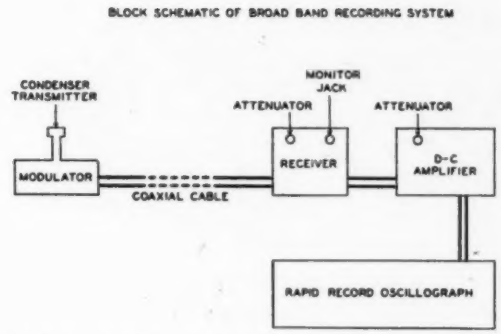

FIG. 11. Block schematic of broad band recording system.

EXPERIMENT

Apparatus

The experimental apparatus used in the broad band recording system consists of the resonant circuit modulator, a receiver, a d.c. amplifier, and a recording string oscillograph. The system is represented by the block schematic Fig. 11.

Resonant Circuit Modulator

The modulator is shown in the simplified schematic Fig. 12. The resonant circuit plate load of a conventional crystal controlled oscillator operating at 4 mc is coupled at low impedance (2 ohms) to the modulator circuit. The latter circuit is provided with a coaxial jack to which the condenser transmitter is attached by means of a coaxial line about one foot long inside of a brass tube. The complete resonant modulator circuit then consists of, the inductance L_1, the variable tuning condenser C_1 of 50 $\mu\mu$f, the coaxial line of 25 $\mu\mu$f and the type 640 condenser transmitter of 50 $\mu\mu$f. The voltage appearing across this total capacity is put on the grid of a tube, and the output is obtained on a coaxial line from a resonant circuit plate load. Measurements on this much of the circuit gave $Q\cong25$ and 10 percent modulation at 1000 bars sound pressure. This agrees with theory which gives 18.8 percent modulation for $Q=25$ and a sound field of 1000 bars, when it is remembered that the total capacity in the resonant circuit is about 100 $\mu\mu$f instead of 50 $\mu\mu$f of the type 640 transmitter and consequently the percentage modulation is half as much.

To obtain 10 percent modulation at 100 bars and 10 bars, carrier suppression is necessary.

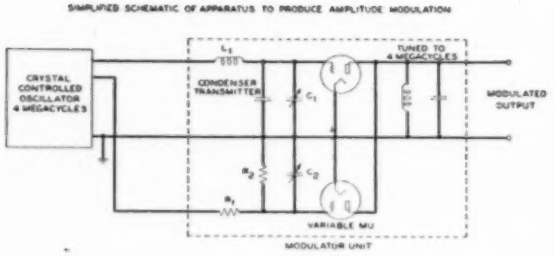

FIG. 12. Simplified schematic of resonant circuit modulator with additional circuit for producing partial carrier suppression.

This was accomplished by means of the lower half of the circuit shown in Fig. 12. Some of the oscillator output which is obtained by suitable coupling is sent through a voltage divider and phase shifter onto the grid of a variable mu tube. The output from the plate of this tube is connected to the plate of the modulator tube, such as to cancel some of the carrier. Cancellation of the carrier is achieved by properly adjusting the phase of the coupling to the resonant circuit plate load of the oscillator and by means of the voltage divider and variable phase shifter which consist of the resistances R_1 and R_2 and the capacity C_2. The tube gain is controlled by the proper cathode bias. Two bias conditions were used such that for one the carrier was suppressed to 0.1 of its original value and for the other it was suppressed to 0.01 of its value. This gave three operating conditions for the modulator of 10 percent modulation at 10, at 100 and at 1000 bars sound field pressure. For the 1000 bar operating condition the carrier suppression circuit was turned off.

As stated the condenser transmitter was connected to the resonant circuit by means of a coaxial line inside a brass tube. This construction was used in order to prevent the coaxial line from acting itself as a condenser transmitter. On the outside of this brass tube a low pass acoustic filter was constructed which was connected to the back plate of the condenser transmitter in order to allow changes in atmospheric pressure to equalize on both sides of the diaphragm. This filter was about 1 db down at 0.1 c.p.s. If it were not for changes in atmospheric pressure, the air leak in the condenser transmitter could be sealed and then the transmitter and modulator would respond to frequencies all the way down to 0 c.p.s.

Receiver

The receiver, designed to operate at 4 mc, consists of two r-f stages of amplification having a gain of 30 db per stage followed by a linear diode rectifier. The coupling transformers are broad band (50 kc wide 1 db down) so as not to cut off any of the significant side bands of the phase modulated carrier. A low pass filter connected to the diode rectifier is uniform in frequency response to 8000 c.p.s. and 0.5 ± 0.1 db down at 10,000 c.p.s. A milliammeter was inserted in the diode circuit to measure the rectified d.c. component and also to aid in balancing it out. The maximum distortionless audio output from the receiver when connected to the modulator was 1 volt for sound fields of 10, of 100, and of 1000 bars applied to the condenser transmitter. This voltage is more than sufficient when applied to the input of the d.c. amplifier to drive the string on the rapid record oscillograph to maximum amplitude.

D.C. Amplifier and Rapid Record Oscillograph

The d.c. amplifier was one developed for use with the rapid record oscillograph.[5] The amplifier is provided with an equalizer such that if the oscillograph string is tuned to 4000 c.p.s., the frequency response of the d.c. amplifier and oscillograph combined is uniform to within ± 0.5 db from 0 to 10,000 c.p.s.

Measurements

Measurements of linearity, frequency response, distortion, and noise were made on the receiver, and on the combined d.c. amplifier and rapid record oscillograph. They were found to be linear and distortionless within the limits of measurement. Their frequency response was uniform to within ± 0.5 db from 0 to 10,000 c.p.s. and their noise level was lower than could be conveniently measured. The measured range of the receiver was 60 db and that of the combined d.c. amplifier, rapid record oscillograph was 30 db. The oscillograph is the limiting element in the system,

[5] A. M. Curtis, Bell Sys. Tech. J. **12**, 76 (1933).

because the limit of resolution of the trace of the string is 30 db.

Measurements of the modulator characteristics were made at the output of the receiver. Known sound fields were applied to the type 640 condenser transmitter by means of a calibrated Western Electric Type 711A Receiver driven by an audio oscillator and coupled to the transmitter. For frequencies below 20 c.p.s. a pistonphone was used. Distortion, linearity, and noise measurements were made using 1000 c.p.s. sound fields of 10, of 100, and of 1000 bars for the three operating conditions. The modulator was found to be linear over a 50-db range for each of the operating conditions within the limits of measurement ±1 db. The noise level could be determined only in the case of the 10-bar operating condition, and for this case not very accurately. It was found to be greater than 40 db below 1 bar. Distortion measurements for the three operating conditions of the modulator over the 50-db range of each showed that each harmonic component was less than 1 percent of the fundamental. Frequency response measurements are shown in Fig. 13. The response is uniform from 0.5 to 1000 c.p.s. It is down about 1 db at 0.1 c.p.s. because of the low pass acoustic filter associated with the condenser transmitter and has a peak of 5 db at 7500 c.p.s. because of the resonance of the transmitter diaphragm. This frequency response characteristic is what would be expected for a type 640 condenser transmitter operated without the customary polarizing potential.

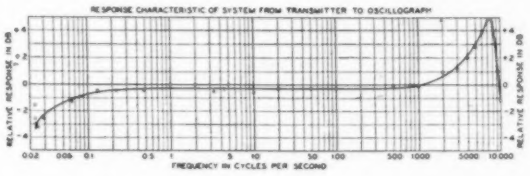
RESPONSE CHARACTERISTIC OF SYSTEM FROM TRANSMITTER TO OSCILLOGRAPH
RELATIVE RESPONSE IN DB
FREQUENCY IN CYCLES PER SECOND

FIG. 13. Frequency response of broad band recording system employing resonant circuit modulator with type 640 Western Electric condenser transmitter.

These measurements are in good agreement with the theory of the resonant circuit modulator. As the theory shows the modulator should be linear over the straight line portion of the resonance curve and low in distortion. The noise level should be below that of ordinary sound fields encountered and the frequency response should be that of the condenser transmitter.

As a final test the entire system was assembled and records were taken on the rapid record oscillograph of sinusoidal sound fields. These records corroborated the measurements in every way.

CONCLUSIONS

The theory of a resonant circuit modulator employing a condenser transmitter is outlined and it is shown that such a modulator should respond linearly to sound fields and should have low distortion and noise. The frequency response is that of the condenser transmitter used, and with proper construction can be made to cover a wide frequency range and in particular can be made to go to frequencies approaching 0 c.p.s.

Using this modulator, an experimental recording system is described which has a frequency response from 0.1 to 10,000 c.p.s. Measurements made upon this modulator and recording system were found to be in agreement with theory.

I wish to express my indebtedness to Messrs. N. G. Wade, R. T. Jenkins, J. B. Kelly, and Dr. E. C. Wente of the Bell Telephone Laboratories for their valuable suggestions and aid during the course of this work.

Transient Temperatures around Heating Pipes Maintained at Constant Temperature

ANDREW GEMANT
The Detroit Edison Company, Detroit, Michigan
(Received June 6, 1946)

This paper deals with the transient temperature distribution caused by conduction around cylindrical heating pipes maintained at definite constant temperatures. The theoretical equation for this case known from the literature is integrated numerically and presented in graphs. The amounts of heat dissipated are also computed and presented. As an application, the influence of pipe diameter upon temperatures obtained at given times is shown for a particular case. For practical installations, the characteristics of which usually deviate from those upon which the theoretical equation is based, the graphs may be used for obtaining close estimates as an aid in designing the installation. It is shown that on two actual installations a satisfactory agreement between measured and computed temperatures (maximum deviation about 10 degrees F) was obtained.

THE PROBLEM

IN connection with the practical problem of melting snow upon sidewalks by means of heated pipes, of which more will be said later, the author has had the opportunity of looking into the theoretical equations describing the process. The basic problem is the characteristics of the transient heat flow caused by conduction into an infinite medium from a cylindrical heat source that is kept at a certain temperature different from the surroundings. This two-dimensional heat flow is described by an equation, discussed in the next section, that contains a definite integral of a certain combination of Bessel functions. It occurred to the author that this integral was not entirely suitable for numerical calculations. While the integral could be expanded in series and integrated by terms, such procedure would have practical use only under certain limited conditions, and not in the whole range of variables encountered. Thus, a numerical integration of the equation and presentation of the results in graphical form seemed desirable.

Such a presentation permits the determination of temperature for any combination of variables. It is strictly valid for one cylinder in an infinite medium. In practical installations these conditions are never exactly fulfilled: There are often several pipes in the ground; also, the extent of the ground in the vertical upward direction is limited. It is thought, however, that even in such cases the theoretical equation and the graphs obtained from it might serve for obtaining a close estimate of expected temperatures and be of help in the design of the installation. This expectation was verified in the case of two actual installations, as will be shown in a later section of this paper.

The equations and the graphs are valid not only for heating, but for cooling pipes as well.

THE NUMERICAL INTEGRATION OF THE TRANSIENT EQUATION

Let us consider a cylinder of radius a in a medium of thermal diffusivity κ. At a time $t=0$ the pipe is suddenly brought to a temperature corresponding to a temperature difference T_0 above the surroundings and maintained at this level. The question is in what manner does the temperature difference T between any point in the medium and the surroundings depend on the time t and the distance r of that point from the axis of the pipe ($r>a$). The solution was obtained by Carslaw and Jaeger[1] among others and is given by

$$\frac{T}{T_0}=1+\frac{2}{\pi}\int_0^\infty \exp(-\kappa u^2 t) \times \frac{J_0(ur)N_0(ua)-J_0(ua)N_0(ur)}{J_0^2(ua)+N_0^2(ua)}\frac{du}{u}, \quad (1)$$

where u is a variable having the dimension of a reciprocal length extending from zero to infinity, J_0 and N_0 = Bessel functions of first and second kind, both of zero order.

[1] H. S. Carslaw and J. C. Jaeger, Phil. Mag. **26**, 473 (1938).

It is advantageous to transform this integral by replacing all quantities occurring in it by dimensionless variables. The substitutions required are the dimensionless temperature ratio

$$\theta = T/T_0, \tag{2}$$

the dimensionless distance ratio

$$\rho = r/a, \tag{3}$$

the dimensionless time function

$$\tau = \kappa t/a^2, \tag{4}$$

and, instead of u,

$$v = au. \tag{5}$$

With these substitutions, Eq. (1) becomes

$$\theta = 1 + \frac{2}{\pi}\int_0^\infty \exp(-\tau v^2) \times \frac{J_0(\rho v)N_0(v) - J_0(v)N_0(\rho v)}{J_0^2(v) + N_0^2(v)} \frac{dv}{v}. \tag{6}$$

The integration of Eq. (6) was carried out numerically by dividing the total integral in three parts:

$$\int_0^\infty = \int_0^{v_1} + \int_{v_1}^{v_2} + \int_{v_2}^\infty. \tag{7}$$

It can be shown that for v_1 smaller than a certain limit the first term, after expansion in a series, can be solved explicitly, and for v_2 larger than a certain limit the third term can be neglected. It remains then to compute numerically the second term between the limits specified.

Concerning the limit for v_1, it must fulfill the two conditions: $\tau v_1^2 \ll 1$ and $\rho v_1 \ll 1$. The largest value of τ considered was 10^4 and the largest value of ρ was 40. Hence, $v_1 = 10^{-4}$ is seen to fulfill both conditions satisfactorily.

Using the known expansions[2] of the Bessel functions, the first integral, multiplied by $2/\pi$, takes the form:

$$-\ln \rho \int_0^{v_1} \frac{dv}{v \ln^2(\gamma v/2)}, \tag{8}$$

where $\ln(\gamma/2) = -0.116$. This can be integrated directly, giving

$$\ln \rho/(\ln v_1 - 0.116). \tag{9}$$

With regard to the third term, the asymptotic expansion[2] of the Bessel functions can be used as an approximation. The integral, multiplied by $2/\pi$, is then represented by

$$-\frac{2}{\pi\sqrt{\rho}}\int_{v_2}^\infty \exp(-\tau v^2)\frac{\sin[(\rho-1)v]}{v}dv. \tag{10}$$

The value of this integral is certainly smaller than the following, obtained by replacing the sin function by unity and v in the denominator by v_2:

$$-\frac{2}{\pi v_2\sqrt{\rho}}\int_{v_2}^\infty \exp(-\tau v^2)dv,$$

and the condition required is that this last integral should be small as compared with unity. Introducing the error integral ϕ, the third integral can be neglected if

$$\frac{1}{v_2(\pi\rho\tau)^{\frac{1}{2}}}[1 - \phi(v_2\sqrt{\tau})] \ll 1. \tag{11}$$

TABLE I. Numerical integration of Eq. (6) for $\rho = 4$ and $\tau = 100$.

v	Fraction below integral involving Bessel functions	Exponential function	$\frac{2}{\pi}$ times integrand	Geometric average of integrands	Average of integrands times Δv
1×10^{-4}	−0.0243	1.00	−155	−118	−0.0118
2×10^{-4}	−0.0282	1.00	− 90.1	− 77.1	−0.0077
3×10^{-4}	−0.0310	1.00	− 65.8	− 50.8	−0.0152
6×10^{-4}	−0.0369	1.00	− 39.2	− 32.4	−0.0130
1×10^{-3}	−0.0420	1.00	− 26.8	− 20.8	−0.0208
2×10^{-3}	−0.0510	1.00	− 16.2	− 14.1	−0.0141
3×10^{-3}	−0.0580	1.00	− 12.3	− 9.77	−0.0293
6×10^{-3}	−0.0730	0.996	− 7.75	− 6.43	−0.0257
1×10^{-2}	−0.0841	0.990	− 5.31	− 4.31	−0.0431
2×10^{-2}	−0.114	0.961	− 3.49	− 3.07	−0.0307
3×10^{-2}	−0.138	0.914	− 2.69	− 1.98	−0.0594
6×10^{-2}	−0.196	0.698	− 1.45	− 0.940	−0.0376
0.1	−0.258	0.368	− 0.606	− 0.117	−0.0117
0.2	−0.386	0.0183	− 0.0225	− 0.00167	−0.0002
0.3	−0.476	0.000123	− 0.000124		
				Sum:	−0.3203
				First integral, expression (9):	−0.1482
				Total integral:	−0.4685
				θ:	0.53

[2] E. Jahnke and F. Emde, *Tables of Functions* (Dover Publications, New York, 1943).

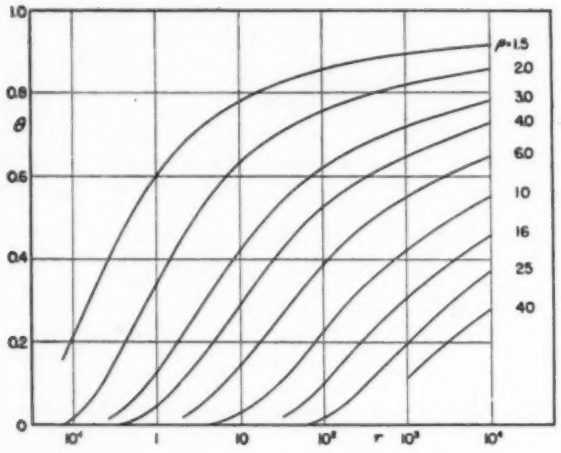

FIG. 1. Temperature as a function of time of heating for various distances from the axis of the pipe.

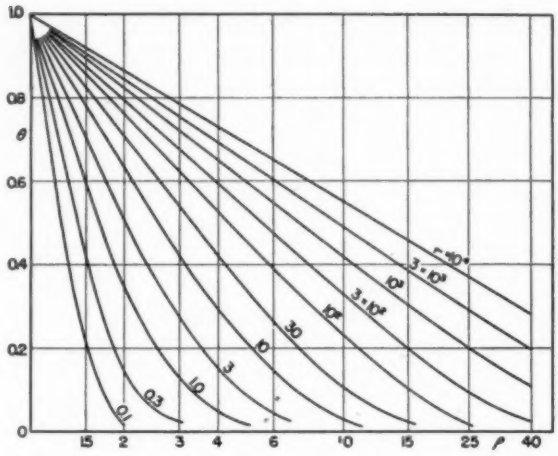

FIG. 2. Temperature as a function of the distance from the axis of the pipe for various times of heating.

From tables[2] of the error integral it is known that the square bracket in Eq. (11) is very small as compared with unity for arguments equal to or larger than 3. Hence, the limiting value of v_2 is given by

$$v_2 \geqq 3/\sqrt{\tau}. \tag{12}$$

The integration of Eq. (6) was thus carried out numerically between the limits $v_1=10^{-4}$ and $v_2=3/\sqrt{\tau}$; the term (9) was then added to the result of the summation.

Concerning the range of the parameters ρ and τ of the integration, it should be recalled that κ for various materials varies between about 10^{-3} and 10^{-1}. The heating times that might be encountered in practical applications vary between, say, 10 minutes and a day. The radii of heating pipes range roughly between 1 and 10 cm, and the distances from the axis of the pipe between 1 and 100 cm. These ranges are fairly well, although not completely, covered by the range of ρ between 1.5 and 40 and τ between 10^{-1} and 10^4.

As an example of the numerical integration, Table I for $\rho=4$ and $\tau=100$ is given.

THE USE OF THE GRAPHS

The results of the calculations as outlined in the foregoing sections are presented in Figs. 1 and 2. Figure 1 presents θ as a function of τ for various values of ρ, and Fig. 2 presents θ as function of ρ for various values of τ; the abscissae of both graphs are logarithmic.

There exists extensive literature for the numerical calculation of heat transients *inside* certain enclosures, including cylinders. Patton[3] uses a stepwise graphical computation, Emmons[4] and Dusinberre[5] apply approximate numerical methods. Graphs, calculated from the rigorous equations, are applied to the interior of enclosures by Newman,[6] Olson and Jackson,[7] and Olson and Schultz.[8] The present writer has not yet found in the literature the application of this principle to the exterior of a cylinder.

The method of using the two graphs, Figs. 1 and 2, is rather obvious, but a few remarks may be made. From the constants of a given installation and the distance and time for which the temperature is required, ρ and τ are computed from Eqs. (3) and (4). Generally the specific values of these two parameters will not be represented by any of the curves on Figs. 1 or 2. From the particular value of τ, the values of θ for a few values of ρ near the one required are read from Fig. 1 and plotted *vs.* log ρ. From a curve drawn through these points, θ for the particular ρ can then be read. Or the same procedure can be carried out starting from the particular ρ and plotting θ *vs.* log τ, whichever of the two alternatives appears better suited to

[3] T. C. Patton, Ind. Eng. Chem. **36**, 990 (1944).
[4] H. W. Emmons, Trans. ASME **65**, 607 (1943).
[5] G. M. Dusinberre, Trans. ASME **67**, 703 (1945).
[6] A. B. Newman, Ind. Eng. Chem. **28**, 545 (1936).
[7] F. C. W. Olson and J. M. Jackson, Ind. Eng. Chem. **34**, 337 (1942).
[8] F. C. W. Olson and O. T. Schultz, Ind. Eng. Chem. **34**, 874 (1942).

the case. From θ the temperature is given by Eq. (2).

INFLUENCE OF PIPE DIAMETER ON TEMPERATURE

A practical application of the graphs given in Figs. 1 and 2 is the evaluation of the effect of the pipe diameter upon temperatures attained at certain times and distances from the center of the pipe. It is obvious that with increasing pipe diameter the temperature at a given point increases, but the question is whether this increase is sufficiently large to justify the installation of larger pipes.

An answer to this question can be given only if all the other quantities involved are known. As an illustration of such a case, some data are presented in Fig. 3. A medium of diffusivity $\kappa=0.01$ is taken, and a distance of 10 cm from the pipe axis is assumed. The question is: How does the temperature after certain heating times vary with the pipe radius? From the various data, ρ and τ are computed and θ is read using Figs. 1 and 2 as explained in the previous section. The result for four different heating times is plotted on Fig. 3.

As can be seen, for the range of radii of 1 to 3 cm the increase in temperature difference is nearly proportional to the increase in radius for a 30-minute heating time, but for somewhat longer times, for instance 1 hour and 30 minutes, the effect is less than proportional: The temperatures for 1- and 3-cm radii being in the ratio of 1.0:1.95.

THE AMOUNT OF HEAT DISSIPATED

Further information that can be obtained by using Eq. (1) is the amount of heat Q that is dissipated per unit time per unit length of the cylinder. It is interesting in this connection to compare the present case of heating pipes with the companion case of cables, as discussed by Sticher and the author,[9] among others. In the case of cables, the amount of heat dissipated is constant while the temperature, in the absence of a sink, would continue to rise indefinitely. In the present case of a pipe of constant temperature the heat dissipated is theoretically infinite at the first moment and gradually decreases, in the absence of a sink, indefinitely.

This function, Q *vs.* time is now calculated from Eq. (1). The heat flow at any radius r is

$$Q_r=-2\pi rg(dT/dr),$$

with g=thermal conductivity of the medium. Using θ and ρ as before

$$Q_r/T_0=-2\pi\rho g(d\theta/d\rho). \tag{13}$$

Remembering the general relation for any Bessel function

$$Z_0'=-Z_1,$$

one has

$$\frac{d\theta}{d\rho}=-\frac{2}{\pi}\int_0^\infty \exp(-\tau v^2)\times\frac{J_1(\rho v)N_0(v)-J_0(v)N_1(\rho v)}{J_0^2(v)+N_0^2(v)}dv. \tag{14}$$

Since we are interested in the value of Q_r for $r=a$, we have

$$\frac{Q}{T_0 g}=4\int_0^\infty \exp(-\tau v^2)\frac{J_1(v)N_0(v)-J_0(v)N_1(v)}{J_0^2(v)+N_0^2(v)}dv. \tag{15}$$

Carrying out the numerical integration of Eq. (15) for various values of τ following the pattern of Eq. (6), the function in question can be obtained.

It is of interest to note that the same function is obtainable from Fig. 2 without any additional

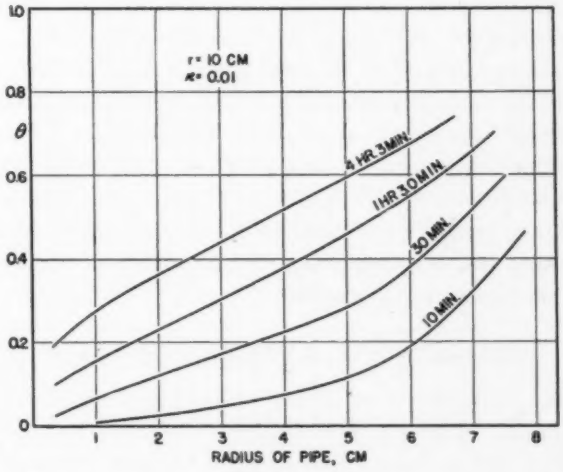

FIG. 3. Effect of pipe diameter upon temperature for various times in a given case, as shown. The notation on the upper curve should read "4 hr. 30 min."

[9] Andrew Gemant and Joseph Sticher, Trans. AIEE 65, 475 (1946).

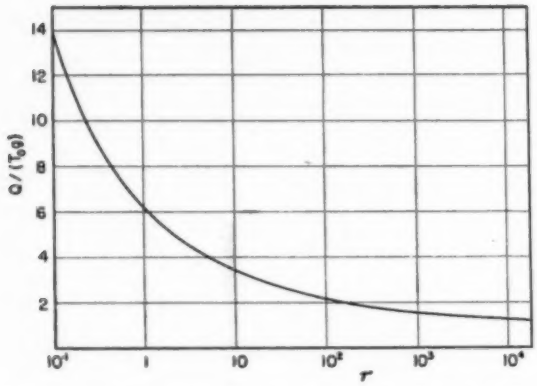

FIG. 4. Heat dissipated per unit time and unit length of pipe as a function of time.

computation. From Eq. (13) one has

$$\frac{Q}{T_0 g} = -\frac{2\pi}{2.30}\left(\frac{d\theta}{d \log \rho}\right)_{\rho=1}, \qquad (16)$$

and the quantity in the bracket is simply the initial slope of the various curves in Fig. 2.

Figure 4 was constructed by actually calculating numerically the integral in Eq. (15). As a check for the computation, Eq. (16) in conjunction with Fig. 2 was used; the agreement, as was to be expected, was good within 1 percent, the accuracy aimed at for the final results of the numerical computations. In Fig. 4 the dimensionless heat dissipated, $Q/(T_0 g)$, is plotted *vs.* τ, from which Q is obtained for any specific case and any given time.

Let us calculate an example. A pipe of 8-cm diameter in soil of diffusivity 0.005, thermal resistivity 100 thermal ohms, and an ambient temperature of 20°C is heated to 100°C. What is the heat dissipated per sec. per cm of pipe length, after 10 minutes and after 1 hour? The values of τ are 0.19 and 1.12, and the ordinates read from Fig. 4 are 10.8 and 6.0, respectively. Thus, with $T_0 = 80$ and $g = 10^{-2}$, the heats dissipated per sec. are 8.6 and 4.8 watts/cm at the two moments in question.

APPLICATION TO A PRACTICAL PROBLEM

A verification on an experimental basis of the graphs given is obviously not necessary since Eq. (1) is based on straight-forward mathematics. It is shown, however, in this section that the graphs can be used for purposes of close estimates in practical cases in which the conditions underlying Eq. (1) are not fulfilled.

Equation (1) is based on one heating pipe in an infinite medium. In practical cases three deviations from these conditions occur: (a) The pipes are of finite length. This limitation, except for very short pipes, does not seriously affect the applicability of Eq. (1). (b) There are usually several parallel pipes. This circumstance is probably not too serious, either, because the influence of the pipes diminishes rapidly with increasing distance from the pipe. An approximation for not too long heating times may be obtained by simply adding the temperature differences produced by the pipes in the immediate neighborhood of the point in question. (c) The medium in which the pipes are embedded is of limited dimensions. This circumstance will generally invalidate Eq. (1), so that for this reason it cannot be expected to yield other than approximate values.

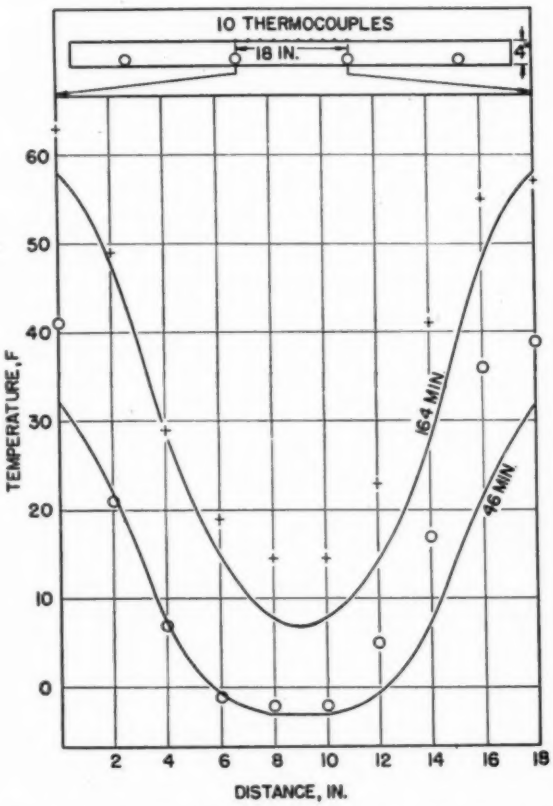

FIG. 5. Temperature distribution on top of a slab containing heating pipes for two different times of heating.

○ and + are measured data.
Solid lines are computed from graphs in Figs. 1 and 2.

Application of the graphs to the problem of snow melting by means of heat is now shown. The Detroit Edison Company, with which the author is associated, has made some trial snow-melting installations. A cross-sectional schematic diagram of one of these installations is shown at the top of Fig. 5. It is a concrete slab 4 inches deep, simulating a sidewalk, containing four parallel pipes, $1\frac{5}{8}$ in. o.d., spaced 18 inches from center to center. As shown, ten thermocouples were arranged on top of the slab for temperature determinations. The temperature of the surroundings was -3°F and the pipes carried water at 170°F.

In order to apply the graphs, the diffusivity of the embedding medium, concrete, has to be known. The density of concrete was taken as 2.0 g/cc, the specific heat as 0.21 cal./g deg. C, and the thermal conductivity as 0.0029 cal./sec. cm deg. C, as listed for concrete containing 10 percent water; all data were taken from the Landolt-Börnstein Tables.[10] From these data one has $\kappa = 0.007$.

The points given in Fig. 5 indicate the measured temperatures after the water had been flowing for 46 and 164 minutes. The curves were computed from the graphs; the maximum deviation between measured and computed data is about 10°F. From these data the conclusion was drawn that the temperature distribution over the surface was too uneven for the purpose; a similar installation with the pipes on 6-inch centers was then decided upon. Measurements with such an installation, only 12 in. wide, indicated a fairly even temperature distribution; a surface temperature of 32°F, necessary for melting the snow, was reached in about 35 minutes. Computation on such an arrangement also showed even distribution; a temperature of 32°F at a distance from the pipes corresponding to the top surface is reached in about 50 minutes. Considering the relatively small dimensions of the slabs, the agreement between measurements and the estimate from the graphs is satisfactory

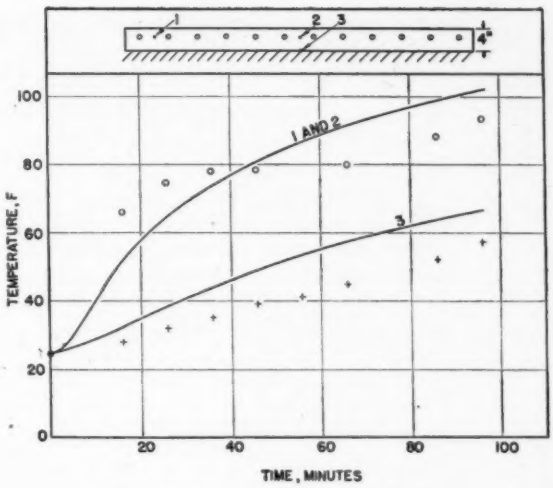

FIG. 6. Temperature as a function of time in a slab containing heating pipes.

Numbers 1 to 3 refer to three thermocouples.
○ and + are measured data.
Solid lines are computed from graphs in Figs. 1 and 2.

and shows the usefulness of the latter. Since the installations were in a small cold room, the measured data are higher than the estimates because of the low diffusivity of air.

A cross-sectional sketch of a trial field installation is shown at the top of Fig. 6. The 4-inch deep concrete slab contained twelve iron pipes, 0.84 in. o.d., on 5-in. centers. Three thermocouples were installed as indicated. The temperature of the surroundings was 25°F, that of the water 160°F. The points in Fig. 6 show the measured temperatures as a function of time, the circles being averages of data obtained from thermocouples 1 and 2; the lines represent the estimates from the graphs. The maximum deviation is 12°F. In this case the measured temperatures at the bottom of the slab and partly also near the top are lower than the estimates; this is explainable as a result of the wet ground below the slab and the convection loss caused by wind above the slab. However, even in such an unfavorable case, estimates from the graphs might be useful for designing installations of this kind.

The author is indebted to his colleague, C. M. Weinheimer, for having placed at his disposal the data on the two experimental installations.

[10] Landolt-Börnstein, *Physikalisch-Chemische Tabellen* (Edwards Brothers, Ann Arbor, 1943).

The Effect of Temperature on the Strength and Fatigue of Glass Rods

B. VONNEGUT* AND J. L. GLATHART
Preston Laboratories, Butler, Pennsylvania
(Received July 31, 1946)

By the use of an electrodynamic quick-loading device, the strength of scratched soda-lime glass rods was measured at various temperatures between −190°C and 520°C for load durations of 0.1 second, 10 seconds, and 100 seconds. It was found that the strength was highest at the lowest temperature, declined to a minimum at 100°–200°C, and then increased for higher temperatures. Static fatigue was exhibited at all temperatures, being maximum in the region of minimum strength. Comparisons with the results of other experimenters are made.

INTRODUCTION

THE strength of glass, defined in terms of the stress required to cause fracture, has been a subject of investigation for many years. Most of these investigations have been carried out at room temperature and under ordinary atmospheric conditions. However, glass is frequently called upon to bear large stresses at other temperatures, both lower and higher. As examples we may cite Dewar flasks for holding liquid air, carbonated beverage bottles on ice, and gauge glasses of steam boilers. A knowledge of the way in which the strength of glass depends upon temperature is thus of economic importance as well as being necessary to a full understanding of the fundamental properties and behavior of glass as an example par excellence of a brittle solid.

The experimental results of T. C. Baker, in the years 1938–40, on the mechanical properties of glass have recently been described by Baker, Preston, and Glathart.[1,2] In 1939, Baker declared that the subject matter seemed to be threatening to escape from the field of physics proper into that of physical chemistry. Accordingly, it became necessary to assign a chemist to the problem, and the senior author's brief connection therewith (1939–40) arose from Baker's feeling. However, the work here described may be said to be straightforward physics. It follows the line of thought reported by Preston[3] that, when the very nature of the problem is obscure, it may be useful to find out how the phenomena vary when the temperature is changed.

The effect of temperature upon the strength of glass has been studied by a number of investigators.[4–10] The results reported have been somewhat discordant, some tending to show that the strength is independent of temperature,[4,5] at least up to about 500°C, while other experiments [6–10] indicate definite temperature effects. This is not surprising, perhaps, when it is remembered that data obtained by different experimenters on the strength of glass at room temperature are not consistent. This is undoubtedly due to the fact that the breaking stress of glass is a function of many variables. Among these are the size and shape of the specimen, the condition of its surface, its chemical composition, and its thermal history, as well as the rate of loading and the water and CO_2 content[1] of the surrounding atmosphere. These are variables which are not always under control in the usual experiment.

The experimental work reported herein was done by the senior author at the Preston Laboratories in 1940, before this country became involved in the war. The changes in personnel and press of war work at the Laboratories prevented publication at the time, and it has only recently been possible for one of us (J.L.G.) to

* Formerly Hartford-Empire Company research fellow at Preston Laboratories. Present address: General Electric Company, Schenectady, New York.

[1] T. C. Baker and F. W. Preston, J. App. Phys. **17**, 162–188 (1946).

[2] J. L. Glathart and F. W. Preston, J. App. Phys. **17**, 189 (1946).

[3] F. W. Preston, J. App. Phys. **13**, 10, 629 (1942).

[4] H. von Wartenberg, Zeits. f. tech. Physik. **13**, 479 (1932).

[5] G. O. Jones and W. E. S. Turner, J. Soc. Glass Tech. **26**, 35 (1942).

[6] K. Mengelkoch, Zeits. f. Physik **97**, 46 (1935).

[7] M. Eichler, Zeits. f. Physik **98**, 280 (1935).

[8] J. S. Gregorius, Bull. Am. Ceram. Soc. **15**, 271 (1936).

[9] A. Smekal, Ergeb. d. exakt. Naturwiss. **15**, 106 (1936).

[10] W. Dawihl and W. Rix, Zeits. tech. Physik. **19**, 294 (1938).

collect the old data and prepare the present summary.

These results are not intended to be interpreted as the last word on the question of strength *versus* temperature. That must wait for a more adequate appreciation of all the factors involved. However, these data will add just that much more evidence to the view that the temperature coefficient of the strength of glass is by no means negligible.

APPARATUS AND PROCEDURE

The specimens used were annealed soda-lime glass rods six inches long and 7/32 inch in diameter. They were tested in cross bending, between knife edges five inches apart, with central knife-edge loading.

In order to insure a greater homogeneity with respect to surface conditions, the glass rods were uniformly abraded with 00 emery paper applied to them as they were rotated in the chuck of an electric drill.

The apparatus for applying the loads was that used by Baker[1] with the addition of devices for maintaining the specimens at various constant temperatures during tests. Briefly, it consisted of a loud-speaker field magnet, in the magnetic field of which was suspended a light armature coil. This coil was attached to the central knife edge, and when both it and the field magnet were energized by the current from storage batteries, a constant load was applied to the specimen. This load was directly proportional to the armature current, and could be varied from zero to a maximum value of 30 pounds.

The loads were applied in increments of 500 lb./sq. in., and for durations of 0.1, 10, and 100 seconds. The time of the shortest interval was measured with a cathode-ray oscillograph.

The equipment used for making the low temperature tests is shown in Fig. 1. It is essentially a horizontal metal tube which could be surrounded with various low temperature mixtures. This tube contained the test rod, mounted on knife edges. Below the center of the specimen was a narrow vertical tube, extending to the outside of the insulated container, through which the wire stirrup from the armature coil passed.

The two low temperatures used were those of dry ice and liquid air, respectively, their values being obtained from the literature.

The measurements made above room temperature employed a simple furnace made of steel tubing which could be closed at both ends. These temperatures were maintained constant by a thermoregulator and measured with a thermocouple.

The general procedure in testing a rod at any given temperature was to apply a light load (small armature current) for the chosen time interval. If the rod did not break, the current was increased and a larger load applied for the same time interval. This process was continued until the specimen broke.

Although tests showed that the rods reached temperature equilibrium with the enclosure in six or seven minutes, they were always left in the apparatus for 15 minutes before testing. During this time they were exposed to the atmosphere in the room, which had come to the temperature of the interior of the apparatus. The low temperature equipment was sufficiently airtight so that there was little circulation of the atmosphere through it. No deposit of frost on the specimen was ever observed.

RESULTS

The effect of temperature on the strength of soda-lime glass is shown by the graph of Fig. 2,

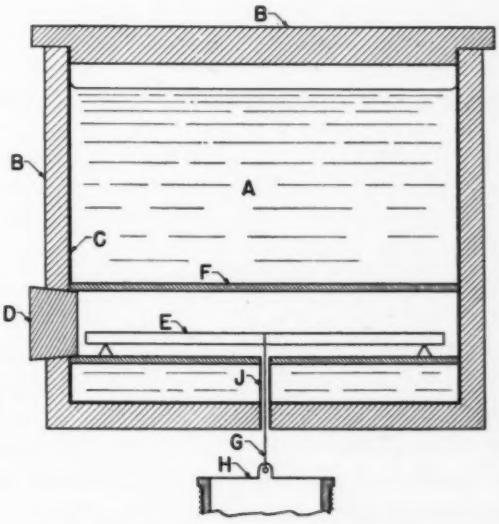

FIG. 1. Low temperature apparatus.

A. Low temperature liquid. *B*. Celotex thermal insulation. *C*. Metal container. *D*. Rubber stopper. *E*. Glass rod specimen. *F*. Metal tube. *G*. Wire loop. *H*. Armature coil. *J*. Wire channel.

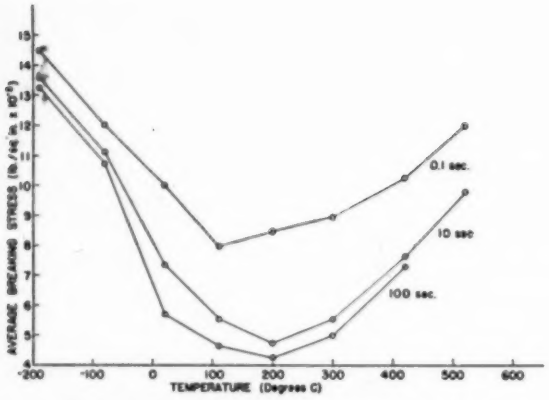

FIG. 2. The breaking strength of glass rods as a function of temperature.

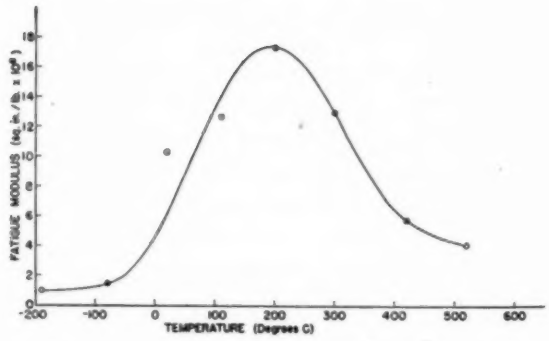

FIG. 3. The fatigue modulus of glass as a function of temperature.

in which the breaking stress in pounds per square inch is plotted against the temperature in degrees centigrade. Each plotted point represents the average for 12 rods, corrected for the loading increment. Since the theoretical form of these curves is unknown, the points are connected by straight lines simply for convenience in associating them.

No determination of the strength of the rods was possible for a load duration of 100 seconds at 520°C. At this temperature, the glass was sufficiently soft that it bent out of shape before its breaking point was reached. For the loads of shorter duration this deformation was not large enough to cause any trouble.

Figure 3 shows the fatigue modulus plotted against the temperature.

DISCUSSION AND COMPARISON OF RESULTS

It can be seen from Fig. 2 that the strength of soda-lime glass, for a 10-sec. duration of stress, decreases from about 13,600 lb./sq. in. at −190°C to about 4800 lb./sq. in. at 200°C. This is a decrease of 65 percent. Beyond 200°C the strength increases, reaching almost 10,000 lb./sq. in. at 520°C. The other two curves follow, in general, the same pattern, with a minimum strength in the 100°–200° range.

Since the chemical composition was the same for all rods used, and since the surface condition was made as nearly uniform as practicable by the abrasion, it is presumed that this temperature effect is due largely to the action of adsorbed moisture. At low temperatures, the weakening effect due to this moisture layer would be small because of its relative inactivity. Above the 100°–200° range the moisture layer would be driven off. It would be likely to have its greatest effect in the very temperature range in which the glass showed minimum strength. It is undoubtedly true that the severe surface abrasion had an effect on the moisture adsorption. It is known that the heat of adsorption in narrow cracks and crevices of an adsorbent differs greatly from that on the plane surface.

The static fatigue phenomenon, that is, the decrease in strength with duration of load, is shown in Fig. 2 by the positions of the three points corresponding to any one of the temperatures at which measurements were made.

The dependence of fatigue on temperature is shown more clearly, however, in Fig. 3. In this figure the ordinate is the fatigue modulus w_{et_o} defined by Glathart and Preston.[2]

$$w_{et_o}=\frac{1}{f_{et_o}}.$$

Here f_{et_o} is the breaking stress for a duration of load et_o, e being the base of natural logarithms, 2.718, and t_o the threshold time, or the least time interval in which a tensile stress, however large, can rupture the material (or the specimen). The fatigue modulus w_{et_o} represents the number of square inches that must be added to the cross-sectional area assigned to carry unit load (one pound) in order to double the life of the specimen.

Figure 3 shows that the fatigue is small at the lowest temperatures, reaches a maximum at about 200°C and thereafter decreases. It is

interesting, and perhaps significant, that the maximum fatigue occurs in the same temperature range in which the strength is least.

Although a smooth curve has been drawn among the plotted points in Fig. 3, there is no reason for believing that it represents the data any better than a number of other curves which might be drawn, including a curve passing exactly through all the points. However, there is some reason for believing that the experimental point at 20°C may be too high, and the line has been drawn accordingly.

It is worth while, perhaps, to compare the fatigue at room temperature of these abraded soda-lime rods with that of the similar unabraded rods used by Baker and Preson.[1] They found that their unabraded rods decreased in strength from 15,900 lb./sq. in. at 0.1-sec. duration of stress to 9100 lb./sq. in. at 100-sec. duration, a decrease of 6800 lb./sq. in. or 42.8 percent. Over the same range, the decrease for the abraded rods of the present report was 4300 lb./sq. in., or 43 percent. This substantiates the conclusion reached by Baker and Preston[1] that scratched glass loses much less strength in a given time interval than does unscratched glass but the percent loss of strength is roughly the same. Their conclusion was based on their results for scratched and unscratched Pyrex glass only. It can now be said to be confirmed even more accurately for soda-lime glass.

The abrading reduced the absolute value of the strength of soda-lime rods at room temperature from 15,900 to 10,000 lb./sq. in. on the 0.1-sec. test, a drop of 37 percent. The corresponding values for the 10-sec. and 100-sec. tests are 29 percent and 38 percent, respectively. Thus abrading alone has the effect of reducing the strength of soda-lime glass about one-third, at room temperature.

The results shown in Fig. 2 are in substantial agreement with those reported by Smekal[9] who tested scratched Thuringer apparatus glass rods over the same temperature range, using constant rates of loading of 420 and 53 g/mm²/sec. He found that the strength reached a minimum at 150°C, a decrease of 62 percent from the −190°C value in the case of his lower loading rate.

Mengelkoch[6] also found a minimum strength at 150°, the decrease from the −190°C value being about 50 percent. Gregorius,[8] on the other hand, found a minimum at 300°C.

The results reported by Jones and Turner,[5] however, are in distinct disagreement with those discussed thus far. They used unabraded flat glass laths thoroughly annealed and firepolished. Their experiments covered the range from 20°C to 560°C, and were apparently very carefully controlled. Up to 500°C they found no change in strength with temperature but beyond 500° the strength declined.*

In spite of this, it is believed that the results herein reported give a correct representation of the change in the strength of glass with temperature, under the conditions of the experiment and for the type of specimens used.

CONCLUSIONS

It is concluded that the strength and the static fatigue of scratched soda-lime glass rods exposed to the atmosphere show a pronounced variation with temperature. A minimum of the strength and a maximum of the fatigue at 100°–200° suggest that the form of the curves obtained may be attributed to the effects of adsorbed layers on the surface of the glass. It would be expected that the effects of the layers would be small at low temperature because of the small activity at low temperatures. At high temperatures the effects would again be small because of the evaporation of the layers. Confirmation of this theory will depend on the results of tests on the strength of glass made over the same temperature range in high vacuum, in the absence of adsorbed films.

* Professor Turner states, in a private communication just received, that later measurements by A. J. Holland have been carried down to −40°C, where an increase of modulus of rupture of 20 percent over that at room temperature was found, as well as an increase in impact strength of 17 percent. This is more in agreement with the results reported here.

Plastic Flow, Creep, and Stress Relaxation

Part I. Plastic Flow

CHARLES MACK
Technical and Research Department, Imperial Oil Limited, Sarnia, Ontario
(Received March 28, 1946)

Plastic substances are considered to be composed of units of flow with various yield values. It is shown that in this case the product of the strain rate and viscosity is equal to the sum of the differences between the applied stress and the yield values. This relationship can be applied to any plastic system free of elastic after-effect and expresses their mechanical properties in terms of a coefficient of viscosity which is independent of the stress applied. With the proper choice of the distribution of yield values any kind of relation between stress and strain rate can be established. This relationship is applied to plastic flow which is defined as a deformation mechanism having a curvilinear relationship between stress and rate of deformation and a constant rate of deformation at constant stress. Equations are given for the coefficient of viscosity of such systems and for the relaxation of stress at constant deformation as a function of time.

INTRODUCTION

IDEAL solids and perfect liquids represent two states of matter and two extremes in mechanical behavior. A stress applied to a perfectly elastic body brings about a deformation, the amount of which is proportional to the stress applied and independent of the duration of its application. Because of the symmetric structure of an ideal solid, the deformation involves a change in the distance between the constituent units against chemical forces, and each constituent particle retains identical neighbors.

A perfect liquid can support no other stresses in a state of rest but a hydrostatic pressure. Internal stresses appear as soon as the various volume elements are set in motion relative to each other. These stresses in turn produce a continuously increasing deformation, the rate of which is only determined by the stresses. These stresses are therefore not connected with the magnitude of the deformation at any moment, and they disappear completely, as soon as no further deformation is produced in the liquid. Consequently the deformation of a liquid cannot give rise to any change in potential energy, as in the case of an ideal solid, and the work performed during the deformation is partly used for maintaining the kinetic energy of each moving volume element, and the remainder is converted into heat.

Many industrially important substances have properties which place them between ideal solids and perfect liquids, i.e., they have rigidity as well as viscosity. The mechanical behavior of such substances is generally referred to as plasticity. The elastic properties of plastic substances are the same as those of ideally elastic bodies except for systems showing the phenomenon of elastic after-effect. Their flow properties, however, deviate from those of perfect liquids in that their relationship between shearing stress and rate of shear is curvilinear. When subjected to a constant stress, plastic substances show two types of plastic deformation as a function of time. In one case the deformation increases linearly with time and the rate of deformation is constant. This type of deformation as a function of time will be termed "plastic flow." The other type has a non-linear relationship between time and deformation, the rate of which decreases with time, and will be referred to as "creep."

The knowledge of the mechanical properties of plastic substances is purely empirical in most cases. It is most desirable to put this knowledge on a more rational basis, since it would make it finally possible to design a plastic substance for a specific use. Much progress has been made by applying the methods of statistical mechanics to molecules.[1,2] These methods become very com-

[1] H. Eyring and co-workers, J. Chem. Phys. **4**, 283 (1936), **5**, 726 (1937); J. App. Phys. **12**, 669 (1941); Ind. Eng. Chem. **33**, 430 (1941).
[2] A. P. Alexandrov and J. S. Lazurkin, Acta Phys. Chim. U.S.S.R. **12**, 647 (1941).

plicated when applied to systems containing molecular aggregates of varying size built up from identical molecules or to systems containing such aggregates with several components. Most mechanical tests involve the measurement of a relationship between stress, deformation, and time, and it is a matter of necessity to express such a relationship in terms of exact quantities. For this purpose recourse is taken to the mechanical models suggested by Burgers.[3] These models consist of elastic and viscous elements rigidly attached to each other. These elements can be coupled in series or in parallel. No more importance should be attached to these elements than that of mathematical symbols.

The behavior of the simpler forms of these models under stress was discussed by Burgers for the condition of lateral confinement of the models. In the following the derivation of the equations covering the deformation mechanism of plastic substances will be discussed for the condition of tension at constant temperature. The results are directly applicable to the condition of shear, and the shearing stress and shear strain can be calculated from the tensile stress and strain.[4]

GENERAL MODEL FOR PLASTIC DEFORMATION

For viscous flow the Burgers model consists of an elastic spring and a viscous element coupled in series. Spring A in Fig. 1 is considered to be perfectly elastic and element B consists of a porous piston moving in a cylinder filled with a perfect liquid. A tensile stress, S, applied at constant temperature causes an immediate elongation of spring A followed by movement of the piston of element B. The total strain of the system consists of the sum of the individual strains, consequently the individual strain rates are also additive.

Plastic substances are poly-disperse systems which contain the disperse phase in various degrees of subdivision ranging from individual units of flow to structural units of varying size. A sufficiently low stress produces a strain in the readily deformable part of the system and a resistance to shear in the structural units. As the stress increases, these units are also deformed at a rate which depends upon their individual yield values. The total strain rate at a given stress is therefore equal to the sum of the strain rates of the individual units.

Such a system can be represented by a model which consists of an elastic element and a number of viscous elements, all coupled in series. Each viscous element has a different yield value. A low stress causes movement of the pistons of all elements with yield values lower than the stress applied. With increasing stress more viscous elements take part in the deformation. Omitting the elastic element, the total strain rate is equal to the sum of the individual strain rates of the viscous elements

$$v=v_1+v_2+v_3+\cdots v_n.$$

The strain rate v is $d\epsilon/dt$, where the strain ϵ is preferentially expressed as the "true strain," the natural logarithm of the ratio length after deformation over original length.[5] With the viscous elements containing the same liquid, the individual strain rates can be replaced by the active stress (applied stress minus yield value) over the

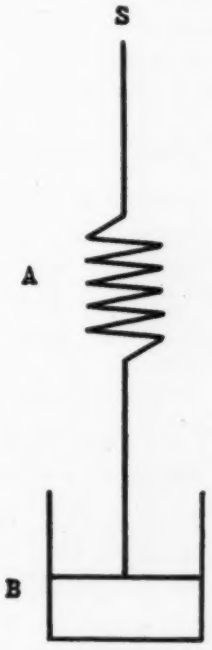

FIG. 1. Model for viscous flow.

[3] J. M. Burgers in *First Report on Viscosity and Plasticity* Acad. Sci., Amsterdam 1935.
[4] A. Nadai, J. App. Phys. **8**, 205 (1937).
[5] For details see Markus Reiner, *Ten Lectures on Theoretical Rheology* (Rubin Mass, Jerusalem, 1943).

coefficient of viscosity

$$v=(S-Sf_1)/\eta+(S-Sf_2)/\eta+\cdots(S-Sf_n)/\eta,$$

or

$$v=\sum (S-Sf_i)/\eta. \quad (1)$$

For the condition of tension, the expression η is understood to have the same dimensions as the coefficient of viscosity and to be proportional to it. When the system contains components of different viscosities, the individual strain rates and hence their fluidities $(1/\eta)$ are also additive, and the above equation becomes

$$v=\sum [(S-Sf_i)/\eta_i]. \quad (2)$$

These equations can be applied to any plastic system, the plastic deformation of which is not recoverable, and express their mechanical properties in terms of a coefficient of viscosity which is independent of the stress applied. With the propriate choice of the distribution of yield values any kind of relation between stress and strain rate can be established.

PLASTIC FLOW

Several empirical equations for plastic flow are given in the literature which cover the relationship between stress and strain rate. The most outstanding equations give the stress as a power function of the strain rate and the stress as a function of the logarithm of the strain rate.

(a) Stress a Power Function of Strain Rate

For many disperse systems the curvilinear part of the stress/strain rate diagram conforms to empirical equations which have been given by de-Waele,[6] Farrow,[7] and Wo. Ostwald.[8] These equations are similar in form and may be expressed as follows:

$$S/S_0=(v/v_0)^b, \quad (3)$$

where b is a dimensionless constant, and S_0 and v_0 are constants with the dimensions of stress and strain rate. If the system has a yield value, then S_0 represents the minimum stress which brings about an observable minimum strain rate v_0.

[6] A. deWaele, J. Oil Col. Chem. Assoc. **4**, 33 (1923).
[7] F. D. Farrow and G. M. Lowe, J. Text. Inst. **14T**, 414 (1923).
[8] Wo. Ostwald, Kolloid Zeits. **36**, 99 (1925).

Written in the following form, $(S/S_0)^{1/b}=v/v_0$, this equation has been criticized by Nadai,[9] because if the direction of the stress is reversed, a material must deform with the same strain rate in the opposite direction. This condition is only satisfied if $1/b=1, 3, 5$, etc., but not for fractional irrational or even exponents $1/b$. Further the viscosity $dS/dv=bS_0^{1/b}/v_0S^{(1-b)/b}$, becomes infinite at $v=0$, $S=0$, which is of course an objectionable conclusion from a physical standpoint. This critique is not justified in view of what has been said.

A system, for which Eq. (3) holds, is deformed at a constant strain rate when a constant stress is applied; hence only the fraction of the system with yield values smaller than the stress applied is deformed. Referring to the model this fraction corresponds to the number of pistons moving. It can be assumed for such a system with one mechanism of viscosity that the summation term is Eq. (1) is proportional to the number of elements deformed and to the applied stress. With n pistons moving

$$\sum (S-Sf_i)=nbS, \quad (4)$$

where b is the proportionality factor which is independent of the stress and has a value between 0 and 1. The distribution of the yield values is here such that their sum is equal to $n(1-b)S$. The term n is equal to ν/N where ν = number of elements deformed and N = total number of elements per unit volume.

The liquid contained in each element of the model has the same viscosity,

$$\eta=dS/dv_i=(S-Sf_i)/v_i.$$

Hence the differential strain rate is constant for each element, $dv_1=dv_2=dv_3$ etc., as can be also demonstrated by differentiating Eq. (1), and the differential of the total strain rate is equal to the differential of the individual strain rate multiplied by the number of elements taking part in the deformation, $dv=ndv_i$ and $dv_i=dv/n$. Combining these terms with Eq. (1) gives

$$\eta v=\sum (S-Sf_i)=vdS/dv/n=nbS \quad (5)$$

and

$$dS/S=bdv/v$$

[9] A. Nadai and P. G. McVetty, Proc. Am. Soc. Test. Mat. **43**, 735 (1943).

which on integration between S and So, v and v_0 leads to Eq. (3), $S/S_0=(v/v_0)^b$.

Equation (5) contains a constant coefficient of viscosity

$$\eta=nbS/v=n_0bS_0/v_0$$

and since $nS/n_0S_0=v/v_0=(S/S_0)^{1/b}$, it follows that

$$\eta=n_0b(S/S_0)^{(1-b)/b}S/v. \tag{6}$$

This equation gives a constant viscosity for plastic flow independent of the stress applied, and contains only S and v as vectors, as $(S/S_0)^{(1-b)/b}$ is equal to n/n_0 and is therefore a scalar. This equation requires the knowledge of the value of n_0, which can be obtained, if the fractional volume of the elements with strain rate v_0 is known. Otherwise the coefficient of viscosity may be replaced by a constant coefficient of plasticity, η/n_0.

At a sufficiently high stress the number of moving pistons of the viscous elements can become constant, in which case Eq. (5) may be written

$$\eta v=\sum(S-Sf_i)=nS-\sum Sf_i. \tag{7}$$

The summation term is constant and has the dimensions of stress. Replacing it by f and considering that n becomes 1 leads to

$$\eta=(S-f)/v, \tag{8}$$

which is equivalent to Bingham's equation[10] giving the stress/strain rate relationship for plastic systems with an extrapolated yield value f. It has to be borne in mind that f does not correspond to the highest yield value present in the system but represents the sum of all yield values of the fractions. Equation (8) also applies to the curvilinear relationship between stress and strain rate, in which case, however, f becomes variable.

Equation (3) was derived by considering a system with only one mechanism of viscosity. It can equally well be applied to systems having elements with various viscosities. In the case of two viscosities, for example, we have from Eq. (4)

$$\begin{aligned} v&=v_1+v_2=n_1b_1S/\eta_1+n_2b_2S/\eta_2 \\ v&=v_1+v_2=b_1Sdv_1/dS+b_2Sdv_2/dS \end{aligned} \tag{9}$$

from which follows

$$v_1/v_2=b_1dv_1/b_2dv_2, \quad \text{and} \quad b_1dv_1/v_1=b_2dv_2/v_2,$$

hence

$$\begin{aligned} vdS/S&=v_1b_2dv_2/v_2+v_2b_1dv_1/v_1 \\ &=(v_1^2b_2dv_2+v_2^2b_1dv_1)/v_1v_2 \\ &=(v_1+v_2)v_2b_1dv_1/v_1v_2=(v_1+v_2)v_1b_2dv_2/v_1v_2. \end{aligned}$$

Adding the last two terms and dividing by $v=(v_1+v_2)$ gives

$$2dS/S=b_1dv_1/v_1+b_2dv_2/v_2,$$

and since $b_1dv_1/v_1=b_2dv_2/v_2$, their sum can be replaced by $2bdv/v$, which on integration leads to

$$S/S_0=(v_1/vo_1)^{b_1/2}\cdot(v_2/vo_2)^{b_2/2}=(v/vo)^b. \tag{10}$$

If the system has two values of S_0 with S_{02} larger than S_{01}, then at stresses lower than S_{02}, the relationship between log S and log v has a slope different from that at stresses larger than S_{02}. With the number of elements of viscosity η_1 being small in comparison with the number of elements of viscosity η_2, a measurable deformation may be obtained only at a stress equal to S_{02}. In cases where the system contains several mechanisms of with different values of S_0, the relationship between log S and log v may be curvilinear for stresses smaller than the value of the largest S_0.

Equations (3) and (10) are based on the assumption that the extensibility of the viscous elements is unlimited. In the case of limited extensibility, a low stress deforms a certain number of elements at a low strain rate. With increasing stress the strain rate of the individual elements increases, but since some of the elements have reached their maximum extensibility, the number of elements taking part in the deformation has decreased. This decrease does not occur suddently with each increment in stress, but is a gradual process and will be treated in detail in connection with the discussion of creep. For a decrease in the number of elements deformed, which hypothetically depends on the stress only, the ratio of the number of elements deformed, n/n_0, is smaller than 1. In these cases the active stress is bS as before, however, because of the limited extensibility of some elements, the strain rate is only a fraction of what it should be and is equal to av, where a is a numerical constant such that $o<a<1$. Hence Eq. (5) assumes the form

$$dS/dv/n=nbS/av$$

and

$$(S/S_0)^a=(v/v_0)^b \tag{11}$$

[10] E. Bingham, *Fluidity and Plasticity* (McGraw-Hill Book Company, Inc., New York, 1923).

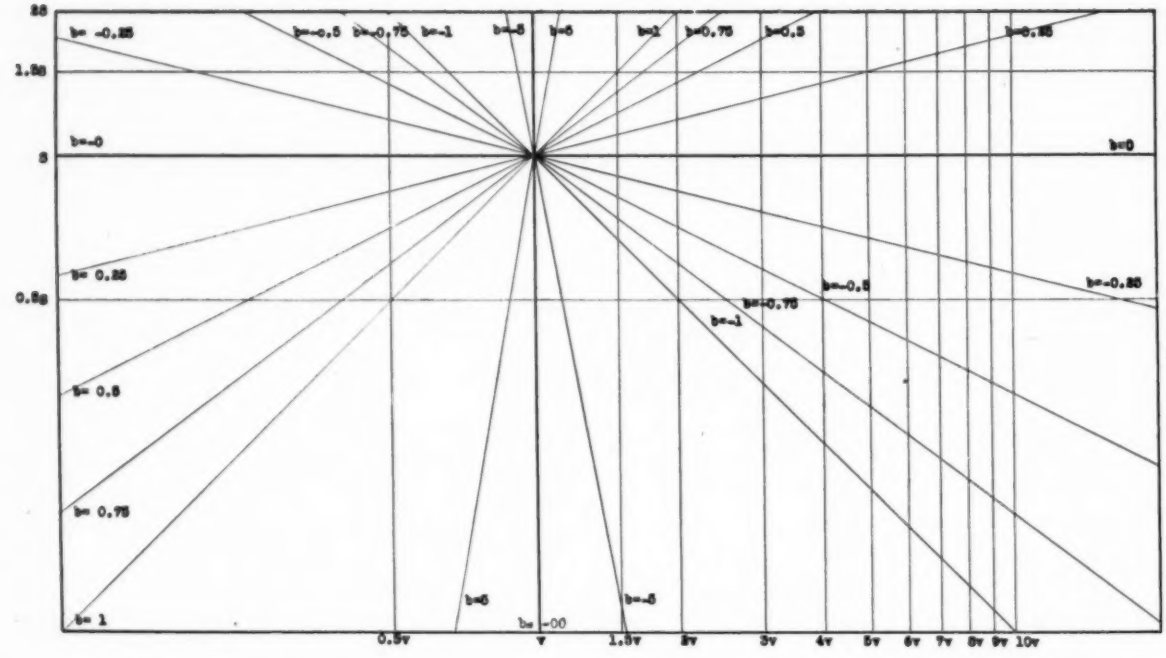

FIG. 2. Relationship between stress and strain rate for various values of b. The notation $b=00$ in the lower center should read $b=\infty$.

or

$$(S/S_0)^{-a}=(v/v_0)^b \qquad (12)$$

the latter term holding for systems where dv is negative, i.e., where the strain rate decreases with increasing stress. The viscosities derived from Eqs. (11) and (12) are

$$\eta=n_0(b/a)(S/S_0)^{(1-b)/b}(S_0/S)^{(1-a)/b}S/v, \qquad (13)$$

and

$$\eta=n_0(b/a)(S/S_0)^{(1-b)/b}(S_0/S)^{(1+a)/b}S/v. \qquad (14)$$

In both cases the ratio n/n_0 is the product of two terms in S, the first expressing the increase in the number of elements deformed with increasing stress and the other representing the increase in the number of elements having reached the limit of their extensibility with increasing stress.

For $b/a>1$ the total strain rate increases with increasing stress, and for $b/a<o$ the total strain rate decreases while the individual strain rates increase with increasing stress. In either case an increase in stress causes an increase in the yield value, since, with n elements having reached their limit of their extensibility, the original yield value is increased to that of the $n+1$st element. Hence a deformation increases the strength of the system, i.e., the stress that can be supported, and this phenomenon may be termed "stress-hardening."

Systems with negative values of b/a are usually connected with a type of flow termed dilatancy. Actually the mechanical behavior of such systems does not allow for any increase in volume. At a sufficiently high load stress the deformation of all the viscous elements will come to a stop. A further increase in stress will distort the system and cause dilation. An example of this kind of behavior will be given in a separate part.

The relationship between stress and strain-rate is represented in Fig. 2 for values of b and b/a varying between $-\infty$ and $+\infty$. With $b=0$ the stress becomes independent of the strain rate. A substance of such properties does not exist, since at $b=0$, the active stress and the viscosity are zero. As b/a increases from 1 to ∞ the strain rate becomes more independent of the stress. The same also holds for b/a decreasing from 0 to $-\infty$. Keeping n_0, S, and v constant, the viscosity decreases with increasing values of b and reaches a minimum at $b=1$ and increases with increasing values of b/a and becomes infinite at $b/a=\infty$.

The same also holds for negative values of b/a. With $b/a=+\infty$ or $-\infty$ the strain rate is constant and independent of the stress applied, and the viscosity is infinite. These conditions are met with an ideal elastic body.

(b) Relaxation of Stress

If the system is first deformed and then the strain kept constant, spring A in Fig. 1 contracts and causes a continued motion of the pistons of the viscous elements, until the potential energy stored in the spring is spent. Under this condition the total strain rate is zero and is composed of the strain rate of the elastic spring and the sum of the individual strain rates of the viscous elements, hence

$$dS/Edt+v=0, \tag{15}$$

where E is the modulus of elasticity of spring A. Substituting v from Eq. (6) and integrating between S and S_i, the stress at the instant when the strain is kept constant, t and 0 gives

$$(S_i/S)^{(1-b)/b}-1=n_0(1-b)(S_i/S_0)^{(1-b)/b}Et/\eta. \tag{16}$$

If the system has a yield value, the stress will relax during an observable time to a value equivalent to that of the yield value and to zero in infinite time. This equation can also be applied to systems which have different mechanisms of elasticity and viscosity, in which case E/η must be replaced by $\sum^1/\eta/\sum^1/E$.

The term E/η is constant with the dimensions of $1/t$ and may be replaced by $1/\tau$ where τ is the relaxation time.

Since $n_0\ (S_i/S_0)^{(1-b)/b}=n_i$, the number of viscous elements deformed at stress S_i, Eq. (16) may be simplified into

$$(S_i/S)^{(1-b)/b}=n_i(1-b)t/\tau+1. \tag{17}$$

Although the term $n_i(1-b)/\tau$ contains the constant relaxation time, τ, its value depends upon n_i and therefore upon S_i. Replacing this term by $1/tr$, where tr is a variable relaxation time depending upon the initial stress, gives

$$(S_i/S)^{(1-b)/b}=t/t_r+1. \tag{18}$$

The variable relaxation time is the time at which the original stress is reduced to a value of $S_i/2^{b/(1-b)}$.

This equation holds only for systems for which $o<b<1$. With $b/a>1$ and $b/a<0$, there is no relaxation, since immediately after the strain is kept constant, all viscous elements with yield values equal to or smaller than S_i, have reached their maximum extensibility. Such systems, therefore, behave at constant strain and temperature like ideal solids.

(c) Strain Rate an Exponential Function of Stress

Another equation which covers curvilinear relationships between stress and strain rate has been suggested by Ludwik[11] and shows the stress to be proportional to the logarithm of strain rate in accordance with

$$\exp\ (S-S_0)/S_0=(v/v_0)^b \tag{19}$$

or

$$\exp\ (S/S_0)=e(v/v_0)^b, \tag{20}$$

where b, S_0, and v_0 have the same meaning as before. This equation was mathematically derived by Prandtl[12] by considering a model consisting of a row of molecules which are bound to their normal positions of rest by forces which increase proportionally with the deviation of the molecule from its particular position of rest, i.e., these forces are of an elastic nature.

Applying statistical mechanics to his reaction rate theory, Eyring[13] arrived at a relationship for plastic flow which is similar to Eq. (19).

$$v=\frac{\lambda kT}{h}\exp\ (-F^{\ddagger}/kT)$$
$$\times[\exp\ (S\lambda/2kT)-\exp\ (-S\lambda/2kT)], \tag{21}$$

where λ = the average distance jumped by a molecule, therefore $S\lambda$ = work done by a potential, $-S\lambda$ is the amount of work for a similar motion in the opposite direction, k = Boltzmann's constant, h = Planck's constant, T = absolute temperature, and $F^{\ddagger}$ = free energy change of going from normal to activated states. If the free energy of activation is large, S must be large before v will have a noticeable value, therefore the second term in the parenthesis is negligible. Introducing

[11] P. Ludwik, *Elements der Technologischen Mechanik* (Verlagsbuchhandlung, Julius Springer, Berlin, 1909).
[12] E. Prandtl, Zeits. f. angew. Math. u. Mech. **8**, 85 (1928).
[13] H. Eyring, J. App. Phys. **4**, 283 (1936).

a similar term for v_0 gives

$$\exp(S-S_0)=(v/v_0)^{2kT/\lambda}. \quad (22)$$

The Eyring equation has been obtained for a system containing molecules of large size for which the free energy of activation is high. Yet substances of high molecular weight are known which behave like perfect liquids under stress. A viscous asphalt,[14] for example, having viscosities of 10^7 and 7.07×10^5 poises at 15 and 25°C, has a value of 22700 for $F\ddagger/k$. Equation (22) has also been found to hold for the curvilinear part of the stress/strain rate diagram of disperse systems such as greases, paints, and clay ships,[15] the total free energy of activation of which is relatively small, although it may be high for individual units of the disperse phase. These considerations seem to indicate that the mechanism of plastic deformation for a substance obeying Eq. (19) is similar to that obtained for Eq. (3). Such a system can also be assumed to consist of an elastic element and a number of viscous elements coupled in series for which Eq. (1) holds

$$v=\sum(S-Sf_i)/\eta.$$

If the summation term is independent of the stress and proportional to the number of the viscous elements deformed, then

$$\eta v=nvdS/dv=n \text{ const.}, \quad (23)$$

where const. has the dimensions of a constant stress. Since S_0 is the lowest stress which produces an observable plastic deformation, bS_0 can substitute for const., and

$$dS=bS_0dv/v$$

which on integration between S and S_0, v and v_0 leads to Eq. (19). From the above equation the following terms for viscosity are obtained

$$\eta=n_0bS_0/v_0=nbS_0/v$$
$$=n_0b\exp[(S-S_0)/bS_0]S_0/v. \quad (24)$$

The distribution of the yield values is in this case such that their sum is equal to $n(S-bS_0)$.

Combining Eq. (24) with the general Eq. (15) for relaxation at constant strain leads to

$$\exp[(S_i-S)/bS_0]$$
$$=n_0(t/\tau)\exp[(S_i-S_0)/bS_0]+1 \quad (25)$$

and with $n_0\exp[(S_i-S_0)/bS_0]=n_i$

$$\exp[(S_i-S)/bS_0]=n_it/\tau+1=t/t_r+1. \quad (26)$$

The term, $\tau/n_i=t_r$, represents the time at which the initial stress is reduced to a value of $S_i-bS_0\ln 2$, and depends on the initial stress in the same way as in Eq. (17). For systems containing several mechanisms of elasticity and viscosity, $1/\tau$ becomes $\sum 1/\eta/\sum 1/E$.

Equations (3) and (19) giving the strain rate as a power function and an exponential function of the stress are applicable to plastic systems of the sol-gel type which are subject to plastic flow and form the basis for more complicated systems. As the latter systems are more frequently encountered, the presentation of data will be reserved for a separate paper. It may be mentioned here that experience so far seems to give preference to Eq. (3) for systems where the structural elements of the substance under test remain in a high degree of disorder. In systems, where the structural units orient themselves to a higher state of order under stress, Eq. (19) appears to be applicable.

[14] C. Mack, unpublished work.
[15] R. E. Powell and H. Eyring, Nature **154**, 427 (1944).

Plastic Flow, Creep, and Stress Relaxation
Part II. Creep

CHARLES MACK
Technical and Research Department, Imperial Oil Limited, Sarnia, Ontario
(Received March 28, 1946)

The general equation covering the deformation of plastic substances given in Part I is applied to creep. Creep is defined as a mechanism of deformation for systems which have a curvilinear relationship between stress and strain rate and a curvilinear relationship between strain and time at constant stress. Creep is connected with changes in the internal structure of a plastic substance and results in an increase in strength of such materials through work-hardening. Equations are derived which give the stress as a function of strain rate and time (time-hardening), as a function of strain rate and strain (strain-hardening) and as a function of strain rate, strain, and time. The difference between time-hardening and strain-hardening is discussed. Expressions are given for the coefficients of viscosity of such systems which are independent of the stress applied. The relaxation of stress at constant strain is discussed, and it is shown that the stress relaxation depends upon the history of the substance under test. The concept of creep is also applied to thixotropic systems which are considered as cases of work-softening.

INTRODUCTION

IN Part I[1] plastic systems of the sol-gel type have been discussed. Gels differ from this type only in degree, in that they contain a larger number of elements of three-dimensional structure. The interlocking of these structural elements gives the system an appearance of rigidity. The formation of three-dimensional structures is caused by attractive forces between the individual molecules which are either of the van der Waals type, or in the case of polar molecules are caused by hydrogen bonds which are caused by the interaction between hydrogen and two other atoms. This bond is highly directional, and therefore resembles to some extent a covalent bond, although the free energy of a hydrogen bond is considerably lower.[2,3]

Amorphous solids such as thermoplastic and thermosetting plastics are generally obtained by polymerization. They also have a gel-like structure, however, as a consequence of the high degree of polymerization, the attractive forces between the individual molecules of the structural elements are to a large extent caused by primary bonds.

Such systems owe their external appearance to a structure resulting from a more or less random distribution of structural units. Owing to the lack of symmetry, the presence of flaws can be assumed to exist as pointed out by Griffith.[4] These flaws play the same role as the holes in a liquid according to Eyring's theory,[5] and represent the space into which the structural elements can slip, when the system is subjected to a stress. As a result of the smallness of the flaws relative to the volume of the structural elements, the mechanism of the movement of the structural elements is complicated. It may consist of a shear movement of the structural units along certain planes or of a migration of molecular segments throughout the structural unit, starting at one side of the unit and crossing it like a wave in the requisite direction.[6] In any case, the individual unit cannot flow in any direction as the molecules in a liquid but moves only in directions which are made available by the location of the flaws.

This process of flow also requires a rotation of the structural units with their long axis in the direction of flow. In view of their more or less random distribution, the structural elements are at different angles to the general direction of flow. It happens, therefore, that units of different orientation tend to move in slightly different directions or even in the opposite direction in the

[1] Charles Mack, J. App. Phys. **17**, 1086 (1946).
[2] T. S. Moore and T. F. Winmill, J. Chem. Soc. **101**, 1635 (1912).
[3] P. Pfeiffer, Ann. **398**, 137 (1913).
[4] A. A. Griffith, Phil. Trans. Roy. Soc. London **221**, 163 (1921).
[5] H. Eyring, J. App. Phys. **4**, 283 (1936).
[6] W. Kauzmann and H. Eyring, J. Am. Chem. Soc. **62**, 3275 (1940).

extreme case. With the change in orientation of the structural units, the shape of the flaws is also altered, and at the sharp end of a flaw there is an excessive strain which results in a concentration of stress at that point accompanied by a reduction in stress at other places. For an elliptical flaw (with the long and short half axis of a and b) under the influence of an exterior stress S perpendicular to the long axis a, Griffith[4] calculated the stress at the sharp edges to be equal to $S(2a+b)/b$. The motion of the structural units will become arrested at such points of stress concentration. As the process continues more units will cease moving, until the total internal stress becomes equal to the external stress, and the deformation of the plastic body under test comes to a stop. An increase in deformation can then only be obtained by the application of a higher stress. It is usually found that when the substance is unloaded and loaded again, deformation does not begin at the same stress as originally observed but at a higher value. This value is often found to be near the value of the stress applied in the experiment, before the unloading took place. Thus the deformation has increased the strength of the material, i.e., the stress which can be supported, and this phenomenon is called "work-hardening." As the number of structural units arrested decreases with time, a constant stress produces a continuously increasing deformation, the rate of which decreases with time. This type of deformation as a function of time is generally termed "creep." During this deformation the neighboring structural units, although moving in slightly different directions, must maintain contact at all points, or a crack will form and spread through the whole substance. To ensure contact, some distortion of the structure of the units must occur particularly at the boundaries. If this distortion becomes large enough in extent, so that the structural units are forced to move mainly in one direction, the creep will change into flow, i.e., the rate of deformation becomes constant.

The concept of creep can also be applied to thixotropic systems. A stress causes a continuous breakdown of the three-dimensional structures without permitting the formation of new connections between the structural elements. These changes in structure reveal themselves in the fact that as soon as the first plastic deformation is obtained, further deformation requires a lower stress than the original. As a result of this, the strength, which can be supported by a thixotropic system, decreases with increasing deformation, and this process may be considered as a case of "work-softening."

CREEP AND WORK-HARDENING

The phenomenon of creep accompanied by work-hardening under constant stress can be represented by the same model, consisting of an elastic element and a number of viscous elements, as given for plastic flow in Part I.[1] Whereas in the latter case the deformability of the viscous elements is unlimited, the extensibility of the elements of a substance subject to creep must be assumed to be limited. A stress applied to such a system sets the pistons of all viscous elements in motion with yield values smaller than the applied stress. As the deformation proceeds, some of the elements reach their maximum extensibility resulting in a decrease in the number of elements deformed and in a reduction of the total strain rate. Finally the motion of all pistons of the viscous elements comes to a stop, and the strain rate becomes zero. With n elements having reached the limit of their extensibility, the original yield value is increased to that of the $n+1$st element, and it requires a stress increment to bring about further deformation. This condition holds only, if the direction of the load stress is kept constant. If a tensile stress is applied to the system for some time and then the direction of loading reversed from tension to compression, the pistons of all elements which have reached their maximum extensibility will start moving again in the opposite direction, and the total strain rate of the system will be increased. This behavior explains the observation that metals, after they are plastically deformed, undergo comparatively large plastic deformations by small loads, when the direction of loading is reversed.[7]

The strain rate of the system can be expressed by Eq. (5) given in Part I

$$v=\sum (S-Sf_i)/\eta=n\varphi(S)/\eta, \qquad (1)$$

where the stress function $\varphi(S)$ is either bS or bS_0 depending upon the applicability of Eq. (3) or

[7] A. Nadai, *Plasticity* (McGraw-Hill Book Company, Inc., New York, 1931).

(20) given in Part I to the system under test. For plastic flow n, the number of viscous elements deformed, is constant at constant stress. In the case of creep, n decreases continually from a maximum to a minimum or to zero and can be a function of the strain or of time. For a system subject to work-hardening, the stress can therefore be a function of strain and strain rate (strain-hardening) or a function of time and strain-rate (time-hardening). Since the time is always a function of the strain for this system, the stress function may be written in the following general form:

$$S=f(\epsilon, v). \tag{2}$$

Differentiation with respect to time gives

$$\frac{dS}{dt}=\frac{\partial S}{\partial \epsilon}\frac{d\epsilon}{dt}+\frac{\partial S}{\partial v}\frac{dv}{dt}. \tag{3}$$

$\partial S/\partial \epsilon$ measures the rate of change of stress with plastic strain at constant strain rate, and may be compared to a coefficient of work-hardening, ψ. In a similar way $\partial S/\partial v$ measures the rate of change of stress with changing strain rate at constant strain. This term has the dimensions of a coefficient of viscosity and may be termed coefficient of plasticity, ϕ. If the deformation is carried out at constant stress, dS is zero, and Eq. (3) becomes

$$\psi d\epsilon/dt=\psi v=-\phi dv/dt. \tag{4}$$

ϕ is a stress function divided by the strain rate, $\phi=\varphi(S)/v$, and

$$-dv/dt=v^2\psi/\varphi(S), \tag{5}$$

i.e., the decrease in strain rate is proportional to the square of the strain rate and to $\psi/\varphi(S)$. At constant stress $\varphi(S)$ is constant, and the coefficient of work-hardening, ψ, can be constant or variable. Equation (5) also implies that, when $\psi=0$, then $dv=0$, and v becomes constant which is the condition for plastic flow.

(a) Coefficient of Work-Hardening is Constant at Constant Stress and Time-Hardening

With ψ being constant, the term $\psi/\varphi(S)$ also becomes constant. If it is replaced by $1/k$, then

$$-v^{-2}dv/dt=1/k,$$

and on integration between v and v_1, the strain rate obtained 1 second after application of the constant stress, and t and 1 second

$$v=d\epsilon/dt=k/(t-1+k/v_1). \tag{6}$$

On second integration between ϵ and 0, t and 0

$$\epsilon=k\ln(t+k/v_1). \tag{7}$$

At $t=0$, $\epsilon=0$, hence $k/v_1=1$ and $k=v_1$, and

$$\epsilon=k\ln(t+1). \tag{8}$$

In this equation and the ones to follow, ϵ represents the plastic strain only. With systems of sufficiently large elastic deformation, ϵ can be replaced by the difference between the total and elastic strains.

With $k=v_1$, it follows from Eq. (6) that

$$v=k/t. \tag{9}$$

Introducing this term into Eq. (1) for v and $v_1=v$ at $t_1=1$ second gives on division of both equations for the condition of constant stress:

$$v/v_1=t_1/t=n/n_1.$$

This term indicates that, since $n<n_1$, the number of elements under deformation decreases with time, and the creep is caused by time-hardening.

It follows from Eq. (8) that the strain is a linear function of the logarithm of time, but since the proportionality factor is constant only for a constant stress, k varies with the stress.

For the evaluation of the coefficient of work-hardening, ψ, it is necessary to define ϕ and $\varphi(S)$. If Eq. (3) of Part I, $S/S_0=(v/v_0)^b$ is applied then $\phi=\partial S/\partial v=bS/v$, and $\varphi(S)=bS$, therefore since $k=\varphi(S)/\psi$

$$\psi=bS/k, \tag{10}$$

$$\phi=bSt/k. \tag{11}$$

These relationships give a coefficient of work-hardening which is constant at constant stress, and a coefficient of plasticity, which increases linearly with time.

Substituting the above terms for ψ and ϕ in Eq. (3) and replacing k by vt gives

$$dS/S=bdt/t+bdv/v,$$

which on integration between S and S_0, t and t_0, v and v_0 yields

$$S/S_0=(vt/v_0t_0)^b, \tag{12}$$

confirming that creep is caused by time-hardening. The constant term of viscosity for this relationship is obtained from Eq. (1) as follows:

$$\eta = nbS/v = n_0 bS_0/v_0.$$

Since $v/v_0 = (S/S_0)^{1/b} t_0/t$

$$n/n_0 = (S/S_0)^{(1-b)/b} t_0/t$$

and the expression for viscosity becomes

$$\eta = n_0 b (S/S_0)^{(1-b)/b} (t_0/t) S/v, \qquad (13)$$

in which S and v are the only vectors. For this case the distribution of yield values is such that their sum is equal to $n_0(1-b)(S/S_0)^{(1-b)/b} t_0 S/t$. This equation in combination with Eq. (15) given in Part I leads to the following term for the relaxation of stress at constant strain:

$$-dS/dt = Ev = n_0 b (S/S_0)^{(1-b)/b} (t_0/t) SE/\eta,$$

and on integration between S and S_i, the stress at the moment where the strain is kept constant, t and o

$$(S_i/S)^{(1-b)/b} = n_0(1-b)(S_i/S_0)(1-b)/b \text{ to } (E/\eta) \ln (t+1) + 1. \qquad (14)$$

Since $n_0 t_0 (S_i/S_0)^{(1-b)/b} = n_i t_i$, where n_i and t_i are the number of elements deformed and the time at the moment where the strain is kept constant, and $E/\eta = 1/\tau$, where τ is the relaxation time, this equation becomes

$$(S_i/S_0)^{(1-b)/b} = (1-b) n_i t_i \ln (t+1)/\tau + 1. \qquad (15)$$

Although this equation has been obtained for a system having one mechanism of elasticity and viscosity, it is also applicable to systems with several such mechanisms, in which case $1/\tau = \sum 1/\eta / \sum 1/E$, as outlined in Part I. The term $(1-b) n_i t_i/\tau$ varies with the number of elements under deformation at the moment where the strain is kept constant, and consequently varies not only with the initial stress, S_i, but also with the time t_i during which the substance was deformed, before the strain was kept constant. Replacing this term by $1/\ln t_r$, where t_r is the variable relaxation time, changes above equation into:

$$(S_i/S)^{(1-b)/b} = \ln (t+1)/\ln t_r + 1, \qquad (16)$$

and $\ln t_r$ is the logarithm of the time at which the original stress is reduced to $S_i/2^{b/(1-b)}$. This equation as well as the others to follow in connection with work-hardening holds only when the system is still subject to work-hardening during the relaxation of stress. Consequently the stress relaxes to a certain lower limit which can be close to the value of the initial stress. In this case the substance remains under strain, and further stress relaxation can be only obtained by heating the substance, which process is carried out by the annealing of glass and tempering of steel.

Applying the Prandtl Eq. (20) given in Part I, $\exp[(S-S_0)/S_0] = (v/v_0)^b$, to the case of time-hardening gives

$$\exp[(S-S_0)/S_0] = (vt/v_0 t_0)^b, \qquad (17)$$

the coefficient of viscosity is

$$\eta = n_0 b \exp[(S-S_0)/bS_0](t_0/t) S_0/v \qquad (18)$$

and the stress at constant strain relaxes according to

$$\exp[(S_i-S)/bS_0] = \ln (t+1)/\ln t_r + 1, \qquad (19)$$

$\ln t_r$ being the logarithm of the time at which the initial stress is reduced to a value of $S_i - bS_0 \ln 2$.

Equations (12) and (17) express the stress as a function of strain rate and time, $S = f(v, t)$. Differentiating this term gives the following general expression:

$$dS = \frac{\partial S}{\partial t} dt + \frac{\partial S}{\partial v} dv = \theta dt + \phi dv, \qquad (20)$$

which implies that at constant stress $\partial S/\partial t = \theta$ approaches zero with high values of t. In this case dv also approaches zero, i.e., at deformations of long duration under constant stress the strain rate becomes finally constant, and creep changes into plastic flow.

These equations have been obtained by assuming, ψ, the coefficient of work-hardening or strain-hardening to be constant at constant stress. Equation (20) leads to an interesting solution when the coefficient of time-hardening is assumed to be constant, at constant stress, in which case

$$\theta dt + \phi dv = \theta dt + \varphi(S) dv/v$$

and

$$\theta/\varphi(S) = 1/\alpha = -v^{-1} dv/dt$$

where α is a constant with the dimension of t.

Integration between v and v_1, t, and 0 gives

$$v = d\epsilon/dt = v_1 \exp(-t/\alpha), \quad (21)$$

and on second integration between ϵ and 0, t and 0

$$\epsilon = \alpha v_1[1 - \exp(-t/\alpha)]. \quad (22)$$

The term αv_1 has the dimension of ϵ and is obviously the limiting value of ϵ, at which creep due to time-hardening at constant stress changes into plastic flow, and is equal to ϵ max.

With $\varphi(S) = bS$ and assuming that α is a constant independent of the stress, the following equation for the stress as a function of strain rate and time is obtained:

$$S/S_0 = (v/v_0)^b \exp[b(t-t_0)/\alpha], \quad (23)$$

from which results the following expression for the coefficient of viscosity

$$\eta = n_0 b (S/S_0)^{(1-b)/b} \exp[-(t-t_0)/\alpha] S/v. \quad (24)$$

The corresponding equations for the condition $\varphi(S) = bS_0$ are:

$$\exp[(S-S_0)/S_0] = (v/v_0)^b \exp[b(t-t_0)/\alpha], \quad (25)$$

$$\eta = n_0 b \exp\{[\alpha(S-S_0) - bS_0(t-t_0)]/\alpha b S_0\} S_0/v. \quad (26)$$

Another solution of Eq. (20) is obtained if $\theta = \varphi(S)/at$, where "a" is a constant, in which case at constant stress

$$\theta dt + \phi dv = \varphi(S)dt/at + \varphi(S)dv/v,$$

and

$$dt/at = -dv/v.$$

With $\varphi(S) = bS$ and assuming that a is a constant independent of the stress and equal to b/c, where c is a new constant, the following equations are obtained: for the stress as a function of strain rate and time

$$S/S_0 = (v/v_0)^b (t/t_0)^c \quad (27)$$

for the coefficient of viscosity

$$\eta = n_0 b (S/S_0)^{(1-b)/b} (t_0/t)^{c/b} S/v \quad (28)$$

and for the relaxation of stress at constant strain

$$(S_i/S)^{(1-b)/b} = (t/t_r)^{(b-c)/b} + 1. \quad (29)$$

(b) Coefficient of Work-Hardening is Variable at Constant Stress and Strain-Hardening

In the previous section the case has been treated for the coefficient of work-hardening, ψ, being constant at constant stress, hence $\psi/\varphi(S)$ = constant. If this term is a function of the strain, so that $\psi/\varphi(S) = 1/\epsilon$, Eq. (5) takes the following form for the condition of constant stress

$$-v^{-2}dv/dt = \psi/\varphi(S) = 1/\epsilon. \quad (30)$$

Substituting the term for ψ in Eq. (3) gives for $\varphi(S) = bS$

$$S/S_0 = (v\epsilon/v_0\epsilon_0)^b, \quad (31)$$

expressing the stress as a function of the strain and the strain rate, and the coefficient of work-hardening becomes a coefficient of strain-hardening. The difference between time-hardening and strain-hardening will be discussed in detail in a later section. It may be mentioned here that the coefficient of strain-hardening obtained from Eq. (30) $\psi = bS/\epsilon$, decreases considerably less with increasing deformation than the coefficient of time-hardening obtained from Eq. (13), $\theta = bS/t$, for the same value of bS. The latter term approaches zero with high values of t, which limit is only reached in the case of strain-hardening with very large values for ϵ, i.e., for elongations which correspond to a large multiple of the original length of the test piece.

The coefficient of viscosity for a substance subject to strain-hardening according to above equation is

$$\eta = n_0 b (S/S_0)^{(1-b)/b} (\epsilon_0/\epsilon) S/v. \quad (32)$$

For the evaluation of the relaxation of stress at constant total strain, the plastic strain is equal to the elastic strain but of opposite sign, and can therefore be replaced by $-S/E$. Introducing this term into Eq. (32) gives the stress relaxation as follows:

$$(S_i/S)^{(1-2b)/b} = t/t_r + 1, \quad (33)$$

where $1/t_r = n_i(1-2b)/\tau$ and t_r depends upon the value of S_i and ϵ_i, the stress and strain prior to the moment where the strain is kept constant.

Introducing into Eq. (31) the term $\varphi(S) = bS_0$ leads to

$$\exp[(S-S_0)/S_0] = (v\epsilon/v_0\epsilon_0)^b \quad (34)$$

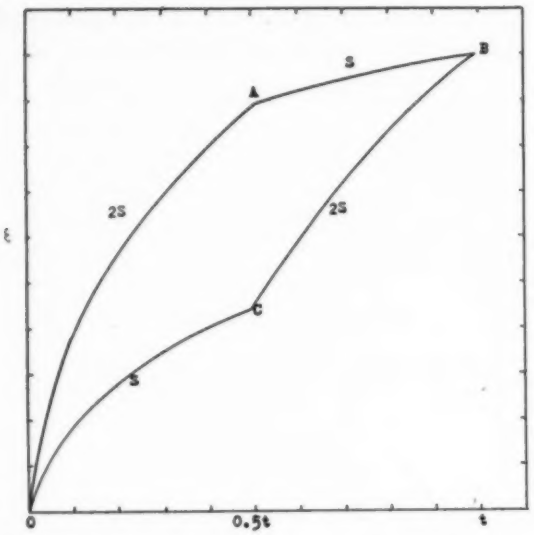

FIG. 1. Effect of strain-hardening: $S/S_0=(v/v_0)^b$; $b=0.5$.

and for the stress relaxation at constant strain

$$[(S-bS_0)/S_0]\exp[(S_i-S)/bS_0] = n_i t/\tau+(S_i-bS_0)/S_0, \quad (35)$$

which is not a simple expression for the stress relaxation as a function of time. A better solution is obtained by substituting the strain in equation (34) by its time function as follows:

$$\exp[(S-S_0)/S_0]=(v/v_0)^{2b}(t/t_0)^b \quad (36)$$

which gives the coefficient of viscosity as

$$\eta=n_0 b(S_0/v)(t_0/t)^{\frac{1}{2}}\exp[(S-S_0)/2bS_0] \quad (37)$$

and the following stress relaxation as a function of time

$$\exp[(S_i-S)/2bS_0]=(t/t_r)^{\frac{1}{2}}+1 \quad (38)$$

where $1/t_r^{\frac{1}{2}}=n_i t_i^{\frac{1}{2}}/\tau$.

In analogy with Eq. (27), ψ can also be assumed to be equal to $\varphi(S)/b\epsilon/m$, where m is a new constant, in which case the stress as a function of strain and strain rate for $\varphi(S)=bS$ takes the form

$$S/S_0=(v/v_0)^b(\epsilon/\epsilon_0)^m. \quad (39)$$

(c) Work-Hardening Depending upon Strain and Time

The equations given in the previous sections express the stress as functions of strain rate and time or as functions of strain rate and strain. Cases may occur where the stress is a function of strain, time and strain rate according to

$$S=f(\epsilon, t, v)$$

and

$$dS=\frac{\partial S}{\partial \epsilon}d\epsilon+\frac{\partial S}{\partial t}dt+\frac{\partial S}{\partial v}dv=\psi d\epsilon+\theta dt+\phi dv. \quad (40)$$

In these cases the number of elements under deformation at constant stress decrease with increasing strain and time.

With $\phi=bS/v$, the application of the corresponding terms for ψ and θ previously given results in the following possible solutions of this equation:

$$S/S_0=(v\epsilon t/v_0\epsilon_0 t_0)^b \quad (41)$$

$$S/S_0=(vt/v_0t_0)^b(\epsilon/\epsilon_0)^m \quad (42)$$

$$S/S_0=(v\epsilon/v_0\epsilon_0)^b\exp[b(t-t_0)/\alpha] \quad (43)$$

$$S/S_0=(v\epsilon/v_0\epsilon_0)^b(t/t_0)^c \quad (44)$$

$$S/S_0=(v/v_0)^b(t/t_0)^c(\epsilon/\epsilon_0)^m. \quad (45)$$

(d) Difference between Time-Hardening and Strain-Hardening

The equations previously given express the stress as functions of strain rate and time, as functions of strain rate and strain or both. In each case the strain is a function of time, and the strain and time functions can be mutually rearranged. The equations given in connection with time-hardening can be expressed as follows:

$$S/S_0=(vt/v_0t_0)^b=(v/v_0)^b \times\exp\{b[\epsilon(S_0/S)^{1/b}-\epsilon_0]/v_0t_0\} \quad (46)$$

$$S/S_0=(v/v_0)^b\exp[b(t-t_0)/\alpha] =\{(v/v_0)+[\epsilon-\epsilon_0(S/S_0)^{1/b}]/\alpha v_0\}^b \quad (47)$$

$$S/S_0=(v/v_0)^b(t/t_0)^c=(v/v_0)^{b-c}(\epsilon/\epsilon_0)^c. \quad (48)$$

Similar equations are obtained for the stress function $\exp[(S-S_0)/S_0]$.

It has been mentioned before that creep due to time-hardening finally changes into plastic flow. This change is borne out by Eqs. (46) and (47) and occurs as soon as the value of $\epsilon(S_0/S)^{1/b}$ in the exponential term has reached the value of ϵ_0, or in Eq. (47) when $\epsilon_0(S/S_0)^{1/b}$ has the value of ϵ. Equation (48) which originally has been derived for creep due to time-hardening is similar

in form to Eq. (39) in connection with strain-hardening. The creep in this case is consequently due to strain-hardening and extends over a wide range of deformation when the values of c are smaller than 1.

The creep at constant stress is of interest, which in the case of Eq. (46) is a linear function of the logarithm of time, and its magnitude increases with increasing stress. In the case of the equations in connection with strain-hardening, the logarithm of strain is a linear function of the logarithm of time, and its slope is independent of the stress applied. For Eq. (47) the logarithm of $\epsilon \max/(\epsilon \max - \epsilon)$ is as shown before a linear function of time independent of the stress applied.

This difference in creep further reveals itself in the behavior of substances subject to work-hardening when they are submitted to stresses in succession. Suppose a test piece subject to strain-hardening is first stretched under a constant stress $2S$ until A in Fig. 1 is obtained at $\frac{1}{2}t$. At this point the stress is reduced to S and kept constant for a second time interval of $\frac{1}{2}t$ during which the creep follows curve AB. A second test piece is subjected to the reversed order of loading, i.e., is first stretched under a constant stress S for the time $\frac{1}{2}t$, and then the stress is increased to $2S$. In this case the creep first follows curve OC and finally meets the strain-time curve at point B and identical time t. Thus if a substance subject to strain-hardening is deformed under various stresses, the strain at a given time will be the same irrespective of the order of loading. This behavior, of course, applies only to the plastic strain and not to the total strain (=elastic +plastic strain). Strain-time diagrams similar to that of Fig. 1 are obtained for substances whose creep is connected with strain-hardening irrespective of the derivation of these equations.

A substance, which is subject to time-hardening in accordance with Eq. (46), when sucessively stretched under the constant stresses S and $2S$, gives a strain-time diagram as presented in Fig. 2. Here the strain obtained after a certain time depends upon the order of loading, and the curves do not meet at the same time t. The strain of such a substance obtained at a given time depends therefore upon previous operations.

Substances obeying Eq. (47) take an intermediate position, in that they show under stress a change from creep to plastic flow as in the case of time-hardening and, when successively stretched, behave like substances due to strain-hardening.

For the cases where the stress is a function of strain-rate, strain and time, it can be shown in the same manner, that the creep is independent of the history of the substance and finally changes into creep due to strain-hardening only.

CREEP AND THIXOTROPY

It has been shown that creep in combination with work-hardening is a process which increases the stress which can be supported by a substance. Thixotropic systems also show the phenomenon of creep which is however accompanied by breakdown of the structure and results in a decrease in stress which can be supported. Thus creep of thixotropic systems is opposite in effect to creep due to work-hardening. Thixotropic systems can therefore be compared with the same model consisting of an elastic element and a number of viscous elements coupled in series. A stress applied to such a system increases the number of elements deformed with time, and the strain rate increases. In view of this effect Eq. (20) can be applied to thixotropic systems with a negative

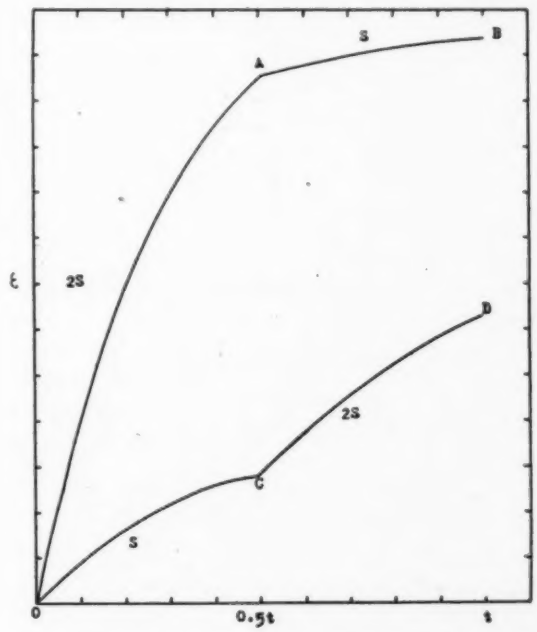

FIG. 2. Effect of time-hardening: $S/S_0=(tv/t_0v_0)^b$; $b=0.5$.

coefficient of time-hardening:

$$dS=\frac{-\partial S}{\partial t}dt+\frac{\partial S}{\partial v}dv=-\theta dt+\phi dv. \qquad (49)$$

This equation also implies that, if θ becomes zero at constant stress, then $dv=0$, and v becomes constant. This condition is fulfilled after breakdown of the thixotropic structure, the amount of which may depend upon the magnitude of the stress applied.

With $\theta=bS/t$, and $\phi=bS/v$, integration of Eq. (49) gives

$$S/S_0=(v/v_0)^b(t/t_0)^{-b}=(vt_0/v_0t)^b \qquad (50)$$

and with $\theta=cS/t$

$$S/S_0=(v/v_0)^b(t_0/t)^c. \qquad (51)$$

For both cases, the logarithm of strain is a linear function of the logarithm of time at constant stress, and the slopes are independent of the stress applied.

The viscosities resulting from these expressions are

$$\eta=n_0b(S/S_0)^{(1-b)/b}(t/t_0)S/v, \qquad (52)$$

$$\eta=n_0b(S/S_0)^{(1-b)/b}(t/t_0)^{c/b}S/v. \qquad (53)$$

With the thixotropic structure still subject to breakdown during relaxation at constant strain, these equations lead to

$$(S_i/S)^{(1-b)/b}=(t/t_r)^2+1, \qquad (54)$$

where $1/t_r^2=[(1-b)/2]n_i/\tau t_i$, and

$$(S_i/S)^{(1-b)/b}=(t/t_r)^{(b+c)/b}+1, \qquad (55)$$

where $1/t_r^{(b+c)/b}=b(1-b)n_i/(b+c)\tau t_i^{c/b}$. In both cases the variable relaxation time t_r depends upon n_i the number of elements deformed at the moment where the strain is kept constant and therefore varies with S_i and t_i the time during which the system was deformed prior to the beginning of relaxation. If the structure is completely destroyed, the stress relaxation follows Eq. (18) Part I, $(S_i/S)^{(1-b)/b}=t/t_r+1$. Another possibility exists if the value of the stress falls below that of the attractive forces of the micelles for each other, in which case the thixotropic structure may be built up again during relaxation.

The expressions giving the stress as functions of strain rate, strain and/or time cover the creep of various systems. Many substances subject to work-hardening have mechanisms of deformation which also exhibit the property of elastic aftereffect. Such systems will be discussed in a separate paper, and the presentation of data for substances subject to work-hardening and thixotropy will be reserved for this part.

Plastic Flow, Creep, and Stress Relaxation

Part III. Creep and Elastic After-Effect

CHARLES MACK
Technical and Research Department, Imperial Oil Limited, Sarnia, Ontario
(Received March 28, 1946)

A large number of substances show the phenomenon of elastic after-effect, and part of their deformation recovers on unloading as a function of time. This portion of the deformation at constant stress has a strain rate which decreases with time and is therefore comparable to creep. Expressions are given for the strain-time relationships of such systems, and the process of stress relaxation at constant strain is discussed. The equations given in connection with plastic flow, creep due to work-hardening, thixotropy, and creep in combination with elastic after-effect are applied to data given in the literature, and it is shown that these equations suffice to describe the deformation and relaxation mechanisms of a variety of materials such as metals, clay soil, food products, acrylic acid polymeride, polyvynil chloride, cellulose acetate, manila ropes, paper laminates, phenolic molding compounds, rubber, asphalt, and bituminous pavements.

INTRODUCTION

THE theory of plastic flow and creep has been discussed in two previous papers.[1,2] It has been shown that these mechanisms of deformation can be represented by a model consisting of an elastic element and a number of viscous elements all coupled in series. The viscous elements represent the structural units of the plastic system and have an unlimited extensibility under tension in the case of plastic flow. In the case of creep their extensibility is limited as a result of a resistance which is caused by the position of the structural units relative to each other. If elastic forces are the cause of limited extensibility, the structural units can be considered as being encased in an elastic sheath. A tensile stress acting on such an element causes a deformation which increases with time up to a certain limit. After removal of the load the elastic sheath will recover its original shape, but, since the element also possesses viscosity, the recovery is a function of time. This phenomenon is generally referred to as elastic after-effect. With structural units of this type present in a substance, the deformation mechanism can be described by models suggested by Burgers[3] consisting of elastic and viscous elements coupled in series as well as in parallel. Such a system is represented by Fig. 1, and the various elements are considered as being rigidly attached to each other. Elements *A* and *B* are perfectly elastic springs, and elements *C* and *D* consist of porous pistons moving in cylinders filled with a viscous liquid. When the model is subjected to a constant tensile stress, spring *A* will immediately elongate followed by movements of the pistons of the viscous elements *C* and *D*. The deformation of element *C* necessitates

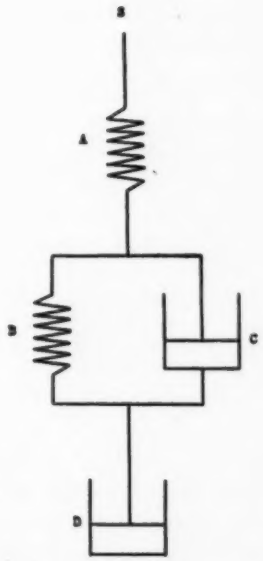

FIG. 1. Model of plastic deformation with elastic after-effect.

[1] Charles Mack, J. App. Phys. **17**, 1086 (1946).
[2] Charles Mack, J. App. Phys. **17**, 1093 (1946).
[3] G. M. Burgers, "First report on viscosity and plasticity," Acad. Sci. Amsterdam (1935).

an elongation of spring B and part of the stress is taken over by this spring.

The deformation of elements C and D can be completely or partially simultaneous, or it can occur that element D will be deformed after element C has reached its maximum extensibility. The latter case is often met with rubber-like substances containing molecules of high degree of polymerization which are large in one dimension only. Such substances consist of a mass of entangled chain molecules which have a repeating unit. Any increase in length of such a substance corresponds to an increase in the distance between the ends of the individual chain molecules and to a change in their relative position. A tensile stress applied will first increase the distance between the individual links in the chain. This affects interatomic distances, and the deformation is purely elastic. Under continued stress the molecule will be further stretched by rotating about the C−C bonds of the main skeleton to a new set of positions. This deformation is also elastic, but requires a certain time, and corresponds to the deformation of the couple formed by elements B and C. Finally, whole portions of chains alter their relative position by sliding over each other, and this part of the deformation is wholly plastic.[4]

CREEP AND ELASTIC AFTER-EFFECT

(a) Deformation Mechanism of Model with Elastic After-Effect

The element causing the elastic after-effect consists of spring B coupled in parallel with the viscous element C. Here the strain is the same for each component. A tensile stress acting on this couple, however, is composed of the sum of the stresses for spring B and element C.

$$S=S_b+S_c=S_b+(S-S_b).$$

The strains of spring A, couple BC, and element D are additive,

$$\epsilon=\epsilon_a+\epsilon_b+\epsilon_d,$$

and substituting the strains by their time-functions leads to an expression for the total strain as functions of time at constant stress, which has been carried out by Burgers for a system containing purely viscous liquids in elements C and D.

[4] R. F. Tuckett, Chem. and Ind. **62**, 430 (1943).

The same procedure can be also applied to a system in which the viscous elements C and D are replaced by elements subject to plastic flow. With element C obeying the relationship $S/S_0=(v/v_0)^b$, S must be replaced by $S_c=S-E\epsilon_b$, the stress acting on this element. Applying the corresponding term for the viscosity gives the strain of the couple BC as

$$\epsilon_b=\epsilon_{b\,\max}\{1-[t/t_{or}+1]^{-b/1-b}\}, \qquad (1)$$

where $\epsilon_{b\,\max}$ is the maximum strain obtained under the stress applied and is S/E. The expression $1/t_{or}$ is equal to $n_0'(1-b)E/\eta$ and has the dimension of inverse time. The term η/E is the same as the relaxation time (see Part I), but since its meaning is different, the term "orientation time," τ_{or}, has been proposed.[4] The expression t_{or} varies with S. With element C obeying the Prandtl equation, $\exp[(S-S_0)/S_0]=(v/v_0)^b$, the strain as a function of time becomes

$$\exp(\epsilon_b/\epsilon_{b\,\max})=(t/t_{or}+1)^b, \qquad (2)$$

where $1/t_{or}=n_0E/\eta$.

Equations (1) and (2) show that the strain-time relationships are the same for loading and unloading but of opposite sign. This behavior is of importance, since by measuring the total strain as a function of time during loading and observing the recovery after unloading as a function of time, the strains of the individual elements at a given time can be obtained for the condition of loading.

In the case where element C is supposed to be subject to work-hardening, the latter effect influences the deformation to such an extent that soon after the application of a constant tensile stress the elongation of element C comes to a stop. The deformation obtained is probably so small that it has no practical significance.

The system causing the elastic after-effect need not be restricted to one spring and viscous or plastic element coupled in parallel and may be composed of several springs and elements all coupled in parallel or may consist of a series of one spring and one element coupled in parallel and the whole series coupled in series. Such systems have been discussed by Alfrey and Doty.[5]

[5] Alfrey and Doty, J. App. Phys. **16**, 700 (1945).

TABLE I. Strain as function of time at constant stress.

Basic relationships for stress as functions of strain-rate	Strain as function of time at constant stress	
	for element D	for spring B after unloading
(1) $S/S_0=v/v_0$	$\epsilon=$const. t	$\epsilon_u/\epsilon=\exp(t/\tau_{or})$
(2) $S/S_0=(v/v_0)^b$	$\epsilon=$const. t	$\epsilon_u/\epsilon=[(t/t_{or})+1]^{b/(1-b)}$
(3) $\exp(S-S_0)/S_0=(v/v_0)^b$	$\epsilon=$const. t	$\epsilon_u-\epsilon=\epsilon_u b\ln[(t/t_{or})+1]$
(4) $S/S_0=(vt/v_0t_0)^b$	$\epsilon=$const. $\ln(t+1)$	
(5) $\exp[(S-S_0)/S_0]=(vt/v_0t_0)^b$	$\epsilon=$const. $\ln(t+1)$	
(6) $S/S_0=(v/v_0)^b\exp[b(t-t_0)/\alpha]$	$\epsilon=$const. $[1-\exp(-t/\alpha)]$	
(7) $\exp[(S-S_0)/S_0]=(v/v_0)^b\exp[b(t-t_0)/\alpha]$	$\epsilon=$const. $[1-\exp(-t/\alpha)]$	
(8) $S/S_0=(v/v_0)^b(t/t_0)^c$	$\epsilon=$const. $t^{(b-c)/b}$	
(9) $\exp[(S-S_0)/S_0]=(v/v_0)^b(t/t_0)^c$	$\epsilon=$const. $t^{(b-c)/b}$	
(10) $S/S_0=(v\epsilon/v_0\epsilon_0)^b$	$\epsilon=$const. t^b	
(11) $\exp[(S-S_0)/S_0]=(v\epsilon/v_0\epsilon_0)^b$	$\epsilon=$const. t^b	
(12) $S/S_0=(v/v_0)^b(\epsilon/\epsilon_0)^m$	$\epsilon=$const. $t^{b/(b+m)}$	
(13) $\exp[(S-S_0)/S_0]=(v/v_0)^b(\epsilon/\epsilon_0)^m$	$\epsilon=$const. $t^{(b+c)/b}$	
(14) $S/S_0=(v/v_0)^b(t_0/t)^c$	$\epsilon=$const. $t^{(b+c)/b}$	
	Where const. has different meaning for each equation.	

(b) Stress Relaxation of Systems with Elastic After-Effect

If the system is strained under tension, and then the strain kept constant, the stress relaxation can consist of two different processes depending upon the value of the moduli of elasticity of the elastic springs A and B relative to each other. When E_a of spring A is larger than E_b of spring B, spring A will contract accompanied by an elongation of the couple B, C and element D. When E_b is larger than E_a, the couple B, C will contract and spring A and element D will be under tension. In either case the relaxation of stress with time follows the general equation:

$$-dS/E_a dt=v=v_c+v_d. \qquad (3)$$

For the case of elements C and D containing perfect liquids with coefficients of viscosity η_c and η_d, this equation becomes on integration

$$S=M\exp[-(p+q)t]+N\exp[-(p-q)t], \qquad (4)$$

where

$$p=\frac{1}{2}\left(\frac{E_a}{\eta_d}+\frac{E_a+E_b}{\eta_c}\right),$$

$$q=\left[\frac{1}{4}\left(\frac{E_a}{\eta_d}+\frac{E_a+E_b}{\eta_c}\right)^2-\frac{E_aE_b}{\eta_c\eta_d}\right]^{\frac{1}{2}},$$

and M and N are constants with the dimensions of stress. It will be noticed that the first exponential term dies away more rapidly than the second and finally approaches the value of zero. At this point the couple B, C is at its maximum elongation for the particular stress at that moment, if E_a is larger than E_b, and the relaxation proceeds according to the second exponential term. Thus the logarithm of stress is first curvilinear with time and becomes finally linear.

This relaxation mechanism is also met with systems for which the elements C and D are subject to plastic flow or creep. In this case Eq. (3) is also applicable. Substituting v_d from $S/S_0=(v/v_0)^b$, and integrating between S and S_i, t and t_i, S_i and t_i being the stress and time at which S becomes equal to S_b, gives

$$(S_i/S)^{(1-b)/b}=[(1-b)/bt_i](t-t_i)+1. \qquad (5)$$

The relaxation process is similar for systems with elements C and D having flow properties different from those of the above case. The corresponding terms are summarized together with the strain/time relationships of the various elements in Tables I and II. It will be noticed that the equations for the final stage of stress relaxation for systems with elastic after-effect are similar in the cases of Eqs. (3), (9), (11), and (13) given in Table II, and do not always allow for a differentiation between relaxation due to plastic flow or due to creep based on strain-hardening.

TABLE II. Relaxation of stress at constant strain.

	Basic relationships for stresses functions of strain-rate	Stress relaxation for systems free of elastic after-effect	Final stage of stress relaxation for systems with elastic after-effect
(1)	$S/S_0=v/v_0$	$S_i/S=\exp\,(t/\tau)$	$S_i/S=\exp\,(t-t_i)/\tau$
(2)	$S/S_0=(v/v_0)^b$	$(S_i/S)^{(1-b)/b}=(t/t_r)+1$	$(S_i/S)^{(1-b)/b}=(t-t_i)/t_r+1$
(3)	$\exp\,[(S-S_0)/S_0]=(v/v_0)^b$	$\exp\,[(S_i-S)/bS_i]=(t/t_r)+1$	$\exp\,[(S_i-S)/bS_i]=(t-t_i)/t_r+1$
(4)	$S/S_0=(vt/v_0\epsilon_0)^b$	$(S_i/S)^{(1-b)/b}=(\ln t/\ln t_r)+1$	$(S_i/S)^{(1-b)/b}=(\ln t-\ln t_i)/\ln t_r+1$
(5)	$\exp\,[(S-S_0)/S_0]=(vt/v_0\epsilon_0)^b$	$\exp\,[(S_i-S)/bS_i]=(\ln t/\ln t_r)+1$	$\exp\,[(S_i-S)/bS_i]=(\ln t-\ln t_i)/\ln t_r+1$
(6)	$S/S_0=(v/v_0)^b\exp\,[b(t-t_0)/\alpha]$	$(S_i/S)^{(1-b)/b}=(\alpha/t_r)[1-\exp\,(-t/\alpha)]+1$	$(S_i/S)^{(1-b)/b}=(\alpha/t_r)\{1-\exp\,[-(t-t_i)/\alpha]\}+1$
(7)	$\exp\,[(S-S_0)/S_0]=(v/v_0)^b\exp\,[b(t-t_0)/\alpha]$	$\exp\,[(S_i-S)/bS_0]=(\alpha/t_r)[1-\exp\,(-t/\alpha)]+1$	$\exp\,[(S_i-S)/bS_i]=(\alpha/t_r)\{1-\exp\,[-(t-t_i)/\alpha]\}+1$
(8)	$S/S_0=(v/v_0)^b(t/t_0)^c$	$(S_i/S)^{(1-b)/b}=(t/t_r)^{(b-c)/b}+1$	$(S_i/S)^{(1-b)/b}=[(t-t_i)/t_r]^{(b-c)/b}+1$
(9)	$\exp\,[(S-S_0)/S_0]=(v/v_0)^b(t/t_0)^c$	$\exp\,[(S_i-S)/bS_0]=(t/t_r)^{(b-c)/b}+1$	$\exp\,[(S_i-S)/bS_i]=(t-t_i)/t_r^{(b-c)/b}+1$
(10)	$S/S_0=(v\epsilon/v_0\epsilon_0)^b$	$(S_0/S)^{(1-2b)/b}=(t/t_r)+1$	$(S_i/S)^{(1-2b)/b}=(t-t_i)/t_r+1$
(11)	$\exp\,[(S-S_0)/S_0]=(v\epsilon/v_0\epsilon_0)^b$	$\exp\,[(S_i-S)/2bS_0]=(t/t_r)^b+1$	$\exp\,[(S_i-S)/2bS_i]=[(t-t_i)/t_r]^b+1$
(12)	$S/S_0=(v/v_0)^b(\epsilon/\epsilon_0)^m$	$(S_i/S)^{(1-b-m)/b}=(t/t_r)+1$	$(S_i/S)^{(1-b-m)/b}=(t-t_i)/t_r+1$
(13)	$\exp\,[(S-S_0)/S_0]=(v/v_0)^b(\epsilon/\epsilon_0)^m$	$\exp\,[(S_i-S)/(b+m)S_0]=(t/t_r)^{b/(b+m)}+1$	$\exp\,[(S_i-S)/b+m)S_i]=[(t-t_i)/t_r]^{b/(b+m)}+1$
(14)	$S/S_0=(v/v_0)^b(t_0/t)^c$	$(S_i/S)^{(1-b)/b}=(t/t_r)^{(b+c)/b}+1$	$(S_i/S)^{(1-b)/b}=(t-t_i)/t_r^{(b+c)/b}+1$
		Where t_r has different meaning for each equation.	Where t_r is a different function of t_i in each case.

COMPARISON OF EQUATIONS FOR PLASTIC FLOW AND CREEP WITH DATA FROM LITERATURE

There is a multitude of strain/time data presented in the literature, but they are in most cases restricted to the condition of loading only, and a possible recovery of strain as a function of time is seldom taken into consideration. It is therefore difficult to obtain a complete picture of the flow characteristics of the substance under test, and only a few cases presented in the literature may be discussed.

(a) Plastic Flow

Examples for plastic flow free of elastic after-effect according to Eqs. (2) and (3) of Table I have been quoted in a previous paper.[1]

(b) Creep and Elastic After-Effect

Leaderman[6] measured the creep of polyvynil chloride plasticized with tricresyl phosphate as a function of time under a constant stress and observed the recovery of strain after unloading. The sample showed almost complete recovery and corresponded essentially to the model presented in Fig. 1 minus element D. The curves given indicate a linear relationship between the strain and the logarithm of time and are in agreement with Eq. (3) in Table I for the couple B, C.

Lutz and Himmelfarb[7] measured the creep of manila ropes under constant tensile stress. The curves given showed for the largest part a linear relationship between strain and logarithm of time, the slope of which increased with increasing stress. No observation of the recovery was made, however, it can be assumed from the fibrous structure of the material, that the manila ropes conform to the same equation as the plasticized polyvynil chloride.

(c) Creep and Time-Hardening

McVetty[8] suggested the following relationship between strain and time at constant stress for steel and its alloys and copper at elevated

[6] Herbert Leaderman, Ind. Eng. Chem. **35**, 314 (1943).
[7] Lutz and Himmelfarb, Proc. Am. Soc. Test. Mat. **40**, 125 (1940).
[8] P. G. McVetty, Proc. Am. Soc. Test. Mat. **43**, 707 (1943).

temperature:

$$\epsilon=\epsilon_0-(c/\alpha)\exp(-\alpha t)+v_0 t,$$

where ϵ is the total strain, ϵ_0 the strain at which the strain-rate becomes constant, v_0=constant strain-rate, t=time, and c and α are constants depending upon the material and temperature. It was suggested that the exponential term serves to define the strain-time relationship during creep. Evidently the term c/α has the dimension of ϵ and corresponds to ϵ_0 being the strain at which the exponential term approaches zero, hence

$$\epsilon=\epsilon_0[1-\exp(-\alpha t)]+v_0 t.$$

The first term of this equation can refer to the mechanical behavior of an elastic element coupled in parallel with a purely viscous element according to Eq. (1) in Table I, which is highly improbable in the case of metals, and therefore refers to creep due to time-hardening according to Eq. (7) in Table I with $1/\alpha$ equal to α in the above equation.

The relationship between stress and the constant strain rate v_0 was found to obey the following hyperbolic sine term

$$v_0=v_1\sinh(S/S_1)=\tfrac{1}{2}[\exp(S/S_1)-\exp(-S/S_1)]$$

in which the second exponential term approaches zero with high values of S, and this equation becomes similar to Eq. (3) in Table I.

The same equation also forms the basis for the stress relaxation of copper at constant strain, for which Boyd[9] gave the following expression at elevated temperatures around 200°C for the last stages of relaxation

$$S=S_i[1-A\ln(Bt+1)]$$

or

$$\exp[(S_i-S)/AS_i]=Bt+1,$$

which is the same as the relaxation term (3) in Table II with $A=b$ and $B=1/t_r$. For the first stage the relationship between stress and logarithm of time forms a curve and seems to be influenced by the elastic after-effect as discussed in the previous section.

Bituminous pavements[10] composed of 80 percent of sand, 10 percent of silica dust, and 10 percent of asphalt were found to correspond in their deformation mechanism to the model given in Fig. 1. The elasticity of spring A of this model is mainly due to the small air pockets present through the pavement, and element D is subject to time-hardening according to Eq. (4) in Table I, $S/S_0=(vt/v_0t_0)^b$. To illustrate the time-hardening effect, the data below may be given which were obtained at 15°C for such a mixture which was compacted in a mold of 5.08 cm in diameter to a cylinder 2.31 cm high under a pressure of 220 kg/cm². The cylinder having an air content of 6.73 percent by volume was subjected to compression tests under constant stress, in such a way that when the deformation came to a stop, i.e., when the initial yield value was increased to that of the stress, the load was increased by constant increments of 0.88 kg/cm². For the non-recoverable deformation the following values of $k=vt$ were obtained:

Stress in kg/cm²	Yield value in kg/cm² at beginning of test	$k\times10^3$
1.55	0.70	0.68
2.43	1.55	0.52
3.31	2.43	0.38
4.19	3.31	0.28
5.07	4.19	0.23
5.95	5.07	0.19
6.82	5.95	0.16
7.70	6.82	0.14
8.58	7.70	0.13
9.46	8.58	0.10

From the data the value of b is -0.89, indicating that the increase in yield value is also affected by the stress as outlined in Part I of this paper.[1] During this stress range the density of 2.038 remained constant after the elastic recovery. At stresses in excess of 9.46 kg/cm² the values of k increased with increasing stress and the density dropped to 2.03 at the application of a stress of 12.10 kg/cm² resulting in opening of the structure and failure of the paving sample.

The modulus of elasticity of spring A was 3940 kg/cm² and that of spring B 9080 kg/cm². Measurements of the strain recovery after unloading showed element C to obey Eq. (2) in Table I, $S_b/S_{b0}=(v/v_0)^b$ with a value of b equal to 0.272. The relaxation of stress at constant strain was mainly due to the expansion of spring B, since its modulus of elasticity was higher than that of spring A.

[9] John Boyd, Proc. Am. Soc. Test. Mat. **37**, 218 (1937).
[10] Charles Mack, unpublished data.

(d) Creep and Strain-Hardening

Creep data given by Sturm[11] for aluminum wire under tension at room temperature showed a linear relationship between the logarithm of strain and the logarithm of time with slopes which are practically independent of the stress applied. The stress was found to be a power function of the strain rate at a given deformation, hence the creep of aluminum wire corresponds to any of the Eqs. (8) to (13) in Table I and is caused by strain-hardening.

Scott Blair and Coppen[12] suggested the following equation for the relationship between stress, strain and time of plastic substances.

$$\psi = St^k/\epsilon,$$

where ψ is a constant measuring "firmness," and k a dimensionless constant. Both constants were found to be independent of the stress in some cases. In most cases ψ was found to vary with the stress, and the following equation was suggested, which was also independently proposed by Nutting.[13]

$$\psi_\beta = S^\beta t^k/\epsilon.$$

Expressing the stress as a function of strain rate and strain, changes these terms into

$$S/S_0 = (v/v_0)^k(\epsilon/\epsilon_0)^{1-k}$$

and

$$S/S_0 = (v/v_0)^{k/\beta}(\epsilon/\epsilon_0)^{(1-k)/\beta}.$$

Both equations cover creep in connection with strain-hardening and correspond in form to Eq. (12) in Table I. The authors found these relationships to hold for a variety of materials under compression at constant stress such as wet and dry clay, worked and unworked butter, cake, apple, cheese, potato, and acrylic acid polymeride. It appears that these substances are free of components giving rise to elastic after-effect or that the latter is so small as to be negligible.

Other substances such as plasticine and its mixtures with rubber and Vaseline showed partial recovery on unloading, and a linear relationship was found to hold between the logarithm of strain and the logarithm of time. In view of the limitation in deformation of element C in Fig. 1 when subject to work-hardening, the elastic recovery appears to conform to the relationship (2) in Table I. The non-recoverable deformation of these materials corresponded to creep due to strain-hardening.

Findley[14] found the following equation to hold for the creep of paper and canvas laminates, cellulose acetate sheets, and a series of phenolic molding compounds:

$$\epsilon - \epsilon_0 = mt^n,$$

where ϵ_0 is the strain at time $t=0$, and m and n are constants. Constant m was found to depend on the stress applied according to

$$m = C[\exp(kS) - 1],$$

where C and k are constants. Combining both terms, he arrived at the following equation for the strain rate

$$v = Cnt^{n-1}[\exp(kS) - 1].$$

With high values of S, -1 can be neglected, which was introduced only in order to satisfy the condition, that $v=0$ when $S=0$; combining this equation with the corresponding term for v_0 gives after substituting bS_0 for $1/k$

$$\exp[(S-S_0)/S_0] = (v/v_0)^b(t/t_0)^{b(1-n)},$$

which is equivalent in form to Eq. (9) given in Table I in connection with strain-hardening. The cellulose acetate also showed the property of elastic after-effect at high stresses.

Buist and Seymour[15] applied the Scott Blair equation mentioned before to data obtained from the compression and elongation of rubber and found a linear relationship between the logarithm of strain and logarithm of time at constant stress. Since the deformation of the couple B, C in Fig. 1 is very rapid in the case of rubber, the deformation as a function of time is measured mainly for element D and represents creep due to strain-hardening.

These results are in agreement with data given by Behre[16] who measured the extrusion of rubber

[11] R. G. Sturm, Proc. Am. Soc. Test. Mat. **43**, 728 (1943).
[12] Scott Blair and J. Coppen, Soc. Chem. Ind. **60**, 190 (1941).
[13] P. G. Nutting, Proc. Am. Soc. Test. Mat. **21**, 1162 (1921).
[14] W. N. Findley, Modern Plastics **22**, 153 (Dec. 1944).
[15] Buist and Seymour, Trans. Inst. Rub. Ind. [XVII] **2**, 366 (1944).
[16] J. Behre, Rubber Chem. and Techn. **18**, 646 (1945) translated from Kautschuk **20**, 15 (1944).

as a function of time and found the following relationship to hold

$$V_{15} = K p^m,$$

where V_{15} is the volume of rubber extruded in 15 seconds, p = pressure applied, K and m are constants. Since the volume extruded and the pressure are proportional to the rate of shear and shearing stress, this term corresponds to Eq. (8) in Table I for strain-hardening with the time being constant.

(e) Creep and Thixotropy

An extensive investigation into the flow characteristics of a plastic asphalt was carried out by Saal and Labout,[17] which consisted in the measurement of the deformation in a rotating cylinder viscometer as a function of time under constant shearing stress, and in measurements of the recovery after unloading and the stress relaxation at constant strain.

The logarithm of deformation was found to be proportional to the logarithm of time at constant stress for the first part with a proportionality factor of 0.38 independent of the stress. This relationship became then curvilinear and finally approached linearity again. The recovery-time curves, with deformation and time at the moment of unloading being 0, coincided with the first part of the deformation-time curves during loading. This part therefore corresponds to the deformation of the couple B, C, in Fig. 1. The deformation of element D was found to be proportional to a power function of time with a value of this function higher than 1. This behavior is in agreement with the break-down of thixotropic structure according to Eq. (14) in Table I. Element C is free of thixotropic disturbance.

Re-evaluation of the stress/time curves during relaxation at constant deformation showed the logarithm of stress to be curvilinear with the logarithm of time for the initial stage due to the effect of the couple B, C. This relationship became then linear with a slope of -0.455. Since the deformation of element C is proportional to $t^{b/(1-b)}$ according to Eq. (2) in Table I and $b/(1-b) = 0.38$, the stress relaxation as a function of time should have the same value for $b/(1-b)$ according to Eq. (2) in Table II. As this value is larger, it follows that the relaxation is still accompanied by break-down of the thixotropic structure and follows the Eq. (14) in Table II, $S_i/S = (t/t_i)^{(b+c)/(1-b)}$, with $b/(1-b) = 0.38$, b becomes 0.275 and c 0.055.

Values of c of this order are frequently found with asphalts. For example[18] a thixotropic asphalt free of elastic disturbance showed in a coaxial falling cylinder viscometer under constant shearing stress at 15°C a linear relationship between the logarithm of deformation and logarithm of time for the period of structural break-down in agreement with Eq. (14) in Table I, $\epsilon = \text{const.}\, t^{(b+c)/b}$. With values of $(b+c)/b$ of 1.090 and 1.092 obtained at two different stresses and $b = 0.95$, c becomes 0.086.

These examples may suffice to show that the equations given have a wide field of application for the description of the deformation mechanism of plastic substances.

[17] Saal and Labout, J. Phys. Chem. **44**, 149 (1940).

[18] Charles Mack, unpublished data.

Asymptotic Solutions for the Normal Modes in the Theory of Microwave Propagation*

C. L. PEKERIS**

(Received July 2, 1946)

In this paper are presented several extensions of the "W.K.B." method in the asymptotic solution of differential equations. The developments were made in the course of a systematic study of the application of asymptotic solutions to the normal-mode theory of microwave propagation. In Section 1 a brief outline is given of the now standard normal-mode theory of propagation of microwaves in an atmosphere with a horizontally stratified index of refraction. Particular emphasis is given in this study to the case of a "surface duct." The case of "leaky modes" is studied in Section 2. Here the aim has been to obtain explicitly the terms after the leading one in the asymptotic expansion of the solution, in order to have an estimate of the order of magnitude of the error introduced by the use of the leading term only. This is achieved in Eq. (20), which is of general applicability to a wide class of physical problems. The first correction term to the phase-integral solution for the characteristic values of the normal modes is set out in Eqs. (28) to (30). An alternative asymptotic solution for the case of leaky modes, which includes the first correction terms, is given in Eqs. (30), (40), and (41). In Section 3 a direct method is given of determining the characteristic values from the phase-integral relation. If the modified index of refraction $y(h)$ is given by a power series (49) then with the aid of Eqs. (50)–(52) one can compute directly the characteristic value Λ_m by Eq. (46), using (47) and (48). The degree of success of this method is illustrated in Table I. The principal contribution of this study is in the development of asymptotic solutions for the case of *transitional modes* which are on the border line between the leaky modes and the trapped modes. The standard "W.K.B." method is inapplicable in this case. The results for the determination of the characteristic values and height-gain functions are as follows. One first obtains v_0 defined in (85), which in the case of an exponential model can be facilitated by the use of Fig. 2. The quantities γ_m^0, $d\gamma_m^0/dv_0$, and $[(\partial P(v_0)/\partial v)\cdot(\partial P(v_0)/\partial\gamma_m^0)]$ are then read off Table IV. The characteristic value is then determined from (87), (88), and (68), particular examples of which are given in (89) and (90) for the "exponential model," and in (94) and (96) for the "power law" model. These include a correction term Δ_m which was obtained from the perturbation theory of transitional modes developed in Section 4D. A comparison between exact characteristic values and those obtained from the theory of transitional modes is shown in Tables II and III for the "exponential" and "power law" models, respectively. It is seen that the theory of transitional modes developed here yields accurate characteristic values over a wide region, extending into the leaky modes on one side and into the trapped modes on the other side. The height-gain functions can be obtained from (60), (69), (76), (77), (83), and (101). In the case of an exponential model the variables u and v can be computed with the aid of Fig. 2. The asymptotic theory of trapped modes developed in Section 5 follows Langer's method, whereby the difficulty with the Stokes phenomenon is completely obviated. The procedure used is to develop the solutions around the two turning points h_1 and h_2 shown in Fig. 1 and to join the solutions at the duct height h_0. The relation determining the characteristic values thus obtained is (140), which bears a similarity to the corresponding equation for a "bilinear" model. Indeed, Eqs. (131), (132), (136), and (137) give the transformation required to turn the model with a continuous $y(h)$ curve shown in Fig. 1 into one where $y(h)$ is represented by two straight lines that intersect at h_0. It is shown in Eq. (159) how one can derive the Furry-Gamow formula for the decrement of *completely trapped modes* from Eq. (140). Equations (160) to (163) give expressions for the height-gain functions for highly trapped modes. These cover the whole range of height including the vicinity of the two turning points.

1. INTRODUCTION

THIS paper gives an account of several developments in the theory of asymptotic solutions for the normal modes in microwave propagation. In the theory of microwave propagation we are interested in determining the electromagnetic field generated by a dipole antenna which is situated at some elevation above the ground. Of particular interest is the effect of atmospheric refraction on propagation into regions below the horizon. The field can be determined from a Hertzian potential Ψ[1] which satisfies the wave equation

$$\nabla^2\Psi+k^2\mu^2\Psi=0. \tag{1}$$

Here

$$k=2\pi/\lambda, \tag{2}$$

$$k^2\mu^2=(\epsilon\omega^2-i\sigma\omega)/c^2, \tag{3}$$

* This paper is based on work done for the Naval Research Laboratory under contract No. N5-ori-90 with the Navy's Office of Research and Inventions.

** Columbia University Mathematical Physics Group, on leave of absence from M.I.T.

[1] See Arnold Sommerfeld's article in Frank-Mises *Differentialgleichungen der Physik* (M. S. Rosenberg, New York), Vol. II, p. 918.

μ denotes the index of refraction and a time factor $e^{i\omega t}$ has been assumed. For vertical polarization Ψ represents the vertical component of the electric Hertzian potential, while for horizontal polarization it represents the vertical component of the magnetic Hertzian potential. The observed field intensity is proportional to $|\Psi|$ in each case. Equation (1) is to be solved subject to the following boundary conditions:

(a) Ψ should reduce to the form e^{-ikR}/R for small distances R from the source,
(b) Ψ should vanish at the ground, and
(c) Ψ should represent an outgoing wave at great distances from the source.

The boundary condition (b) is not strictly true, but it is a good approximation for the low order normal-mode solutions of Eq. (1).

The quantity μ appearing in Eq. (1) represents the index of refraction of the air, which will be assumed to vary only with height above the ground, and the boundary condition (b) is to be satisfied at the spherical surface of the earth. The analysis can be simplified by the use of a device attributed originally to Schelleng, Burrows, and Ferrell[2] and later developed by M. H. L. Pryce,[3] whereby space is transformed so as to make the surface of the earth plane and the rays curved. The transformation can be accomplished by using in Eq. (1) instead of μ the so-called *modified index of refraction* N defined by

$$N=r\mu(r)/b\mu(b),$$

where r denotes the distance from the center of the earth and b is the radius at some reference level. Taking $b=a$, the radius of the earth, we have

$$\frac{r}{a}=1+\frac{h}{a},$$

$$\frac{\mu(r)}{\mu(a)}=1+\dot{\mu}h+\mu'(h), \tag{4}$$

$$N\cong 1+h\left(\dot{\mu}+\frac{1}{a}\right)+\mu'(h). \tag{5}$$

Here h denotes height above ground, $\dot{\mu}$ the vertical gradient of the index of refraction in the *standard atmosphere*, and $\mu'(h)$ denotes the *refraction anomaly* or the deviation of the refractive index from standard conditions. The term $h\dot{\mu}$ in Eq. (5) has the effect of modifying the radius of the earth a to an effective value a_e determined by

$$1/a_e=1/a+\dot{\mu};$$

the value of a_e/a is generally taken as 4/3. In practice it is convenient to use the quantity M defined by

$$M-M_0=10^6(N-1).$$

Substituting in Eq. (5) and using the dependence of μ on atmospheric pressure p (millibars), temperature T (absolute scale) and the partial pressure of water vapor e (millibars), one finds that

$$M=\frac{79p}{T}+\frac{3.8\times 10^5 e}{T^2}+.048h,$$

where h is expressed in feet. Here the term $.048h$ is $10^6(h/a)$; under standard conditions the sum of the first two terms in the expression for M varies with height like $-.012h$, giving

$$M_{\text{std}}=M_0+.036h.$$

The increase of M_{std} with height results in a curving of the rays away from the ground, in the framework of the flattened earth, the radius of curvature of the rays being constant in a standard atmosphere and equal to a_e. Under certain atmospheric conditions the modified index of refraction increases with elevation in the ground layer at a more rapid rate than under standard conditions. We then have a case of *substandard refraction*, and transmission is generally poorer than in the standard atmosphere. On the other hand, when the modified index decreases with elevation in the ground layer at a less rapid rate than in the standard atmosphere, or when the initial slope of $M(h)$-curve is negative, we have a state of *super-refraction*, and transmission is generally improved. A state of super-refraction which starts at the ground is called a *surface-duct*; super-refraction may also occur at some elevation, in which case it is referred to as an *elevated duct*.

[2] J. C. Schelleng, C. R. Burrows, and E. B. Ferrell, Proc. I.R.E. **21**, 427 (1933); J. E. Freehafer, Radiation Laboratory Report 447 (1943); C. L. Pekeris, Phys. Rev. **70**, 518 (October, 1946).
[3] Unpublished report.

Barring certain pathological cases,[4] which we need not consider here, it is possible to obtain a solution of (1) satisfying the boundary conditions in terms of *normal modes* as follows:

$$\Psi = -i\pi \sum_1^\infty H_0^{(2)}(k_m\rho)\, U_m(h_1)\, U_m(h_2), \quad (6)$$

where ρ denotes horizontal distance along the surface of the earth, h_1 and h_2 the heights of transmitter and receiver, and k_m are characteristic complex numbers. The height-gain functions $U_m(h)$ are solutions of the equation

$$\frac{d^2U_m}{dh^2} + (k^2N^2 - k_m^2)\, U_m = 0. \quad (7)$$

$U_m(h)$ must further satisfy the following boundary conditions:

(a) The phase of $U_m(h)$ should decrease with elevation at great heights h;
(b) The tangential components of the electric and magnetic fields should be continuous at the earth's surface.

Under certain conditions[4] the boundary condition (b) can be replaced by the simpler one

$$U_m(0) = 0. \quad (8)$$

Equation (8) is a good approximation for the low order modes in case of propagation over the ocean. Since $N^2 \simeq 1$ and $k_m \simeq k$, it is convenient to write

$$N^2(h) = 1 + y(h), \quad k_m^2 = k^2(1 - \Lambda_m),$$

whereby Eq. (7) is transformed into

$$\frac{d^2U_m}{dh^2} + k^2[\Lambda_m + y(h)]\, U_m = 0. \quad (9)$$

When used in Eq. (6) to represent radiation from a dipole the solutions of (9) must be normalized by the condition

$$\lim_{I(k)\to 0^-} \int_0^\infty U_m^2(h)\, dh = 1 = -\frac{1}{k^2}\frac{\partial U_m(0)}{\partial h}\cdot\frac{\partial U_m(0)}{\partial \Lambda_m}. \quad (10)$$

The different types of solution which arise in the treatment of non-standard propagation in the case of a "surface duct" can be illustrated with reference to the modified-index curve $y(h)$ shown in Fig. 1.

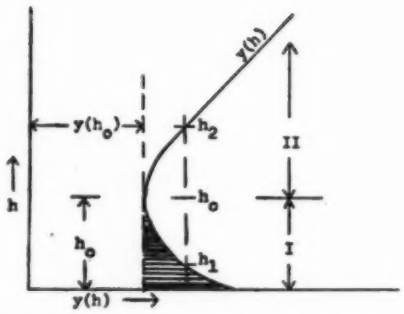

FIG. 1. Variation of the modified index of refraction $y(h)$ with height h in case of a surface duct.

When for any mode of order m the integral

$$F(h_0) \equiv k\int_0^{h_0} [y(h) - y(h_0)]^{\frac{1}{2}} dh$$

is less than the value $v_m \simeq \pi(m - \frac{1}{4})$ (k is small, or the shaded area in the figure is small) the characteristic values Λ_m have imaginary parts (positive) which are comparable in magnitude to their real parts, and the mode is said to be *leaky*. This is because the height-gain function $U_m(h)$ is then found to increase rapidly with height, and the factor $H_0^{(2)}(k_m\rho)$ to decrease at a moderate exponential rate with range ρ. As F approaches the value v_m, $Im(\Lambda_m)$ becomes small and $Re(\Lambda_m) \simeq -y(h_0)$. We then have a *transitional mode* which forms the principal topic of this investigation.

When $F(h_0) \gg v_m$ there is a value $h_1 < h_0$ for which

$$F(h_1) = k\int_0^{h_1} [y(h) - y(h_1)]^{\frac{1}{2}} dh = v_m.$$

The imaginary part of Λ_m is then extremely small, and to a high approximation $\Lambda_m = -y(h_1)$. The mode is said to be *trapped* in this case, because $U_m(h)$ is then concentrated almost entirely at levels below h_1, and the factor $H_0^{(2)}(k_m\rho)$ does not exhibit an exponential attenuation with range ρ.

In the following we discuss the asymptotic solutions of (9) in the three cases of leaky, transitional, and trapped modes. Since the basic theory for the leaky and trapped modes has

[4] Radiation Laboratory Report 680, 1945 by W. H. Furry; and C. L. Pekeris, J. Acous. Soc. Am. **18**, 295 (October, 1946).

already been fully dealt with by Furry[4] we shall confine our discussion of these cases to certain extensions which have been developed subsequent to Furry's report. Thus, in order to have an estimate of the order of magnitude of the error involved in the use of an asymptotic solution for a given value of k, we derive explicit expressions for the terms after the leading one in the asymptotic expansion (in inverse fractional powers of k) of the solutions of (9). We also use the Langer[5] method throughout and obtain solutions which do not suffer from the Stokes phenomenon, and which, furthermore, can be used to compute $U_m(h)$ in the vicinity of the turning points. The latter is, of course, required for determining the field. In addition, a direct method is given for computing the characteristic value from the "phase integral relation" which is particularly useful in case of substandard refraction. The principal contribution of this paper is however in the extension of the method of asymptotic solutions to cover *transitional modes*.

2. ASYMPTOTIC SOLUTIONS FOR LEAKY MODES

In case of leaky modes the imaginary part of the characteristic value Λ_m is comparable in magnitude to the real part, and the expression in brackets in the equation

$$d^2U_m/dh^2+k^2[\Lambda_m+y(h)]U_m=0 \qquad (9')$$

does not vanish on the real axis of h. It was pointed out by Eckersley[6] that asymptotic solutions of (9) can be obtained by determining a *turning point* h_1 (complex) defined by

$$\Lambda_m+y(h_1)=0, \qquad (11)$$

and developing the solutions around that point. Following Langer's method[5] we write

$$U_m(h)=\frac{G(h)}{[Q(h)]^{\frac{1}{2}}}, \quad Q^2=k^2[\Lambda_m+y(h)], \qquad u(h)=\int_{h_1}^{h} Q(h)dh \qquad (12)$$

and obtain from (9)

$$\frac{d^2G}{dh^2}-\frac{\dot{Q}}{Q}\frac{dG}{dh}+\left(-\frac{d^2Q/dh^2}{2Q}+\frac{3}{4}\frac{\dot{Q}^2}{Q^2}+Q^2\right)G=0, \qquad (13)$$

where dots denote differentiation with respect to h. We now introduce u as an independent variable in place of h, and obtain from (13):

$$d^2G(u)/du^2+P(u)G(u)=0, \qquad (14)$$

$$P(u)=1+\frac{1}{4Q^2}\left(\frac{dQ}{du}\right)^2-\frac{1}{2Q}\frac{d^2Q}{du^2}. \qquad (15)$$

From its definition in (12) we develop $u(h)$ into a power series in $(h-h_1)$, invert this series and then express Q as a power series in u. From the latter we find that

$$P(u)=1+\frac{5}{36u^2}+\frac{A}{k^{4/3}u^{2/3}}+\frac{B}{k^2}+\frac{Cu^{2/3}}{k^{8/3}}+\cdots, \qquad (16)$$

where

$$A=\frac{(1.5)^{4/3}}{315(\dot{y})^{2/3}}\left[9\left(\frac{\ddot{y}}{\dot{y}}\right)^2-10\left(\frac{d^3y/dh^3}{\dot{y}}\right)\right], \qquad (17)$$

$$B=\frac{1}{450\dot{y}}\left[-25\left(\frac{d^4y/dh^4}{\dot{y}}\right)+70\left(\frac{\ddot{y}(d^3y/dh^3)}{\dot{y}^2}\right)-42\left(\frac{\ddot{y}}{\dot{y}}\right)^3\right], \qquad (18)$$

and

$$\dot{y}=\frac{dy(h_1)}{dh}, \quad \ddot{y}=\frac{d^2y(h_1)}{dh^2}, \quad \text{etc.} \qquad (19)$$

Using (16) in (14) and expanding $G(u)$ in a descending power series in k we obtain

$$G(u)=u^{\frac{1}{2}}H_{1/3}^{(2)}(u)+\frac{3A}{2k^{4/3}}u^{5/6}H_{-2/3}^{(2)}(u)-\frac{B}{2k^2}u^{3/2}H_{4/3}^{(2)}(u)+0(k^{-8/3})+\cdots, \qquad (20)$$

where we have chosen the Hankel function of the *second kind* in order to assure an outgoing wave at great heights.

The asymptotic expansion (20) of the solution of Eq. (14) is useful for moderate values of u and in the limit of large values of k. This combi-

[5] R. E. Langer, Phys. Rev. **51**, 669 (1937); see also H. Jeffreys, Phil. Mag. **33**, 451 (1943).
[6] T. L. Eckersley, Proc. Roy. Soc. **A132**, 83 (1931); **136**, 499 (1932); **137**, 158 (1932); T. L. Eckersley and G. Millington, Phil. Trans. Roy. Soc. **A237**, 273 (1938).

nation of values of u and k actually occurs in many applications of (20), such as, for example, the finding of the zeros of $G(u)$, and the problem under consideration. Taking the boundary condition at the ground as

$$G[u(0)]=0, \quad u(0)=k\int_{h_1}^{0}[\Lambda_m+y(h)]^{\frac{1}{2}}dh, \quad (7')$$

we seek an expansion for $u(0)$ of the form

$$u(0)=c+\frac{c_1}{k^{4/3}}+\frac{c_2}{k^2}+\frac{c_3}{k^{8/3}}+\cdots. \quad (21)$$

Substituting in (20) we find

$$H_{1/3}^{(2)}(c)=0; \quad c=e^{i\pi}v_m, \quad (22)$$

where the v_m are the roots of the equation

$$J_{1/3}(v_m)+J_{-1/3}(v_m)=0, \quad v_m\simeq\pi(m-\tfrac{1}{4}), \quad m=1, 2, 3, \cdots. \quad (22')$$

When this value of $u(0)$ is used in (7') we obtain *Eckersley's phase integral condition:*

$$k\int_0^{h_1}[\Lambda_m+y(h)]^{\frac{1}{2}}dh = k\int_0^{h_1}[y(h)-y(h_1)]^{\frac{1}{2}}dh=v_m. \quad (23)$$

This gives a relation for determining the value (complex) of the turning point h_1, from which Λ_m is then evaluated by Eq. (11). The numerical solution of (23) for h_1 is, however, a difficult problem, and no method of solution of general applicability is at present available, especially for the case of leaky modes. In the following section we develop an approximate, but direct, method of solving Eq. (23), which is effective in the case when $y(h)$ is a monotone function of h.

Proceeding now with the asymptotic expansion (21) we find that

$$c_1=-\frac{3A}{2}\left[\frac{c^{1/3}H_{-2/3}^{(2)}(c)}{\dot{H}_{1/3}^{(2)}(c)}\right]=-\frac{3A}{2}c^{1/3}, \quad (24)$$

$$c_2=\frac{B}{2}\left[\frac{cH_{4/3}^{(2)}(c)}{\dot{H}_{1/3}^{(2)}(c)}\right]=-\frac{Bc}{2}. \quad (25)$$

Hence the roots $u(0)$ of $G(u)$ in (20) are given by

$$u(0)=e^{i\pi}v_m-\frac{3A}{2k^{4/3}}e^{i\pi/3}v_m^{1/3}+\frac{Bv_m}{2k^2}+\cdots. \quad (26)$$

With this expansion, the phase integral condition (23) is replaced by

$$k\int_0^{h_1}[\Lambda_m+y(h)]^{\frac{1}{2}}dh = v_m+\frac{3A}{2k^{4/3}}e^{i\pi/3}v_m^{1/3}-\frac{Bv_m}{2k^2}+\cdots. \quad (27)$$

Let now

$$\Lambda_m=\Lambda_m^{(0)}+\frac{\Delta}{k^{7/3}}+\cdots, \quad (28)$$

substitute in (27) and obtain

$$k\int_0^{h_1}[\Lambda_m^{(0)}+y(h)]^{\frac{1}{2}}dh=v_m, \quad (23')$$

$$\Delta=\frac{3A}{\theta}e^{i\pi/3}(v_m)^{1/3}, \quad (29)$$

where

$$\theta=\int_0^{h_1}\frac{dh}{[\Lambda_m^{(0)}+y(h)]^{\frac{1}{2}}}. \quad (30)$$

To summarize, the determination of the characteristic values Λ_m in case of leaky modes proceeds as follows. First one finds the turning point h_1 and Λ_m by solving (23'), where

$$\Lambda_m^{0}=-y(h_1). \quad (11')$$

One then evaluates the derivatives of $y(h)$ at h_1 and finds A by (17), as well as θ from (30). Λ_m is then given by

$$\Lambda_m=\Lambda_m^{(0)}+\frac{3A}{\theta k^{7/3}}e^{i\pi/3}(v_m)^{1/3}+\cdots. \quad (28')$$

The last term indicates the order of magnitude of the error involved in the use of $\Lambda_m^{(0)}$ for Λ_m. It will be noted that the factor A contains inverse powers of $\dot{y}(h)$, so that the accuracy of the phase integral method for determining the characteristic values depends on (a) k being large and on (b) the turning point h_1 being removed from a place where $\dot{y}(h_1)=0$. The last condition is violated, in case of a surface duct, when the mode becomes transitional, i.e., when h_1 approaches the real value of the "duct height" h_0 shown in Fig. 1.

As for the height-gain functions, we have in

the first approximation

$$U_m(h)=\frac{C_m u^{\frac{1}{3}}H_{1/3}^{(2)}(u)}{[y(h)+\Lambda_m]^{1/4}}, \tag{31}$$

where

$$u=k\int_{h_1}^{h}[y(h)+\Lambda_m]^{\frac{1}{2}}dh,$$

and the normalization factor C_m is to be determined from Eq. (10). We find that at $h=0$

$$\frac{\partial U_m}{\partial h}=C_m k[y(0)+\Lambda_m]^{1/4}u_0^{\frac{1}{3}}\dot{H}_{1/3}^{(2)}(u_0), \tag{32}$$

$$\frac{\partial U_m}{\partial \Lambda_m}=-\tfrac{1}{2}C_m k\theta[y(0)+\Lambda_m]^{-1/4}u_0^{\frac{1}{3}}\dot{H}_{1/3}^{(2)}(u_0), \tag{33}$$

$$\dot{H}_{1/3}^{(2)}(u_0)=\frac{2}{3^{\frac{1}{3}}}e^{i\pi/6}\left(\frac{2u_m}{v_m}\right)^{\frac{1}{3}};$$

$$u_m\equiv\frac{v_m}{2}[J_{2/3}(v_m)-J_{-2/3}(v_m)]^2\backsimeq\frac{3}{\pi}. \tag{34}$$

Substituting in (10) we determine C_m, and then obtain

$$U(h)=\frac{e^{-i2\pi/3}(3u)^{\frac{1}{3}}H_{1/3}^{(2)}(u)}{2(\theta u_m)^{\frac{1}{3}}[y(h)+\Lambda_m]^{1/4}}. \tag{35}$$

One finds from (35) that

$$\frac{dU_m(0)}{dh}=k\left(\frac{2}{\theta}\right)^{\frac{1}{3}}[y(0)+\Lambda_m]^{1/4}. \tag{36}$$

In evaluating the height-gain function it is convenient to use the Harvard tables of the function

$$h_2(\chi)\equiv(\tfrac{2}{3})^{1/3}\chi^{\frac{1}{3}}H_{1/3}^{(2)}(\tfrac{2}{3}\chi^{3/2})=u^{1/3}H_{1/3}^{(2)}(u);$$
$$\chi\equiv\left(\frac{3u}{2}\right)^{2/3}, \tag{37}$$

which is tabulated for complex values of the argument χ. In terms of this function we have

$$U_m(h)=\frac{3^{\frac{1}{3}}u^{1/6}e^{-i2\pi/3}h_2(\chi)}{2(\theta u_m)^{\frac{1}{3}}[y(h)+\Lambda_m]^{1/4}}. \tag{38}$$

If we include the term after the leading one in (20), the function $H_{1/3}^{(2)}(u)$ in (35) is to be replaced by $[H_{1/3}^{(2)}(u)+(3A/2k^{4/3})u^{1/3}H_{-2/3}^{(2)}(u)]$, or the function $h_2(\chi)$ in (38) by $[h_2(\chi)+(3/2)^{2/3}\times(A/k^{4/3})h_2'(\chi)]$.

It may be pointed out that if we use the first three terms of $P(u)$ in (16) the *exact* solution of (14) is

$$G=u^{1/6}(u^{2/3}+A/k^{4/3})^{\frac{1}{3}}H_{1/3}^{(2)}[(u^{2/3}+A/k^{4/3})^{3/2}]$$
$$=u^{1/6}h_2\left[\left(\frac{3u}{2}\right)^{2/3}+\left(\frac{3A^{3/2}}{2k^2}\right)^{2/3}\right]. \tag{39}$$

Equation (26) is then replaced by

$$[u(0)^{2/3}+A/k^{4/3}]^{3/2}=e^{i\pi}v_m, \tag{40}$$

and Eq. (29) by

$$\Delta=\frac{2v_m k^{4/3}}{\theta}[(1+Ae^{i\pi/3}/k^{4/3}v_m^{2/3})^{3/2}-1]. \tag{41}$$

3. AN APPROXIMATE METHOD OF DETERMINING THE CHARACTERISTIC VALUES FROM THE PHASE INTEGRAL EQUATION

The problem of solving for the characteristic values Λ_m by the phase integral equation is to determine a turning point h_1 (generally complex) which satisfies the equation

$$F(h_1)=k\int_0^{h_1}[y(h)-y(h_1)]^{\frac{1}{2}}dh=v_m, \tag{42}$$

where $y(h)$ is a given continuous function representing the variation of the modified refractive index with height, and v_m is a known constant. The method of solving (42) to be described presently is particularly suited to the case when the function $y(h)$ is monotone, so that h is a single-valued function of y. The idea is to write

$$\int_0^{h_1}[y(h)-y(h_1)]^{\frac{1}{2}}dh=\int_{y(0)}^{y(h_1)}[y-y(h_1)]^{\frac{1}{2}}\left(\frac{dh}{dy}\right)dy, \tag{43}$$

and consider (dh/dy) as a function of y. Let

$$[y(0)+\Lambda_m]^{\frac{1}{2}}=[y(0)-y(h_1)]^{\frac{1}{2}}\equiv x; \tag{44}$$

then by integrating partially with respect to y we obtain from (42)

$$-\frac{2}{3}\dot{h}x^3+\frac{4}{15}\left(\frac{d^2h}{dy^2}\right)x^5-\frac{8}{105}\left(\frac{d^3h}{dy^3}\right)x^7+\frac{16}{945}\left(\frac{d^4h}{dy^4}\right)x^9-\cdots=v_m/k. \tag{45}$$

Equation (45) is now inverted to express x as a power series in $e^{i\pi/3}(v_m)^{1/3}$. Upon squaring the latter series we obtain, on using (44),

$$\Lambda_m = x^2 - y(0) = -y(0) + \tau^2 + \frac{4}{15}h_2\tau^4 + \tau^6\left[\frac{4}{25}h_2^2 - \frac{8}{105}h_3\right] + \frac{16}{27}\tau^8\left[\frac{77}{375}h_2^3 - \frac{33}{175}h_2h_3 + \frac{1}{35}h_4\right] + \cdots, \quad (46)$$

where

$$h_2 = \left(\frac{d^2h/dy^2}{\dot{h}}\right), \quad h_3 = \left(\frac{d^3h/dy^3}{\dot{h}}\right), \quad \text{etc.}, \quad (47)$$

$$\tau = e^{i\pi/3}(3v_m/2k\dot{h})^{1/3}. \quad (48)$$

When $\dot{h}$ is positive the phase of τ is $\pi/3$; in case of a surface duct the phase of τ is zero. In the latter case Eq. (46) yields a real value for Λ_m.

Let $y(h)$ be given as a power series in h:

$$y(h) = y(0) + b_1h + b_2h^2 + \cdots + b_nh^n + \cdots, \quad (49)$$

then

$$\dot{h} = \frac{dh}{dy}(h=0) = 1/b_1, \quad \frac{d^2h}{dy^2} = -2b_2/b_1^3, \quad (50)$$

$$d^3h/dy^3 = (-6b_1b_3 + 12b_2^2)/b_1^5, \quad (51)$$

$$d^4h/dy^4 = (120b_1b_2b_3 - 24b_1^2b_4 - 120b_2^3)/b_1^7, \quad \text{etc.} \quad (52)$$

Equation (46) then gives an explicit expression for Λ_m in terms of the coefficients in the power series expansion (49) of the modified index of refraction curve $y(h)$. This expression is of the nature of an asymptotic formula; it should be terminated when the individual terms begin to increase, and the error in Λ_m is then of the order of magnitude of the last term retained.

In an actual case the value of Λ_m obtained from (46) should be checked by computing h_1 from $y(h_1) = -\Lambda_m$, or from

$$h_1 = -\dot{h}x + \frac{d^2h/dy^2}{2!}x^2 - \frac{d^3h/dy^3}{3!}x^3 + \cdots, \quad (53)$$

and evaluating the phase integral $F(h_1)$ in (42). An improved value of h_1 can then be obtained by Newton's method, using the relation

$$\frac{dF(h_1)}{dh_1} = -\frac{k}{2\dot{y}(h_1)}\int_0^{h_1}\frac{dh}{[y(h)-y(h_1)]^{\frac{1}{2}}}. \quad (54)$$

TABLE I. Approximate determination of Λ_1 from (56) and the verification that $\int_0^{h_1}[y(h)+\Lambda_1]^{\frac{1}{2}}dh = 2.383$.

α	λ	Λ_1 from (56)	h_1 from $y(h_1) = -\Lambda_1$	$\int_0^{h_1}[y(h)+\Lambda_1]^{\frac{1}{2}}dh$	v_1
−20	.6356	$12.360+9.775i$	$.3997-.9518i$	$2.370+.004i$	2.383
−10	.6356	$4.878+6.302i$	$.4745-1.1982i$	$2.397+.010i$	2.383
− 5	.6356	$1.499+4.257i$	$.5691-1.4692i$	$2.393+.009i$	2.383
− 2	.6356	$-.246+2.902i$	$-.764-1.787i$	$2.363-.008i$	2.383

The degree of accuracy that can be obtained by the method described above will now be illustrated for the case of an exponential model, where

$$y(h) = h + \alpha e^{-\lambda h}, \quad k = 1.* \quad (55)$$

In this case Eq. (46) reduces to

$$\Lambda_m = -\alpha + \tau^2 - \frac{4}{15}\frac{\alpha\lambda^2}{(1-\alpha\lambda)^2}\tau^4 + \frac{4}{525}\frac{\alpha\lambda^3(\alpha\lambda-10)\tau^6}{(1-\alpha\lambda)^4} - \frac{16\alpha\lambda^4\tau^8}{70875(1-\alpha\lambda)^6}(75+105\alpha\lambda-\alpha^2\lambda^2) + \cdots. \quad (56)$$

$$\tau = e^{i\pi/3}[3v_m(1-\alpha\lambda)/2]^{1/3}. \quad (57)$$

It is seen from Table I that the values for Λ_1 obtained from (56) for the cases treated satisfy the phase integral equation rather closely. Another case treated was $\alpha = +20$, $\lambda = .6356$, where a real value for Λ_1 of -10.22 was obtained from (56). This is to be compared with the exact value of $\Lambda_1 = -10.21 + 1.07\times10^{-13}i$ obtained for this case by Pearcey and Whitehead.

4. ASYMPTOTIC SOLUTIONS FOR TRANSITIONAL MODES

A. Formal Solution

In the case of transitional modes the characteristic value Λ_m has a small imaginary part, the real part being very nearly equal to $-y(h_0)$, where h_0 denotes the duct height (see Fig. 1). The quantity in brackets in

$$\frac{d^2U_m}{du^2} + k^2[\Lambda_m + y(h)]U_m = 0, \quad (9')$$

* The specification of $k=1$ means simply that we are using natural units, which one would do in an actual problem.

therefore vanishes in the complex h plane at a point h_1 (turning point) which is very close to h_0 on the real axis. Since h_0 is defined by

$$\dot{y}(h_0)=0, \tag{58}$$

the proximity of h_1 to h_0 implies that the asymptotic expansion (20), which proceeds in inverse powers of $\dot{y}(h_1)$, breaks down for transitional modes.

Our method of dealing with the case of transitional modes is to develop the solution around y_0 as a turning point.† In place of (12) we now write

$$Q^2=k^2[y(h)+\Lambda_m{}^0], \quad \Lambda_m{}^0=-y(h_0), \tag{59}$$

$$u(h)=k\int_{h_0}^{h}[y(h)-y(h_0)]^{\frac{1}{2}}dh, \tag{60}$$

$$U_m(h)=\frac{G(h)}{[Q(h)]^{\frac{1}{2}}},$$

and find that

$$\frac{d^2U_m}{dh^2}+[Q^2(h)+k^2(\Lambda_m-\Lambda_m{}^0)]U_m=0, \tag{61}$$

$$\frac{d^2G}{dh^2}-\frac{\dot{Q}}{Q}\frac{dG}{dh}+\left[-\frac{d^2Q/dh^2}{2Q}+\frac{3}{4}\frac{\dot{Q}^2}{Q^2}+Q^2+k^2(\Lambda_m-\Lambda_m{}^0)\right]G=0, \tag{62}$$

$$\frac{d^2G(u)}{du^2}+P(u)G(u)=0, \tag{63}$$

$$P(u)=1+\frac{1}{4Q^2}\left(\frac{dQ}{du}\right)^2-\frac{1}{2Q}\frac{d^2Q}{du^2}+\frac{k^2(\Lambda_m-\Lambda_m{}^0)}{Q^2}. \tag{64}$$

As in Eq. (13), the dots in (62) denote differentiation with respect to h.

In contrast to the case of leaky modes the quantities u, Q, and $\Lambda_m{}^0$ are now real.

† Subsequent to the completion of this investigation the writer learned of a paper by S. Goldstein, Proc. Lond. Math. Soc. **33,** 246 (1932), where the same idea had been used in another connection. Also, Dr. T. Pearcey informed the writer that he independently treated the transitional case by a similar method.

Next, we proceed with the development of $P(u)$ into a power series in u. This is accomplished by first expressing u as a power series in $(h-h_0)$ using (60), inverting this series, and then using it in (59) to obtain a power series in u for Q. When substituted in (64) it yields

$$P(u)=1+\frac{3}{16u^2}+\frac{\gamma}{u}+\frac{N}{u^{\frac{1}{2}}}+\cdots, \tag{65}$$

$$\gamma=k(\Lambda_m-\Lambda_m{}^0)/[2\ddot{y}(h_0)]^{\frac{1}{2}}+\frac{1}{576c}(7y_3{}^2-9y_4), \tag{66}$$

$$N=-\frac{4}{9}\frac{y_3\gamma}{(2c)^{\frac{1}{2}}}+\frac{1}{97200\sqrt{2}c^{3/2}}\times(-1944y_5+3645y_3y_4-1715y_3{}^3), \tag{67}$$

where

$$c=k[\ddot{y}_0(h)/2]^{\frac{1}{2}}, \quad y_3=\left[\frac{d^3y(h_0)}{dy^3}\right]\Big/\ddot{y}(h_0), \quad y_4=\left[\frac{d^4y(h_0)}{dy^4}\right]\Big/\ddot{y}(h_0), \text{ etc.} \tag{68}$$

This expansion for $P(u)$ is to be used for $h>h_0$, with u defined in (60). For $0<h<h_0$ it is convenient to introduce the variable

$$v=k\int_{h}^{h_0}[y(h)-y(h_0)]^{\frac{1}{2}}dh, \tag{69}$$

and to develop P into a power series in v. In doing that, one must keep in mind that Q is a positive function of v, as it is of u. One thus finds that

$$P(v)=1+\frac{3}{16v^2}+\frac{\gamma}{v}-\frac{N}{v^{\frac{1}{2}}}+\cdots.** \tag{70}$$

It will be shown later that the product $k(\Lambda_m-\Lambda_m{}^0)$, and with it γ, remains finite in the limit of large k, so that N is of the order of $1/k^{\frac{1}{2}}$ relative to γ. We therefore treat N as a small perturbation term and write

$$G(u)=W(u)+Nw(u)+\cdots, \tag{71}$$

** A comparison of (70) with (65) shows that in going from $h>h_0$ to $h<h_0$ the phase of u can be considered as undergoing a change of 2π.

where

$$\frac{d^2W(u)}{du^2}+\left(1+\frac{3}{16u^2}+\frac{\gamma}{u}\right)W(u)=0, \quad h>h_0, \quad (72)$$

$$\frac{d^2W(v)}{dv^2}+\left(1+\frac{3}{16v^2}+\frac{\gamma}{v}\right)W(v)=0, \quad h<h_0, \quad (73)$$

$$\frac{d^2w(u)}{du^2}+\left(1+\frac{3}{16u^2}+\frac{\gamma}{u}\right)w(u)=-\frac{W(u)}{u^{\frac{1}{2}}}, \quad h>h_0, \quad (74)$$

$$\frac{d^2w(v)}{dv^2}+\left(1+\frac{3}{16v^2}+\frac{\gamma}{v}\right)w(v)=+\frac{W(v)}{v^{\frac{1}{2}}}, \quad h<h_0. \quad (75)$$

The solutions of (72) and (73) are confluent hypergeometric functions of arguments $2iu$ and $2iv$, respectively. Since the phase of $W(u)$ must decrease for large u, the appropriate solution of (72) is

$$W_m(u)=C_mW_{\kappa,1/4}(2iu), \quad \kappa=-i\gamma/2, \quad (76)$$

where $W_{\kappa,m}(z)$ is Whittaker's function:[7]

$$W_{\kappa,1/4}(2iu)=\frac{2\pi^{\frac{1}{2}}}{\Gamma(\frac{1}{4}-\kappa)}M_{\kappa,1/4}(2iu)+\frac{\pi^{\frac{1}{2}}}{\Gamma(\frac{1}{4}-\kappa)}M_{\kappa,-1/4}(2iu), \quad (77)$$

$$M_{\kappa,1/4}(z)=z^{3/4}e^{-z/2}F(\tfrac{3}{4}-\kappa,\tfrac{3}{2};z);$$
$$M_{\kappa,-1/4}(z)=z^{1/4}e^{-z/2}F(\tfrac{1}{4}-\kappa,\tfrac{1}{2};z). \quad (78)$$

For large z, $W_{\kappa,m}(z)$ behaves like

$$W_{\kappa,m}(z)\to z^{\kappa}e^{-z/2}F\left(\tfrac{3}{4}-\kappa,\tfrac{1}{4}-\kappa;-\frac{1}{z}\right), \quad -\pi<\arg z<\pi,$$
$$W_m(u)\to C_m\{1+[\tfrac{1}{16}-(\kappa-\tfrac{1}{2})^2]/2iu+\cdots\}\times\exp\{-iu+\kappa[\ln(2u)+i\pi/2]\}. \quad (79)$$

In the region below the duct height ($h<h_0$) we set

$$W_m(v)=C_m[pM_{\kappa,1/4}(2iv)+qM_{\kappa,-1/4}(2iv)], \quad (80)$$

and determine the constants p and q from the conditions that at $h=h_0(u=v=0)$

$$U_m(u)=\frac{W_m(u)}{[Q(u)]^{\frac{1}{4}}}=\frac{W_m(v)}{[Q(v)]^{\frac{1}{4}}}=U_m(v), \quad (81)$$

and

$$\frac{d}{dh}U_m(u)=Q(u)\frac{d}{du}U_m(u)=\frac{d}{dh}U_m(v)=-Q(v)\frac{d}{dv}U_m(v). \quad (82)$$

We shall omit the details of the calculation here, and shall merely state that from condition (81) it follows that $q=\pi^{\frac{1}{2}}/\Gamma(\frac{3}{4}-\kappa)$, while condition (82) requires that $p=2\pi^{\frac{1}{2}}/\Gamma(\frac{1}{4}-\kappa)$. Hence we have

$$W_m(v)=C_m\left[\frac{2\pi^{\frac{1}{2}}}{\Gamma(\frac{1}{4}-\kappa)}M_{\kappa,1/4}(2iv)+\frac{\pi^{\frac{1}{2}}}{\Gamma(\frac{3}{4}-\kappa)}M_{\kappa,-1/4}(2iv)\right]. \quad (83)$$

B. Determination of the Characteristic Values

The characteristic values Λ_m are now determined by the boundary condition (8) at the ground.

$$P(\gamma,v_0)\equiv\frac{2\pi^{\frac{1}{2}}}{\Gamma(\frac{1}{4}-\kappa)}M_{\kappa,1/4}(2iv_0)+\frac{\pi^{\frac{1}{2}}}{\Gamma(\frac{3}{4}-\kappa)}M_{\kappa,-1/4}(2iv_0)=0, \quad (84)$$

$$v_0=k\int_0^{h_0}[y(h)-y(h_0)]^{\frac{1}{2}}dh. \quad (85)$$

For a given value of v_0, as determined from the modified refractive index curve $y(h)$, Eq. (84) yields characteristic values (complex) of $\kappa_m=-i\gamma_m/2$, from which Λ_m is then evaluated by Eq. (66). The values of Λ_m thus obtained will be the more accurate the smaller the values of γ_m.

In order to have an estimate of the error to which the values $\gamma_m{}^0$ obtained from Eq. (84) are subject, we derive in section D below a first-order correction term arising from the $w(u)$ term in (71). The result is

$$\gamma_m=\gamma_m{}^0-N(v_0)^{\frac{1}{2}}\frac{d\gamma_m{}^0}{dv_0}, \quad (86)$$

where N is defined in (67), and $d\gamma_m{}^0/dv_0$ is the slope of the $\gamma_m{}^0(v_0)$ curve resulting from (84).

[7] E. T. Whittaker and G. N. Watson, *Modern Analysis* (Cambridge University Press, New York, 1935), p. 339.

Substituting this result in (66) we arrive at an expression for the characteristic values:

$$\Lambda_m=\Lambda_m{}^1+\Delta_m;$$

$$\Lambda_m{}^1=-y(h_0)+\frac{[2\ddot{y}(h_0)]^{\frac{1}{2}}}{k}\gamma_m{}^0-\frac{1}{576c}(7y_3{}^2-9y_4), \tag{87}$$

$$\Delta_m=-\frac{[2\ddot{y}(h_0)]^{\frac{1}{2}}}{k}N(v_0)^{\frac{1}{2}}\frac{d\gamma_m{}^0}{dv_0}. \tag{88}$$

Here, $\gamma_m{}^0$ is to be used for the γ appearing in the expression for N. The term Δ serves not only as an indicator of the order of magnitude of the error in the leading term, but, as will be shown presently, considerably reduces the error when it is not large.

Table II shows how the characteristic values Λ_m computed from (87) compare with the exact values computed by Professor Hartree's associates on the differential analyzer for the case of the exponential model defined in Eq. (55). In this case Eqs. (87) and (88) reduce to

$$\Lambda_m=\Lambda_m{}^1+\Delta_m;$$

$$\Lambda_m{}^1=-(1+\ln\alpha\lambda)/\lambda+(\lambda^2/144)+(2\lambda)^{\frac{1}{2}}\gamma_m{}^0, \tag{89}$$

$$\Delta_m=-(2\lambda v_0)^{\frac{1}{2}}\frac{d\gamma_m{}^0}{dv_0}(.3737\lambda^{3/4}\gamma_m{}^0+.000171\lambda^{9/4}). \tag{90}$$

The quantity v_0 defined in (85) can be obtained from

$$v_0=f(x)/\lambda^{3/2},\quad x=\ln\alpha\lambda,$$
$$f(x)=\int_0^x(e^z-1-z)^{\frac{1}{2}}dz. \tag{91}$$

The universal function $f(x)$ is plotted in Fig. 2. With the aid of this function one can also obtain u and v in (60) and (69) for the purpose of computing the height-gain functions from Eqs. (76) and (83).

A similar comparison is shown in Table III for the "Power law" model defined by

$$y(h)=h-5h^{1/5},\quad k=G^{\frac{1}{2}}. \tag{92}$$

Here

$$h_0=1,\quad v_0=.4591G^{\frac{1}{2}}. \tag{93}$$

$$\Lambda_m=\Lambda_m{}^1+\Delta_m;$$
$$\Lambda_m{}^1=4+.5807\gamma_m{}^0/v_0+.0166/v_0{}^2, \tag{94}$$

$$\Delta_m=-\frac{d\gamma_m{}^0}{dv_0}\left[\frac{.2798\gamma_m{}^0}{v_0}+\frac{.0370}{v_0{}^2}\right]. \tag{95}$$

TABLE II. Comparison of exact characteristic values Λ_m with values obtained from the theory of transitional modes in case of an exponential model. The exact values were computed by Professor Hartree's group on the differential analyzer.

α	λ	Mode No. m	η_0	$\Lambda_m{}^1$ (89)	$\Lambda_m{}^1+\Delta_m$ (90)	Λ_m exact
10	1.2713	1	2.2374	$-2.724+.154i$	$-2.727+.198i$	$-2.72+.187i$
10	.5938	1	3.0694	$-5.038+.019i$	$-5.115+.016i$	$-5.123+.015i$
15	1.5840	1	2.7676	$-2.946+.066i$	$-3.080+.069i$	$-3.10+.05i$
15	.5074	2	5.2285	$-5.893+.097i$	$-5.887+.118i$	$-5.88+.12i$
15	.3024	2	5.8603	$-8.423+.028i$	$-8.440+.029i$	$-8.44+.026i$
20	2.6458	1	2.3234	$-1.830+.193i$	$-1.860+.281i$	$-1.85+.27i$
20	1.7886	1	3.1596	$-3.244+.027i$	$-3.610+.014i$	$-3.74+.008i$
20	.9979	2	4.7989	$-3.704+.228i$	$-3.667+.324i$	$-3.68+.31i$
20	.6357	2	6.3283	$-5.955+.018i$	$-6.066+.016i$	$-6.07+.01i$
20	.6357	3	6.3283	$-4.882+.572i$	$-4.884+.807i$	$-4.95+.77i$
20	.4307	3	7.6663	$-7.071+.171i$	$-7.050+.220i$	$-7.00+.2i$
20	.2969	3	8.6816	$-9.389+.042i$	$-9.394+.048i$	$-9.39+.04i$
20	.1928	3	8.9718	$-12.264+.019i$	$-12.274+.020i$	$-12.27+.02i$

Tables II and III show that the method developed here for computing characteristic values is not only effective for strictly transitional modes but is also applicable over a considerable region extending into the leaky modes on the one side and into the trapped modes on the other side.

Values of $\gamma_m{}^0$ derived from Eq. (84) are shown in Table IV for the first three modes. In computing these, the Γ-functions were obtained from Stirling's asymptotic series[8] after raising the arguments by a few units. The M-functions were computed from the power series (78) for values of v_0 up to 5.5. For larger values of v_0 the following asymptotic expansions were used

$$M_{\kappa,1/4}(z)\rightarrow\frac{\pi^{\frac{1}{2}}z^{-\kappa}e^{z/2}}{2\Gamma(\frac{3}{4}-\kappa)}F\left(\tfrac{3}{4}+\kappa,\ \tfrac{1}{4}+\kappa;\ \frac{1}{z}\right)$$
$$+\frac{\pi^{\frac{1}{2}}z^{\kappa}e^{-z/2}}{2\Gamma(\frac{3}{4}+\kappa)}\exp\left[-i\pi(\kappa-\tfrac{3}{4})\right]$$
$$\times F\left(\tfrac{1}{4}-\kappa,\ \tfrac{3}{4}-\kappa;\ -\frac{1}{z}\right), \tag{96}$$

$$M_{\kappa,-1/4}(z)\rightarrow\frac{\pi^{\frac{1}{2}}z^{-\kappa}e^{-z/2}}{\Gamma(\frac{1}{4}-\kappa)}F\left(\tfrac{1}{4}+\kappa,\ \tfrac{3}{4}+\kappa;\ \frac{1}{z}\right)$$
$$+\frac{\pi^{\frac{1}{2}}z^{\kappa}e^{-z/2}\exp\left[-i\pi(\kappa-\frac{1}{4})\right]}{\Gamma(\frac{1}{4}+\kappa)}$$
$$\times F\left(\tfrac{3}{4}-\kappa,\ \tfrac{1}{4}-\kappa;\ -\frac{1}{z}\right), \tag{97}$$

which are valid when $-\pi/2<\arg z<3\pi/2$. With

[8] Reference 7, p. 251.

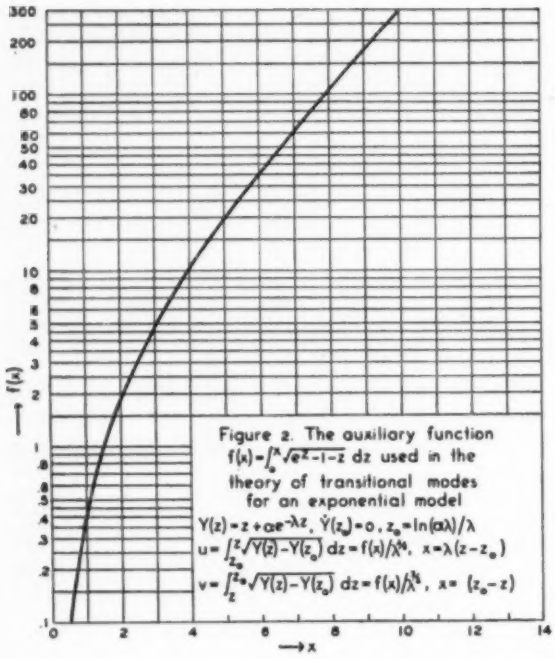
f(x)
x
Figure 2. The auxiliary function f(x) = ∫ √(e^z − 1 − z) dz used in the theory of transitional modes for an exponential model
Y(z) = z + αe^{−λz}, Ẏ(z_0) = 0, z_0 = ln(αλ)/λ
u = ∫ √(Y(z) − Y(z_0)) dz = f(x)/λ^{1/2}, x = λ(z − z_0)
v = ∫ √(Y(z) − Y(z_0)) dz = f(x)/λ^{1/2}, x = (z_0 − z)

FIG. 2.

the aid of these asymptotic series one finds that for large v_0

$$W_m(v)\to C_m\{1-\exp[-F_m(\gamma,v)]\}\times\exp\left[\kappa\ln(2v)+i\left(\frac{\pi}{2}-\frac{3\pi\kappa}{2}-v\right)-\frac{i\kappa(1-\kappa)}{2v}+\cdots\right], \quad (98)$$

where

$$F_m(\gamma,v)=(1+i\gamma)\ln(\tfrac{3}{2}+i\gamma)-\ln(\tfrac{1}{2}+i\gamma)-\gamma\left[\frac{\pi}{2}+i(1+\ln 4+\ln v)\right]+\left[-\frac{3}{2}+i\left(-2v-\frac{\pi}{2}+2m\pi\right)\right]+\frac{1}{(18+i12\gamma)}+\cdots. \quad (99)$$

Equation (84) is, therefore, replaced by $F_m(\gamma, v_0)=0$.

C. Evaluation of the Normalization Factors

For the purpose of evaluating the height-gain functions we need to know the normalization constants C_m in (76) and (83). These constants are determined from the normalization condition

$$1=-\frac{1}{k^2}\frac{\partial U_m(0)}{\partial h}\cdot\frac{\partial U_m(0)}{\partial\Lambda_m}. \quad (10')$$

With $U_m(h)=W_m(v)/[Q(v)]^{\frac{1}{4}}$, $\partial/\partial h=-Q(\partial/\partial v)$, we have

$$\frac{\partial U_m(0)}{\partial h}=-[Q(v_0)]^{\frac{1}{4}}\frac{\partial W_m(v_0)}{\partial v};\qquad \frac{\partial U_m(0)}{\partial\Lambda_m}=\frac{k}{[2\ddot{y}(h_0)]^{\frac{1}{2}}}\frac{1}{[Q(v_0)]^{\frac{1}{4}}}\frac{\partial W_m(v_0)}{\partial\gamma_m}. \quad (100)$$

Substituting in (10′) we get

$$C_m{}^2=\frac{k[2\ddot{y}(h_0)]^{\frac{1}{2}}}{\left[\dfrac{\partial P(\gamma,v_0)}{\partial v}\cdot\dfrac{\partial P(\gamma,v_0)}{\partial\gamma}\right]}, \quad (101)$$

where $P(\gamma, v)$ is defined in (84). Values of $[(\partial P(v_0)/\partial v)\cdot(\partial P(v_0)/\partial\gamma)]$ are shown in Table IV. These were computed by the use of the asymptotic formulae (98) and (99), from which

TABLE III. Comparison of exact characteristic values Λ_m with values obtained from the theory of transitional modes in case of a power law model. The exact values were computed by Professor Hartree's group on the differential analyzer.

$G^{\frac{1}{2}}$	v_0	Mode No. m	$\Lambda_m{}^1$ (94)	$\Lambda_m{}^1+\Delta_m$ (95)	Λ_m exact
10.242	4.701	1	3.841 + 0i	3.791 + 0i	3.749 + 0i
9.126	4.190	1	3.867 + 0i	3.828 + 0i	3.802 + 0i
8.134	3.734	1	3.894 + .0005i	3.866 + 0i	3.851 + .00012i
7.249	3.328	1	3.921 + .0017i	3.902 + .0014i	3.879 + .00107i
6.458	2.964	1	3.948 + .0043i	3.938 + .0041i	3.942 + .0050i
5.758	2.643	1	3.974 + .0102i	3.969 + .0115i	3.978 + .0146i
5.132	2.356	1	4.000 + .0195i	4.001 + .0238i	4.013 + .0304i
4.574	2.100	1	4.027 + .0325i	4.031 + .0415i	4.045 + .0507i
4.077	1.871	1	4.055 + .0521i	4.060 + .068i	4.073 + .076i
3.633	1.668	1	4.084 + .0744i	4.089 + .098i	4.098 + .108i
3.239	1.487	1	4.116 + .101i	4.119 + .135i	4.119 + .150i
2.886	1.325	1	4.147 + .140i	4.143 + .187i	4.140 + .198i
2.572	1.181	1	4.180 + .183i	4.166 + .244i	4.157 + .254i
2.292	1.052	1	4.222 + .232i	4.195 + .310i	4.169 + .316i
16.23	7.450	2	3.932 + 0i	3.914 + 0i	3.907 + 0i
14.46	6.640	2	3.958 + .0008i	3.950 + .0006i	3.949 + .0004i
12.89	5.918	2	3.984 + .0031i	3.981 + .0032i	3.984 + .0031i
11.49	5.275	2	4.007 + .0099i	4.008 + .0120i	4.012 + .0151i
10.24	4.701	2	4.030 + .0221i	4.032 + .0280i	4.035 + .0334i
9.126	4.190	2	4.052 + .0406i	4.054 + .0525i	4.053 + .0600i
8.134	3.734	2	4.076 + .0661i	4.075 + .0862i	4.070 + .0967i
7.249	3.328	2	4.102 + .099i	4.097 + .130i	4.088 + .143i
16.23	7.450	3	4.026 + .017i	4.027 + .022i	4.028 + .025i
14.46	6.640	3	4.047 + .036i	4.048 + .047i	4.044 + .050i

it follows that

$$\frac{\partial P(\gamma, v_0)}{dv} = -2i\left[1+\frac{\gamma}{2v_0}-\frac{\gamma^2}{8v_0^2}\right]\exp\left[\kappa \ln (2v_0) + i\left(\frac{\pi}{2}-\frac{3\pi\kappa}{2}-v_0\right)-\frac{i\kappa(1-\kappa)}{2v_0}\right], \quad (102)$$

$$\frac{\partial P(\gamma, v_0)}{\partial \gamma} = \frac{\partial F_m(\gamma, v_0)}{\partial \gamma}\exp\left[\kappa \ln (2v_0) + i\left(\frac{\pi}{2}-\frac{3\pi\kappa}{2}-v_0\right)-\frac{i\kappa(1-\kappa)}{2v_0}\right], \quad (103)$$

where $F_m(\gamma, v)$ is defined in (99).

D. Perturbation Theory for Transitional Modes

In this section we shall derive the result stated in Eq. (86), namely that the correction to γ_m arising from the neglected $w(u)$ term in (71) is $-N(v_0)^{\frac{1}{2}}d\gamma_m{}^0/dv_0$ to within the first power in N. Actually it is possible to develop a perturbation theory in which N is not assumed to be small, as will be shown presently. Let Eq. (63) and its companion be written as

$$\frac{d^2G}{du^2}+\left[1+\frac{3}{16u^2}+\frac{\gamma}{u}+f(u)\right]G=0, \quad h>h_0 \quad (104)$$

$$\frac{d^2G}{dv^2}+\left[1+\frac{3}{16v^2}+\frac{\gamma}{v}+g(v)\right]G=0, \quad h<h_0 \quad (105)$$

and set

$$G(u)=\sum_{n=1}^{\infty} A_n W_n(u), \quad G(v)=\sum_{n=1}^{\infty} A_n W_n(v), \quad (106)$$

where

$$\frac{d^2W_n(u)}{du^2}+\left[1+\frac{3}{16u^2}+\frac{\gamma_n}{u}\right]W_n(u)=0, \quad (72')$$

$$\frac{d^2W_n(v)}{dv^2}+\left[1+\frac{3}{16v^2}+\frac{\gamma_n}{v}\right]W_n(v)=0. \quad (73')$$

When (106) is substituted in (104) and (105) we get

$$\sum A_n W_n(u)\left[\frac{\gamma-\gamma_n}{u}+f(u)\right]=0, \quad (107)$$

$$\sum A_n W_n(v)\left[\frac{\gamma-\gamma_n}{v}+g(v)\right]=0. \quad (108)$$

TABLE IV. Values of auxiliary functions used in the theory of transitional modes for the determination of characteristic values and normalization factors.

v_0 (85)	Mode No. m	$\gamma_m{}^0$ (84)	$\frac{d\gamma_m{}^0}{dv_0}$ (86)	$\left[\frac{\partial P(v_0)}{dv_0}\cdot\frac{\partial P(v_0)}{d\gamma_m{}^0}\right]$ (102) and (103)
1.0	1	$+.386+.439i$	$-.160-.458i$	$+1.67+1.71i$
1.5	1	$+.276+.255i$	$-.265-.302i$	$2.23+3.34i$
2.0	1	$+.122+.132i$	$-.339-.195i$	$3.88+6.03i$
2.5	1	$-.067+.057i$	$-.409-.110i$	$9.03+10.69i$
3.0	1	$-.290+.0191i$	$-.482-.048i$	$26.1+18.2i$
3.5	1	$-.551+.0047i$	$-.553-.014i$	$85.6+25.3i$
4.0	1	$-.843+.0008i$	$-.610-.003i$	$306.7-4.94i$
4.5	1	$-1.161+.0001i$	$-.651-.0004i$	$1200.-296.i$
5.0	1	$-1.496+.0i$	$-.681-.0i$	$5146.-2074.i$
5.5	1	$-1.845+.0i$	$-.704-.0i$	$24250.-11610.i$
3.0	2	$+.651+.695i$	$-.261-.398i$	$+.868+1.37i$
3.5	2	$+.539+.500i$	$-.229-.356i$	$.781+2.07i$
4.0	2	$+.420+.340i$	$-.244-.284i$	$.986+3.05i$
4.5	2	$+.292+.216i$	$-.269-.215i$	$1.52+4.66i$
5.0	2	$+.149+.124i$	$-.303-.152i$	$3.00+7.34i$
5.5	2	$-.013+.062i$	$-.343-.097i$	$7.06+11.87i$
6.0	2	$-.203+.025i$	$-.395-.050i$	$18.5+20.2i$
6.5	2	$-.413+.012i$	$-.447-.021i$	$54.3+31.0i$
7.0	2	$-.649+.002i$	$-.496-.006i$	$159.3+39.6i$
7.5	2	$-.907+.0005i$	$-.535-.001i$	$503.-3.9i$
8.0	2	$-1.183+.0i$	$-.567-.0i$	$1677.-336.i$
6.0	3	$+.695+.613i$	$-.244-.330i$	$+.426+1.80i$
6.5	3	$+.566+.453i$	$-.248-.291i$	$.360+2.44i$
7.0	3	$+.442+.319i$	$-.251-.243i$	$.499+3.42i$
7.5	3	$+.314+.211i$	$-.261-.192i$	$.952+5.01i$
8.0	3	$+.179+.131i$	$-.283-.141i$	$2.27+7.59i$
8.5	3	$+.033+.070i$	$-.312-.096i$	$5.44+11.6i$
9.0	3	$-.136+.029i$	$-.351-.056i$	$13.4+18.7i$
9.5	3	$-.322+.012i$	$-.393-.026i$	$37.0+29.3i$
10.0	3	$-.528+.005i$	$-.435-.010i$	$102.+40.2i$
10.5	3	$-.757+.001i$	$-.473-.003i$	$287.+37.6i$
11.0	3	$-1.00+.0i$	$-.503-.001i$	$839.-70.i$

Upon multiplying (107) by $W_m(u)$ and integrating from 0 to ∞, also upon multiplying (108) by $W_m(v)$ and integrating from 0 to v_0, and then adding the results we get

$$\sum A_n\beta_{nm}=0, \quad (109)$$

$$\beta_{nm}=(\gamma-\gamma_n)\left[\int_0^{\infty} W_n(u)W_m(u)\frac{du}{u}+\int_0^{v_0} W_n(v)W_m(v)\frac{dv}{v}\right]+\left[\int_0^{\infty} W_n(u)W_m(u)f(u)du+\int_0^{v_0} W_n(v)W_m(v)g(v)dv\right]. \quad (110)$$

Since the consistency condition for (109) requires that $|\beta_{nm}|=0$, we have here a secular equation for the determination of γ, provided we can evaluate the elements β_{nm}. This can be accomplished for the case

$$f(u)=N/u^{\frac{1}{2}}, \quad g(v)=-N/v^{\frac{1}{2}}, \quad (111)$$

where it is found that

$$\beta_{nm}=(\gamma-\gamma_n)\dot{W}_n W_n'\delta_{nm}-N(v_0)^{\frac{1}{2}}\dot{W}_n\dot{W}_m/[1+(\gamma_n-\gamma_m)^2], \quad (112)$$

$$\dot{W}_n\equiv\frac{\partial W_n(v_0)}{\partial v}, \quad W_n'\equiv\frac{\partial W_n(v_0)}{\partial\gamma},$$

$$\dot{W}_n/W_n'=-\frac{d\gamma}{dv}. \quad (113)$$

In a first-order perturbation theory the vanishing of β_{nm} yields Eq. (86).

The detailed derivation of (112) is rather lengthy, and we shall therefore limit ourselves here to an outline of the proof. To begin with it follows from (72′) and (73′) that

$$(\dot{W}_n W_m-W_n\dot{W}_m)_{u=0}=(\gamma_n-\gamma_m)\int_0^\infty W_n(u)W_m(u)\frac{du}{u}, \quad (114)$$

$$(\dot{W}_n W_m-W_n\dot{W}_m)\Big|_{v=0}^{v=v_0}=(\gamma_n-\gamma_m)\int_0^{v_0} W_n(v)W_m(v)\frac{dv}{v}. \quad (115)$$

Also, it can be shown from (76), (77), and (83) that

$$[\dot{W}_n(v)W_m(v)-W_n(v)\dot{W}_m(v)]_{v=0}=2i\pi C_nC_m\left[\frac{1}{\Gamma(\frac{1}{4}-\kappa_n)\Gamma(\frac{3}{4}-\kappa_m)}-\frac{1}{\Gamma(\frac{1}{4}-\kappa_m)\Gamma(\frac{3}{4}-\kappa_n)}\right]=-[\dot{W}_n(u)W_m(u)-W_n(u)\dot{W}_m(u)]_{u=0}. \quad (116)$$

Since $W_n(v_0)=W_m(v_0)=0$, it follows that

$$\alpha_{nm}\equiv\int_0^{v_0} W_n(v)W_m(v)\frac{dv}{v}+\int_0^\infty W_n(u)W_m(u)\frac{du}{u}=0, \quad n\neq m. \quad (117)$$

In order to obtain the value of α_{mm} we pass to the limit of $n\to m$ in the relation

$$(\gamma_n-\gamma_m)\alpha_{nm}=-(\dot{W}_nW_m-W_n\dot{W}_m)_{v=v_0}, \quad (118)$$

which follows from adding (114) and (115), and using (116). The result is

$$\alpha_{mm}=\int_0^{v_0} W_m^2(v)\frac{dv}{v}+\int_0^\infty W_m^2(u)\frac{du}{u}=\dot{W}_m\cdot W_m'. \quad (119)$$

There remains now the task of evaluating

$$\tau_{nm}=\int_0^\infty W_n(u)W_m(u)\frac{du}{u^{\frac{1}{2}}}-\int_0^{v_0} W_n(v)W_m(v)\frac{dv}{v^{\frac{1}{2}}}. \quad (120)$$

This expression involves integrals over the product $F_{nm}(u)$ of the functions $W_n(u)$ and $W_m(u)$

$$F_{nm}(u)\equiv W_n(u)W_m(u), \quad (121)$$

each of which satisfies a linear differential equation of the second order (72′). From the general theory of the products of solutions of linear differential equations of the second order[9] it follows that

$$u\left(\frac{d^4F}{du^4}\right)+\frac{d^3F}{du^3}+\left[4u+\frac{3}{4u}+2(\gamma_n+\gamma_m)\right]\left(\frac{d^2F}{du^2}\right)+\left[4-\frac{3}{2u^2}-\frac{(\gamma_n+\gamma_m)}{u}\right]\dot{F}+\left[\frac{3}{2u^3}+\frac{(\gamma_n+\gamma_m)}{u^2}+\frac{(\gamma_n-\gamma_m)^2}{u}\right]F=0, \quad (122)$$

where we have written F for F_{nm}. This equation yields the useful relation

$$\frac{d}{du}\left\{u^{\frac{1}{2}}\left(u\frac{d^3F}{du^3}-\frac{1}{2}\cdot\frac{d^2F}{du^2}+\left[4u+\frac{1}{u}+2(\gamma_n+\gamma_m)\right]\dot{F}+\left[-2-\frac{1}{u^2}-\frac{2}{u}(\gamma_n+\gamma_m)\right]F\right)\right\}=-[1+(\gamma_n-\gamma_m)^2]\frac{F}{u^{\frac{1}{2}}}, \quad (123)$$

[9] G. N. Watson, *Theory of Bessel Functions* (The Macmillan Company, New York, 1944), p. 146.

or

$$\frac{d}{du}\left\{u^{\frac{1}{2}}\left(-\left[1+\frac{1}{16u^2}+\frac{(\gamma_n+\gamma_m)}{2u}\right]W_nW_m+\left[\frac{1}{4u}+\gamma_n+\gamma_m\right](\dot{W}_nW_m+W_n\dot{W}_m)\right.\right.$$

$$\left.\left.-2\gamma_nW_n\dot{W}_m-2\gamma_nW_m\dot{W}_n-\dot{W}_n\dot{W}_m\right)\right\}=-[1+(\gamma_n-\gamma_m)^2]W_nW_m/u^{\frac{1}{2}}. \quad (124)$$

Using (124) and the defining Eqs. (76), (77), and (83) we now deduce that

$$\int_0^\infty W_n(u)W_m(u)\frac{du}{u^{\frac{1}{2}}}=\frac{-[B_nB_m+2(\gamma_n+\gamma_m)A_nA_m]}{4[1+(\gamma_n-\gamma_m)^2]}, \quad (125)$$

$$\int_0^\infty W_n(v)W_m(v)\frac{dv}{v^{\frac{1}{2}}}=\frac{\{-[B_nB_m+2(\gamma_n+\gamma_m)A_nA_m]+4(v_0)^{\frac{1}{2}}\dot{W}_n(v_0)\dot{W}_m(v_0)\}}{4[1+(\gamma_n-\gamma_m)^2]}, \quad (126)$$

$$A_n\equiv\frac{\pi^{\frac{1}{2}}2^{1/4}e^{i\pi/8}C_n}{\Gamma(\frac{3}{4}-\kappa_n)}, \quad B_n\equiv\frac{2(\pi)^{\frac{1}{2}}2^{3/4}e^{i3\pi/8}C_n}{\Gamma(\frac{1}{4}-\kappa_n)}. \quad (127)$$

Adding (125) and (126) we finally get

$$\tau_{nm}=\int_0^\infty W_n(u)W_m(u)\frac{du}{u^{\frac{1}{2}}}-\int_0^{v_0} W_n(v)W_m(v)\frac{dv}{v^{\frac{1}{2}}}=-\frac{(v_0)^{\frac{1}{2}}\dot{W}_n(v_0)\dot{W}_m(v_0)}{[1+(\gamma_n-\gamma_m)^2]}. \quad (128)$$

This completes the proof of Eq. (112), and with it of Eq. (86). Values of $d\gamma_m{}^0/dv_0$ are shown in Table IV.

5. ASYMPTOTIC SOLUTIONS FOR TRAPPED MODES

So far we have treated the asymptotic solutions for leaky modes and transitional modes, and have found that the formula derived for the characteristic values of transitional modes can be used with sufficient accuracy over a region extending into the leaky modes on one side and into the trapped modes on the other side. There remains now the treatment of completely trapped modes. The asymptotic theory of these modes has been developed by Furry[4] along the lines of Gamow's treatment of the problem of radioactive decay in wave mechanics. Furry follows the technique of the W.K.B. method in which the height-gain functions are given different (asymptotic) representations in each of three regions of height, and the characteristic values are determined from Jeffreys'[10] "connecting formulae." This method does not supply height-gain functions in two isolated regions centered around the two turning points. The principal aim of this section is to fill in these gaps by developing the theory *ab initio* along Langer's method,[5] in which the difficulty with the Stokes phenomena is completely obviated. The expression for the characteristic value we arrive at is, in the limiting case of completely trapped modes treated, identical with Furry's result. However, the method developed here can be applied also to cases of incomplete trapping when Furry's formula becomes inaccurate. The latter extension is reserved for another occasion.

Referring to Fig. 1, a trapped mode of order m is characterized by the condition that

$$F(h_0)=k\int_0^{h_0}[y(h)-y(h_0)]^{\frac{1}{2}}dh$$

$$>v_m\simeq\pi(m-\tfrac{1}{4}). \quad (129)$$

The quantity in brackets in the differential equation

$$\frac{d^2U_m(h)}{dh^2}+k^2[\Lambda_m+y(h)]U_m(h)=0 \quad (130)$$

vanishes at *two* turning points which, though complex, are extremely close to the real values

[10] H. Jeffreys, Proc. Lond. Math. Soc. [2] **23**, 428 (1923); Phil. Mag. **33**, 451 (1943).

h_1 and h_2 shown in the figure. We shall use different representations of $U_m(h)$ in the regions I($h<h_0$) and II($h>h_0$). In region I let

$$u_1(h)=k\int_{h_1}^{h}[y(h)+\Lambda_m]^{1/2}dh$$

$$=e^{i\pi}k\int_{h}^{h_1}[y(h)+\Lambda_m]^{1/2}dh, \quad 0<h<h_1, \quad (131)$$

$$u_1(h)=e^{-i\pi/2}k\int_{h_1}^{h}[-y(h)-\Lambda_m]^{1/2}dh,$$

$$h_1<h<h_0. \quad (132)$$

Here h_1 is strictly speaking a complex number which is the root of $[y(h_1)+\Lambda_m]$, but since the integrand vanishes in the neighborhood of h_1, and Imh_1 is small, we may replace the lower limit by Reh_1; the same holds for h_2 below. In Langer's theory the leading term in the asymptotic expansion of (130) is according to Eqs. (12), (14), (16), and (20), given by

$$U_m^{\mathrm{I}}(h)=\frac{AF^{(1)}(u_1)}{[y(h)+\Lambda_m]^{1/4}}+\frac{BF^{(2)}(u_1)}{[y(h)+\Lambda_m]^{1/4}}, \quad (133)$$

where

$$F^{(1)}(u_1)\equiv(u_1)^{1/2}H_{1/3}^{(1)}(u_1),$$
$$F^{(2)}(u_1)\equiv(u_1)^{1/2}H_{1/3}^{(2)}(u_1). \quad (134)$$

The constants A and B are subject to the boundary conditions $U_m(0)=0$, from which it follows that

$$U_m^{\mathrm{I}}(h)=\frac{C_m}{[y(h)+\Lambda_m]^{1/4}}[H_{1/3}^{(2)}(u_0)F^{(1)}(u_1)$$

$$-H_{1/3}^{(1)}(u_0)F^{(2)}(u_1)]; \quad u_0\equiv u_1(0). \quad (135)$$

In region II let

$$u_2(h)=k\int_{h_2}^{h}[y(h)+\Lambda_m]^{1/2}dh, \quad h>h_2, \quad (136)$$

$$u_2(h)=e^{-i3\pi/2}k\int_{h}^{h_2}[-y(h)-\Lambda_m]^{1/2}dh,$$

$$h_0<h<h_2, \quad (137)$$

then a solution which represents an outgoing wave at great heights is

$$U_m^{\mathrm{II}}(h)=\frac{E_mF^{(2)}(u_2)}{[y(h)+\Lambda_m]^{1/4}}. \quad (138)$$

The relation between E_m and C_m, and the value of Λ_m are determined from the required continuity of $U_m(h)$ and of $[dU_m(h)/dh]$ at $h=h_0$. The equation determining Λ_m is

$$\frac{1}{U_m^{\mathrm{I}}(h_0)}\frac{dU_m^{\mathrm{I}}(h_0)}{dh}=\frac{1}{U_m^{\mathrm{II}}(h_0)}\frac{dU_m^{\mathrm{II}}(h_0)}{dh}, \quad (139)$$

or

$$\frac{H_{1/3}^{(2)}(u_0)}{H_{1/3}^{(1)}(u_0)}=\frac{[F^{(2)}(u_2)F^{(2)}(u_1)-F^{(2)}(u_2)F^{(2)}(u_1)]}{[F^{(2)}(u_2)\dot{F}^{(1)}(u_1)-\dot{F}^{(2)}(u_2)F^{(1)}(u_1)]}, \quad (140)$$

where now

$$u_1=u_1(h_0)=e^{-i\pi/2}k\int_{h_1}^{h_2}[-y(h)-\Lambda_m]^{1/2}dh;$$
$$u_2=u_2(h_0)=e^{-i3\pi/2}k\int_{h_0}^{h_2}[-y(h)-\Lambda_m]^{1/2}dh. \quad (141)$$

Equation (140) serves to determine Λ_m, no matter what the magnitude of the arguments of the functions H and F may be, the only restriction being that the quantity A defined in (17) shall be small at both turning points so as to assure that the leading term in (20) is a sufficient approximation to $G(u)$. We shall however limit the discussion here to the case of highly trapped modes when the arguments of the functions in (140) are found to be large, thus allowing their representation by asymptotic expressions. In view of the phases of the u's given in (141) the

appropriate asymptotic expressions are

$$F^{(2)}(u_1)\rightarrow\left(\frac{2}{\pi}\right)^{\frac{1}{2}}\exp\left[i\left(-u_1+\frac{5\pi}{12}\right)\right]P(u_1),$$
$$-2\pi<\arg u_1<\pi, \quad (142)$$

$$\dot{F}^{(2)}(u_1)\rightarrow-i\left(\frac{2}{\pi}\right)^{\frac{1}{2}}\exp\left[i\left(-u_1+\frac{5\pi}{12}\right)\right]Q(u_1),$$
$$-2\pi<\arg u_1<\pi, \quad (143)$$

$$F^{(1)}(u_1)\rightarrow\left(\frac{2}{\pi}\right)^{\frac{1}{2}}\exp\left[i\left(u_1-\frac{5\pi}{12}\right)\right]\bar{P}(u_1),$$
$$-\pi<\arg u_1<2\pi, \quad (144)$$

$$\dot{F}^{(1)}(u_1)\rightarrow i\left(\frac{2}{\pi}\right)^{\frac{1}{2}}\exp\left[i\left(u_1-\frac{5\pi}{12}\right)\right]\bar{Q}(u_1),$$
$$-\pi<\arg u_1<2\pi, \quad (145)$$

$$F^{(2)}(u_2)\rightarrow\left(\frac{2}{\pi}\right)^{\frac{1}{2}}\left[\exp\left[i\left(-u_2+\frac{5\pi}{12}\right)\right]P(u_2)+\tfrac{1}{2}\exp\left[i\left(u_2-\frac{\pi}{12}\right)\right]\bar{P}(u_2)\right],^{*}$$
$$-3\pi<\arg u_2<\pi, \quad (146)$$

$$\dot{F}^{(2)}(u_2)\rightarrow-i\left(\frac{2}{\pi}\right)^{\frac{1}{2}}\left[\exp\left[i\left(-u_2+\frac{5\pi}{12}\right)\right]Q(u_2)-\tfrac{1}{2}\exp\left[i\left(u_2-\frac{\pi}{12}\right)\right]\bar{Q}(u_2)\right],$$
$$-3\pi<\arg u_2<\pi, \quad (147)$$

where

$$P(x)\equiv1+\frac{5i}{72x}-\frac{385}{10368x^2}+\cdots, \quad (148)$$

$$Q(x)=1+\frac{5i}{72x}+\frac{335}{10368x^2}+\cdots$$
$$=P(x)+i\dot{P}(x), \quad (149)$$

and the bar denotes the complex conjugate function. Using these expressions we find that

$$\frac{[F^{(2)}(u_2)\dot{F}^{(2)}(u_1)-\dot{F}^{(2)}(u_2)F^{(2)}(u_1)]}{[F^{(2)}(u_2)\dot{F}^{(1)}(u_1)-\dot{F}^{(2)}(u_2)F^{(1)}(u_1)]}\rightarrow\epsilon,$$
$$\epsilon=\tfrac{1}{2}\exp\left[i\left(-2u_1+\frac{5\pi}{6}\right)\right][P(u_1)Q(u_2)-P(u_2)Q(u_1)]-\tfrac{1}{4}\exp\left[i\left(2u_2-2u_1+\frac{\pi}{3}\right)\right]$$
$$\times[\bar{P}(u_2)Q(u_1)+\bar{Q}(u_2)P(u_1)]. \quad (150)$$

Here, the second term is of lower order of magnitude than the first, but it has been included because it alone contributes to the *imaginary part* of Λ_m, whereas the first term though larger, merely introduces a small change in the real part of Λ_m.

With regard to the left-hand member of Eq. (140) we set

$$u_0=e^{i\pi k}\int_0^{h_1}[\gamma(h)+\Lambda_m]dh=e^{i\pi v_m}+\Delta, \quad (151)$$

where v_m is a root of Eq. (22′). Assuming that Δ is small in the case of completely trapped modes we find from (140):

$$\frac{H_{1/3}^{(2)}(u_0)}{H_{1/3}^{(1)}(u_0)}\simeq\frac{e^{i\pi/6}\Delta}{\pi v_m J_{1/3}^2(v_m)}=\epsilon, \quad (152)$$

$$\Delta=-\tfrac{1}{2}\pi v_m J_{1/3}^2(v_m)\exp(-i2u_1]\times[P(u_1)Q(u_2)-P(u_2)Q(u_1)]-\tfrac{1}{4}\pi v_m J_{1/3}^2(v_m)\exp\left[i\left(2u_2-2u_1+\frac{\pi}{2}\right)\right]$$
$$\times[\bar{P}(u_2)Q(u_1)+\bar{Q}(u_2)P(u_1)]. \quad (153)$$

Since Λ_m is to a high approximation a purely real number, Eq. (141) shows that u_1 and u_2 are purely imaginary (negative and positive, respectively) numbers. From this fact it follows that the expressions in brackets in (153) are both real, the latter being approximately equal to 2. Hence

$$Im(\Delta)=-\frac{\pi}{2}v_m J_{1/3}^2(v_m)\exp[i(2u_2-2u_1)]$$
$$=-\frac{\pi}{2}v_m J_{1/3}^2(v_m)e^{-2\tau}, \quad (154)$$

$$\tau=k\int_{h_1}^{h_2}[-\gamma(h)-\Lambda_m]^{\frac{1}{2}}dh. \quad (155)$$

* The factor $\frac{1}{2}$ appearing in the brackets of (146) and (147) was introduced by Dr. W. F. Eberlein as leading to the correct Gamow formula. In textbooks two alternative formulae are given, with this factor having either a value of 1 or 0.

In order to determine Λ_m we write

$$\Lambda_m = \Lambda_m{}^0 + i\delta \tag{156}$$

and obtain from (151)

$$k\int_0^{h_1}[y(h)+\Lambda_m]^{\frac{1}{2}}dh = k\int_0^{h_1}[y(h)+\Lambda_m{}^0]^{\frac{1}{2}}dh + \tfrac{1}{2}k\delta\theta i = v_m - \Delta, \tag{157}$$

$$k\int_0^{h_1}[y(h)+\Lambda_m{}^0]^{\frac{1}{2}}dh = v_m - Re(\Delta), \tag{158}$$

$$\delta = -\frac{2Im(\Delta)}{k\theta} = \frac{\pi v_m J_{1/3}(v_m)e^{-2\tau}}{k\theta} \simeq \frac{e^{-2\tau}}{2k\theta}; \qquad \theta = \int_0^{h_1}\frac{dh}{[y(h)+\Lambda_m{}^0]^{\frac{1}{2}}}. \tag{159}$$

The last expression agrees with Furry's result obtained by the W.K.B. method.

Here we shall point out that although in the matter of the determination of characteristic values we have so far merely shown that our method leads to results agreeing with those obtained by the W.K.B. method for the limiting case of highly trapped modes, expression (140) can actually be used also to determine characteristic values for modes which are only moderately trapped by applying a technique developed by the writer for the bilinear model. These developments will, however, be reported in another communication.

The derivation of the height-gain functions as well as of the normalization factors can be carried out in the manner shown in previous sections. We shall therefore limit ourselves here to a statement of results for the case of *highly trapped modes:*

1. $0 \le h \le h_1$.

$$x = \int_h^{h_1}[y(h)+\Lambda_m{}^0]^{\frac{1}{2}}dh, \qquad U_m(h) = \frac{x^{\frac{1}{2}}[J_{1/3}(x)+J_{-1/3}(x)]}{(u_m\theta)^{\frac{1}{2}}[y(h)+\Lambda_m{}^0]^{1/4}}. \tag{160}$$

2. $h_1 \le h \le h_0$.

$$y = k\int_{h_1}^{h}[-y(h)-\Lambda_m{}^0]^{\frac{1}{2}}dh, \qquad U_m(h) = \frac{y^{\frac{1}{2}}[I_{-1/3}(y)-I_{1/3}(y)]}{[u_m\theta]^{\frac{1}{2}}[-y(h)-\Lambda_m{}^0]^{1/4}}. \tag{161}$$

3. $h_0 \le h \le h_2$.

$$y_0 = k\int_{h_1}^{h_0}[-y(h)-\Lambda_m{}^0]^{\frac{1}{2}}dh, \qquad w_0 = k\int_{h_0}^{h_2}[-y(h)-\Lambda_m{}^0]^{\frac{1}{2}}dh, \qquad w = k\int_{h}^{h_2}[-y(h)-\Lambda_m{}^0]^{\frac{1}{2}}dh,$$

$$U_m(h) = U_m(h_0)\left[\frac{-y(h_0)-\Lambda_m{}^0}{-y(h)-\Lambda_m{}^0}\right]^{1/4} \times \frac{w^{\frac{1}{2}}[I_{1/3}(w)+e^{-i\pi/3}I_{-1/3}(w)]}{(w_0)^{\frac{1}{2}}[I_{1/3}(w_0)+e^{-i\pi/3}I_{-1/3}(w_0)]}. \tag{162}$$

4. $h \ge h_2$.

$$v = k\int_{h_2}^{h}[y(h)+\Lambda_m{}^0]^{\frac{1}{2}}dh,$$

$$U_m(h) = U_m(h_0)\left[\frac{-y(h_0)-\Lambda_m{}^0}{-y(h)-\Lambda_m{}^0}\right]^{1/4} \times \frac{v^{\frac{1}{2}}[-J_{1/3}(v)+e^{-i\pi/3}J_{-1/3}(v)]}{w^{\frac{1}{2}}[I_{1/3}(w_0)+e^{-i\pi/3}I_{-1/3}(w_0)]}. \tag{163}$$

Here, $u_m(\simeq 3/\pi)$ is defined in Eq. (34).

We note that Eq. (160) yields

$$\frac{dU_m(0)}{dh} = k\left(\frac{2}{\theta}\right)^{\frac{1}{2}}[y(0)+\Lambda_m{}^0]^{1/4}, \tag{164}$$

which agrees formally with Eq. (36) for the case of leaky modes.

Letters to the Editor

Concerning "Computer for Solving Linear Simultaneous Equations"

C. C. EAGLESFIELD
The Mullard Radio Valve Company, Ltd., Bournemouth, England

I HAVE read with great interest the paper by Berry, Wilcox, Rock, and Washburn[1] describing a computer for solving simultaneous equations.

I notice that the operation of this machine follows the classical method (named by Southwell the "relaxation method") of satisfying each equation in turn until a desired degree of approximation is reached.

I am wondering whether the authors considered a somewhat different method, hardly suited to arithmetical computation, but well suited to an electrical computer.

If the equations to be solved are

$$a_{11}x_1+a_{12}x_2+\cdots+m_1=0,$$
$$a_{21}x_1+a_{22}x_2+\cdots+m_2=0,$$
$$\text{etc.},$$

and if for arbitrary values of the variables x_1, x_2, etc.

$$a_{11}x_1+a_{12}x_2+\cdots+m_1=d_1,$$
$$a_{21}x_1+a_{22}x_2+\cdots+m_2=d_2,$$
$$\text{etc.}$$

Then of course the solution can be obtained by modifying x_1, etc., so that $d_1=d_2=\cdots=0$; the usual way of doing this is by adjusting x_1 until $d_1=0$, then adjusting x_2 until $d_2=0$, and so on.

The method I have in mind is to adjust x_1 until Σd^2 is reduced to a minimum, then adjust x_2 until Σd^2 is reduced to a (lower) minimum, and so on until a sufficient approximation is reached.

It is almost self-evident that this method is convergent, and very probable that it is more rapidly convergent than the line-by-line method. The latter is by no means always convergent, and in any case careful preparation of the relative size of the coefficients and the order of the equations is necessary. This preparation would not be necessary with the method I am suggesting.

In the machine described d_1, etc., are obtained as a.c. voltages, so that it is a simple matter to get an indicating instrument responding to Σd^2 by applying each d to a separate square law rectifier and adding the rectified currents.

From the point of view of the practical operation of the computer, it is evident that other types of rectifier could conveniently be substituted for the square law rectifiers. The essential thing would seem to be that the indication should be independent of the signs of the d's, and should be weighted in favor of the large d's. Thus "average" rectifiers would seem to be quite suitable.

Another interesting possibility is to use "peak" rectifiers. If each d is applied to the anode of a separate diode and, the cathodes being strapped, the circuit is completed by a single capacitance, then the capacitance will be charged to the peak value of the largest d. An indicator of this type would thus respond to the d which was numerically largest, instead of to a summation of the d's.

The peak rectifier is probably the most convenient practically, followed by the average rectifier and the square law rectifier in that order.

While it is doubtful whether convergence could be formally proved for any but the square law rectifier, it seems very probable that both the average and the peak rectifier would give converging results.

The substitution of the over-all balance for the line-by-line balance modifies the design of the computer considerably, of course, but I do not think it brings in any great problems. It should give a computer which is easier and quicker to use, particularly with sets of equations which converge slowly, if at all, on the line-by-line computer.

July 24, 1946 (received July 29)

Thank you for allowing me to read the interesting letter from Mr. C. C. Eaglesfield.

Several months ago Dr. W. M. Bleakney of Lockheed Aircraft Corporation suggested use of the same mathematical method to me in a private communication. In fairness to Dr. Bleakney I should like to see a statement of this appear at the same time as the letter from Mr. Eaglesfield.

Clifford E. Berry
Consolidated Engineering Corporation
Pasadena, California

[1] J. App. Phys. **17**, 262 (1946).

Preparing Pigments for the Electron Microscope

A. M. CRAVATH
Shell Development Company, Emeryville, California
September 16, 1946

ONE of the most satisfactory methods of preparing pigments for electron microscopy does not seem to have been reported. It is an adaptation of the well-known Green's method used in light microscopy. It produces better dispersions than the other methods tried by the author and is convenient and rapid. Its greatest advantage, however, in comparison with other methods in which the pigment is dispersed in the film forming solution is that it does not impair the definition. Presumably this is caused by the film being attached to the particle at a spot in the shadow instead of around the periphery as it is when cast on water.

The technique is not critical and is easily modified to suit the particular problem. One version is as follows:

Place 1 mm³ of the pigment on a microscope slide. Add two drops of 4 percent parlodion in 70 percent amyl acetate plus 30 percent diisobutyl ketone. Rub smooth with a narrow spatula (made by filing and polishing ¼" drill rod) which has a blade with slightly elliptical instead of rectangular cross section and therefore rubs over the sample instead of scraping it up. The slowness of evaporation of the diisobutyl ketone prolongs the period during which the mixture is highly viscous. Violent rubbing during this period is a very convenient way to concentrate a large amount of work on a small amount of material and thoroughly break up agglomerates if they are not too strongly cemented. If this viscous shearing work is too mild, a $\frac{3}{16}$" glass rod instead of a spatula may be used. Rolling and rubbing the rod over the very small sample in the early fluid stage breaks up the hard lumps more completely and conveniently than use of a muller, for lumps are more often missed by the point contact of the muller than by the line contact of the rod. When the paste is nearly dry add four drops of butyl acetate and mix thoroughly until half of the solvent has evaporated. Touch the wet spatula or rod crosswise to a clean microscope slide 1 cm from the end. Place the dry part of the rod across the slide between the wet stripe and the end and with one quick light stroke smear the liquid along the slide. Agglomerates which may have reformed since the mixing are broken up by the violent shearing as the thin layer is spread out and they have no chance to reform because the film dries so rapidly. When the film is dry breathe on it and float it off on distilled water. The thickness will not be uniform. Place the specimen screens where the thickness appears to be correct.

Specimens in which the sample is not incorporated within the film may be prepared by a slight modification of the method. The sample is mixed in a volatile nonsolvent and smeared over a slide previously coated with film by dipping in ¼ percent parlodion solution and drying. However, no advantages have been observed to justify this more difficult procedure.

Coordination Number in Solid Solutions—A Mathematical Paradox

DOUGLAS RENNIE HUDSON
University of Leeds, Leeds, England
July 24, 1946

DURING the last ten years the application of statistical methods to the theory of solubility has proceeded apace, and striking progress has been made, especially in Britain. To apply these theoretically interesting results usually requires a knowledge of the *number* of A molecules surrounding a dissolved B molecule of different size or shape.

In investigating the number of metal atoms X surrounding another metal atom Y in solid solution, the simplest possible model is usually set up in which both

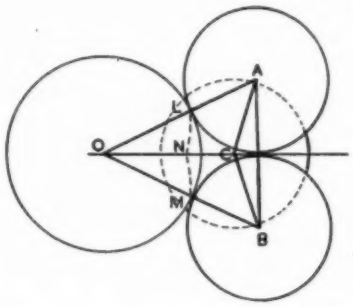

FIG. 1.

are assumed to be rigid spheres differing in diameter. In the course of calculation the following paradox has been discovered which may interest x-ray crystallographers and physicists generally.

If three spheres of radius r (atom X) with centers at A, B, C, are in contact with one another and with a large sphere of radius R (atom Y) with center at 0, ABC is a plane equilateral triangle of side $2r$. Similarly the corresponding points of contact of the outer spheres with the kernel sphere, at L, M, N, form an equilateral spherical triangle on the surface of the latter. (Fig. 1.)

If now the radius of the larger sphere shrinks to r, with suitable accommodation of the smaller spheres, the lengths OA, OB, OC, will shrink to $2r$ from $(R+r)$, giving four equal spheres in contact.

Then each side of the spherical triangle LMN will subtend an angle of 60° at the center 0, or in mathematical notation each *side* of the triangle, LM, MN, or NL, is 60° or $\pi/3$. Then by the formula

$$\sin\left(\frac{\theta}{2}\right)=\tfrac{1}{2}\sec\left(\frac{\text{side } LM}{2}\right)=\frac{1.15470}{2}=.57735,$$

whence θ, the spherical angle, is found to be 70° 31.8′, at L, M, and N. Since the spherical triangle LMN is equilateral, the spherical excess is $3\times(70°\ 31.8')-180°$, or 31° 35.4′, or .55141 radians, and the area of the spherical triangle is $.55141r^2$. Now the total surface of the sphere is $4\pi r^2$ and if this be divided by $.55141r^2$ the total number of such triangles which can be inscribed on the surface would appear to be $(4\pi r^2/.55141r^2)=22.8$. But it is well known that in close packing, whether hexagonal or cubic, the number of spheres surrounding a given sphere is 12. Explanation of the paradox may entertain geometers and afford a half-hour's amusement to readers of mathematical bent.

Note on a Paper of H. Bateman

F. W. J. Olver
Mathematics Division, National Physical Laboratory, Teddington, England
September 30, 1946

In a paper[1] entitled "Some Integral Equations of Potential Theory" the late Professor Bateman includes a table of $P_n(1-2e^{-t})$ to 15D for $n=1(1)10$, $t=1(1)20$. A number of errors were noticed in this table and subsequent investigation showed the need for complete recomputation. This has been done and the new table, in which the values given are correct to within 0.52 units of the 15th decimal, is appended.

Attention is also drawn to the erroneous value given[2] for $P_4(\mu)$ where $\mu=1-2e^{-\pi}$; the last four decimals given should read $\cdots$ 7662 instead of $\cdots$ 5162.

[1] J. App. Phys. 17, 91–102 (1946).
[2] Reference 1, p. 99.

$P_n(1-2e^{-t})$

n / t	1	2	3	4	5
1	+ 0·26424 11176 57115	0·39526 49476 08978	− 0·35023 61643 16206	+ 0·13449 18185 76736	0·34115 78146 74563
2	0·72932 94335 26775	| + 0·29788 21339 12729	| | + 0·12412 92757 10654	| + 0·38164 10855 26292	0·40197 48761 18927
3	0·90042 58632 64272	0·71615 01028 52814	0·47444 95488 03890	0·21049 99508 35291	0·03838 98178 26693
4	0·96336 87222 22532	0·89211 89424 35010	0·79015 33279 25199	0·66302 65464 69307	0·51760 76040 28999
5	0·98852 41060 01829	0·95984 47175 84062	0·92050 05158 57439	0·86928 43716 52798	0·80722 55650 05097
6	0·99504 24956 46667	0·98516 45522 14122	0·97043 89956 51009	0·95097 58060 23902	0·92691 92142 65318
7	0·99817 62360 68891	0·99453 36973 78988	0·98908 23471 09798	0·98163 70921 66184	0·97281 77376 76441
8	0·99932 90747 44195	0·99798 78994 43633	0·99597 78237 65385	0·99330 00703 23373	0·98995 97324 16840
9	0·99975 31803 91827	0·99925 96325 55358	0·99851 95392 12762	0·99753 31743 53326	0·99630 09031 20756
10	0·99990 92001 40475	0·99972 76127 88347	0·99945 52626 75587	0·99909 21868 95476	0·99863 84348 96986
11	0·99996 65965 98420	0·99989 97914 68939	0·99979 95879 58828	0·99966 59910 86756	0·99949 90075 52514
12	0·99998 77115 75293	0·99996 31349 52388	0·99992 62705 84296	0·99987 71191 50522	0·99981 56815 57053
13	0·99999 54793 41186	0·99998 64380 54213	0·99997 28762 00389	0·99995 47938 71677	0·99993 21911 90693
14	0·99999 83369 42562	0·99999 50108 31834	0·99999 00216 76114	0·99998 33694 87847	0·99997 50542 83629
15	0·99999 93881 95359	0·99999 81645 86638	0·99999 63291 74961	0·99999 38819 62012	0·99999 08229 50036
16	0·99999 97749 29651	0·99999 93247 89028	0·99999 86495 78283	0·99999 77492 97645	0·99999 66239 47418
17	0·99999 99172 01246	0·99999 97516 03747	0·99999 95032 07525	0·99999 91720 12610	0·99999 87580 19044
18	0·99999 99695 40041	0·99999 99086 20123	0·99999 98172 40250	0·99999 96954 00426	0·99999 95431 00656
19	0·99999 99887 94407	0·99999 99663 83222	0·99999 99327 66444	0·99999 98879 44074	0·99999 98319 16113
20	+ 0·99999 99958 77693	+ 0·99999 99876 33078	+ 0·99999 99752 66157	+ 0·99999 99587 76928	+ 0·99999 99361 65392

n / t	6	7	8	9	10
1	+ 0·05464 80014 52797	0·26817 48073 26644	0·18068 47715 50211	0·14819 38418 87370	0·23701 82165 74609
2	| + | 0·21928 12946 63080	| + | 0·04754 01893 22603	| + | 0·25688 19941 06463	+ + | | 0·31162 84080 67465	+ + | | 0·20063 77689 23104
3	0·23878 90479 34200	0·36640 21347 36359	0·40965 57551 92309	0·37105 35279 20304	0·26611 15873 97219
4	0·36166 40008 03395	0·20339 42262 98305	0·05093 83202 15463	0·08810 25878 44205	0·20710 75153 98279
5	0·73556 67348 63206	0·65573 61016 67475	0·56931 56160 02127	0·47800 57812 79961	0·38358 79750 75831
6	0·89844 75100 59999	0·85577 13712 05337	0·82813 21271 91742	0·78879 97720 45136	0·74507 07436 35930
7	0·96204 89278 14871	0·94956 00689 40862	0·93538 52422 93312	0·91956 30995 25272	0·90213 67456 06779
8	0·98595 77710 19097	0·98129 90110 20097	0·97598 81367 27241	0·97003 04866 29698	0·96343 20474 32386
9	0·99482 31816 62974	0·99310 05569 44490	0·99113 36665 21426	0·98892 32382 79290	0·98647 00901 33615
10	0·99809 40684 77302	0·99745 91617 72468	0·99673 38012 46168	0·99591 80856 70643	0·99501 21261 41742
11	0·99929 86457 16643	0·99906 48156 19968	0·99879 78289 73037	0·99849 73991 57471	0·99816 36412 25220
12	0·99974 19589 36336	0·99965 59526 47257	0·99955 76642 75112	0·99944 70956 31578	0·99932 42487 54670
13	0·99990 50683 10705	0·99987 34254 15632	0·99983 72627 20043	0·99979 65804 69155	0·99975 13789 38830
14	0·99996 50760 84201	0·99995 34349 14456	0·99994 01308 03434	0·99992 51637 84321	0·99990 85338 94456
15	0·99998 71521 41841	0·99998 28695 40795	0·99997 79751 50830	0·99997 24689 76435	0·99996 63510 22665
16	0·99999 52735 27981	0·99999 36980 39790	0·99999 18974 83377	0·99998 98718 59350	0·99998 76211 68393
17	0·99999 82612 26878	0·99999 76816 36173	0·99999 70192 47002	0·99999 62740 59447	0·99999 54460 73600
18	0·99999 93603 40948	0·99999 91471 21310	0·99999 89034 41751	0·99999 86293 02282	0·99999 83247 02917
19	0·99999 97646 82563	0·99999 96862 43423	0·99999 95965 98696	0·99999 94957 48383	0·99999 93036 92485
20	+ 0·99999 99134 31550	+ 0·99999 98845 75400	+ 0·99999 98515 96945	+ 0·99999 98144 96182	+ 0·99999 97732 73114

Here and There

New Appointments

J. H. Dillon, assistant director of the Firestone Research Laboratories, Akron, Ohio, and formerly chairman of the Division of High-Polymer Physics, American Physical Society, has been appointed director of research of the Textile Research Institute, with offices and laboratories at Princeton, New Jersey.

Leo Szilard has been appointed to the faculty of the University of Chicago, and will divide his time between the new Institute for Radiobiology and Biophysics and the division of social sciences.

Stanley S. Ballard joined the faculty of Tufts College, Medford, Massachusetts, this fall as professor of physics and chairman of the Department of Physics. His last previous academic association was at the University of Hawaii. During the war he served as a Commander in the United States Naval Reserve, and was a member of the technical staff, Joint Task Force One, during Operation Crossroads.

Professor G. H. Henderson of the Department of Physics, Dalhousie University, Halifax, Nova Scotia, has returned to his post after having been engaged for the past six years in research for the Royal Canadian Navy.

Varnakale L. Jones, formerly with the Stanolind Oil and Gas Company, has rejoined the engineering staff of The University of Tulsa as assistant professor of geophysics and head of the newly created Department of Geophysics.

Henry H. Young, Price D. Wickersham, Jr., William W. Niven, Jr., and George L. Tuer, Jr., have joined the technical staff of the Midwest Research Institute.

Albert M. Stone, formerly with the Radiation Laboratory, Massachusetts Institute of Technology, has received an appointment as a physicist with the Office of Naval Research. He will be stationed at its London office, serving in a liaison capacity between European and American physicists.

Lee A. DuBridge is the new president of California Institute of Technology, succeeding Dr. R. A. Millikan, who retired last spring. Dr. DuBridge was formerly with the Department of Physics at the University of Rochester and later at the NDRC Radiation Laboratory, Cambridge, Massachusetts.

William A. Lewis, Jr., formerly research professor of electrical engineering at Illinois Institute of Technology, became dean of the Institute's graduate school on September 1.

Honors and Awards

Raymond D. Mindlin, associate professor of civil engineering at Columbia University, was recently awarded the Medal for Merit for his wartime work in the development of the radio proximity fuse.

In recognition of war research on fire-control instruments for better marksmanship in shooting down enemy aircraft, 27-year-old Wayne G. Norton of the Eastman Kodak Company received the Adolph Lomb medal from the Optical Society of America on October 4. The award is made annually "to a person under 30 years of age who shall have made a noteworthy contribution to optics."

Eugene C. Crittenden, associate director of the National Bureau of Standards, has been elected to membership in the International Committee on Weights and Measures. Commented Dr. E. U. Condon, director of the Bureau: "Dr. Crittenden's election is not only a distinct personal honor, but is recognition of the leading role played by the United States through the Bureau of Standards in the field of measurements." Dr. Crittenden is an authority on the measurement of light.

New Division at Brown University

Science reports that a new graduate division of applied mathematics has been organized at Brown University as an interdepartmental project of the Departments of Mathematics and Physics and the Division of Engineering, to meet the needs of schools and research laboratories for engineers, physicists, and mathematicians whose training extends beyond the accepted boundaries of their respective fields. The following professors have been appointed to the new division: William Prager (chairman), applied mechanics; John Henry Marchant (director of research), engineering; Maurice Anthony Biot, applied physical sciences; George Frances Carrier, engineering; James Arthur Krumhansl, physics; Chia Chiao Lin, applied mathematics; and Rohn Truell, physics.

Students are admitted who have excellent undergraduate records in two of the following subjects: engineering, physics, and mathematics. Training in research is stressed for the advanced students. Fellowship funds have been provided by the Rockefeller Foundation.

Radio Physics Department at Tufts College

On September 1 a Department of Radio Physics was established at Tufts College, with Professor Jamison R. Harrison appointed as head. Work in the department will comprise the field of radio and the allied fields of acoustics and electromagnetics. While the new department will be administered independently of the department of physics, the two departments will operate on a close cooperative basis. A broad foundation in physics will be required of majors in radio physics, and the urgent need on the part of majors in physics today for basic knowledge of electronics will be met by courses in radio physics.

The following personnel are associated with Professor Harrison in the new department while serving also in the

department of physics: Charles R. Mingins, associate professor of physics and radio communication; Carl A. Stevens, assistant professor of physics and radio communication; Domina Eberle Spencer, assistant professor of physics.

Information Clearing House

A library research service of special interest to industrial and scientific organizations not having ready access to the wealth of scientific literature in New York City is now offered by the Technical Library Consultants, 347 Madison Avenue, New York 17. The service is specifically designed to meet the literature research needs of executive, sales, and research departments.

Humble Oil Lectures

Establishment of an annual series of scientific lectures to be given at its Baytown Refinery and to be known as "Humble Lectures in Science" has been announced by Humble Oil and Refining Company. The series is designed especially to keep Humble technical personnel abreast of the latest developments in science and engineering. Outstanding scientists will be invited each year to present topics in their fields of special study and research.

Pittsburgh Physical Society Officers

Following are the 1946–47 officers of the Physical Society of Pittsburgh: president, Dr. I. Estermann, Carnegie Institute of Technology; vice president, Dr. Frank Morgan, Gulf Research and Development Corporation; secretary-treasurer, Dr. E. Stickley, Pittsburgh Plate Glass Company.

Atomic Research Center on Long Island

Nine leading educational institutions of the East have cooperated to form Associated Universities, Inc., which will operate as contractor with the government a large atomic research center at Camp Upton, Long Island. The camp has been transferred from surplus to the Manhattan Engineer District. Director of scientific research for Associated Universities will be Dr. Philip M. Morse, professor of physics at Massachusetts Institute of Technology and wartime consultant on scientific projects to the Navy Department.

The primary purpose of the project will be one of pure research, looking toward the peacetime application of atomic energy in industrial and medical fields and toward the training of more experts in the field of atomic research. Design of machines, which will cost approximately $5,000,000, will start immediately. Research, according to Dr. Morse, will be under way by early spring.

New Curriculum at Brooklyn Polytechnic

A new curriculum leading to the degree of Master of Science in Applied Mechanics has been announced by the Polytechnic Institute of Brooklyn, "to make available to graduate engineers a broad knowledge of the principles of mechanics which became so all-important in the new concepts of design developed during the war." These studies are incorporated in the new Department of Aeronautical Engineering and Applied Mechanics headed by Professor R. P. Harrington.

Universal Oil Products Company Expansion

The physics division of Universal Oil Products Company has recently moved into a new home, a functional building designed largely by the scientists who are to work in it. The building is completely air conditioned, and all the equipment is mounted on steel supports resting on spread concrete footings and insulated from the floor by cork gaskets. The laboratory is located at Riverside, Illinois. Dr. G. M. Webb is director of the physics division.

Kimberly-Clark Fellowships

The Kimberly-Clark Corporation, Neenah, Wisconsin, has announced a program of fellowships, with grants offered to the University of Wisconsin, the University of Minnesota, and the Massachusetts Institute of Technology. The fellowships are in the fields of physics, physical chemistry, and chemical engineering.

Louisville Physics Society

The Louisville Physics Society ended its first year with a dinner meeting on June 6. The new officers for the coming year were installed: Dr. Peter L. Vissat, president, and Dr. H. T. Smyth, secretary-treasurer.

Pittsburgh Spectroscopists

The Spectroscopy Society of Pittsburgh was organized in August. It will cooperate in the sponsoring of an Applied Spectroscopy Conference to be held at the University of Pittsburgh November 15, 1946. For information about the Society address Dr. Mary E. Warga, University of Pittsburgh, Pittsburgh 13, Pennsylvania.

Westinghouse Program for Fundamental Research

Westinghouse Research Laboratories have announced a broad program of research into nuclear physics and the problems associated with the conversion of atomic energy into a useful source of power for the peacetime world. The program will be in direct charge of Dr. W. E. Shoupp, Manager of the Electronics Department. First step will be modernization of the atom-smasher at the East Pittsburgh Laboratory.

Radioisotopes from the Manhattan Project

A detailed announcement on the availability and procurement of pile-produced radioisotopes from the Manhattan Project appeared in the June 14 issue of *Science*. Tables are included giving pertinent data on the characteristics and the quantities which may be made available of around 100 isotopes and isotopic mixtures. For practical reasons isotopes with a half-life less than 12 hours are not considered for distribution. Most of the isotopes are produced by fission or (n, γ) processes. Only four isotopes are produced by the (n, p) process with sufficient yield for distribution. Other processes are either not sufficiently productive or do not occur.

The article emphasized that (1) present piles were not designed for tracer and therapeutic isotope production, (2) waste plutonium process solutions are not a feasible source for separated fission isotopes, (3) routine production methods and facilities are not yet developed for most isotopes, (4) isotopes which can now be made available are only experimental lots resulting from research and development proceedings, (5) technical problems involved in the irradiation and processing of essential materials has been and will continue to be responsible for the delay in making certain isotopes available by routine production.

Allocation and distribution will be effected on the basis of the general policies, as well as on recommendations regarding specific applications, made by well qualified advisory groups nominated for Manhattan District appointment by the National Academy of Sciences. Charges will be made for materials and services on the basis of "out-of-pocket" operational expenses to the government necessitated by the non-project production and service program. Costs for construction or rental of major plant facilities and the expenses of research and development on isotope production will be assumed by the Project.

All correspondence concerning radioisotope procurement should be addressed to the Isotopes Branch, Research Division, Manhattan District, P.O. Box E, Oak Ridge, Tennessee. Reference to the original article for pertinent details is recommended before instituting inquiries or requests.

Bulletin of Mathematical Biophysics

Following is the table of contents for the December 1946 issue of *The Bulletin of Mathematical Biophysics:*

The Half-Life of a Drug in Relation to its Therapeutic Index—H. D. LANDAHL

Contributions to the Mathematical Theory of the Stability of Metabolizing Systems with Variable Surface Tension—ALFONSO SHIMBEL

Asynchrony of Labrinthine Receptors as a Physical Factor in Motion Sickness—MANUEL F. MORALES

A Mathematical Description of Metabolizing Systems: I—HERMAN BRANSON

The University of Chicago Press, Chicago, Illinois. Volume 8, Number 4.

Placement Register

In response to many requests from physicists and employers of physicists, the American Institute of Physics will operate another one of its Placement Registers in connection with the joint meeting of the American Physical Society and the American Association of Physics Teachers on January 30 and 31, and February 1, 1947.

The Register affords an effective supplement to the continuing Placement Service carried on by the Institute. The continuing service provides an opportunity for those desiring new employment to place their records on file at the Institute office. Here they may be consulted by employers or sent out to employers for consideration.

The Register itself provides an on-the-spot mechanism for bringing applicants and employers' representatives together. One or more rooms will be reserved for the Register and interviews will be scheduled as requested. Because employers will have opportunity to consult the records of applicants before the interview period begins, pre-registration on the part of the applicants is essential for the maximum effectiveness of the Register.

Registration forms and further information may be obtained from the Institute, 57 East 55 Street, New York 22, New York.

Addendum

There should have been a footnote to the title of E. P. Wigner's paper on "Theoretical Physics in the Metallurgical Laboratory of Chicago," November, 1946, *Journal of Applied Physics*, which should read as follows:

This document is based on work performed under Contract No. W-7401-eng-37 for the Manhattan Project of the Metallurgical Laboratory at the University of Chicago.

New Books

Piezoelectricity

BY WALTER G. CADY. Pp. 806+xxiii, Figs. 166, 6×9 in. International Series in Pure and Applied Physics. McGraw-Hill Book Company, New York, 1946. Price $9.00.

The purpose and scope of this book is compactly stated in the sub-title: An Introduction to the Theory and Applications of Electromechanical Phenomena in Crystals. Because of the increasing importance of this subject and many applications, Professor Cady's book is a needed addition to the literature in this field, much of which has been heretofore scattered in scientific and technical journals in several languages.

A thorough study of piezoelectricity, such as this, must necessarily draw on much of the material of crystal physics. This is because piezoelectricity is closely related to the elastic and dielectric properties of crystals and less closely to pyroelectric and to piezo- and electro-optical effects. The Weiss theory of ferromagnetism which finds a close analogy in the theory of the Seignette-electric crystals is also discussed. There is an extensive treatment of resonator theory which makes full use of the electromechanical analogy and explains how the equivalent electrical constants of vibrating crystals may be computed over any range of frequencies. Details of electrical circuits, however, are generally omitted since they may be found in other books. In like manner, while there is a good chapter on practical applications, only the general principles are discussed, the details being left to an extensive list of classified references. In view of the wide use of oblique crystal cuts, the great number of specialized

formulae for calculating crystal constants for rotated axes will be found very useful.

Since the book is intended for research workers as well as for students of physics and for radio amateurs, parts of it will be found difficult or incomprehensible to many in the latter group. In order to fully understand all of this book, familiarity with theoretical physics and circuit theory is essential, though many parts may be read profitably with less background.

A commendable feature is the list of symbols and abbreviations giving the number of the section in which each quantity is first introduced. The reviewer, however, found it annoyingly inconvenient to look back for equations referred to only by number, there being an extremely large number of such cross references. It would appear that page references along with the numbers would have made this task much easier. There is an extensive bibliography at the end of the book. The tables of numerical constants, which are indexed for ready reference, will be found very useful to workers in this field. Some of the data included have not been published elsewhere, being taken from investigations carried out at Wesleyan University by students of Professor Cady and Van Dyke. Gaps in existing data are pointed out, and suggestions for further research to settle controversial topics may be found in many places.

Besides the few misprints, there is not much fault that one may find with this book. However, in defining a Seignette-electric crystal it is asserted that the possession of a Curie point on one side of which the dielectric properties show non-linearity and hysteresis is the basic criterion. Shortly thereafter one finds the statement that perhaps some day a crystal will be discovered which is stable only in the Seignette-electric range so that no Curie point is observable. Surely then, the existence of a Curie point cannot be regarded as basic a criterion as the non-linearity and hysteresis themselves.

Furthermore, it seems contradictory to attribute practically all hysteresis effects in Rochelle salt to the clamped dielectric properties (p. 479), suggesting that a free crystal would not show such effects, and then to state that the constraints imposed by cement, electrodes, clamping, and water-proofing greatly reduce the effects of temperature and hysteresis (p. 670). It is well known that the anomalies of Rochelle salt were discovered in crystals which were not clamped except for the constraint imposed by the electrodes and that in many cases this was quite negligible.

The use of literary quotations at the head of each chapter add interest to the book, giving it a certain cultural seasoning. Many of the quotations aptly express some central idea in the chapter, but some of them are so irrelevant that they would have been better omitted.

The wide variety of subjects treated testifies to Professor Cady's broad, scholarly interests, and thorough knowledge of his specialty. This book is a distinguished addition to the growing number of important volumes in the International Series in Pure and Applied Physics.

JOSEPH VALASEK
University of Minnesota

New Booklets

Mathematical Tables Project of the National Bureau of Standards, 150 Nassau Street, New York, New York, has published three short notes bearing on tables now in progress, as follows: Mathieu functions, exponential integrals for complex arguments, and functions related to certain confluent hypergeometric functions.

The Ohio Valley Spectrographic Society, Engineers Club Building, Dayton, Ohio, is distributing *Collected Abstracts, Published during 1945 on Spectrochemical Analysis*, compiled by Edwin S. Hodge. 64 pages, well indexed. $1 postpaid for cash orders, $1.25 when billing is required. Discount of 15 percent on lots of 10 or more copies.

North American Philips Company, Inc., 100 East 42 Street, New York 17, New York, has issued a new 8-page booklet (R1041) titled *The Geiger-Mueller X-Ray Spectrometer*. It explains the history and construction details covering the instrument, along with circuits and data pertinent to correct usage. Free.

General Electric Company, Schenectady, New York, has assembled in booklet form six addresses on *Applications of Atomic Power* given by staff members of the General Electric Research Laboratory on the Science Forum Program, Station WGY, Schenectady, during the fall of 1945. 26 pages.

Ampro Corporation, 2835 North Western Avenue, Chicago, Illinois, has issued a new price sheet, showing the general trend in prices of its 16-mm motion picture equipment and accessories to be slightly upwards. 4 pages.

Reiner Electronics Company, Inc., 152 West 25 Street, New York 1, New York, has published a new 4-page bulletin (105) providing a complete description of the new laboratory instruments now being produced by the company. The design of these volt-ammeters makes available for the first time a method of manual insertion of accurately calibrated shunts and multipliers with values always visible in the unit. This self-instructing feature teaches the student as he works. The principles of operation are thoroughly described and all applications and specifications are given in detail.

Interchemical Review for Spring 1946, published by the Research Laboratories of Interchemical Corporation, 432 West 45 Street, New York 19, New York, features the following articles: "Synthetic Amino Acids" and "A Brief Review of Atomic Physics." 28 pages.

Carson Micrometer Corporation, 28 Edison Place, Newark 2, New Jersey, has announced production of four redesigned models of its electronic micrometers for precise thickness measurement. They are described in a 4-page leaflet. Address Department 72 of the company.

Author Index to Volume 17

References with (L) are to Letters to the Editor.

Adams, H. E. and P. O. Powers. Thermal polymerization of drying oils—325
Akeley, E. S. Study of a certain type of resonant cavity and its application to a charged particle accelerator—1056
Albright, John G. Book review—537
van Amerongen, G. J. Permeability of different rubbers to gases and its relation to diffusivity and solubility—972
Andrews, R. D., A. V. Tobolsky, and E. E. Hanson. Theory of permanent set at elevated temperatures in natural and synthetic rubber vulcanizates—352
Anthony, Robert L. (see Guth, Eugene)—347
Arnold, Orlan M. (see Rathbun, Mary E.)—759

Baker, R. F. (see Hillier, James)—12
Baker, T. C. and F. W. Preston. Effect of water on the strength of glass—179
—— Fatigue of glass under static loads—170
—— Wide range static strength testing apparatus for glass rods—162
Bargmann, V. and H. F. Ludloff. Elastic limit for dynamic loading—63 (L)
Barnes, R. Bowling, Robert S. McDonald, and Van Zandt Williams. Erratum: Small prism infra-red spectroscopy—532
Barry, Arthur J. Viscometric investigation of dimethylsiloxane polymers—1020
Bateman, H. Some integral equations of potential theory—91
Baum, Richard F. Design of broad band I. F. amplifiers—519
—— Part II—721
Beams, J. W., J. L. Young, III, and J. W. Moore. Production of high centrifugal fields—886
Beck, Hugo M. (see Faust, William R.)—749
Bekkedahl, Norman (see Wood, Lawrence A.)—362
Berry, Clifford E. (see Eaglesfield, C. C.)—1125 (L)
——, **Doyle E. Wilcox, Sibyl M. Rock, and H. W. Washburn.** Computer for solving linear simultaneous equations—262
Birks, L. S. and H. Friedman. Particle size determination from x-ray line broadening—687
Blewett, John P. Oxide coated cathode literature, 1940–1945—643
Bloch, F., K. M. Hamermesh, and M. Phillips. Radar reflections from long conductors—1015
Boyer, R. F. (see Spencer, R. S.)—398
Brentano, J. C. M. Parafocusing properties of microcrystalline powder layers in x-ray diffraction applied to the design of x-ray goniometers—420
Bridgman, P. W. Effect of hydrostatic pressure on plastic flow under shearing stress—692
—— Studies of plastic flow of steel, especially in two-dimensional compression—225
—— Tensile properties of several special steels and certain other materials under pressure—201
Brittin, Wesley E. Liquid rise in a capillary tube—37
Brown, Gordon P., Albert DiNardo, George K. Cheng, and Thomas K. Sherwood. Flow of gases in pipes at low pressures—802
Bruck, George G. Letter to the editor—213
Bryant, J. M. and M. Newman. Lightning recorded by aeroplane propeller—555
Buerger, M. J. Interpretation of Harker syntheses—579
—— **and Gilbert E. Klein.** Correction of diffraction amplitudes for Lorentz and polarization factors—285
—— Erratum—743
Burington, Richard S. Book review—409
Busse, W. F., J. M. Lambert, and R. B. Verdery. Tackiness of GR-S and other elastomers—376

Carter, J. L. (see Osborne, M. F. M.)—871
Champaygne, E. F. (see McLachlan, Dan, Jr.)—1006
Cheng, George K. (see Brown, Gordon P.)—802
Chilton, Ernest G. Dynamic characteristics of rubber supports from vibration table data—492
Coggeshall, Norman D. and Eleanor L. Saier. Analyses of mixtures of light gases by infra-red absorption—450
Coomes, Edward A. Pulsed properties of oxide cathodes—647
Cravath, A. M., A. E. Smith, J. R. Vinograd, and J. N. Wilson. Preparation of electron microscope specimens for determination of particle size distribution in aqueous suspensions—309
Cravath, Austin M. Preparing pigments for the electron microscope—1125 (L)
Crittenden, Eugene C., Jr. (see Parkins, William E.)—447
—— **and William E. Parkins.** Methods for betatron or synchrotron beam removal—444

Dart, S. L. and Eugene Guth. Elastic properties of cork. I. Stress relaxation of compressed cork—314
Debye, P. P. Photoelectric instrument for light scattering measurements and a differential refractometer—392
Dienes, G. J. and H. F. Klemm. Theory and application of the parallel plate plastometer—458
DiNardo, Albert. (see Brown, Gordon P.)—802

Eaglesfield, C. C.; Clifford E. Berry. Concerning "computer for solving linear simultaneous equations"—1125 (L)
Eastwood, Mary J. (see Rathbun, Mary E.)—759
Eisenstein, A. Study of oxide cathodes by x-ray diffraction methods. Part I. Methods, conversion studies, and thermal expansion coefficients—434
—— Part II. Oxide coating composition—654
—— X-ray method for measuring the thickness of thin crystalline films—874
—— (see Fineman, A.)—663
Ewell, Arthur W. Recent ozone investigations—908

Faust, William R. and Hugo M. Beck. Oscillation conditions in single tuned amplifiers—749
Feenberg, Eugene. Elementary treatment of longitudinal debunching in a velocity modulation system—852
—— Relation between nodal positions and standing wave ratio in a composite transmission system—530
—— **and David Feldman.** Theory of small signal bunching in a parallel electron beam of rectangular cross section—1025
Feldman, David. (see Feenberg, Eugene)—1025
Field, J. E., D. E. Woodford, and S. D. Gehman. Applications of infra-red methods in the structural examination of synthetic rubber—386
Field, Robert F. Formation of ionized water films on dielectrics under conditions of high humidity—318
Fineman, A. and A. Eisenstein. Studies of the interface of oxide coated cathodes—663
Fisher, J. R. (see Teal, G. K.)—879
Forsythe, George E. Book review—535
Friedman, H. (see Birks, L. S.)—687
Frocht, Max M. Numerical solution of Laplace's equation in composite rectangular areas—730
Froelich, H. C. Depreciation of fluorescent lamps without passage of current—573
Fry, D. L., R. E. Nusbaum, and H. M. Randall. Analysis of multicomponent mixtures of hydrocarbons in the liquid phase by means of infra-red absorption spectroscopy—150
Fuertes, Fidel Alsina. Letter to the editor on the "power function"—712 (L)
Fulcher, Gordon S. Interpolation with the aid of a plot of first differences—617

Gehman, S. D. (see Field, J. E.)—386
Gemant, Andrew. Induction heating of hollow metallic cylinders—195
—— Transient temperatures around heating pipes maintained at constant temperature—1076
Glathart, J. L. (see Vonnegut, B.)—1082
—— **and F. W. Preston.** Fatigue modulus of glass—189
Gregory, J. H. (see Smith, Alva W.)—33
Guth, Eugene (see Dart, S. L.)—314
——, **Paul E. Wack, and Robert L. Anthony.** Significance of the equation of state for rubber—347

Hall, C. E. Book review—538
Hammermesh, K. M. (see Bloch, F.)—1015
Hansen, W. W. Erratum: On maximum gain-band width product in amplifiers—109
Hanson, E. E. (see Andrews, R. D.)—352
—— (see Kelsey, R. H.)—675
Harris, Louis. Evaporation of antimony—757 (L)
Harvey, E. Newton (see McMillen, J. Howard)—541
Havenhill, R. S. Book review—539
——, **H. C. O'Brien, and J. J. Rankin.** Electrostatic and tensile properties of rubber and GR-S at elevated temperatures—338
Heidenreich, R. D., L. Sturkey, and H. L. Woods. Investigation of secondary phases in alloys by electron diffraction and the electron microscope—127
Heisler, Michael P. (see Paschkis, Victor)—246
Herman, Robert C. and Charles F. Meyer. Thermoluminescence and conductivity of phosphors—743
Hershberger, W. D. Absorption of microwaves by gases—495
—— (see Walter, John E.)—814
Hillier, James. Further improvement in the resolving power of the electron microscope—307
—— Study of distortion in electron microscope projection lenses—411
—— **and R. F. Baker.** On the improvement of resolution in electron diffraction cameras—12
von Hippel, A., J. H. Schulman, and E. S. Rittner. New electrolytic selenium photo-cell—315
—— (see Roberts, S.)—610
Hollomon, J. H. (see Zener, Clarence)—69
—— **and Clarence Zener.** Problems in fracture of metals—82
Honold, Edith (see Wakeham, Helmut)—698
Horvath, William J. (see Iskenderian, Haig P.)—255
Howlett, J. Film-lubrication between spherical surfaces: with an application to the theory of the four-ball lubricant testing instrument—137
Hudson, Douglas Rennie. Coordination number in solid solutions—a mathematical paradox—1126 (L)
Hull, Albert W. Stresses in cylindrical glass-metal seals with glass inside—685
Hull, Gordon Ferrie, Jr. Resonant circuit modulator for broad band acoustic measurements—1066
Hunter, Lloyd P. Energy build-up in magnetrons—833
Hurd, J. M. (see Smoluchowski, R.)—864

Ingersoll, H. G. Fine structure of viscose rayon—924
Iskenderian, Haig P. and William J. Horvath. Determination of the temperature rise and the maximum safe current through multiconductor electric cables—255

Jacobs, Harold. Dissociation energies of surface films of various oxides as determined by emission measurements of oxide coated cathodes—596
Johnson, J. B. Cathode-ray tube for viewing continuous patterns—891

Kaufmann, K. (see Watson, John H. L.)—996
Kelsey, R. H. and E. E. Hanson. Method for preparing rubber latex specimens for the electron microscope—675
King, Allen L. Pressure-volume relation for cylindrical tubes with elastomeric walls: the human aorta—501
King, D. D. Measured impedance of cylindrical dipoles—844
King, Ronold (see Middleton, David)—273
Kingdon, K. H. (see Lafferty, J. M.)—894
Klein, Gilbert E. (see Buerger, M. J.)—285, 743
Klemm, H. F. (see Dienes, G. J.)—458
Korff, Serge A. Book review—408
Krzywoblocki, M. Zbigmew. Approximate calculation of the range of a winged jet projectile—515

Lafferty, J. M. Millimeter-wave reflex oscillator—1061
—— **and K. H. Kingdon.** Improvements in the stability of the FP-54 electrometer tube—894

Lambert, J. M. (see Busse, W. F.)—376
Landsberg, Peter T. On plane rotations in n dimensions—60 (L)
Langmuir, D. B. (see Malter, L.)—456
Liebhafsky, Herman A. Picturesque oxidation of molybdenum vacuum-tube leads—901
Lucht, C. M. (see Smoluchowski, R.)—864
Ludeke, Carl A. Experimental investigation of forced vibrations in a mechanical system not having a non-linear restoring force—603
Ludloff, H. F. (see Bargmann, V.)—63 (L)
Lynn, J. T. (see Smith, Alva W.)—33
Lyons, W. James. General relations of flow in solids and their application to the plastic behavior of tire cords—472

Mack, Charles. Plastic flow, creep, and stress relaxation. Part I-Plastic flow—1086
—— Plastic flow, creep, and stress relaxation. Part II-Creep—1093
—— Plastic flow, creep, and stress relaxation. Part III-Creep and elastic after-effect— 1101
MacLean, William R. Microwave dielectric loss measuring technique—558
Makinson, K. Rachel (see Makinson, R. E. B.)—567
Makinson, R. E. B., J. M. Somerville, K. Rachel Makinson, and P. Thonemann. Magnetically-controlled gas discharge tubes—567
Malter, L. and D. B. Langmuir. Methods of minimizing lead loss in emissivity and resistivity determinations—456
Marcum, Jess. Interchange of energy between an electron beam and an oscillating electric field—4
Margenau, Henry. Book review—641
Mayer, Ernest. Resonant frequencies of the nosed-in cavity—1046
McCuskey, S. W. Book review—536
McDonald, Robert S. (see Barnes, R. Bowling)—532
McLachlan, Dan, Jr. and E. F. Champaygne. Machine for the application of sand in making Fourier projections of crystal structures—1006
McMillen, J. Howard and E. Newton Harvey. Spark shadowgraphic study of body waves in water—541
McReynolds, Andrew W. Electrical observations of the Austenite-Martensite transformation in steel—823
Meyer, Charles F. (see Herman, Robert C.)—743
Middleton, David. Response of biased, saturated linear, and quadratic rectifiers to random noise—778
—— (see Van Vleck, J. H.)—940
—— **and Ronold King.** Thin cylindrical antenna: a comparison of theories—273
Moon, Parry and Domina Eberle Spencer. Approximations to Planckian distributions—506
Moore, J. W. (see Beams, J. W.)—886
Morris, M. Book review—312
Mueller, C. W. Erratum: Secondary electron emission of Pyrex glass—62

Newman, M. (see Bryant, J. M.)—555
North, H. Q. Properties of welded contact germanium rectifiers—912
Nusbaum, R. E. (see Fry, D. L.)—150

O'Brien, H. C. (see Havenhill, R. S.)—338
Olver, F. W. J. Note on a paper of H. Bateman—1127 (L)
Osborne, M. F. M. and J. L. Carter. Transient analysis of linear systems, using underwater explosion waves—871
Osgood, Thomas H. Book review—540

Parkins, William E. (see Crittenden, Eugene C., Jr.)—444
—— **and Eugene C. Crittenden, Jr.** Graphical method for determining particle trajectories—447
Paschkis, Victor and Michael P. Heisler. Accuracy of lumping in an electric circuit representing heat flow in cylindrical and spherical bodies—246
Pekeris, C. L. Asymptotic solutions for the normal modes in the theory of microwave propagation—1108
—— Perturbation theory of the normal modes for an exponential M-curve in non-standard propagation of microwaves—678
Phillips, M. (see Bloch, F.)—1015
Pickett, Gerald. Letter to the editor—61
Powers, P. O. (see Adams, H. E.)—325
Preston, F. W. (see Baker, T. C.)—162, 170, 179
—— (see Glathart, J. L.)—189

Randall, H. M. (see Fry, D. L.)—150
Rankin, J. J. (see Havenhill, R. S.)—338
Rathbun, Mary E., Mary J. Eastwood, and Orlan M. Arnold. Supplementary bibliography of electron microscopy—759
Read, Thomas A. and E. P. T. Tyndall. Internal friction and plastic extension of zinc single crystals—713
Reissner, Eric. On vibrations of shallow spherical shells—1038
Rittner, E. S. (see Von Hippel, A.)—215
Roberts, S. and A. Von Hippel. New method for measuring dielectric constant and loss in the range of centimeter waves—610
Robinson, A. L. Book review—537
Rock, Sibyl M. (see Berry, Clifford E.)—262
Rosenthal, Jenny E. On a novel form of refrigerator—62 (L)
Roseveare, W. E. (see Waller, R. C.)—482

Saier, Eleanor L. (see Coggeshall, Norman D.)—450
Sard, R. D. Calculated frequency spectrum of the shot noise from a photo-multiplier tube—768
Schroeder, Alfred C. (see Sziklai, George C.)—763
Schulman, J. H. (see von Hippel, A.)—215
Schulman, James H. Luminescence of $(Zn,Be)_2SiO_4$:Mn and other manganese-activated phosphors—902
Schwerdtfeger, H. Erratum: On the representation of rigid rotations—109
Sears, W. C. Book review—536
Sherwood, Thomas K. (see Brown, Gordon P.)—802
Smith, A. E. (see Cravath, A. M.)—309

Smith, Alva W., J. H. Gregory, and J. T. Lynn. Electrical resistance of iron wires and permalloy strips at radio frequencies—33
Smoluchowski, R., C. M. Lucht, and J. M. Hurd. Composition and diffraction effects in x-ray microradiographs—864
Somerville, J. M. (see Makinson, R. E. B.)—567
Spencer, Domina Eberle (see Moon, Parry)—506
Spencer, R. S. and R. F. Boyer. Thermal expansion and second-order transition effects in high polymers. III. Time effects—398
Stockman, Harry. Calculation of the output from non-linear mixers—110
Stoker, R. L. Method of determining the size of droplets dispersed in a gas—243
Sturkey, L. (see Heidenreich, R. D.)—127
Sziklai, George C. and Alfred C. Schroeder. Electronic spectroscopy—763

Tai, C. T. Shunt and series sections of transmission line for impedance matching—44
Teal, G. K., J. R. Fisher, and A. W. Treptow. New bridge photo-cell employing a photo-conductive effect in silicon. Some properties of high purity silicon—879
Thonemann, P. (see Makinson, R. E. B.)—567
Tobolsky, A. V. (see Andrews, R. D.)—352
Treptow, A. W. (see Teal, G. K.)—879
Tyndall, E. P. T. (see Read, Thomas A.)—713

Valesek, Joseph. Book review—1130
Van Vleck, J. H. and David Middleton. Theoretical comparison of the visual, aural, and meter reception of pulsed signal in the presence of noise—940
Verdery, R. B. (see Busse, W. F.)—376
Vinograd, J. R. (see Cravath, A. M.)—309
Von Karman, Theodore. Atomic engineering—2
Vonnegut, B. and J. L. Glathart. Effect of temperatures on the strength and fatigue of glass rods—1082

Wack, Paul E. (see Guth, Eugene)—347
Wakeham, Helmut and Edith Honold. Hysteresis and related elastic properties of tire cords—698
Walker, L. R. and Nelson Wax. Non-uniform transmission lines and reflection coefficients—1043
Waller, R. C. and W. E. Roseveare. Fatigue failure of rayon tire cord—482
Walsh, Thomas J. Book review—409
Walter, John E. and W. D. Hershberger. Absorption of microwave by gases. II—814
Washburn, H. W. (see Berry, Clifford E.)—262
Watson, John H. L. Filmless sample mounting for the electron microscope—121
—— **and K. Kaufmann.** Electron microscope examination of the microphysical properties of the polymer cuprene —996
Wax, Nelson. (see Walker, L. R.)—1043
Weyl, W. A. Use of color and fluorescence indicators for determining the structure of glass—628
Wigner, E. P. Theoretical physics in the metallurgical laboratory of Chicago—857; Addendum—1130
Wilcox, Doyle E. (see Berry, Clifford E.)—262
Wildschut, A. J. On the proportion of crystalline and amorphous components in stretched vulcanized rubber—51
Williams, Robley C. Book review—538
—— **and Ralph W. G. Wyckoff.** Applications of metallic shadow-casting to microscopy—23
Williams, Van Zandt (see Barnes, R. Bowling)—532
Wilson, J. N. (see Cravath, A. M.)—309
Wood, Lawrence A. and Norman Bekkedahl. Crystallization of unvulcanized rubber at different temperatures—362
Woodford, D. E. (see Field, J. E.)—386
Woods, H. L. (see Heidenreich, R. D.)—127
Wright, D. K., Jr. Book reviews—312, 535
Wyckoff, Ralph W. G. (see Williams, Robley C.)—23

Young, J. L., III (see Beams, J. W.)—886

Zener, Clarence (see Hollomon, J. H.)—82
—— **and J. H. Hollomon.** Problems in non-elastic deformation of metals—69
Ziegler, George E. Midwest Research Institute—a new scientific research institution—669

Subject Index to Volume 17

References with (L) are to Letters to the Editor.

Absorption of microwaves by gases, W. D. Hershberger—495
—— Part II, John E. Walter and W. D. Hershberger—814
Abstracts of papers presented at meeting of Division of High Polymer Physics—405
Accuracy of lumping in an electric circuit representing heat flow in cylindrical and spherical bodies, Victor Paschkis and Michael P. Heisler—246
Acoustic measurements, Resonant circuit modulator for broad band acoustic measurements, Gordon Ferrie Hull, Jr.—1066
Aeroplane propeller, Lightning recorded by, J. M. Bryant and M. Newman—555
Alloys, Investigation of secondary phases in alloys by electron diffraction and the electron microscope, R. D. Heidenreich, L. Sturkey, and H. L. Woods—127
Amplifiers, Design of broad band I.F. amplifiers, Richard F. Baum—519
—— Part II—721
Amplifiers, On maximum gain-band width product in amplifiers, W. W. Hansen—109 (erratum)
Amplifiers, Oscillation conditions in single tuned amplifiers, William R. Faust and Hugo M. Beck—749
Analyses of mixtures of light gases by infra-red absorption, Norman D. Coggeshall and Eleanor L. Saier—450
Analysis of multicomponent mixtures of hydrocarbons in the liquid phase by means of infra-red absorption spectroscopy, D. L. Fry, R. E. Nusbaum, and H. M. Randall—150
Antenna, Thin cylindrical antenna: a comparison of theories, David Middleton and Ronold King—273
Antimony, Evaporation of, Louis Harris—757 (L)
Applications of infra-red methods in the structural examination of synthetic rubber, J. E. Field, D. E. Woodford, and S. D. Gehman—386
Applications of metallic shadow-casting to microscopy, Robley C. Williams and Ralph W. G. Wyckoff—23
Approximate calculation of the range of a winged jet projectile, M. Zbigmew Krzywoblocki—515
Approximations to Planckian distributions, Parry Moon and Domina Eberle Spencer—506
Asymptotic solutions for the normal modes in the theory of microwave propagation, C. L. Pekeris—1108
Atomic engineering, Theodore Von Karman—2
Atomic scientists, Federation of—108
Austenite-Martensite transformation in steel, Electrical observations of the, Andrew W. McReynolds—823

Bateman, Note on a paper of H. Bateman, F. W. J. Olver—1127 (L)
Betatron, Methods for betatron or synchrotron beam removal, Eugene C. Crittenden, Jr., and William E. Parkins—444
Bibliography of electron microscopy, Supplementary, Mary E. Rathbun, Mary J. Eastwood, and Orlan M. Arnold—759
Body waves in water, Spark shadowgraphic study of, J. Howard McMillen and E. Newton Harvey—541

Calculated frequency spectrum of the shot noise from a photo-multiplier tube, R. D. Sard—768
Calculation of the output from non-linear mixers, Harry Stockman—110
Capillary tube, Liquid rise in a, Wesley E. Brittin—37
Cathode-ray tube for viewing continuous patterns, J. B. Johnson—891
Cathodes, oxide coated, Dissociation energies of surface films of various oxides as determined by emission measurements of, Harold Jacobs—596
Centimeter waves, New method for measuring dielectric constant and loss in the range of, S. Roberts and A. von Hippel—610
Centrifugal fields, Production of high centrifugal fields, J. W. Beams, J. L. Young, III, and J. W. Moore—886
Circuit modulator, Resonant circuit modulator for broad band acoustic measurements, Gordon Ferris Hull, Jr.—1066
Color and fluorescence indicators for determining the structure of glass, Use of, W. A. Weyl—628
Composition and diffraction effects in x-ray microradiographs, R. Smoluchowski, C. M. Lucht, and J. M. Hurd—864
Computer for solving linear simultaneous equations, Clifford E. Berry, Doyle E. Wilcox, Sibyl M. Rock, and H. W. Washburn—262
Computer for solving linear simultaneous equations, C. C. Eaglesfield; Clifford E. Berry—1125 (L).
Conductors, Radar reflections from long conductors, F. Bloch, M. Hamermesh, and M. Phillips—1015
Continuous patterns, Cathode-ray tube for viewing continuous patterns, J. B. Johnson—891
Coordination number in solid solutions—a mathematical paradox, Douglas Rennie Hudson—1126 (L)
Cork, Elastic properties of. I. Stress relaxation of compressed cork, S. L. Dart and Eugene Guth—314
Correction of diffraction amplitudes for Lorentz and polarization factors, M. J. Buerger and Gilbert E. Klein—285
Correction of diffraction amplitudes for Lorentz and polarization factors, M. J. Buerger and Gilbert E. Klein—743 (erratum)
Creep, Plastic flow, creep, and stress relaxation. Part I—Plastic flow, Charles Mack—1086
—— Part II—Creep—1093
—— Part III—Creep and elastic after-effect—1101
Crystal structures, Machine for the application of sand in making Fourier projections of crystal structures, Dan McLachlan, Jr., and E. F. Champaygne—1006
Crystalline films, x-ray method for measuring the thickness of thin crystalline films, A. Eisenstein—874
Crystallization of unvulcanized rubber at different temperatures, Lawrence A. Wood and Norman Bekkedahl—362

Cuprene, Electron microscope examination of the microphysical properties of the polymer cuprene, John H. L. Watson and K. Kaufmann—996
Cylinders, Induction heating of hollow metallic cylinders, Andrew Gemant—195
Cylindrical dipoles, Measured impedance of, D. D. King—844

Debunching, Elementary treatment of longitudinal debunching in a velocity modulation system, Eugene Feenberg—852
Deformation of metals, Problems in non-elastic deformation of metals, Clarence Zener and J. H. Hollomon—69
Depreciation of fluorescent lamps without passage of current, H. C. Froelich—573
Design of broad band I. F. amplifiers, Richard F. Baum—519
—— Part II—721
Determination of the temperature rise and the maximum safe current through multiconductor electric cables, Haig P. Iskenderian and William J. Horvath—255
Dielectric constant and loss in the range of centimeter waves, New method for measuring, S. Roberts and A. von Hippel—610
Dielectric loss measuring technique, Microwave, William R. MacLean—558
Dielectrics, Formation of ionized water films on dielectrics under conditions of high humidity, Robert F. Field—318
Dimethylsiloxane polymers, Viscometric investigation of, Arthur J. Barry—1020
Dissociation energies of surface films of various oxides as determined by emission measurements of oxide coated cathodes, Harold Jacobs—596
Division of High Polymer Physics, Abstracts—405
Dynamic characteristics of rubber supports from vibration table data, Ernest G. Chilton—492

Effect of hydrostatic pressure on plastic flow under shearing stress, P. W. Bridgman—692
Effect of temperature on the strength and fatigue of glass rods, B. Vonnegut and J. L. Glathart—1082
Effect of water on the strength of glass, T. C. Baker and F. W. Preston—179
Elastic limit for dynamic loading, V. Bargmann and H. F. Ludloff—63 (L)
Elastic properties of cork. I. Stress relaxation of compressed cork, S. L. Dart and Eugene Guth—314
Elastomers, Tackiness of GR-S and other elastomers, W. F. Busse, J. M. Lambert, and R. B. Verdery—376
Electric cables, Determination of the temperature rise and the maximum safe current through multiconductor electric cables, Haig P. Iskenderian and William J. Horvath—255
Electric circuit, Accuracy of lumping in an electric circuit representing heat flow in cylindrical and spherical bodies, Victor Paschkis and Michael P. Heisler—246
Electrical observations of the Austenite-Martensite transformation in steel, Andrew W. McReynolds—823
Electrical resistance of iron wires and permalloy strips at radiofrequencies, Alva W. Smith, J. H. Gregory, and J. T. Lynn—33
Electron beam, Interchange of energy between an electron beam and an oscillating electric field, Jess Marcum—4
Electron beam, Theory of small signal bunching in a parallel electron beam of rectangular cross section, Eugene Feenberg and David Feldman—1025
Electron diffraction cameras, Improvement of resolution in, James Hillier and R. F. Baker—12
Electron diffraction and the electron microscope, Investigation of secondary phases in alloys by, R. D. Heidenreich, L. Sturkey, and H. L. Woods—127
Electron microscope examination of the microphysical properties of the polymer cuprene, John H. L. Watson and K. Kaufmann—996
Electron microscope, Filmless sample mounting for the, John H. L. Watson—121
Electron microscope, Further improvement in the resolving power of the, James Hillier—307
Electron microscope, Method for preparing rubber latex specimens for the, R. H. Kelsey and E. E. Hanson—675
Electron microscope, Preparing pigments for the, A. M. Cravath—1125 (L)
Electron Microscope Society of America, Report of the Committee on Resolution of the—989
Electron Microscope Society of America. Third Annual meeting—66
Electron microscope specimens, Preparation of, for determination of particle size distribution in aqueous suspensions, A. M. Cravath, A. E. Smith, J. R. Vinograd, and J. N. Wilson—309
Electron microscope, Study of distortion in electron microscope projection lenses, James Hillier—411
Electron microscopy, Supplementary bibliography of, Mary E. Rathbun, Mary J. Eastwood, and Orlan M. Arnold—759
Electronic spectroscopy, George C. Sziklai and Alfred C. Schroeder—763
Electrostatic and tensile properties of rubber and GR-S at elevated temperatures, R. S. Havenhill, H. C. O'Brien, and J. J. Rankin—338
Elementary treatment of longitudinal debunching in a velocity modulation system, Eugene Feenberg—852
Emission measurements of oxide coated cathodes, Dissociation energies of surface films of various oxides as determined by, Harold Jacobs—596
Energy build-up in magnetrons, Lloyd P. Hunter—833
Equation of state, Significance of the equation of state for rubber, Eugene Guth, Paul E. Wack, and Robert L. Anthony—347
Evaporation of antimony, Louis Harris—757 (L)
Experimental investigation of forced vibrations in a mechanical system having a non-linear restoring force, Carl A. Ludeke—603

Fatigue failure of rayon tire cord, R. C. Waller and W. E. Roseveare—482
Fatigue of glass under static loads, T. C. Baker and F. W. Preston—170
Fatigue modulus of glass, J. L. Glathart and F. W. Preston—189
Federation of atomic scientists—108

Filmless sample mounting for the electron microscope, John H. L. Watson—121
Film-lubrication between spherical surfaces: with an application to the theory of the four-ball lubricant testing instrument, J. Howlett—137
Fine structure of viscose rayon, H. G. Ingersoll—924
Flow of gases in pipes at low pressures, Gordon P. Brown, Albert DiNardo, George K. Cheng, and Thomas K. Sherwood—802
Flow in solids, General relations of flow in solids and their application to the plastic behavior of tire cords, W. James Lyons—472
Fluorescent lamps, Depreciation of, without passage of current, H. C. Froelich—573
Formation of ionized water films on dielectrics under conditions of high humidity, Robert F. Field—318
Four-ball lubricant testing instrument, Film-lubrication between spherical surfaces: with an application to the theory of, J. Howlett—137
Fourier projections, Machine for the application of sand in making Fourier projections of crystal structures, Dan McLachlan, Jr., and E. F. Champaygne—1006
FP-54 electrometer tube, Improvements in the stability of the, J. M. Lafferty and K. H. Kingdon—894
Frequency discriminator, George G. Bruck—213 (L)
Frequency spectrum, Calculated frequency spectrum of the shot noise from a photo-multiplier tube, R. D. Sard—768
Further improvement in the resolving power of the electron microscope, James Hillier—307

Gas discharge tubes, Magnetically-controlled, R. E. B. Makinson, J. M. Somerville, K. Rachel Makinson, and P. Thonemann—567
Gas, Method of determining the size of droplets dispersed in a, R. L. Stoker—243
Gases, Absorption of microwaves by gases. II, John E. Walter and W. D. Hershberger—814
Gases, Flow of gases in pipes at low pressures, Gordon P. Brown, Albert DiNardo, George K. Cheng, and Thomas K. Sherwood—802
Gases, Permeability of different rubbers to gases and its relation to diffusivity and solubility, G. J. van Amerongen—972
General relations of flow in solids and their application to the plastic behavior of tire cords, W. James Lyons—472
Glass, Effect of water on the strength of, T. C. Baker and F. W. Preston—179
Glass, Fatigue of glass under static loads, T. C. Baker and F. W. Preston—170
Glass, Fatigue modulus of, J. L. Glathart and F. W. Preston—189
Glass-metal seals, Stresses in cylindrical glass-metal seals glass inside, Albert W. Hull—685
Glass rods, Effect of temperature on the strength and fatigue of, B. Vonnegut and J. L. Glathart—1082
Glass rods, Wide range static strength testing apparatus for, T. C. Baker and F. W. Preston—162
Glass, Use of color and fluorescence indicators for determining the structure of, W. A. Weyl—628
Graphical method for determining particle trajectories, William E. Parkins and Eugene C. Crittenden, Jr.—447
GR-S, Electrostatic and tensile properties of rubber and GR-S at elevated temperatures, R. S. Havenhill, H. C. O'Brien, and J. J. Rankin—338
GR-S, Tackiness of, and other elastomers, W. F. Busse, J. M. Lambert, and R. B. Verdery—376

Harker syntheses, Interpretation of, M. J. Buerger—579
Heat flow, Accuracy of lumping in an electric circuit representing heat flow in cylindrical and spherical bodies, Victor Paschkis and Michael P. Heisler—246
Human aorta, Pressure-volume relation for cylindrical tubes with elastomeric walls: the human aorta, Allen L. King—501
Hydrocarbons, Analysis of multicomponent mixtures of hydrocarbons in the liquid phase by means of infra-red absorption spectroscopy, D. L. Fry, R. E. Nusbaum, and H. M. Randall—150
Hysteresis and related elastic properties of tire cords, Helmut Wakeham and Edith Honold—698

Impedance matching, Shunt and series sections of transmission line for, C. T. Tai—44
Impedance, Measured impedance of cylindrical dipoles, D. D. King—844
Improvement of resolution in electron diffraction cameras, James Hillier and R. F. Baker—12
Improvements in the stability of the FP-54 electrometer tube, J. M. Lafferty and K. H. Kingdon—894
Induction heating of hollow metallic cylinders, Andrew Gemant—195
Infra-red absorption, Analyses of mixtures of light gases by, Norman D. Coggeshall and Eleanor L. Saier—450
Infra-red absorption spectroscopy, Analysis of multicomponent mixtures of hydrocarbons in the liquid phase by means of, D. L. Fry, R. E. Nusbaum, and H. M. Randall—150
Infra-red, Applications of infra-red methods in the structural examination of synthetic rubber, J. E. Field, D. E. Woodford, and S. D. Gehman—386
Infra-red spectroscopy, Small prism, R. Bowling Barnes, Robert S. McDonald, and Van Zandt Williams—532 (erratum)
Integral equations of potential theory, Some, H. Bateman—91
Interchange of energy between an electron beam and an oscillating electric field, Jess Marcum—4
Internal friction and plastic extension of zinc single crystals Thomas A. Read and E. P. T. Tyndall—713
Interpolation with the aid of a plot of first differences, Gordon S. Fulcher—617
Interpretation of Harker syntheses, M. J. Buerger—579
Investigation, Experimental, of forced vibrations in a mechanical system having a non-linear restoring force, Carl A. Ludeke—603
Investigation of secondary phases in alloys by electron diffraction and the electron microscope, R. D. Heidenreich, L. Sturkey, and H. L. Woods—127
Ionized water films, Formation of, on dielectrics under conditions of high humidity, Robert F. Field—318

Jet projectile, Approximate calculation of the range of a winged jet projectile, M. Zbigmew Krzywoblocki—515
Journal of Applied Physics, Reconversion of the—1

Laplace's equation, Numerical solution of, in composite rectangular areas, Max M. Frocht—730
Lead loss, Methods of minimizing lead loss in emissivity and resistivity determinations, L. Malter and D. B. Langmuir—456
Light gases, Analyses of mixtures of light gases by infrared absorption, Norman D. Coggeshall and Eleanor L. Saier—450
Light scattering measurements, Photoelectric instrument for light scattering measurements and a differential refractometer, P. P. Debye—392
Lightning recorded by aeroplane propeller, J. M. Bryant and M. Newman—555
Linear simultaneous equations, Computer for solving, Clifford E. Berry, Doyle E. Wilcox, Sibyl M. Rock, and H. W. Washburn—262
Linear simultaneous equations, Computer for solving, C. C. Eaglesfield; Clifford E. Berry—1125 (L)
Linear systems, Transient analysis of, using underwater explosion waves, M. F. M. Osborne and J. L. Carter—871
Liquid rise in a capillary tube, Wesley E. Brittin—37
Lorentz and polarization factors, Correction of diffraction amplitudes for, M. J. Buerger and Gilbert E. Klein—285
—— 743 (erratum)
Luminescence of $(Zn, Be)_2SiO_4$:Mn and other manganese-activated phosphors, James H. Schulman—902

Machine for the application of sand in making Fourier projections of crystal structures, Dan McLachlan, Jr., and E. F. Champaygne—1006
Magnetically-controlled gas discharge tubes, R. E. B. Makinson, J. M. Somerville, K. Rachel Makinson, and P. Thonemann—567
Magnetrons, Energy build-up in, Lloyd P. Hunter—833
Maximum gain-band width product in amplifiers, W. W. Hansen—109 (erratum)
Measured impedance of cylindrical dipoles, D. D. King—844
Mechanical system having a non-linear restoring force, Experimental investigation of forced vibrations in a, Carl A. Ludeke—603
Metallic shadow-casting, Applications of metallic shadow-casting to microscopy, Robley C. Williams and Ralph W. G. Wyckoff—23
Metallurgical laboratory of Chicago, Theoretical physics in the, E. P. Wigner—857; Addendum—1130
Metals, Problems in fracture of, J. H. Hollomon and C. Zener—82
Metals, Problems in non-elastic deformation of, Clarence Zener and J. H. Hollomon—69
Method of determining the size of droplets dispersed in a gas, R. L. Stoker—243
Method for preparing rubber latex specimens for the electron microscope, R. H. Kelsey and E. E. Hanson—675
Methods for betatron or synchrotron beam removal, Eugene C. Crittenden, Jr., and William E. Parkins—444
Methods of minimizing lead loss in emissivity and resistivity determinations, L. Malter and D. B. Langmuir—456
Microscopy, Applications of metallic shadow-casting to, Robley C. Williams and Ralph W. G. Wyckoff—23
Microwave dielectric loss measuring technique, William R. MacLean—558
Microwave propagation, Asymptotic solutions for the normal modes in the theory of, C. L. Pekeris—1108
Microwaves, Absorption of microwaves by gases. W. D. Hershberger—495
—— Part II, John E. Walter and W. D. Hershberger—814
Microwaves, Perturbation theory of the normal modes for an exponential *M*-curve in non-standard propagation of microwaves, C. L. Pekeris—678
Midwest Research Institute—a new scientific research institution, George E. Ziegler—669
Millimeter-wave reflex oscillator, J. M. Lafferty—1061

New bridge photo-cell employing a photo-conductive effect in silicon. Some properties of high purity silicon, G. K. Teal, J. R. Fisher, and A. W. Treptow—879
New electrolytic selenium photo-cell, A. von Hippel, J. H. Schulman, and E. S. Rittner—215
New method for measuring dielectric constant and loss in the range of centimeter waves. S. Roberts and A. von Hippel—610
Noise, Response of biased, saturated linear and quadratic rectifiers to random noise, David Middleton—778
Non-linear mixers, Calculation of the output from, Harry Stockman—110
Non-uniform transmission lines and reflection coefficients, L. R. Walker and N. Wax—1043
Nosed-in cavity, Resonant frequencies of the, Ernest Mayer—1046
Note on a paper of H. Bateman, F. W. J. Olver—1127 (L)
Novel form of refrigerator, Jenny E. Rosenthal—62 (L)
Numerical solution of Laplace's equation in composite rectangular areas, Max M. Frocht—730

Oils, Thermal polymerization of drying oils, H. E. Adams and P. O. Powers—325
Oscillation conditions in single tuned amplifiers, William R. Faust and Hugo M. Beck—749
Oscillator, Millimeter-wave reflex oscillator, J. M. Lafferty—1061
Oxide cathodes, Pulsed properties of, Edward A. Coomes—647
Oxide cathodes, Study of, by x-ray diffraction methods. Part I. Methods, conversion studies, and thermal expansion coefficients, A. Eisenstein—434
—— Part II. Oxide coating composition—654
Oxide coated cathode literature, 1940–1945, John P. Blewett—643
Oxide coated cathodes, Dissociation energies of surface films of various oxides as determined by emission measurements of, Harold Jacobs—596
Oxide coated cathodes, Studies of the interface of, A. Fineman and A. Eisenstein—663
Ozone, Recent ozone investigations, Arthur W. Ewell—908

Parafocusing properties of microcrystalline powder layers in x-ray diffraction applied to the design of x-ray goniometers, J. C. M. Brentano—420
Parallel plate plastometer, Theory and application of the, G. J. Dienes and H. F. Klemm—458
Particle accelerator, Study of a certain type of resonant cavity and its application to a charged particle accelerator, E. S. Akeley—1056
Particle size determination from x-ray line broadening, L. S. Birks and H. Friedman—687
Particle size distribution, Preparation of electron microscope specimens for determination of particle size distribution in aqueous suspensions, A. M. Cravath, A. E. Smith, J. R. Vinograd, and J. N. Wilson—309
Particle trajectories, Graphical method for determining particle trajectories, William E. Parkins and Eugene C. Crittenden, Jr.—447
Permeability of different rubbers to gases and its relation to diffusivity and solubility, G. J. van Amerongen—972
Perturbation theory of the normal modes for an exponential M-curve in non-standard propagation of microwaves, C. L. Pekeris—678
Phosphors, Luminescence of $(Zn, Be)_2SiO_4$:Mn and other manganese-activated phosphors, James H. Schulman—902
Phosphors, Thermoluminescence and conductivity of, Robert C. Herman and Charles F. Meyer—743
Photo-cell, New bridge photo-cell employing a photoconductive effect in silicon. Some properties of high purity silicon, G. K. Teal, J. R. Fisher, and A. W. Treptow—879
Photo-cell, New electrolytic selenium photo-cell, A. von Hippel, J. H. Schulman, and E. S. Rittner—215
Photoelectric instrument for light scattering measurements and a differential refractometer, P. P. Debye—392
Photo-multiplier tube, Calculated frequency spectrum of the shot noise from a, R. D. Sard—768
Picturesque oxidation of molybdenum vacuum-tube leads, Herman A. Liebhafsky—901
Pigments, Preparing pigments for the electron microscope, A. M. Cravath—1125 (L)
Pipes, Transient temperatures around heating pipes maintained at constant temperature, Andrew Gemant—1076
Planckian distributions, Approximations to, Parry Moon and Domina Eberle Spencer—506
Plane rotations in n dimensions, Peter T. Landsberg—60 (L)
Plastic extension, Internal friction and plastic extension of zinc single crystals, Thomas A. Read and E. P. T. Tyndall—713
Plastic flow, creep, and stress relaxation. Part I—Plastic flow, Charles Mack—1086
—— Part II—Creep—1093
—— Part III—Creep and elastic after-effect—1101
Plastic flow, Effect of hydrostatic pressure on plastic flow under shearing stress, P. W. Bridgman—692
Plastic flow of steel, Studies of, especially in two-dimensional compression, P. W. Bridgman—225
Polymer cuprene, Electron microscope examination of the microphysical properties of the, John H. L. Watson and K. Kaufmann—996
Polymer, Division of High Polymer Physics, Abstracts—405
Polymerization, Thermal polymerization of drying oils, H. E. Adams and P. O. Powers—325
Polymers, Thermal expansion and second-order transition effects in high polymers. III. Time effects, R. S. Spencer and R. F. Boyer—398
Polymers, Viscometric investigation of dimethylsiloxane polymers, Arthur J. Barry—1020
Power function, Fidel Alsina Fuertes—712 (L)
Preparation of electron microscope specimens for determination of particle size distribution in aqueous suspensions, A. M. Cravath, A. E. Smith, J. R. Vinograd, and J. N. Wilson—309
Preparing pigments for the electron microscope, A. M. Cravath—1125 (L)
Pressure-volume relation for cylindrical tubes with elastomeric walls: the human aorta, Allen L. King—501
Problems in fracture of metals, J. H. Hollomon and C. Zener—82
Problems in non-elastic deformation of metals, Clarence Zener and J. H. Hollomon—69
Production of high centrifugal fields, J. W. Beams, J. L. Young, III, and J. W. Moore—886
Properties of welded contact germanium rectifiers, H. Q. North—912
Proportion of crystalline and amorphous components in stretched vulcanized rubber, A. J. Wildschut—51
Pulsed properties of oxide cathodes, Edward A. Coomes—647
Pulsed signal, Theoretical comparison of the visual, aural, and meter reception of pulsed signal in the presence of noise, J. H. Van Vleck and David Middleton—940
Pyrex glass, Secondary electron emission of, C. W. Mueller—62 (erratum)

Radar reflections from long conductors, F. Bloch, M. Hamermesh, and M. Phillips—1015
Radiofrequencies, Electrical resistance of iron wires and permalloy strips at, Alva W. Smith, J. H. Gregory, and J. T. Lynn—33
Range of centimeter waves, New method for measuring dielectric constant and loss in the, S. Roberts and A. von Hippel—610
Rayon, Fine structure of viscose rayon, H. G. Ingersoll—924
Rayon tire cord, Fatigue failure of, R. C. Waller and W. E. Roseveare—482
Recent ozone investigations, Arthur W. Ewell—908
Reconversion of the Journal of Applied Physics—1
Rectifiers, Properties of welded contact germanium rectifiers, H. Q. North—912
Rectifiers, Response of biased, saturated linear and quadratic rectifiers to random noise, David Middleton—778
Reflection coefficients, Non-uniform transmission lines and, L. R. Walker and N. Wax—1043

Refractometer, Photoelectric instrument for light scattering measurements and a differential refractometer, P. P. Debye—392
Refrigerator, Novel form of, Jenney E. Rosenthal—62 (L)
Relation between nodal positions and standing wave ratio in a composite transmission system, Eugene Feenberg—530
Report of the Committee on Resolution of the Electron Microscope Society of America—989
Representation of rigid rotations. H Schwerdtfeger—109 (erratum)
Resonant cavity, Study of a certain type of, and its application to a charged particle accelerator, E. S. Akeley—1056
Resonant circuit modulator for broad band acoustic measurements, Gordon Ferrie Hull, Jr.—1066
Resonant frequencies of the nosed-in cavity, Ernest Mayer—1046
Response of biased, saturated linear and quadratic rectifiers to random noise, David Middleton—778
Rigid rotations, On the representation of, H. Schwerdtfeger—109 (erratum)
Rubber, Applications of infra-red methods in the structural examination of synthetic rubber, J. E. Field, D. E. Woodford, and S. D. Gehman—386
Rubber, Crystallization of unvulcanized rubber at different temperatures, Lawrence A. Wood and Norman Bekkedahl—362
Rubber, Electrostatic and tensile properties of rubber and GR-S at elevated temperatures, R. S. Havenhill, H. C. O'Brien, and J. J. Rankin—338
Rubber latex, Method for preparing rubber latex specimens for the electron microscope, R. H. Kelsey and E. E. Hanson—675
Rubber, On the proportion of crystalline and amorphous components in stretched vulcanized rubber, A. J. Wildschut—51
Rubber, Significance of the equation of state for rubber, Eugene Guth, Paul E. Wack, and Robert L. Anthony—347
Rubber supports, Dynamic characteristics of rubber supports from vibration table data, Ernest G. Chilton—492
Rubber vulcanizates, Theory of permanent set at elevated temperatures in natural and synthetic rubber vulcanizates, R. D. Andrews, A. V. Tobolsky, and E. E. Hanson—352
Rubbers, Permeability of different rubbers to gases and its relation to diffusivity and solubility, G. J. van Amerongen—972

Sand, Machine for the application of sand in making Fourier projections of crystal structures, Dan McLachlan, Jr., and E. F. Champaygne—1006
Secondary electron emission of Pyrex glass, C. W. Mueller—62 (erratum)
Shells, Vibrations of shallow spherical shells, Eric Reissner—1038
Shunt and series sections of transmission line for impedance matching, C. T. Tai—44
Signal bunching, Theory of small signal bunching in a parallel electron beam of rectangular cross section, Eugene Feenberg and David Feldman—1025
Significance of the equation of state for rubber, Eugene Guth, Paul E. Wack, and Robert L. Anthony—347
Silicon, New bridge photo-cell employing a photo-conductive effect in silicon. Some properties of high purity silicon, G. K. Teal, J. R. Fisher, and A. W. Treptow—879
Small prism infra-red spectroscopy, R. Bowling Barnes, Robert S. McDonald, and Van Zandt Williams—532 (erratum)
Solid solutions, Coordination number in solid solutions—a mathematical paradox, Douglas Rennie Hudson—1126 (L)
Some integral equations of potential theory, H. Bateman—91
Spark shadowgraphic study of body waves in water, J. Howard McMillen and E. Newton Harvey—541
Spectroscopy, Electronic, George C. Sziklai and Alfred C. Schroeder—763
Static strength testing apparatus, Wide range, for glass rods, T. C. Baker and F. W. Preston—162
Steel, Electrical observations of the Austenite-Martensite transformation in, Andrew W. McReynolds—823
Steel, Studies of plastic flow of steel, especially in two-dimensional compression, P. W. Bridgman—225
Steels, Tensile properties of several special steels and certain other materials under pressure, P. W. Bridgman—201
Stress relaxation, Elastic properties of cork. I. Stress relaxation of compressed cork, S. L. Dart and Eugene Guth—314
Stress relaxation, Plastic flow, creep, and stress relaxation. Part I—Plastic flow, Charles Mack—1086
—— Part II—Creep—1093
—— Part III—Creep and elastic after-effect—1101
Stresses in cylindrical glass-metal seals with glass inside, Albert W. Hull—685
Structure of glass, Use of color and fluorescence indicators for determining the, W. A. Weyl—628
Studies of the interface of oxide coated cathodes, A. Fineman and A. Eisenstein—663
Studies of plastic flow of steel, especially in two-dimensional compression, P. W. Bridgman—225
Study of a certain type of resonant cavity and its application to a charged particle accelerator, E. S. Akeley—1056
Study of distortion in electron microscope projection lenses, James Hillier—411
Study of oxide cathodes by x-ray diffraction methods. Part I. Methods, conversion studies, and thermal expansion coefficients, A. Eisenstein—434
—— Part II. Oxide coating composition—654
Supplementary bibliography of electron microscopy, Mary E. Rathbun, Mary J. Eastwood, and Orlan M. Arnold—759
Surface films of various oxides as determined by emission measurements of oxide coated cathodes, Dissociation energies of, Harold Jacobs—596
Surface tension, Gerald Pickett—61 (L)

Synchrotron, Methods for betatron or synchrotron beam removal, Eugene C. Crittenden, Jr., and William E. Parkins—444

Tackiness of GR-S and other elastomers, W. F. Busse, J. M. Lambert, and R. B. Verdery—376
Temperatures, Transient temperatures around heating pipes maintained at constant temperature, Andrew Gemant—1076
Tensile properties of several special steels and certain other materials under pressure, P. W. Bridgman—201
Theoretical comparison of the visual, aural, and meter reception of pulsed signal in the presence of noise, J. H. Van Vleck and David Middleton—940
Theoretical physics in the metallurgical laboratory of Chicago, E. P. Wigner—857; Addendum—1130
Theory and application of the parallel plate plastometer, G. J. Dienes and H. F. Klemm—458
Theory of permanent set at elevated temperatures in natural and synthetic rubber vulcanizates, R. D. Andrews, A. V. Tobolsky, and E. E. Hanson—352
Theory of small signal bunching in a parallel electron beam of rectangular cross section, Eugene Feenberg and David Feldman—1025
Thermal expansion and second-order transition effects in high polymers. III. Time effects, R. S. Spencer and R. F. Boyer—398
Thermal polymerization of drying oils, H. E. Adams and P. O. Powers—325
Thermoluminescence and conductivity of phosphors, Robert C. Herman and Charles F. Meyer—743
Thin cylindrical antenna: a comparison of theories, David Middleton and Ronold King—273
Tire cords, General relations of flow in solids and their application to the plastic behavior of, W. James Lyons—472
Tire cords, Hysteresis and related elastic properties of, Helmut Wakeham and Edith Honold—698
Transient analysis of linear systems, using underwater explosion waves, M. F. M. Osborne and J. L. Carter—871
Transient temperatures around heating pipes maintained at constant temperature, Andrew Gemant—1076
Transmission lines, Non-uniform, and reflection coefficients, L. R. Walker and N. Wax—1043
Transmission system, Relation between nodal positions and standing wave ratio in a composite transmission system, Eugene Feenberg—530
Tubes, Magnetically-controlled gas discharge tubes, R. E. B. Makinson, J. M. Somerville, K. Rachel Makinson, and P. Thonemann—567

Underwater explosion waves, Transient analysis of linear systems, using underwater explosion waves, M. F. M. Osborne and J. L. Carter—871
Use of color and fluorescence indicators for determining the structure of glass, W. A. Weyl—628

Vacuum-tube leads, Picturesque oxidation of molybdenum vacuum-tube leads, Herman A. Liebhafsky—901
Velocity modulation system, Elementary treatment of longitudinal debunching in a, Eugene Feenberg—852
Vibrations, forced, in a mechanical system having a non-linear restoring force, Experimental investigation of, Carl A. Ludeke—603
Vibrations of shallow spherical shells, Eric Reissner—1038
Viscometric investigation of dimethylsiloxane polymers, Arthur J. Barry—1020
Viscose rayon, Fine structure of, H. G. Ingersoll—924

Water, Effect of water on the strength of glass, T. C. Baker and F. W. Preston—179
Wide range static strength testing apparatus for glass rods, T. C. Baker and F. W. Preston—162
Wires, Electrical resistance of iron wires and permalloy strips at radiofrequencies, Alva W. Smith, J. H. Gregory, and J. T. Lynn—33

X-ray diffraction methods, Study of oxide cathodes by x-ray diffraction methods. Part I. Methods, conversion studies, and thermal expansion coefficients, A. Eisenstein—434
—— Part II. Oxide coating composition—654
X-ray diffraction, Parafocusing properties of microcrystalline powder layers in x-ray diffraction applied to the design of x-ray goniometers, J. C. M. Brentano—420
X-ray goniometers, Parafocusing properties of microcrystalline powder layers in x-ray diffraction applied to the design of x-ray goniometers, J. C. M. Brentano—420
X-ray line broadening, Particle size determination from, L. S. Birks and H. Friedman—687
X-ray method for measuring the thickness of thin crystalline films, A. Eisenstein—874
X-ray microradiographs, Composition and diffraction effects in, R. Smoluchowski, C. M. Lucht, and J. M. Hurd—864

Zinc single crystals, Internal friction and plastic extension of, Thomas A. Read and E. P. T. Tyndall—713
$(Zn, Be)_2SiO_4$:Mn and other manganese-activated phosphors, Luminescence of, James H. Schulman—902

Eimac TUBES — THE COUNTERSIGN OF DEPENDABILITY IN ANY ELECTRONIC EQUIPMENT

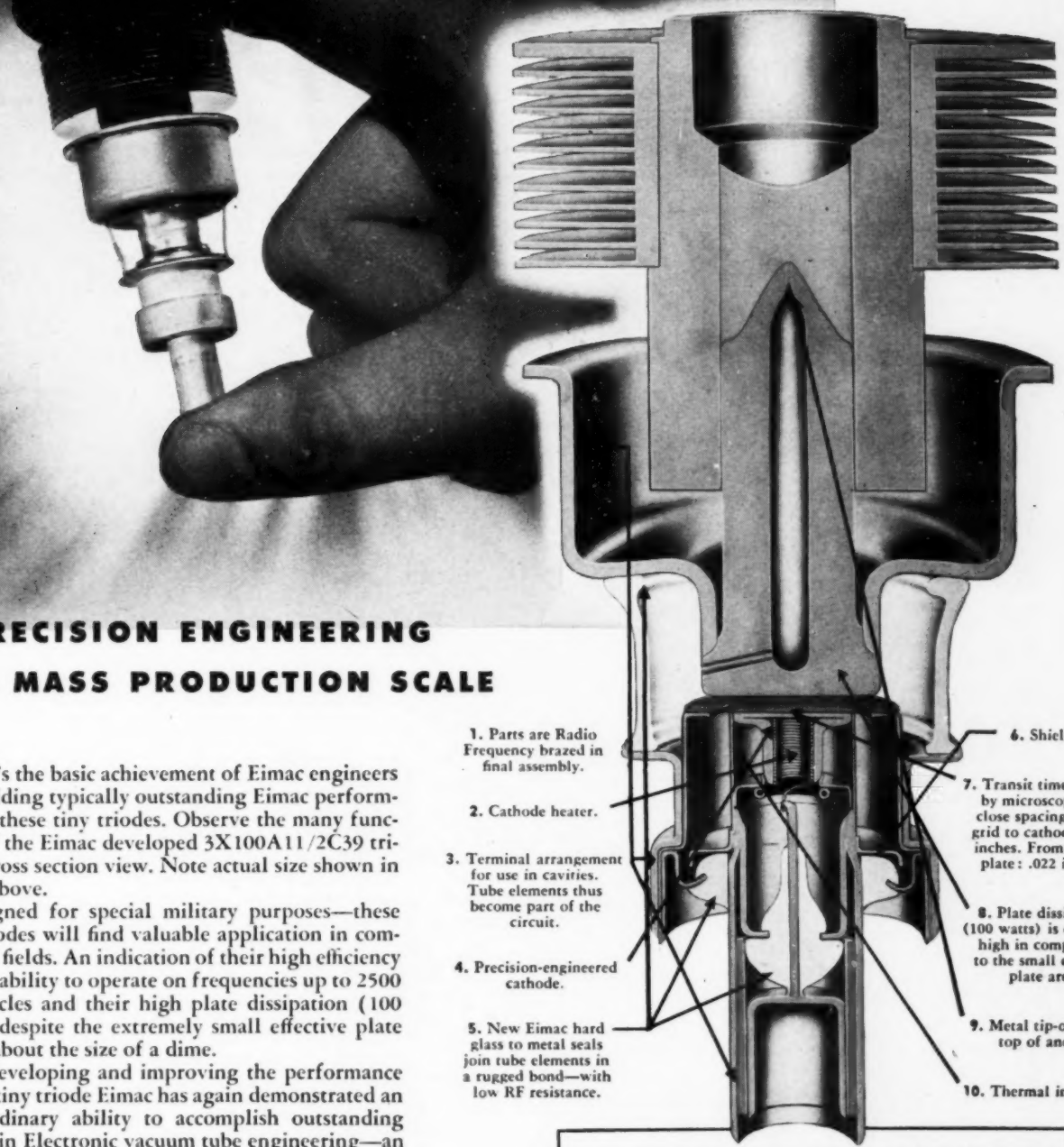
1. Parts are Radio Frequency brazed in final assembly.
2. Cathode heater.
3. Terminal arrangement for use in cavities. Tube elements thus become part of the circuit.
4. Precision-engineered cathode.
5. New Eimac hard glass to metal seals join tube elements in a rugged bond—with low RF resistance.
6. Shield.
7. Transit time reduced by microscopically close spacing. From grid to cathode: .005 inches. From grid to plate: .022 inches.
8. Plate dissipation (100 watts) is extremely high in comparison to the small effective plate area.
9. Metal tip-off at the top of anode.
10. Thermal insulation.

PRECISION ENGINEERING ON A MASS PRODUCTION SCALE

... that's the basic achievement of Eimac engineers in providing typically outstanding Eimac performance in these tiny triodes. Observe the many functions of the Eimac developed 3X100A11/2C39 triode—cross section view. Note actual size shown in photo above.

Designed for special military purposes—these tiny triodes will find valuable application in commercial fields. An indication of their high efficiency is their ability to operate on frequencies up to 2500 megacycles and their high plate dissipation (100 watts) despite the extremely small effective plate area—about the size of a dime.

By developing and improving the performance of this tiny triode Eimac has again demonstrated an extraordinary ability to accomplish outstanding results in Electronic vacuum tube engineering—an ability which has established Eimac as first choice of leading Electronics engineers throughout the world.

1148

FOLLOW THE LEADERS TO Eimac TUBES

EITEL-McCULLOUGH, INC., 1148 San Mateo Ave., San Bruno, Calif.

Plants located at: San Bruno, Calif., and Salt Lake City, Utah

Export Agents: Frazar and Hansen, 301 Clay St., San Francisco 11, Calif., U S.A.

TYPE 3X100A11/2C39 EIMAC TRIODE
GENERAL CHARACTERISTICS

ELECTRICAL	
Cathode: Coated unitpotential	
Heater Voltage	6.3 volts
Heater Current	1.1 amps
Amplification Factor (Average) 100	
Direct Interelectrode Capacitances (Average)	
Grid-Plate	1.95 μμfd
Grid-Cathode	6.50 μμfd
Plate-Cathode	0.030 μμfd
Transconductance (i_B=75 ma., E_B=600 v.) (Av.)	20,000 μmhos
Maximum Plate Dissipation	100 watts
MECHANICAL	
-Maximum Overall Dimensions	
Length . 2.75 inches	Diameter . 1.26 inches

CALL IN AN EIMAC ENGINEER FOR RECOMMENDATIONS

ROYAL J. HIGGINS (W9AIO).. 600 South Michigan Avenue, Room 818, Chicago 5, Illinois. Phone: Harrison 5948. Illinois, Wisconsin, Michigan, Indiana, Ohio, Kentucky, Minnesota, Missouri, Kansas, Nebraska and Iowa.

VERNER O. JENSEN, General Sales Co., 2616 Second Avenue, Seattle 1, Washington. Phone: Elliott 6871. Washington, Oregon, Idaho and Montana.

M. B. PATTERSON (W5CI)...1124 Irwin-Kessler Bldg., Dallas 1, Texas. Phone: Central 5764. Texas, Oklahoma, Arkansas and Louisiana.

ADOLPH SCHWARTZ (W2CN)...220 Broadway, Room 2210, New York 7, N Y. Phone: Cortland 7-0011. New York, Pennsylvania, New Jersey, Maryland, Delaware and District of Columbia.

HERB B. BECKER (W6QD)...1406 South Grand Avenue, Los Angeles 15, California. Phone: Richmond 6191. California, Nevada and Arizona.

TIM COAKLEY (W1KKP)...11 Beacon St., Boston 8, Mass. Phone: Capitol 0050. Maine, Vermont, New Hampshire, Massachusetts, Connecticut, Rhode Island.

CAUTION! Look for the latest serial numbers on Eimac Tubes. Be sure you get the newest types.

Recent Applications of Physics

Prepared by CLARK GOODMAN, Associate Editor

Material to be included in this section should be submitted to Dr. Clark Goodman, Massachusetts Institute of Technology, Cambridge 39, Massachusetts.

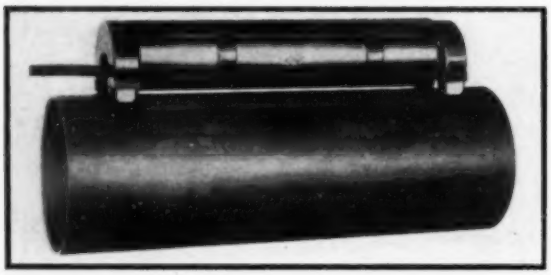

Thickness Measurements Routine checks to determine the thickness of the walls of pipes or pressure vessels are quickly and easily made with an uncertainty of about 3 percent by means of a new gamma-ray device known as the Penetron. This instrument, developed by Dr. Gerhard Herzog of the Texas Company, measures either the amount of radiation transmitted through the wall or the amount of back-scattered radiation, depending on whether a 1-mg radium source is placed inside or outside the pipe or vessel. The detector is a special type of Geiger-Müller counter. The pulses from the counter are amplified and integrated to produce a direct current measured by a microammeter.

The magnetic holder shown in the above figure has been designed to place the counter in a fixed geometry on ferrous tubing. The power supply, amplifier, and integrating circuit are contained in a single unit, shown below, which operates from a 110-volt 60-cycle line.

The Penetron measures the average thickness of metal over an area of approximately one square inch. Calibration is by means of tubing and flat plates of appropriate thickness and composition. If the pipe or vessel contains fluid, the calibration must include this material. Conversely, the specific gravity of fluids in closed containers or pipes of known thickness can be determined with fair accuracy.

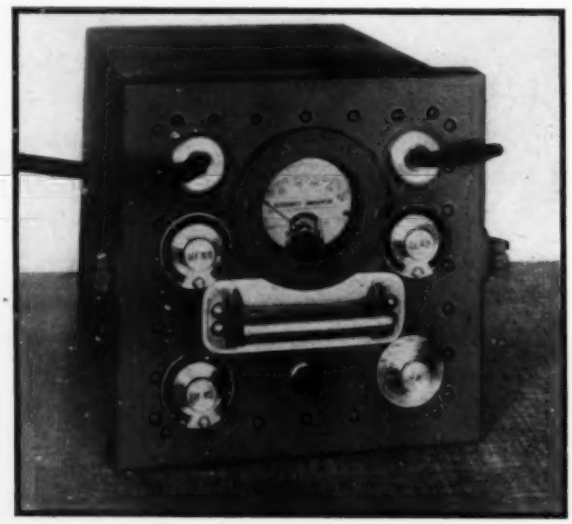

Highway Traffic With the rescission of gasoline rationing, the increase in highway traffic has not only replaced "A," "B," and "C" coupons as a subject of conversation, but has become one of the important post-war problems. A number of recent articles have shown an increasing realization of the need for a scientific approach to this subject. Systematic studies have been made of the skidding characteristics of tires on roadway surfaces and of the stopping distance and brake condition of automotive vehicles. A particularly timely investigation[1] has been an application of principles of physics to traffic movements and road conditions.

Traffic is considered as a flow of successive *influence spaces* through a continuous system of channels. Each vehicle occupies a mathematically defined, two-dimensional area whose width is slightly greater than the actual width of the vehicle and whose length is the sum of three terms: (i) the distance traveled during the perception and reaction time of the driver, (ii) the distance required to stop after application of the brakes, and (iii) the actual length of the vehicle plus a reasonable separation of vehicles at rest. Using these simple concepts, it is possible to establish absolute and relative efficiencies of highways as regards traffic volumes and to dictate optimum speeds for safe and efficient utilization of arteries of traffic. Safety is assured if the influence spaces do not overlap, economy of traffic if there are no wide gaps between the influence spaces. Optimum speeds, arrangements of intersections, and timing and spacing of signals are derivable from these studies. Numerous common misconceptions are revealed. For example, it is easily shown that the capacity of a highway with many intersections is not increased by introducing the progressive traffic-signal system, where signals are timed with respect to each other so as to allow undelayed motion at a planned speed, even though this system may be beneficial to the individual driver.

It seems highly desirable for our post-war design of new highways and reorganization of existing traffic facilities to be based on a real scientific study of the problem, rather than the rule-of-thumb methods that have been used so prevalently in the past.

---

[1] E. M. J. Herrey and H. Herrey, Am. J. Phys. **13**, 1–14 (1945).

Electrostatic Deposition The familiar Cottrell process recently has been used to improve the deposition of phosphors in the manufacture of fluorescent glass tubing and of abrasives in the manufacture of sandpaper.

The conventional process for coating fluorescent tubing has been to allow a suspension of phosphor powder in solution to flow through the carefully cleaned glass tubing. The liquid is removed by subsequent baking. In the electrostatic method, using Westinghouse Precipitrons, the tubing is slipped over an electrically charged wire which serves to ionize a smoke of the dry phosphor as it is blown through the tube. The phosphor particles acquire a positive charge and under the influence of the strong electrostatic field are driven to the glass walls where they give up their charge and adhere firmly. A blast of moisture-saturated warm air smooths the inner surface. The liquid-flow method causes some draining which results in a non-uniform deposition. The greater uniformity of the electrical method increases the light efficiency by three to four percent. The hazard attendant to volatile solvents and the need for cleaning of the tubing are eliminated by this newer technique.

In the manufacture of sandpaper, the sifted abrasive particles are fed from a hopper to an endless belt which carries them through a high-tension electrostatic field. Simultaneously, the glue-covered paper or cloth moves through the field above the belt. As a result of induced charges, the abrasive particles become oriented with their long axes normal to the backing surface and uniformly

A VERSATILE VACUUM!

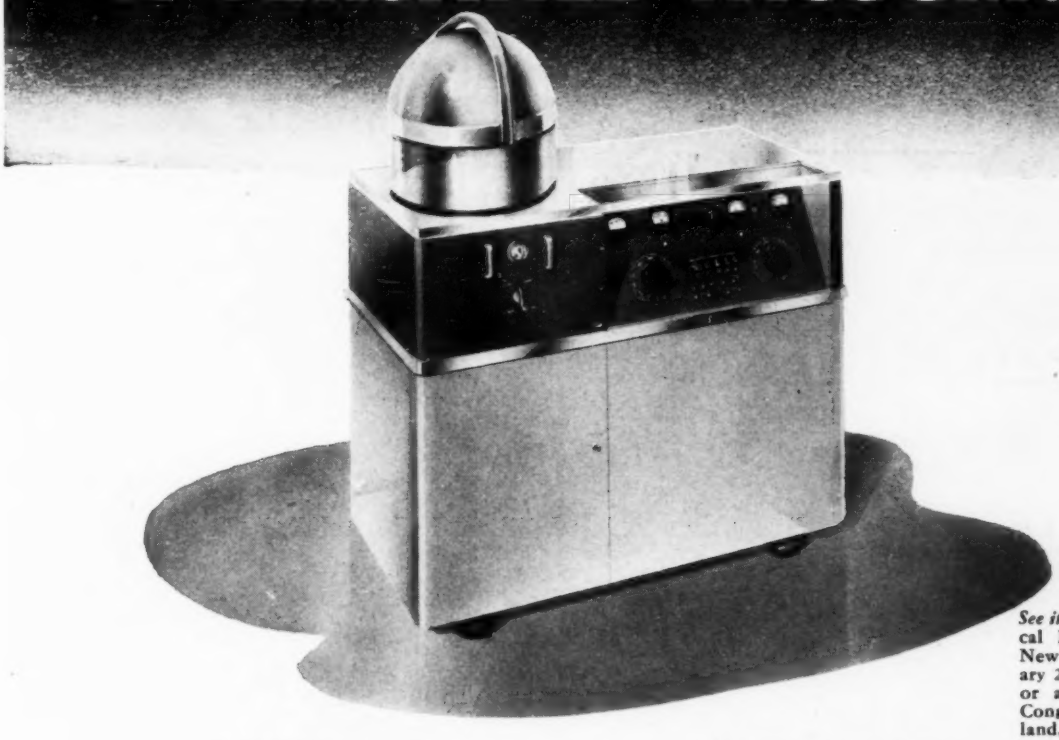

See it at the Chemical Exposition in New York, February 25 to March 2 or at the Metals Congress in Cleveland, Feb. 4 to 8.

NEW RCA VACUUM UNIT

speeds many laboratory and factory processes

Here are a few jobs this unit will help you do easier, quicker, and better: mirror making; lens coating; vacuum or freeze drying; evaporating, condensing, or sputtering of materials on metal or non-metallic surfaces; and experiments where various gases at reduced pressures are required.

The RCA vacuum unit (Type EMV) consists of a vacuum chamber or bell jar, a high-speed pumping system (with simplified valving) to evacuate it, a control system, and meters and gages for reading currents, voltages, and vacuum pressures.

Within the bell jar are nine pairs of terminals.

Six of these are each capable of carrying 50 amperes. They are used to light filaments for the evaporation of metals or other materials. The power available for these circuits is 5 kva.

Another set of terminals will carry up to 5000 volts at 80 milliamperes—useful for ionization cleaning and for sputtering metals.

The two remaining pairs are useful in making measurements in the vacuum chamber while it is being pumped out, and for supplying power to heaters or other equipment within the bell jar.

If desired, gases can be admitted into the vacuum chamber after the air is removed.

Two bell jars are provided: one 18 by 18 inches, the other 18 by 29 inches (height). A vacuum of better than ½ micron (mercury) pressure is rapidly achieved in 7 or 10 minutes depending upon the size of the chamber used.

Write for new bulletin today, c/o Dept. 44A.

RCA

SCIENTIFIC INSTRUMENTS

RADIO CORPORATION of AMERICA

ENGINEERING PRODUCTS DIVISION, CAMDEN, N.J.

distributed. The field is sufficient to cause the particles to move toward the upper electrode where they become firmly imbedded in the adhesive. Because the grains stand on end with their sharp points facing out, the cutting efficiency of such electrocoated papers is increased by 20 to 60 percent. Coatings of garnet, silicon carbide, and alumina can equally well be made in all grades from "fine" to "coarse."

Jet-Propulsion Engine As security restrictions are relaxed, there undoubtedly will be much interesting information released concerning jet propulsion. The first detailed description that has come to our attention is of an American jet engine developed by G. M. Giannini and Company in conjunction with the

U. S. Army Air Forces at Wright Field. A sectional view is shown in the above drawing. A test model, 2 feet in length, and approximately 2 inches in diameter, for use in wind-tunnel testing, is illustrated below. This engine is made of aluminum alloy and stainless steel, weighs only 5 ounces, but develops a thrust of 2 pounds. It is fully controllable, burns either gasoline or kerosene and, after being started by means of a small spark plug, runs without ignition at a firing rate up to about 250 explosions per second. The efficiency is sufficient to enable the engine, plus a small light-weight fuel tank, to be launched from an inclined platform and to fly through the air without wings.

Potential use of the full-scale engine is still a subject under governmental restriction. However, it is evident that the engine is only practical for aircraft traveling at speeds of greater than 500 miles per hour, that is in the neighborhood of sonic velocities or greater.

Photo Strain Test A previous article[1] described the use of strain gauges and brittle lacquer coatings for strain measurements. Grid patterns have also been used for this purpose, but the application of the fine rulings is often tedious and difficult. Douglas Aircraft and Carnegie Illinois Steel have simplified the problem by employing a new light sensitive paint known as Transfax. The material is applied with an ordinary spray gun, after which a reduced negative of linear coordinate graph paper is placed in contact with the metal and the whole exposed for a few minutes to the light of a flood-type lamp. The surface of the metal is washed with a weak solution of ammonia water and a fine grid

remains as a set of narrow white lines. As shown in the photograph, these lines are examined with a low power microscope which includes a reticle having accurately spaced parallel lines. By aligning the reticle pattern with the lines on the sample, a direct measure is made of the amount and direction of movement of the metal in the sample during the forming operation. From this information both elongation and compression of the material can be analyzed.

[1] J. App. Phys. **15**, xx (1944).

Timely
McGRAW-HILL BOOKS

PRINCIPLES OF RADAR

By Members of the Staff of the Radar School, Massachusetts Institute of Technology. Second edition. 960 pages, $5.00

Originally prepared for the technical training of Radar Officers in the Armed Forces, this text is devoted to the engineering principles of the pulse circuits and high-frequency devices common to nearly all radar equipment. Explanations of circuit operation are based on physical concepts and make free use of numerical examples.

AN INDEX OF MATHEMATICAL TABLES

By A. FLETCHER, J. C. P. MILLER and L. ROSENHEAD, University of Liverpool. 450 pages, $16.00

A complete index to all published and some unpublished mathematical tables, compiled by three of the foremost recognized experts in the international field of mathematical tables and their reliability. Part I is an index according to Functions. Part II is a complete list of the published material referred to in Part I, arranged alphabetically according to authors. The volume contains more than 2000 entries.

THE THEORY OF FUNCTIONS OF REAL VARIABLES

By LAWRENCE M. GRAVES, The University of Chicago. 321 pages, $4.00

A compact and well integrated presentation of the theorems and methods which are fundamental for research in analysis. The more essential and generally useful aspects of the theory of functions of real variables are treated in detail. Many topics not usually found in standard treatises are included, such as some of the theorems on implicit functions, differential equations, and Lebesgue and Stieltjes integrals.

WAVE PROPAGATION IN PERIODIC STRUCTURES. Electric Filters and Crystal Lattices

By LÉON BRILLOUIN, Columbia University. *International Series in Pure and Applied Physics.* 315 pages, $4.00

Incorporates a variety of problems linked by a common mathematical background, extending from electrical engineering to electromagnetism and wave mechanics of the spinning electron. All problems deal with periodic structures of various kinds, which invariably, whether they are electric lines or crystal lattices, behave like band-pass filters.

GERMAN-ENGLISH SCIENCE DICTIONARY. For Students in Chemistry, Physics, Biology, Agriculture, and Related Sciences. *New second edition.*

By LOUIS DE VRIES, Iowa State College. 558 pages, $4.50

This widely distributed volume has been revised to make it of greater use to chemists. At the same time, the number of terms in biology, physics, mathematics, geology, agriculture, and forestry have been substantially increased. Many more idioms have been added, and the number of abbreviations at least doubled. The appendix contains Conversion Table, Atomic Table, Thermodynamic Symbols, Electric Units of Measure, Abbreviations of Periodicals, List of Measurements, and Geographic Names.

Send for copies on approval

McGRAW-HILL BOOK COMPANY, Inc.

330 West 42nd Street **New York 18, N. Y.**

For Permanent Records

OF HIGH-SPEED PHENOMENA

THE NEW HEILAND CATHODE-RAY RECORDER

Type CR-43A

A wide frequency range, and compact, rugged construction make this new recorder ideally suited to both laboratory and field studies of high speed, transient or steady state, phenomena.

The HEILAND CR-43A Cathode-Ray Recorder has four recording channels, each consisting of a one-stage balanced amplifier direct-coupled to a 3" short persistence Cathode-Ray tube. Records are made of the waves appearing on the tube screen by a 35 mm. built-in camera which can be operated at one of four quickly selected speeds. The optical system can be readily shifted to photograph either 2 or 4 channels. Time markers are provided by means of a fork-controlled discharge tube producing 100 marks per second.

Daylight loading magazines assure easy film loading. A viewing door provides convenient visual observation. The response is flat from 0 to 40 Kc. direct or through the amplifiers.

Write today
for complete information to

Heiland Research Corporation
DENVER

STATHAM

PRESSURE TRANSMITTER

MODEL P10

The Model P10 Pressure Transmitter, newest member of our line of remote reading instruments, is now available.

Increased accuracy is combined with the simplicity of operation, ruggedness, small size and light weight which characterize all Statham Instruments.

Its high natural frequency permits measurements of the rapidly fluctuating pressures in fluid or gas lines. No elaborate amplifiers or other electronic equipment is required for most applications. Dry cells are usually suitable for the power supply, although the instruments may be used with an A. C. supply or a carrier system.

The indicating instrument may be a panel type microammeter, recording galvanometer recording potentiometer, or cathode ray oscilloscope.

A large selection of ranges is available, from 0-50 psi to 0-5000 psi.

Size: 1⅜ x 4 in.
Weight: 14 oz.

Statham Laboratories also makes Pressure Transmitters with full ranges as low as ± 0.2 psi, accelerometers, and dynamometers. Our engineering department is at your service to analyze your problem and make specific suggestions for solving them. Write for our catalog.

STATHAM LABORATORIES INSTRUMENT MAKERS

8222 BEVERLY BOULEVARD · LOS ANGELES 36, CALIF.

Physics books

by HENRY SEMAT

Associate Professor of Physics
College of The City of New York

INTRODUCTION TO ATOMIC PHYSICS

412 pp., $4.50

Revised and Enlarged

This successful text for the one-semester course in atomic physics has now been brought up to date. Highlights of the revision include

Major changes in the section on The Nucleus

New material on the discovery of new elements, sources of nuclear energy, the measurement of nuclear magnetic moments

More extensive treatment of the production of transuranic elements, the fission of nuclei, and nuclear isomers

A description of the betraton with diagrams and photograph.

FUNDAMENTALS OF PHYSICS

xii + 593 pp., $4.00

Selects topics of major importance and treats them fully.

Develops fundamentals with clarity in a scope restricted to that actually attainable in a first-year college course.

Solves illustrative examples in a way to encourage the student to understand rather than imitate method.

Rinehart & Company, Inc.

232 Madison Avenue **New York 16**

Super

NON-INDUCTIVE RESISTORS

FOR HIGH R-F USES

Sprague Koolohm type SIF super non-inductive resistors have solved many serious problems in high-frequency radar and communications work involving dummy loads and dummy antennae, line terminations, rhombic antenna phasing resistors, and others—wherever there is need for power wire-wound resistors having extremely small phase angles.

These SIF units are made in seven types, with power rating from 15 to 150 watts. Typical maximum phase angle values, measured at 3MC are as follows:

5 ohms to 26 ohms . . . 20°
27 ohms to 99 ohms . . . 12°
100 ohms and higher . . . 6°

For complete details write for the new catalog of Sprague Koolohm wire-wound resistors for every requirement.

A Large Government Laboratory Reports:

"Preliminary measurements on the Sample No. 878, Type 120SIF resistors have indicated that these resistors should fulfill the requirements of the intended service. Over a frequency range from 6 to 15 Mc and with six units connected in parallel the impedance (R±JX) varied from 49+J4.3 to 51+J6.3. At a frequency of 10 Mc and with each unit measured singly, the resistance of six units varied from 295 to 306.5 ohms and the reactance varied from 0 to −4.2 ohms. The higher reactance obtained for the parallel arrangement is partially due to the necessary connecting buss bars."

SPRAGUE ELECTRIC COMPANY
RESISTOR DIVISION NORTH ADAMS, MASS.

SPRAGUE KOOLOHM RESISTORS
Reg. U. S. Pat. Off.

WIRE-WOUND POWER TYPES • BOBBIN TYPES • METER MULTIPLIERS • MEGOMAX, ETC.

AMERICAN INSTITUTE OF PHYSICS

Member Societies: AMERICAN PHYSICAL SOCIETY OPTICAL SOCIETY OF AMERICA
ACOUSTICAL SOCIETY OF AMERICA SOCIETY OF RHEOLOGY
AMERICAN ASSOCIATION OF PHYSICS TEACHERS

Associated Societies: AMERICAN SOCIETY FOR X-RAY AND ELECTRON DIFFRACTION
ELECTRON MICROSCOPE SOCIETY OF AMERICA
PHYSICS CLUB OF CHICAGO PHYSICS CLUB OF PHILADELPHIA
PHYSICAL SOCIETY OF PITTSBURGH

FOR the most part, the expenses incurred in carrying out the work of the American Institute of Physics are defrayed by its Member Societies. The Institute exists to do the work which these Societies have assigned to it—work toward objectives which they have in common. These Societies are being materially aided by a significant added contribution from the dues of the Associates of the Institute. The Associates are a group of forward looking companies and laboratories who believe it is valuable to them and to America to maintain a vigorous advance of physical science. In aiding the Institute they are helping physicists to secure for themselves and their science the necessary opportunities and facilities for effective service to industry and to society in general.

Associates of the Institute

Allegheny Ludlum Steel Corporation
Aluminum Company of America
American Can Company
American Cyanamid Company
American Optical Company
Armour Research Foundation
The Atlantic Refining Company
The Barrett Division
Allied Chemical & Dye Corporation
Battelle Memorial Institute
Bausch & Lomb Optical Company
Bell & Howell Company
Bell Telephone Laboratories
Bendix Aviation Corporation
Boeing Aircraft Company
The Bristol Company
Bristol-Myers Company
Carbide & Carbon Chemicals Corporation
Celanese Corporation of America
Central Scientific Company
Columbia Broadcasting System, Inc.
Corning Glass Works
Crane Co.
The Detroit Edison Company
A. B. Dick Company
Douglas Aircraft Company, Inc.
Dow Chemical Company
E. I. du Pont de Nemours & Company
Eastman Kodak Company
Ethyl Corporation
Farnsworth Television & Radio Corporation
Federal Telecommunication Laboratories, Inc.
The Firestone Tire & Rubber Company
General Aniline & Film Corporation
General Electric Company
General Motors Corporation
The B. F. Goodrich Company
Grinnell Corporation
Gulf Research & Development Company
Hercules Powder Company
Humble Oil & Refining Company
Keuffel & Esser Co.
Koppers Company, Inc.
Leeds & Northrup Company
Lever Brothers Company
Libby-Owens-Ford Glass Company
Lockheed Aircraft Corporation
The Loomis Laboratory
Magnolia Petroleum Company
Massachusetts Institute of Technology
Department of Physics
Division of Industrial Cooperation
Midwest Research Institute
Monsanto Chemical Company
The National Cash Register Company
North American Philips Company, Inc.
Owens-Illinois Glass Company
Philco Corporation
Phillips Petroleum Company
Pittsburgh Plate Glass Company
Glass Division
Polaroid Corporation
The Pure Oil Company
Radio Corporation of America
Raytheon Manufacturing Company
Research Corporation
The Sharples Corporation, Research Laboratories
Shell Development Company
Sperry Gyroscope Company, Inc.
Sprague Electric Company
Standard Brands Incorporated
Standard Oil Development Company
Stromberg-Carlson Company
Sun Oil Company
Sylvania Electric Products Inc.
Taylor Instrument Companies
The Texas Company
Tung-Sol Lamp Works Inc.
Union Oil Company of California
Union Switch & Signal Company
United States Rubber Company
Universal Oil Products Company
Waugh Laboratories
Westinghouse Electric Corporation
Weston Electrical Instrument Corporation

The American Institute of Physics cordially invites other interested corporations to become its Associates and will welcome their inquiries addressed to the Director.

AMERICAN INSTITUTE OF PHYSICS, 57 EAST 55 STREET, NEW YORK 22, NEW YORK

INDUSTRIAL HIGH VACUUM COATING UNIT NO. 3103

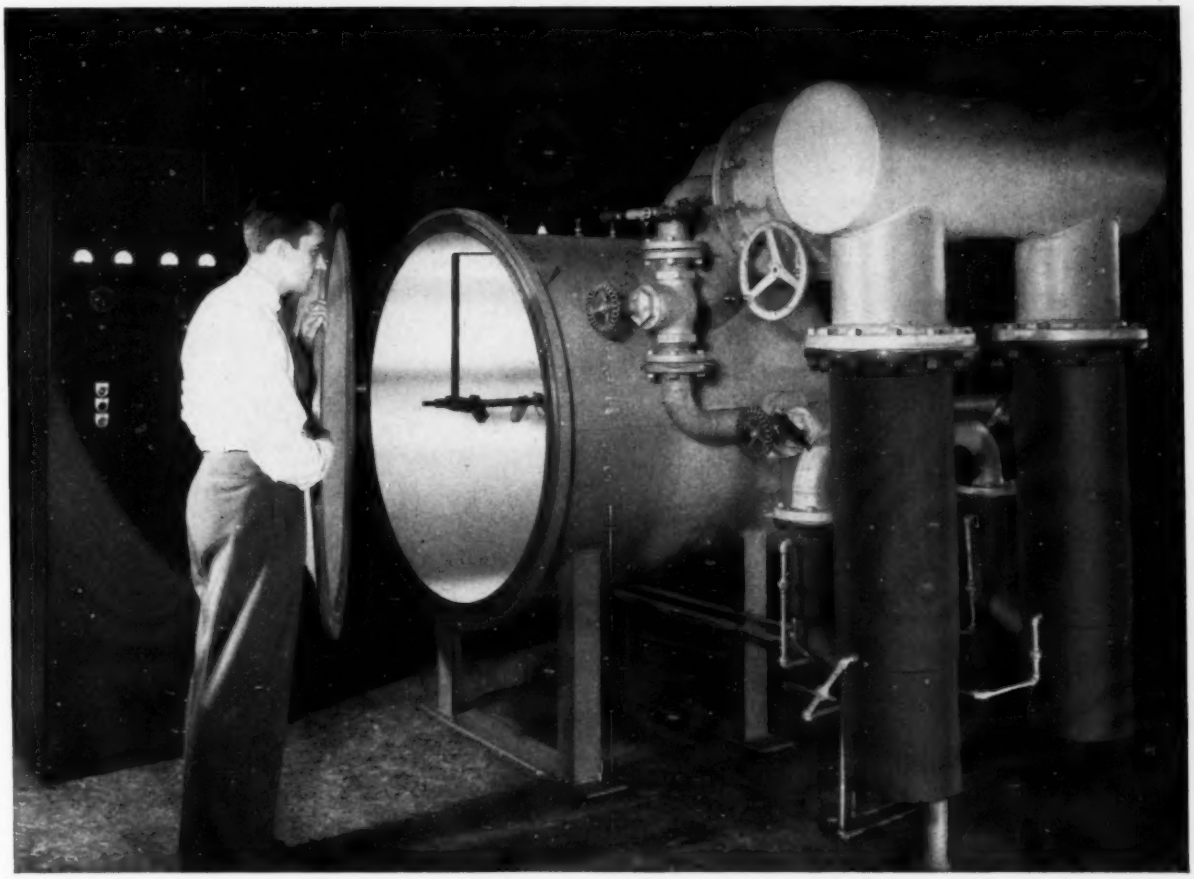

This High Vacuum Coating Unit is designed for low-cost production of evaporated films on glass and plastics.

The capacity of the stainless steel tank — 48" diameter, 48" long — makes possible processing of large batches and large pieces on a production basis.

The pumping system has ample speed to handle the outgassing of plastics and consistently maintains rapid coating cycles.

For further details, write VACUUM ENGINEERING DIVISION, National Research Corporation, Boston 15, Massachusetts.

HIGH VACUUM FOR INDUSTRY

NATIONAL RESEARCH CORPORATION

Vacuum ENGINEERING DIVISION

To suit each need . . .

POWERSTAT VARIABLE TRANSFORMERS

ARE MADE WITH VARIOUS TERMINAL ARRANGEMENTS

Shown above are three POWERSTATS of identical physical and electrical size. Each unit is rated at 115 volts, 50/60 cycles, single phase input with 0-135 volts, 15.0 amperes output. The difference is in terminal arrangement. This is just one example of how POWERSTATS are built . . . to suit each need.

- For the laboratory — Type 2PF1126 with totally enclosed terminal box, fuse protection, output receptacle and input cord-plug.
- As a component — Type 1126 with exposed terminal studs for direct wiring.
- For other needs — Type F1126 with terminal studs, fuse protection, and bakelite terminal cover.

For further details —

Send for BULLETIN 150SR

THE SUPERIOR ELECTRIC COMPANY

874 LAUREL STREET • BRISTOL, CONNECTICUT, U. S. A.

Save *TIME* in Analysis— Two Ways *with* SPECTROSCOPIC ANALYSIS

FIRST of all, Spectroscopic Analysis is FAST! The complete analysis of a material can be run in a very few minutes. This makes Spectroscopic Analysis ideal for on-the-spot analyses.

This established method saves time in another way: When operated on a routine basis, Spectroscopic Analysis takes up fewer man-hours per analysis . . . because it can analyze a large number of samples with the same equipment in a short space of time. Often it is possible in one spectrogram to analyze for as many as ten different elements, thus reducing to one-tenth the usual time for analysis!

It pays to use "National" Spectroscopic Electrodes. Extreme accuracy with Spectroscopic Analysis is possible only when the electrode is of known purity. That is why National Carbon Company, Inc., has developed ways to make carbon and graphite electrodes of unmatched purity. And, to enable the analyst to know exactly the properties of each particular lot, a "Statement of Purity" accompanies each lot of "National" Special Spectroscopic Electrodes. This gives qualitative estimates of the relative intensities of the most sensitive lines present in the electrodes.

Yes . . . using Spectroscopic Analysis with "National" Electrodes can save you much valuable time and trouble.

The word "National" is a registered trade-mark of National Carbon Company, Inc.

OTHER USES FOR SPECTROSCOPIC ANALYSIS:

- Extremely sensitive to 1/10,000,000 of a gram
- Makes possible analysis without destroying or mechanically removing material from the sample
- Detects unsuspected metals
- Makes possible analysis when only a minute quantity is available
- Provides a permanent record
- Differentiates between two substances very similar chemically.

NATIONAL CARBON COMPANY, INC.
Unit of Union Carbide and Carbon Corporation
UCC
30 East 42nd Street, New York 17, N. Y.
Division Sales Offices:
Atlanta, Chicago, Dallas, Kansas City, New York, Pittsburgh, San Francisco

GEIGER COUNTER SPECTROMETER

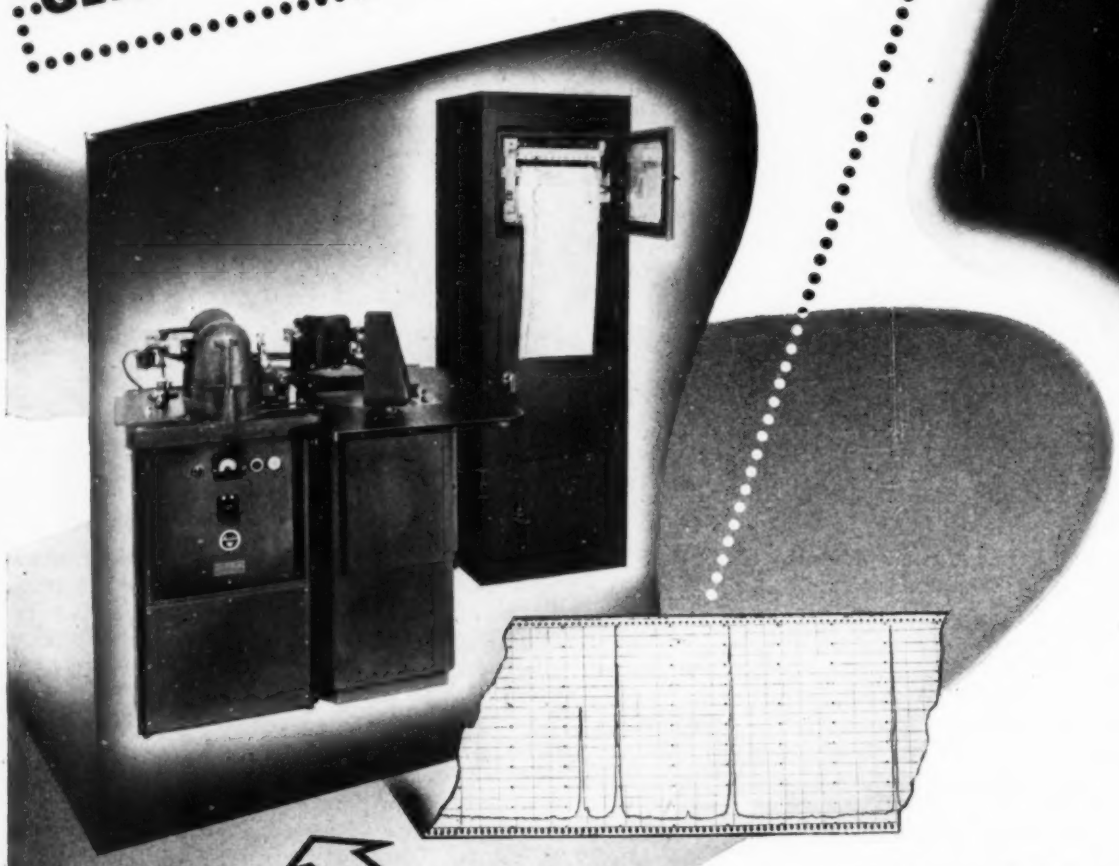

The Norelco Geiger counter X-ray Spectrometer makes use of a Geiger counter tube by means of which intensities and space distribution of X-ray reflections are easily and quickly determined.

Through the use of electronic circuits, characteristic reflections are registered directly on a scaled chart—showing at a glance, line positions and intensities.

This method, besides being accurate, saves considerable time in process work where continuous control is necessary and results must be obtained as rapidly as possible.

The apparatus does not require constant attention. Relatively unskilled operators can perform routine tests.

Time consumed in photographic processing and the possibility of human error in intensity evaluation are eliminated.

Norelco
Reg. U. S. Pat. Off.

ELECTRONIC PRODUCTS

NORTH AMERICAN PHILIPS COMPANY, INC.

DEPT. 2-12, 100 EAST 42ND STREET
NEW YORK 17, N. Y.

It's VERSATILE

It's EFFICIENT

It's PRECISE

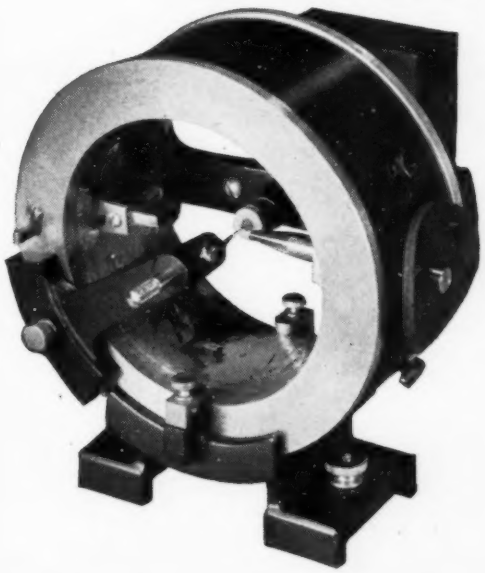

...it's the G-E MODEL XRD POWDER CAMERA

If you are interested in x-ray diffraction analysis of crystalline substances—check the outstanding features of the G-E Model XRD Powder Camera.

It's VERSATILE—all practical variations of the Debye-Scherrer-Hull-Davey technics can be accomplished. The sample shape may be varied rather than limited to cylindrical. The sample may be oscillated or rotated in a variety of holders. The camera sides are open so that large samples may extend into the center.

It's EFFICIENT—in the XRD Powder Camera the effective diameter is related to the number of degrees in a radian so that a distance on the film will be related to the Bragg angle by a round number. The size chosen produces the most favorable dispersion of the pattern as an optimum compromise between the requirements of speed and resolution. And the effective resolving power is variable through a choice of collimators and sample size.

It's PRECISE—designed to exacting standards and precision manufactured, you can depend upon the G-E Model XRD Powder Camera to routinely produce precision results of hair-line quality. And because it is a precision instrument, the XRD Powder Camera provides exceptional operating convenience that simplifies the production of patterns.

There are sound reasons why the majority of the nation's leading industries and laboratories have selected the G-E Model XRD X-Ray Diffraction Unit and cameras. They protected their investment by investigating. If you have problems that require x-ray diffraction, why not investigate the G-E Model XRD? For complete information on the XRD Unit and its cameras, write to General Electric X-Ray Corporation, 175 Jackson Boulevard, Chicago 4, Illinois. Department 2513.

GENERAL ELECTRIC X-RAY CORPORATION

•ACCURATE •SPEEDY •DEPENDABLE

Electrical Measurements with **WELCH METERS**

D.C. PANEL INSTRUMENTS

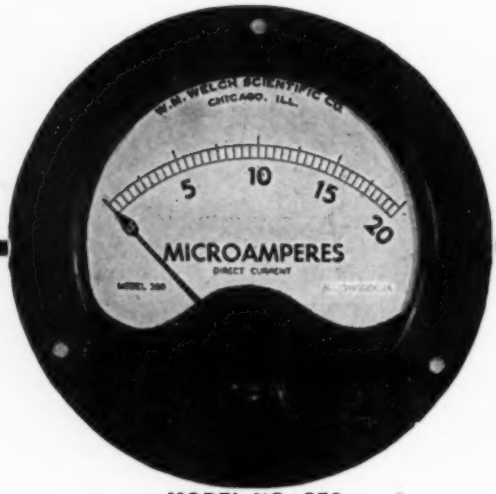

MODEL NO. 350

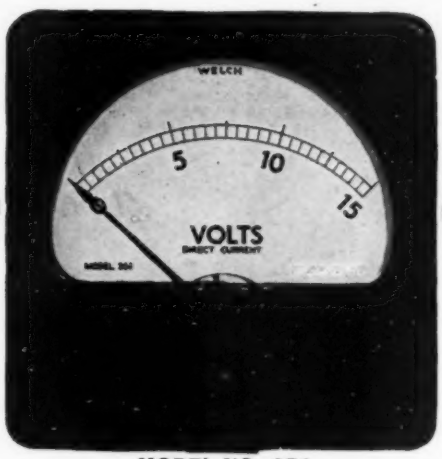

MODEL NO. 351

- Alnico Magnets
- Sapphire Jewel Bearings
- Selected Steel Pivots
- Fume-proof White Metal Scales
- Extremely Rigid Mounting
- High Torque Ratio
- Cases Moulded Bakelite for Flush Mounting

MODELS

350—3½ inch round—2.4 inch scale
351—3 inch square—2.4 inch scale
451—4½ inch rectangular—3.5 inch scale

TYPES

Microammeters 0–20 up to 0–500
Milliammeters 0–1 up to 0–500
Ammeters 0–1 up to 0–30
Voltmeters, various ranges, 100 to 50,000 ohms per volt
Zero Center Ammeters
DB Meters
Rectifier Instruments
Thermocouple Meters
Special Scaled Meters

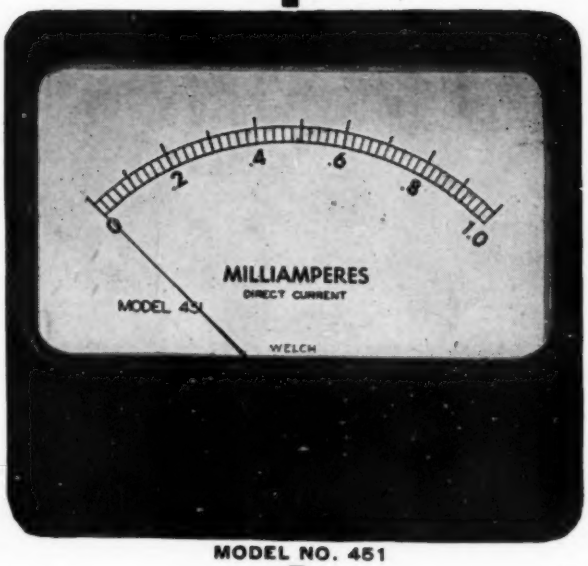

MODEL NO. 451

WRITE FOR OUR METER CATALOG

W. M. WELCH SCIENTIFIC COMPANY

Established 1880

1515 SEDGWICK STREET, DEPT. C-I CHICAGO 10, ILLINOIS, U.S.A.

Kodak develops special emulsions to record individual corpuscular tracks

For ready identification of nuclear reactions, Kodak research provides fine grain Alpha Particle Plates and Film to record alpha particles, deuterons, and protons as individual tracks rather than over-all exposure density.

These emulsions, 25 microns thick, reveal particle paths as close-spaced grains . . . with few gaps . . . low background fog. They are relatively insensitive to light and gamma radiation. To accentuate deuteron and proton sensitivity, boron can be introduced into the emulsion either in manufacture or by pre-exposure bathing. Kodak can supply these plates and films in any size to meet individual convenience.

Kodak invites you to write for more information about the specialized properties that emulsion research can build into photographic materials for nucleonics.

How to process Kodak fine grain Alpha Particle Plates

1. **Develop 2 minutes in Kodak Developer D-19 at 68° F, *without agitation*.**
2. **Rinse thoroughly in running water or in Kodak Stop Bath SB-3.**
3. **Fix in Kodak Fixing Bath F-5 for twice the time to clear.**
4. **Wash 30 minutes in running water. Note: Use Wratten Series I safelight.**

EASTMAN KODAK COMPANY
Rochester 4, N. Y.

Visit the Kodak exhibit at the Boston A.A.A.S. meeting . . . booth A50-51

Nuclear particle recording . . .
another important function of photography

Kodak

PROFESSIONAL SOCIETIES IN PHYSICS

AMERICAN PHYSICAL SOCIETY

The Society has as its object the advancement and diffusion of the knowledge of physics. All branches of fundamental and applied physics are generally included in its scope. Both experimental and theoretical researches are reported in its journals and meetings.

Publications: *The Physical Review* (24 issues annually), *Reviews of Modern Physics* (quarterly), and the *Bulletin* (7 issues, constituting the advance programs and abstracts of papers to be presented at meetings). Members receive *The Physical Review*, the *Bulletin*, and also *Science Abstracts A* (Physics section) without additional charge.

Dues: Members, $10; Fellows, $14.

Address: Karl K. Darrow, Secretary, Columbia University, New York 27, New York.

OPTICAL SOCIETY OF AMERICA

The Society devotes itself to the advancement of optics, pure and applied, in all its branches. It promotes the interests of investigators of optical problems and of designers, manufacturers, and users of optical instruments and apparatus.

Publications: The *Journal of the Optical Society of America* (12 issues annually) and advance programs of meetings with abstracts of papers to be presented. Members receive the Journal and programs without additional charge.

Dues: Associate Members, $6; Regular Members, $8.50; Corporate Members, $50; Patrons, $1000.

Address: Arthur C. Hardy, Secretary, Massachusetts Institute of Technology, Cambridge 39, Massachusetts.

ACOUSTICAL SOCIETY OF AMERICA

The Society's purpose is to increase and diffuse the knowledge of acoustics and promote its practical applications. The scope includes fundamental researches on the intensity, transmission and absorption of sound; also on noise, reverberation in rooms, the processes of speech and hearing, the performance and reproduction of music, etc.

Publications: *The Journal of the Acoustical Society of America* (quarterly) and advance programs of meetings with abstracts of papers to be presented. Members receive the Journal and the programs without additional charge.

Dues: Members, $5; Fellows, $7.50; Sustaining Members, $50.

Address: Wallace Waterfall, Secretary, 350 Fifth Avenue, 64th floor, New York 1, New York.

SOCIETY OF RHEOLOGY

This small but active society is composed of physicists, chemists, and engineers interested in "rheology," which is defined as the science of deformation and flow of matter.

Publications: The *Rheology Bulletin* (quarterly). Members receive the Bulletin without extra charge together with the Annual Rheology issue of the *Journal of Colloid Science*. Sustaining members receive both the *Journal of Applied Physics* and *The Review of Scientific Instruments*.

Dues: Members, $4; Sustaining Members, $25.

Address: R. B. Dow, Secretary-Treasurer, Bureau of Ordnance, Navy Department, Washington 25, D. C.

AMERICAN ASSOCIATION OF PHYSICS TEACHERS

Whereas the other Societies are mainly concerned with research, this Association has provided a much needed forum for the discussion of the problems of teaching. In cooperation with the other groups, the Association promotes the advancement of physics and emphasizes its place in the general culture.

Publications: The *American Journal of Physics* (6 issues annually) and advance programs of meetings. Members receive the Journal and the programs without additional charge.

Dues: Members, $5; Junior Members, $2.50.

Address: C. J. Overbeck, Secretary, Northwestern University, Evanston, Illinois.

The above five Member Societies jointly operate the American Institute of Physics in which they combine their collective strength for the achievement of objectives which they have in common. They publish their journals through the Institute, thus establishing a coordinated publishing program of high standards, efficiency, and economy. Through the Institute they have also opened new opportunities for physicists in industry and elsewhere, they have greatly increased the funds available for publication and they have preserved the spirit of unity among followers of the science.

Also associated with the American Institute of Physics are the following Affiliated Societies:

American Society for X-Ray and Electron Diffraction
Address: J. D. H. Donnay, Secretary, Johns Hopkins University, Baltimore, Maryland.

Electron Microscope Society of America
Address: John Turkevich, Secretary-Treasurer, Frick Chemical Laboratory, Princeton, New Jersey.

Physical Society of Pittsburgh
Address: E. Stickley, Secretary-Treasurer, Research Laboratory, Pittsburgh Plate Glass Company, Creighton, Pennsylvania.

Physics Club of Chicago
Address: H. A. Leedy, Secretary, Armour Research Foundation, 35 West 33 Street, Chicago 16, Illinois.

Physics Club of Philadelphia
Address: Mabel A. Purdy, Secretary-Treasurer, 6830 York Road, Oakhane, Philadelphia 26, Pennsylvania.

The American Institute of Physics exists for the service of the Member Societies and is devoted to the advancement of the science of physics. It publishes, as contributions to the field of physics at large,* The Journal of Chemical Physics, *the* Journal of Applied Physics, *and* The Review of Scientific Instruments. *The last two are available at reduced rates to members of the above Societies.

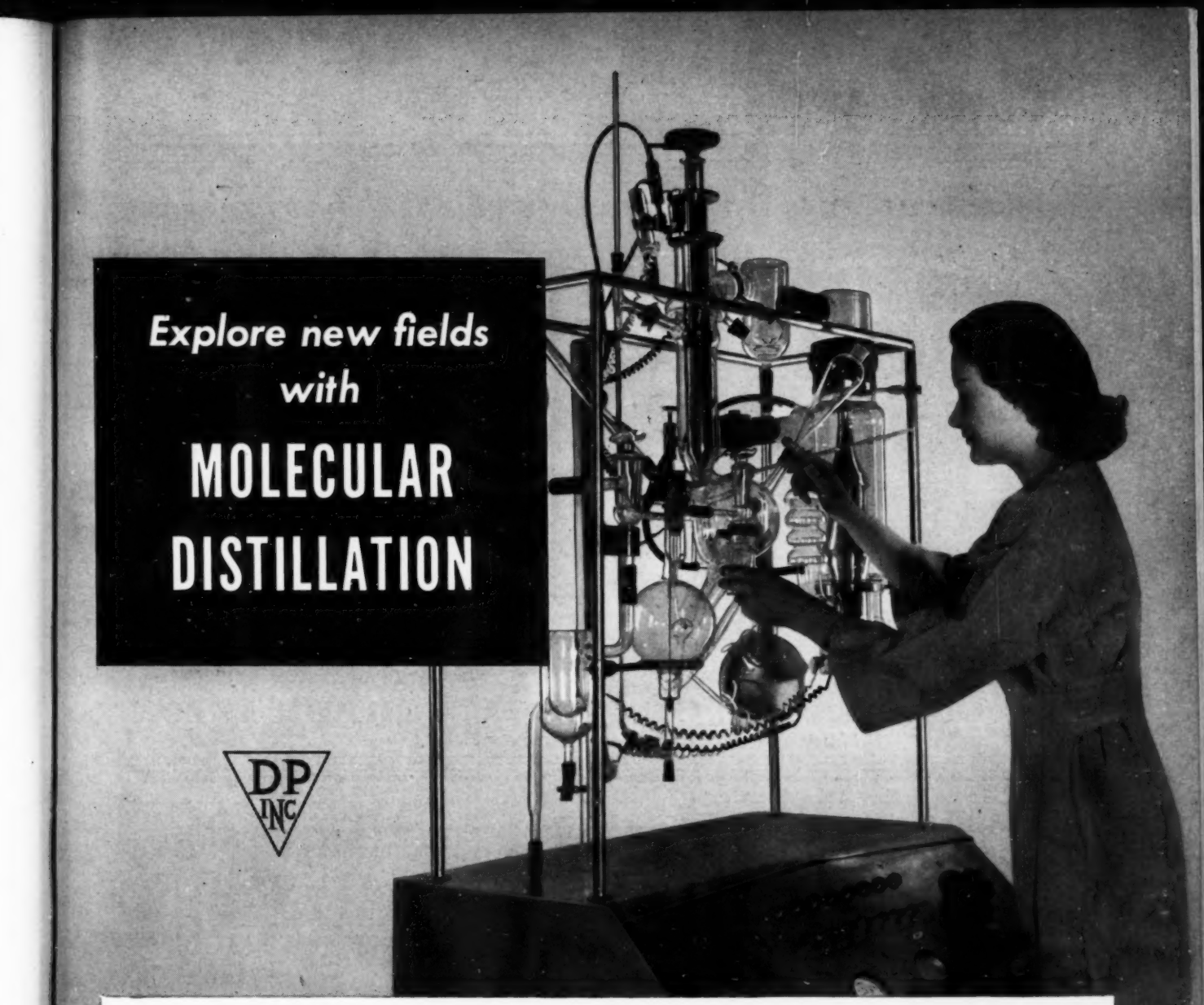

Explore new fields with

MOLECULAR DISTILLATION

DP INC

D.P.I.'s Falling Film Molecular Still gives chemical engineers a versatile tool for distillation... a tool which clearly indicates a vast new range of research possibilities. Perhaps your interest lies in some of the heretofore "undistillable" substances... perhaps in chemicals of high molecular weight... or you may be investigating oil separation, fat products, or other organic compounds. In any of these studies, the Falling Film Molecular Still can play a vital part. Through its use, new products may be discovered—new production methods evolved—and materials now a total waste may be salvaged. And finally, while it provides an invaluable technique for the laboratory, it also accurately points the way to practical commercial processing.

THE FALLING FILM MOLECULAR STILL IS DESCRIBED IN FULL DETAIL IN OUR NEW BOOKLET. WRITE—

Vacuum Equipment Division

DISTILLATION PRODUCTS, INC.,

Rochester 13, N. Y.

GAERTNER

Instruments for Spectrographic Analysis

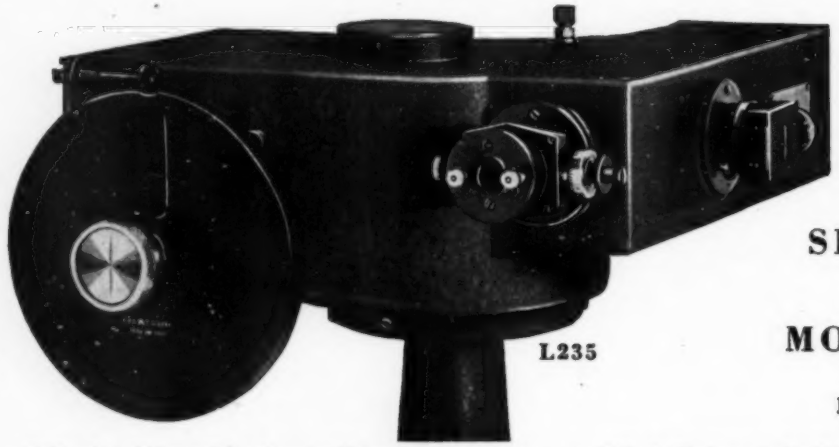

L235

INFRA-RED

SPECTROMETER and MONOCHROMATOR

Range: 0.7μ to 12.0μ

Elimination of Astigmatism and Coma • High Transmission • Extreme Accuracy

together with the skillful design and workmanship incorporated in this instrument render it exceptionally well-fitted for exacting research work.

THE GAERTNER SCIENTIFIC CORPORATION

1212 WRIGHTWOOD AVE. • CHICAGO 14 • U.S.A.

STANDARD

Wherever Power is Handled

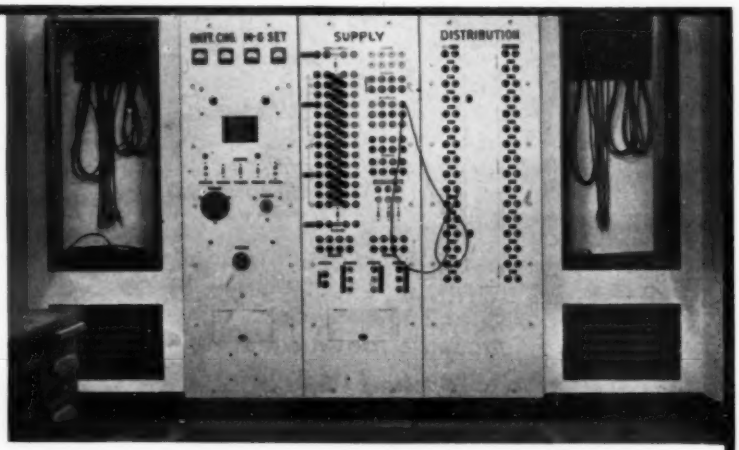

"Standard" Laboratory Panels may be found in the small as well as the larger colleges and universities throughout the entire country. For controlling and distributing electrical services of all kinds to the different laboratory tables, they are safe, convenient, efficient, practical and are great time savers.

If you are planning a new laboratory or remodeling your present one, ask "Standard" to give you the benefit of their many years' experience — with no obligation incurred. 38

Physics Laboratory
Wabash College
Crawfordsville, Ind.

THE STANDARD ELECTRIC TIME CO., SPRINGFIELD 2, MASS.

• Founded 1884 •

Proved RADIOACTIVITY EQUIPMENT

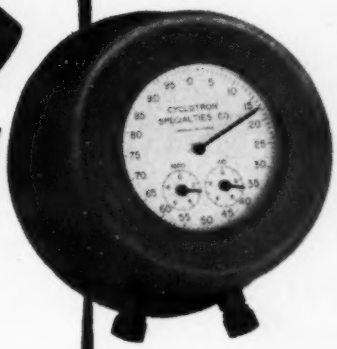

IMPULSE REGISTER

Accurately registers up to *sixty impulses* per second, and will solve your problems in high speed impulse or mechanical operation counting. Price, FOB factory **$55**

Cyclotron Specialties Instruments are readily assembled into a complete apparatus for the rapid and accurate determination of radioactivity. They combine simplicity and economy with all important requirements of the most exacting investigators and have won recognition of the leading workers in this field throughout the world...in educational institutions, industrial plants, laboratories and hospitals.

For new workers, the use of a cathode ray oscillograph, giving an excellent visual pattern of the pulses, is recommended. The counter set is fitted with amplifier and external connections for this purpose. The Cyclotron 401-A Impulse Register is also widely used by itself for high speed impulse recording or mechanical operation counting.

GEIGER MULLER COUNTER

An especially fine piece of equipment with numerous applications in radioactivity work. Price, FOB factory **$345**

THIN MICA WINDOW GEIGER TUBE

A compact, completely enclosed counter tube of sturdy construction with many important features. Used extensively by leading laboratories. Price, FOB factory **$50**

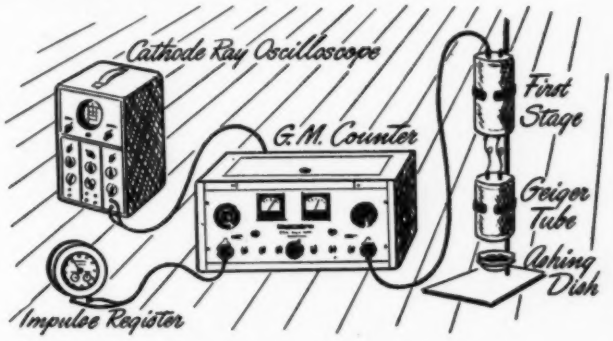

Cyclotron Specialties Instruments are quickly assembled into a complete radioactivity apparatus...

The sample to be tested is placed in an ashing dish where its radioactivity is transmitted into the Geiger Tube through the latter's thin mica window. Impulses from the tube are amplified and extinguished by a First Stage. This passes the impulses on to the Counter Set where they are amplified, scaled on a scale of eight and indicated on the Impulse Register.

Cyclotron Specialties radioactivity instruments are rugged and practically foolproof...made from the highest grade materials and designed for dependable performance under actual working conditions. Place your order now by mail.

Detailed specifications upon request

Cyclotron Specialties Company

Moraga 6, California

Q METER
TYPE 160-A

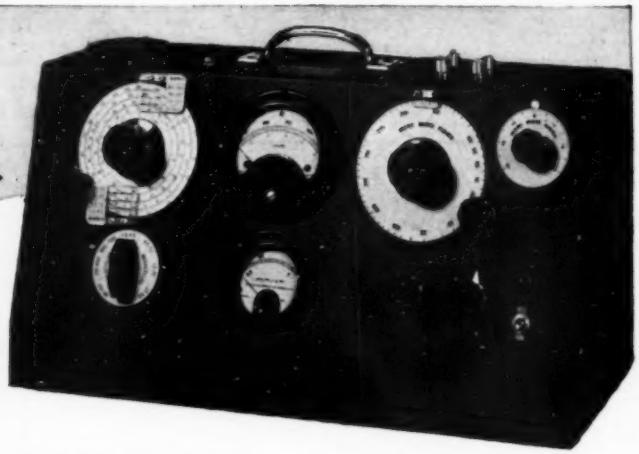

Direct Reading

B. R. C. instruments are designed and manufactured to give accurate and precise direct reading measurements with simplicity of operation.

A Standard for "Q" Measurements with a reputation for accurate and dependable service. Has a Frequency Range of 50 kc to 75 mc which may be extended with external oscillator down to 1 kc.

BOONTON RADIO Corporation
BOONTON, N. J.

DESIGNERS AND MANUFACTURERS OF THE "Q" METER . . . Q-CHECKER . . . FREQUENCY MODULATED SIGNAL GENERATOR . . . BEAT FREQUENCY GENERATOR . . . AND OTHER DIRECT READING TEST INSTRUMENTS

ATOMIC ENERGY IN COSMIC AND HUMAN LIFE: Fifty Years of Radioactivity

***by* GEORGE GAMOW**

The first part of the book, "Modern Alchemy," reviews the general theory of nuclear physics from the discovery of radioactivity in 1896 to the beginning of the second World War. Part II, "Atomic Energy in the Cosmos," discusses the evolution of the universe in terms of atomic transformations. Part III, "How can we use Atomic Energy," gives a clear account of the methods used to release nuclear energy and the facts of the atomic bomb; it concludes with an exciting look into the future.

This book, by the distinguished nuclear physicist, provides the fullest and most interesting background to the whole subject of atomic energy of any book yet published. Illustrated, $3.00

WHAT IS LIFE?: The Physical Aspects of the Living Cell

***by* ERWIN SCHRÖDINGER**

A Nobel Prize winner brings the physicists' discoveries about the structure of ultimate particles to bear upon fundamental particles of biology. The result is an exciting document that is one of the most significant scientific books of this generation. $1.75

THE CAVENDISH LABORATORY

***by* ALEXANDER WOOD**

This small book, containing eight full pages of plate illustrations, describes the foundation and development of the Cavendish Laboratory of Physics under Clerk Maxwell, J. J. Thomson and Rutherford, and it also discusses briefly the work of such scientists as C. T. R. Wilson, W. D. Aston, R. T. Glazebrook, W. N. Shaw, J. Chadwick, Peter Kapitza, and its present head, Sir Lawrence Bragg. $1.00

CAMBRIDGE UNIVERSITY PRESS
THE MACMILLAN COMPANY
60 Fifth Avenue New York 11, N. Y.

PATTERSON PHOSPHORS Provide Fine Detail...Brilliance... in Television Images

High luminescence with low input energy characterizes PATTERSON PHOSPHORS—for television, radar, oscilloscopes and other electronic instruments. E. I. du Pont de Nemours & Co. (Inc.), Patterson Screen Division, Towanda, Pennsylvania.

Patterson

PATTERSON PHOSPHORS ARE AVAILABLE IN A WIDE RANGE OF

1. Colors
2. Grain Size
3. Brilliance
4. Types of Excitation
5. Afterglow
6. Special Blends

DU PONT

LUMINESCENT CHEMICALS

BETTER THINGS FOR BETTER LIVING...*THROUGH CHEMISTRY*

PHOTOVOLT ELECTRONIC PHOTOMETER

A highly sensitive light meter with phototube and amplifier.

For all problems involving the measurement of low light values or thin beams of light.

Densitometry of spectographs and X-ray diffraction negatives.

Exposure determination in photomicrography and metallography.

Measurement of fluorescence and phosphorescence of solids and solutions.

Obtainable with phototubes extending in sensitivity to 200 millimicrons for measurement of ultraviolet emission and absorption.

Write for literature to

PHOTOVOLT CORP.

95 Madison Ave. New York 16, N. Y.

Also

Colorimeters
Reflection Meters
Glossmeters
Fluorescence Meters
Densitometers
Photoelectric pH Meters

FIFTH PLACEMENT REGISTER

of the

AMERICAN INSTITUTE OF PHYSICS

When: Joint meeting, American Physical Society and the American Association of Physics Teachers, January 30, 31, and February 1, 1947.

Where: Columbia University, New York, New York.

INTERESTED IN A NEW POSITION?

Registration forms and further instructions may be obtained from the Institute office. Pre-registration is advisable, as records will be made available to employers before the meeting begins.

DO YOU NEED MEN?

Files will be available to employers the afternoon of the 22nd. Companies or institutions wishing to post notices of positions may send details to the Institute office, or post them upon arrival at the meeting.

INTERVIEWS

It is naturally to the advantage of registrants to be present. Interviews will be arranged as usual between employers' representatives and those applicants attending the meeting.

Please Report to the Register Office Immediately Upon Arrival at Meeting.

American Institute of Physics **57 East 55 Street, New York 22, New York**

New

GEIGER MÜLLER COUNTER

A superlative radiation instrument—setting new performance standards. . . . Many new features including:

1. **Scales of 2, 4, 8, 16, 32 and 64.**
2. **Automatic hi-voltage stabilization.**
3. **Neon lamp interpolators.**

Also available

ELECTRONIC TIME INTERVAL METER

Measures electric or light pulses, from 1/10,000 to 3 seconds.

Descriptive literature on request.

Berkeley Scientific Co.

1908 ALCATRAZ AVE., BERKELEY 3, CALIF.

GEOPHYSICS

Offers the following subscription rates:

	U. S.	Foreign
One year, 4 issues	$6.00	$6.50
Single copies	$2.00	$2.20

Special discounts to public libraries and government agencies

•

Address subscriptions to

SOCIETY OF EXPLORATION GEOPHYSICISTS
P. O. Box 1614
Tulsa, Oklahoma

BARGAINS IN WAR SURPLUS LENSES and PRISMS

NOW! MAKE YOUR OWN BINOCULARS!

Complete Set of LENSES and PRISMS from Navy's 7X50 Model

Save up to $150.00!

Here's an unusual opportunity to secure a fine set of Binoculars at a tremendous saving of money. Build them yourself with all of the very same optics contained in the Navy's 7 Power Glasses. Or you can construct a Monocular (½ a Binocular) in which case exactly one half quantities of the Binocular Components will be furnished. Lenses are cemented and have the new low reflection coating. Complete assembly directions included for either project.

Stock #5102-R—Binocular Set of Lenses and Prisms.....**$25.00 Postpaid**
Stock #5103-R—Monocular Set of Lenses and Prisms....**$12.50 Postpaid**

AIR FORCES GUN SIGHT With Polarizing Variable Density Attachment
Use as Slide Viewer or take apart and get Polarizing Variable Density Attachment, Mangin Concave Mirror, Reflector Plate, Metal Reticle, Lamp Housing, etc. Polarizing attachment alone is worth many times price of entire unit.
Stock #908-R.....**$5.00 Postpaid**
Same Unit Without Polarizing Attachment
Stock #916-R.....**$2.50 Postpaid**

BOMBER SIGHTING STATION—A double end Periscope Type Instrument of highest precision. 6 ft. tall, shipping wt. 360 lbs. Orig. cost $9,850. Consists of numerous Lenses, Prisms, Mirrors, Gears, Motors, Metal Parts and Electrical Gadgets.
Stock #914-R.....**$50 F.O.B. Oklahoma**

SPECTROSCOPE SET.....These sets contain all Lenses and Prisms you need to make a Spectroscope plus FREE 15-page Instruction Booklet.
Stock #1500-R—Hand Type Spectroscope.....**$3.45 Postpaid**
Stock #1501-R—Laboratory Type Spectroscope.....**$6.50 Postpaid**

We have literally millions of war surplus lenses and prisms for sale at bargain prices.
Write for catalog "R"—Sent Free!

Satisfaction Guaranteed • **Order by Stock No.**

EDMUND SALVAGE COMPANY
P. O. AUDUBON NEW JERSEY

WANTED!

ENGINEER, PHYSICIST OR APPLIED MATHEMATICIAN

For research and analysis of the problems of aircraft dynamics, including vibration and flutter. Post-graduate experience in similar work desirable. Excellent opportunity to acquire responsible direction of particular projects.

Write to

CHANCE VOUGHT AIRCRAFT
STRATFORD, CONN.

Silicone News

DC SILICONES

DC Silicone Fluid affords greater sensitivity in temperature control

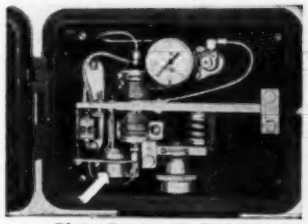

Photo, Courtesy the Swartwout Co.

The Thermo Master Control and other control instruments made by The Swartwout Company of Cleveland have been redesigned and made even more sensitive through use of a damping device filled with one of the Dow Corning Silicone fluids (arrow). Previously no damping device was used because conventional organic fluids are subject to such wide changes in viscosity with temperature that they limit rather than increase the sensitivity of these carefully engineered instruments.

With the introduction by Dow Corning of Silicone Fluids unique among liquids for their flat viscosity-temperature slopes, low volatility, and thermal stability, the long standing problem of effective damping over a wide temperature range was solved.

The Thermo Master Control is widely used for regulating temperature in steam desuperheating involving temperatures ranging from 50° to 950°F. Ambient temperatures may vary from −40°F. to 150°F. Over such a wide temperature span, only silicone fluids remain sufficiently constant in viscosity to damp minor oscillations of the metallic control without lessening the sensitivity of such precision instruments.

More information about DC Silicone Fluids available in several types for a wide variety of applications is contained in catalog No. R 1-3.

DOW CORNING CORPORATION
MIDLAND, MICHIGAN
Chicago Office: Builders' Building
Cleveland Office: Terminal Tower Building
New York Office: Empire State Building
In Canada: Dow Corning Products Distributed by Fiberglas Canada, Ltd., Toronto

Dow Corning
FIRST IN SILICONES

The Golay

INFRA-RED DETECTOR

For over twenty years the Eppley Laboratory, Inc. has endeavored to be of service to Science and Industry in America by supplying thermopiles, pyrheliometers and other equipment for the detection and measurement of radiant energy.

During the war years great forward strides were made in this field, particularly with respect to the detection and measurement of infra-red radiation. At the March meeting of the American Optical Society, held in Cleveland, much of this progress was revealed.

Of particular interest to those present was the disclosure of the Golay infra-red detector, developed at the Signal Corps Engineering Laboratories under the direction of Dr. Marcel J. E. Golay. This device was acclaimed as presenting the best all around characteristics of sensitivity, speed, reliability and spectral uniformity of response.

The Eppley Laboratory, Inc. has begun the manufacture of the Golay detector under the personal supervision of Dr. Golay. Literature is in preparation and it is expected that the units will be available commercially in a short time.

EPLAB

The Eppley Laboratory, Inc.

SCIENTIFIC INSTRUMENTS

NEWPORT
RHODE ISLAND
U. S. A.

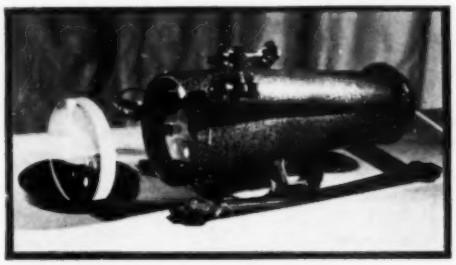

CONVENIENT COMPACT COLLIMATOR

Available are one dozen of these precision instruments. Five-inch cemented achromat, computed to deliver image of point source of light in exactly parallel rays. Focal length 25 inches; first surface flat reduces total length to a compact 14 inches, placing point source conveniently at front end. Auxiliary 6 V. green light-spot system for instant location of correct alignment. Point source not furnished. Cut shows how common radio tube base fits sleeve for easy construction of desired type of pinhole system. Cast aluminum throughout, 3 adjusting screws, cover. Hand figured lens tests near to theoretical perfection. Black crackle. New. Priced at less than cost of objective alone,—only $250.00.

ANTHONY COTTONE & CO.

63 Grand Street New York 13, N. Y.

PHYSICISTS

For research and development in problems of finding and producing oil, a major oil company requires the services of a few well-qualified physicists as permanent research staff members. Preference will be given men with the Ph.D. degree or the equivalent in training and experience.

A modern Southwestern laboratory, established for several years, furnishes complete facilities and pleasant surroundings. The expansion currently being conducted is definitely on a permanent basis.

Time will be saved in consideration of applicants if their initial communications give full information.

Box 1246A, 57 E. 55th Street
New York 22, New York

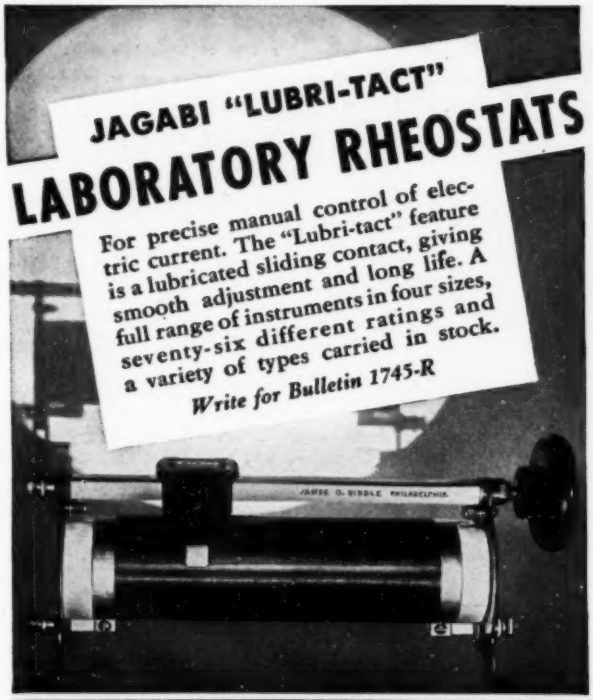

JAGABI "LUBRI-TACT"
LABORATORY RHEOSTATS

For precise manual control of electric current. The "Lubri-tact" feature is a lubricated sliding contact, giving smooth adjustment and long life. A full range of instruments in four sizes, seventy-six different ratings and a variety of types carried in stock.

Write for Bulletin 1745-R

JAMES G. BIDDLE CO.
ELECTRICAL AND SCIENTIFIC INSTRUMENTS
1316 ARCH STREET—PHILADELPHIA 7, PA.

PHYSICIST — CHEMICAL PHYSICIST

A physicist and a chemical physicist required for fundamental research on solid catalysts and molecular structure. Their prime interest should be in devising and interpreting crucial experiments with a secondary interest in instrumentation. The physicist should have experience in x-ray diffraction as well as a good theoretical and mathematical background.

The chemical physicist should have experience or a thorough fundamental training in the field of molecular structure, preferably with an experimental background in infrared absorption spectroscopy.

These men will be members of the physics group of a large research laboratory established for fifteen years and located about fifty miles from New York City. As the scheduled expansion of the present physics group proceeds, qualified men will receive increased responsibility.

Please write fully, including education, experience and expected salary to:

DR. L. C. ROESS
THE TEXAS COMPANY
BEACON, NEW YORK

NEW!

HIGH SPEED GEIGER-MULLER LABORATORY SET MODEL GL532C

Every desirable feature incorporated into one complete instrument:—

1 Regulated high voltage power supply for counter tube continuously variable up to 1500 volts. Regulates to within 1%.

2 Scaling ratios of 2, 4, 8, 16, and 32 can be selected by ratio switch on front panel.

3 Bank of numbered neon indicator lamps on front panel show proper operation of scaling circuits and provide means of interpolation between scalar stages.

4 Five separate power supplies for extremely stable operations and perfect circuit isolation.

BACKED BY 12 YEARS CONTINOUS EXPERIENCE IN THE DESIGN, DEVELOPMENT AND MANUFACTURE OF HIGH QUALITY COMMERCIAL GEIGER-MULLER COUNTER APPARATUS.

PRICE: Counter Set $455.00

MANUFACTURING DIVISION
HERBACH & RADEMAN CO.
Electronics Specialists
517 LUDLOW STREET
PHILADELPHIA 6 PA.

WRITE FOR CATALOGUE

EVAPORATED *metal films* CORPORATION OF ITHACA

Now We Are Three!

CHROLUMINUM
DUOLUX
RHODIUM

•

All are first-surface mirrors, but each has its special use.

CHROLUMINUM is permanently *brilliant.*

DUOLUX is accurately *semi-reflecting.*

RHODIUM is the rugged new-comer. It is as surface-hard as *most steels,* and cannot be tarnished nor corroded under *any known* conditions of use.

•

Write for folder of information and prices.

•

High-vacuum chambers are used in the production of our mirrors.

EVAPORATED METAL
FILMS CORPORATION
ITHACA, NEW YORK

MICRO-MIKER

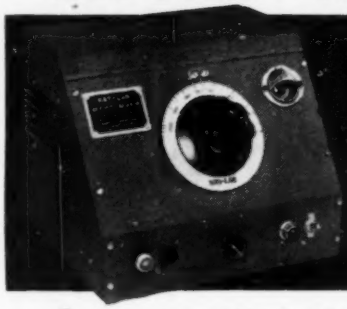

A new type of instrument for the measurement of small capacities

1. Measures capacities from 1 to 230 Micro-Micro-Farads by direct substitution.
2. This capacity is measured at the end of a shielded cable, thereby eliminating connection errors.
3. Wiring capacity in an amplifier may be measured without disconnecting the load resistor. Condensers as small as 1 MMF may be measured when shunted by a 1500 ohm resistor.

Write for Bulletin No. 4L

KAY-LAB

KALBFELL
LABORATORIES
1076 MORENA BLVD.
SAN DIEGO 10, CALIFORNIA

NUCLEAR PHYSICIST

An unusual opportunity for a competent Ph.D. Physicist with experience in nuclear physics. This man will be given an opportunity to carry on nuclear research and also will be required to maintain close contact with nucleonic research throughout the United States. He should have a good theoretical and mathematical background. He will be a member of the physics group in a large research laboratory. As the scheduled expansion of the present group proceeds, he will have a good opportunity for increased responsibility.

Please write fully, including education, experience, and expected salary to:

DR. L. C. ROESS
THE TEXAS COMPANY
BEACON, NEW YORK

TWIN POWER SUPPLY

Electronically Regulated for Precise Measurements

Two independent sources of continuously variable D.C. are combined in this one convenient unit. Its double utility makes it a most useful instrument for laboratory and test station work. Three power ranges are instantly selected with a rotary switch:

175–350 V. at 0–60 Ma., terminated and controlled independently, may be used to supply 2 separate requirements. 0–175 V. at 0–60 Ma. for single supply. 175–350 V. at 0–120 Ma. for single supply.

Twin Power Supply Model 210 - - - Complete $115.00 F.O.B. Chicago

Dimensions: 16″ × 8″ × 8″
Shipping Wt. 35 lbs.
(Other types for your special requirements)

FURST ELECTRONICS
800 W. North Avenue
Chicago 22, Illinois

McDONNELL AIRCRAFT CORPORATION
is augmenting its staff of research physicists as part of its special, long-range, secret development program being undertaken for the armed forces.

There are openings for several men with M. S. or Ph.D. degrees in physics and with two to three years research experience in circuit analysis, ballistics, theoretical physics, or related fields. Salary and position commensurate with ability and experience.

WRITE

McDonnell Aircraft Corporation
Lambert-St. Louis Municipal Airport
Box 516, St. Louis (21)
Missouri

DELIVERIES FROM STOCK

on all standard items—
Specials in less than a week if necessary

ACCURATE
to 0.05% when required

MOUNTING STYLES
to match any need

PHYSICALLY PROTECTED
to specifications

HERMETICALLY-SEALED and TROPICALIZED TYPES
for exacting applications

BULLETIN R tells what you want to know about precision resistors. Write for your copy today.

Shallcross Manufacturing Company
Dept. P-126 **Collingdale, Pa.**

SHALLCROSS
AKRA-OHM PRECISION RESISTORS
Electrical Measuring Apparatus • Precision Switches
Electronic Engineering

TYPE B HIGH PRECISION POTENTIOMETER

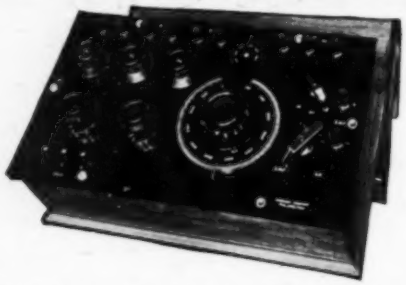

This instrument is widely used for highly precise thermocouple measurements, for the calibration of electrical measuring instruments, and for other critical measurements of DC potentials requiring exceptionally high accuracy. Distinctive features include:

1. Three ranges: 0 to 1.6 volts, 0 to 160 millivolts and 0 to 16 millivolts.
2. Three reading dials—effective scale length of approximately 175 feet for each range. Readings easily estimated to within one part in 100,000 of full-scale ranges.
3. Subpanel switch and slidewire construction for protection of contacts from dust and corrosive fumes.
4. Special provisions to minimize parasitic thermal emf's—including automatic compensation of slidewire thermals and gold contacts in galvanometer key.
5. Exceptional convenience in reading and adjustment.
6. Solid and substantial construction for many years of trouble-free service.

Thoroughly proven by practical application in exacting research investigations for nearly fifteen years. Described in Bulletin 270 with other Rubicon potentiometers, including the popular portable precision models.

Rubicon galvanometers suitable for use with the Type B Potentiometer are listed in Bulletin 320.

OTHER RUBICON INSTRUMENTS

Galvanometers • Resistance Standards • Wheatstone, Kelvin and Mueller Bridges • Evelyn Photoelectric Colorimeter for precise colorimetric chemical analysis • Automatic Recording Photometric Analyzers for NO and H_2S • Magnetic Permeameters • Other equipment involving precise measurement of electrical quantities.

RUBICON COMPANY

ELECTRICAL INSTRUMENT MAKERS

3761 Ridge Avenue, Philadelphia 32, Pa.

RAWSON TWIN MULTIMETER

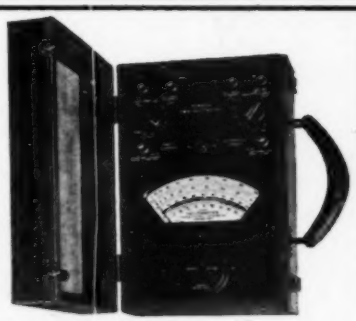

Type 5012 Accuracy ½ of 1% DC
Size 12" x 8" x 6"
A Combination AC. Multimeter and DC Multimeter

Range of Measurements

DC 1 microampere to 1 Ampere.
20 Microvolts to 1000 volts.

AC (thermocouple type)
2 Milliampere to 3 Amperes.
60 Millivolts to 1000 volts.

Write for bulletin

WE ALSO SUPPLY

REGULAR DC METERS
THERMOCOUPLE AC METERS
MULTIMETERS, FLUXMETERS
ELECTROSTATIC VOLTMETERS

Special apparatus built to order

RAWSON ELECTRICAL INSTRUMENT COMPANY
101 POTTER ST. CAMBRIDGE, MASS.

Representatives
CHICAGO LOS ANGELES NEW YORK CITY

WANTED

Prominent Aircraft Company, Eastern United States, needs men with following qualifications:

Experienced engineers with Bachelor's, Master's, Doctor's degrees in Electrical Engineering, Physics, Mathematics. At least two years' experience in design and development of radar and television systems, automatic computers, servomechanisms, target seekers, etc., required. Positions open for preliminary and detail design, research, and development of guided missiles under Army and Navy contracts.

Starting salary commensurate with experience.

Address
BOX 1146
57 East 55 Street, New York 22, N. Y.

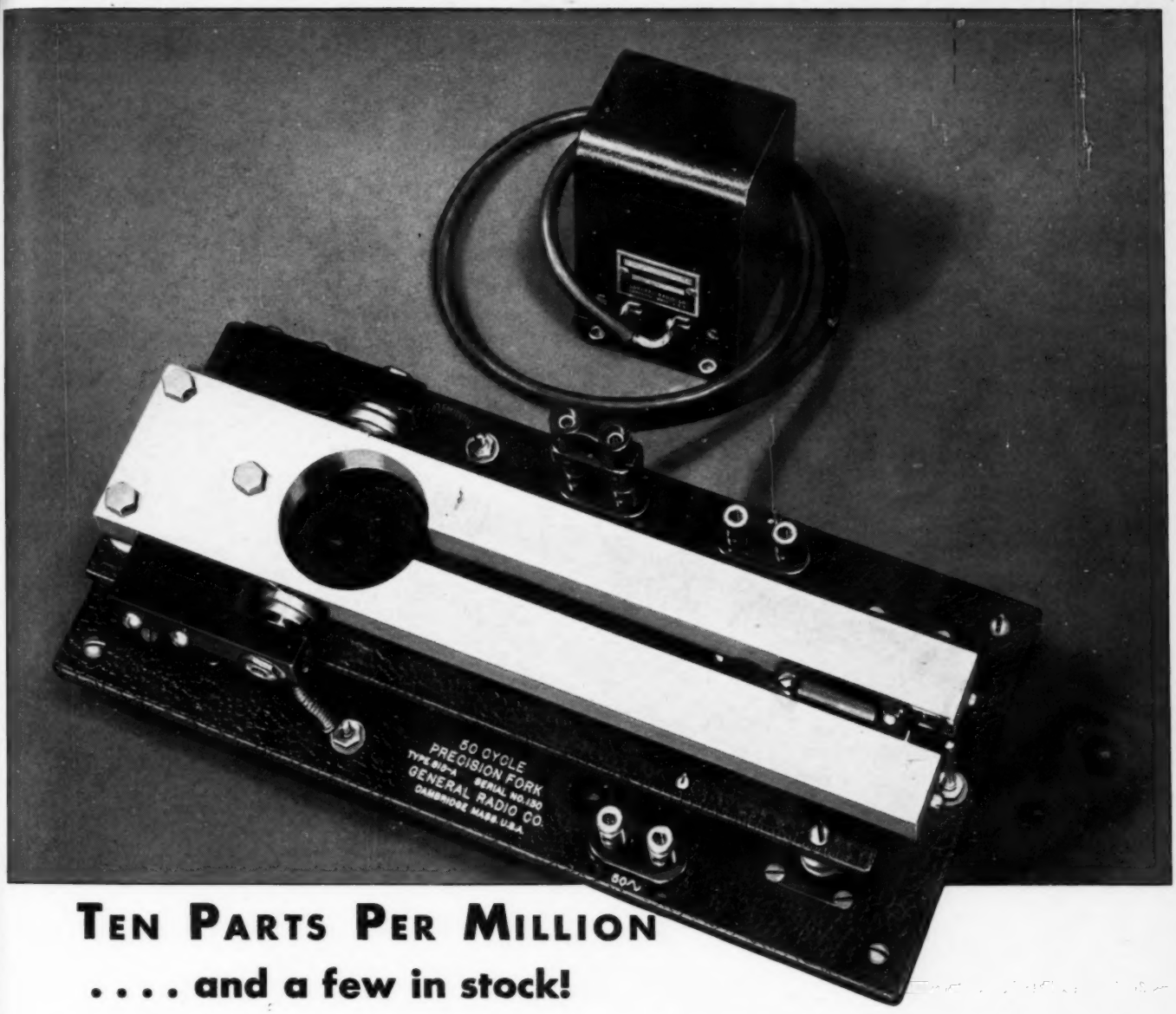

TEN PARTS PER MILLION

. . . . and a few in stock!

Where the ultra refinement of temperature control is not required, the G-R Type 815 Precision Forks have more than sufficient accuracy for use both in the laboratory and in the field. They are supplied in frequencies of 50, 60 and 100 cycles with a calibration accuracy of ten parts per million. They make excellent low-frequency standards.

Stock for the forks is low-temperature-coefficient stainless steel, received by us in bars. A sample fork is made from each bar and the coefficient of the stock is obtained after a protracted temperature run.

The forks are then machined in our shops. When measured to one millicycle, the unmounted fork is about 2 cycles below its nominal frequency. After this initial measurement, the excess material is milled from the end of the tines and a second frequency check is made. Occasionally the forks must be milled a second time.

Two adjustable loading screws are placed in holes drilled and tapped in the end of each tine. The fork is then assembled and the temperature coefficient of the outer tine screw is obtained. If necessary, excess material is removed from the outer tine screw. The screws are adjusted so that the frequency is within ±0.001% of its nominal value. The voltage coefficient of frequency is obtained; it averages about 0.005%. Output voltage and harmonic content are then measured.

When orders are received the forks are returned to the standardizing laboratory, given a half-hour run and the frequency is measured at a driving voltage of exactly four volts. With each fork a calibration certificate is supplied to show: the frequency to within ±0.001% at a stated temperature between 70 and 80 deg. F.; the temperature and voltage coefficients of frequency.

TYPE 815-A	50-CYCLE FORK	$175.00
TYPE 815-B	60-CYCLE FORK	185.00
TYPE 815-C	100-CYCLE FORK	185.00
TYPE 815-P1	Transformer (for use between the fork and relatively high-impedance loads)	6.95

AT THE MOMENT WE HAVE A SMALL STOCK OF THESE FORKS

GENERAL RADIO COMPANY Cambridge 39, Massachusetts

90 West St., New York 6 — 920 S. Michigan Ave., Chicago 5 — 950 N. Highland Ave., Los Angeles 38

HIGH SPEED—HIGH VACUUM

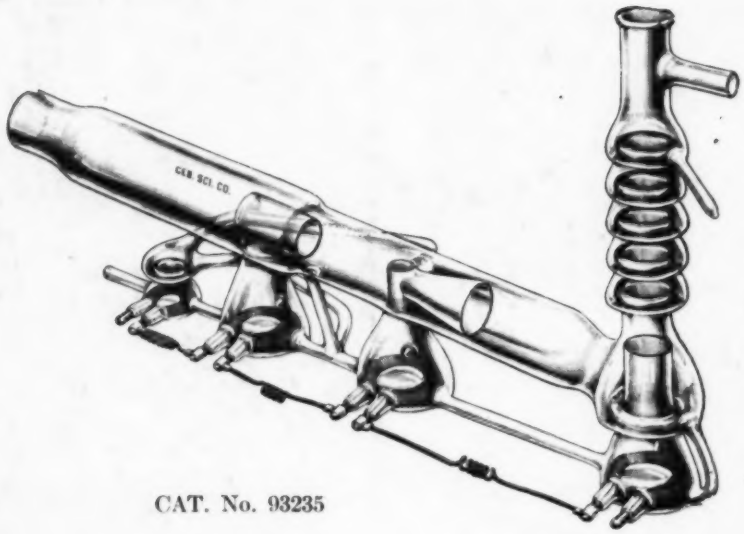

CAT. No. 93235

DP-Four-Compartment, Three-Jet Glass Diffusion Pump—Attains pressures less than $5x10^{-8}$—Speed of pumping at 10^{-4} mm, 30 liters per second. A Cenco-Hyvac or Cenco-Pressovac Pump is an ideal backing unit. Constructed entirely from "Pyrex" brand glass, No. 93235 Diffusion Pump contains three jets, catchment lobes and four fractionating boiling compartments which greatly improve the speed and vacuum obtained. Side tubes are placed to drain the uppermost lobe and for the connection of a gage for measuring the forepressure. Each of the boiling compartments contains heating coils with sealed-in terminals. These are proportioned for proper heating, when connected in series. Current requirements 1.5 to 2.4 amperes..... Each **$215.00**

CENTRAL SCIENTIFIC COMPANY

SCIENTIFIC INSTRUMENTS — CENCO REG. U.S. PAT. OFF. — LABORATORY APPARATUS

NEW YORK TORONTO **CHICAGO** BOSTON SAN FRANCISCO

LANCASTER PRESS, INC., LANCASTER, PA.